THE PROCESS OF CRACK INITIATION AND PROPAGATION IN CONCRETE

by

Michel Pigeon, B.Sc. (LAVAL), D.I.C.

A thesis submitted for the degree of

Master of Philosophy

in the Faculty of Engineering of the
University of London

IMPERIAL COLLEGE OF SCIENCE
AND TECHNOLOGY

LONDON, NOVEMBER 1969

ABSTRACT

In the present thesis, the process of crack initiation and propagation is examined in a particular type of concrete consisting of single-sized glass spheres imbedded in a mortar matrix.

Thin, two-dimensional, slices of such a concrete, containing three different aggregate particle arrays with various spacings between particles to represent various volume fractions of coarse aggregate, were tested in uniaxial compression. Using photoelastic and strain gauge techniques, the 'elastic' strain distribution in the matrix surrounding the particles was determined.

These "plate-models" were subsequently loaded to failure and, using continuous strain recording techniques at the points where initial cracking had been predicted from the above strain analysis, the level of strain of the composite material at fracture initiation was measured. Information regarding the cracking process up to failure was obtained by examination of the crack patterns on the plates at the end of the tests and from photographs taken during the tests of the isochromatic patterns on the photoelastic coatings.

Good quantitative agreement was found between the results of the plate-model tests and those of tests by Newman[13] on three-dimensional specimens of the concrete. In addition, uniaxial compression tests on gap-graded gravel concrete cylinders showed that these concretes behaved similarly to glass-marble concrete.

It was thus concluded that the plate-models gave valid indications of the cracking phenomenon in the two types of concrete considered and probably in plain concrete as well.

ACKNOWLEDGEMENTS

The author wishes to express his gratitude to:

Professor A.L.L. Baker, under whose supervision the research program was conducted.

Mr. J.B. Newman, head of the Concrete Materials Research Group, for his invaluable help and advice throughout the past year and especially for his patience when reviewing the manuscript.

Mr. K. Newman, for useful comments and suggestions concerning the research program.

The other members of the Concrete Materials Research Group, R. Glen, P.R. Mitchell and P. Corles, for their expert technical advice and constant cheerfulness. Special thanks are due to Mr. Mitchell for his skill in taking the photographs.

Miss J. Ward, who typed the manuscript.

The Athlone Fellowships Committee who provided the author with financial support during his stay in England.

The Construction Industries Research and Information Association (C.I.R.I.A.), for granting the funds required for the experimental research.

Contents

	Page No
Abstract	2
Acknowledgements	3
Contents	4
Sign Convention and Abbreviations	7
Chapter I Introduction	8
Chapter II Determination of Plate-Model Characteristics	14
Section 1. Introduction	14
Section 2. Aggregate Particle Arrays	14
Section 3. Spacing of Particles	21
Section 4. Determination of the Coarse Aggregate Content Represented by each Model	22
Chapter III Experimental Technique	27
Section 1. Materials	27
Section 2. Casting and Curing	27
Section 3. Photoelastic Technique	28
a) Birefringent Coatings	28
b) Optical Instruments	29
c) Use of Coatings	29
d) Validity of Measurements	29
Section 4. Loading System	32
Chapter IV The Fracture Initiation Envelope for Mortar	35
Section 1. Introduction	35
Section 2. Uniaxial Tests on Mortar	36
Section 3. Changes in the Fracture Initiation Envelope	43
Chapter V Strain Distribution Analysis in Plate-Models	46
Section 1. Introduction	46
Section 2. Testing Procedure	47

	Page No
a) Grid Scribed	47
b) Load Cycling	47
c) Determination of Isoclinic Values	47
d) Placing of Strain Gauges	54
e) Shrinkage Pattern Readings	56
f) Isochromatic and Strain Gauge Readings	56
g) Face Correction Factor	59
h) Determination of Principal Strains	59
i) Composite Strains	63
j) Critical Point Analysis	69
Section 3. Discussion of Results	71
a) Results	71
b) Validity of Results	73
c) Critical Zones	74
Chapter VI Loading Tests to Failure of the Plate-Models	120
Section 1. Introduction	120
Section 2. Testing Procedure	120
a) Position of Strain Gauges	120
b) Loading Arrangements	122
c) Recording of Strains and Applied Load	122
d) Photographs	124
Section 3. Determination of Fracture Initiation Point	124
a) Results	124
b) Relation between Composite Strains at Fracture Initiation and Coarse Aggregate Content	131
c) Comparison with McCreaths Results	135
d) Comparison with Tests on Three-Dimensional Concretes	137

	Page No
Section 4. Strains up to Failure	144
Section 5. Crack Patterns	147
a) Crack Patterns prior to Loading	147
b) Influence of Shrinkage Cracks	149
c) Crack Patterns Observed after Failure	150
Section 6. Photographs of Isochromatic Patterns	157
Section 7. Discussion of Results and Conclusions	167
a) Applicability of Plate-Model Test Results to Concrete	167
b) The Process of Crack Initiation and Propagation	172
Chapter VII Tests on Three-Dimensional Concretes	175
Section 1. Introduction	175
Section 2. Testing Procedure	175
a) Materials	175
b) Casting	176
c) Air Content	176
d) Curing	177
e) Preparation of Specimens for Testing	177
f) Loading System and Strain Recording	177
Section 3. Compressive Composite Material Strain at Fracture Initiation	178
Section 4. Discussion of Results and Conclusions	186
Chapter VIII Conclusions	190
References	194

SIGN CONVENTION

The sign convention used throughout this thesis is as follows:

for principal stresses;

$$\sigma_1 > \sigma_2 > \sigma_3 \text{ , tension positive}$$

for principal strains;

$$\varepsilon_1 > \varepsilon_2 > \varepsilon_3 \text{ , tension positive}$$

ABBREVIATIONS

V_f C.A. ; Volume fraction of coarse aggregate

f.i. ; Fracture initiation

comp. ; Composite material

CHAPTER I

Introduction

Nowadays, it is generally accepted that the application to concrete of simple failure criteria (such as maximum stress or strain) is neither satisfactory nor realistic because, in such a complex material cracking occurs at loads well below those required for final failure.

Internal cracking of concrete specimens before failure was first recognized by Richart, Brandtzaeg and Brown[1] in 1928. Since then, several investigators have devised methods to determine at which point in the loading history this cracking initiates. A comprehensive list of these methods can be found in a paper by Newman and Newman[2]. McCreath[3], in his thesis, discusses the sensitivity of these various methods.

To fully understand the behaviour of concrete under load, however, the basic causes of this phenomenon of internal cracking must be examined. Such an investigation can be carried out either theoretically or experimentally.

Theoretical Investigations

The basis of most of the theoretical work on this subject is related, directly or indirectly, to Griffith's[4-5] theory. At first it would seem that Griffith's postulate of the existence of small flaws in brittle materials, acting as stress-raisers and causing early cracking, would apply to concrete very well indeed. But, because of the complexity of it's nature, concrete does not resemble Griffith's ideal brittle material.

Any analysis based on Griffith's work[6-7] requires basic assumptions of the properties of the components of concrete at the micro-

scopic level. But due to the nature of concrete and to the presence of air and water filled cavities in it's structure[8], these properties, such as elastic modulus values, are extremely variable at this level and any attempt to attribute fixed values to them must be viewed with suspicion.

It must therefore be concluded that any quantitative application of Griffith's theory to concrete is not practical. It must be mentioned, however, that qualitative work on the subject might prove of great interest and importance in understanding the phenomenon of crack propagation in concrete. Work such as that carried out by Hoek[9] on the propagation of Griffith cracks in biaxial stress fields is considered for instance as highly significant.

Experimental Investigations

a) In 1963, Hsu, Slate, Sturman and Winter[10] published the results of a series of tests aimed at correlating the mechanism of fracture with the shape of the stress-strain curve for concrete. Plain concrete cylinders, loaded to predetermined axial strain values, were sliced in a direction perpendicular to that of the applied load and examined for cracks with a dyeing and stereo-microscope (40 x magnification) technique. On each slice, the total length of crack around the aggregate particles and in the mortar matrix were calculated.

The results of these tests showed that, generally, cracking occurred first around the aggregate particles and not until 70 - 90% of the uniaxial compressive strength was it evident in the mortar matrix. The point on the stress-strain curve where there was a marked deviation from approximate linearity was found to correspond to the axial strain value at which a significant increase in the measured

crack length occurred.

Unfortunately, it is difficult to evaluate the significance of these results. The observation of cracks was certainly limited by the technique used, i.e. a certain length and width of crack was needed to be detected, but no mention was made of these limitations. In addition, the investigators themselves admit that, sometimes, cracking around the aggregate particles was difficult to detect because the cracks appeared "fuzzy". Finally, it must be mentioned that the crack patterns were observed on a plane perpendicular to the direction of the applied load. As the investigators themselves qualify the mode of fracture of their specimens as "vertical instead of the usual hour-glass type" the propagation of cracks would probably have best been investigated if the cylinders had been sliced in a direction parallel to that of the applied load.

b) Dantu[11] was probably the first investigator to analyse the strain distribution in a typical slice of concrete with the use of birefringent coatings. Unfortunately, he published only a small amount of data. This consisted of the shear-strain value at various points along a line parallel to the direction of applied load which indicated that, generally, the shear strain in the aggregate particles was much lower than in the surrounding mortar matrix.

c) Swamy[12] also reports a study of the internal strain distribution in concrete with the use of birefringent coatings.

At various points on a typical slice of concrete he measured the shear strain value at different load levels. He also showed stress-intensification to occur at the aggregate-mortar interface using the above shear strain values and the values of the elastic modulus for mortar and aggregate.

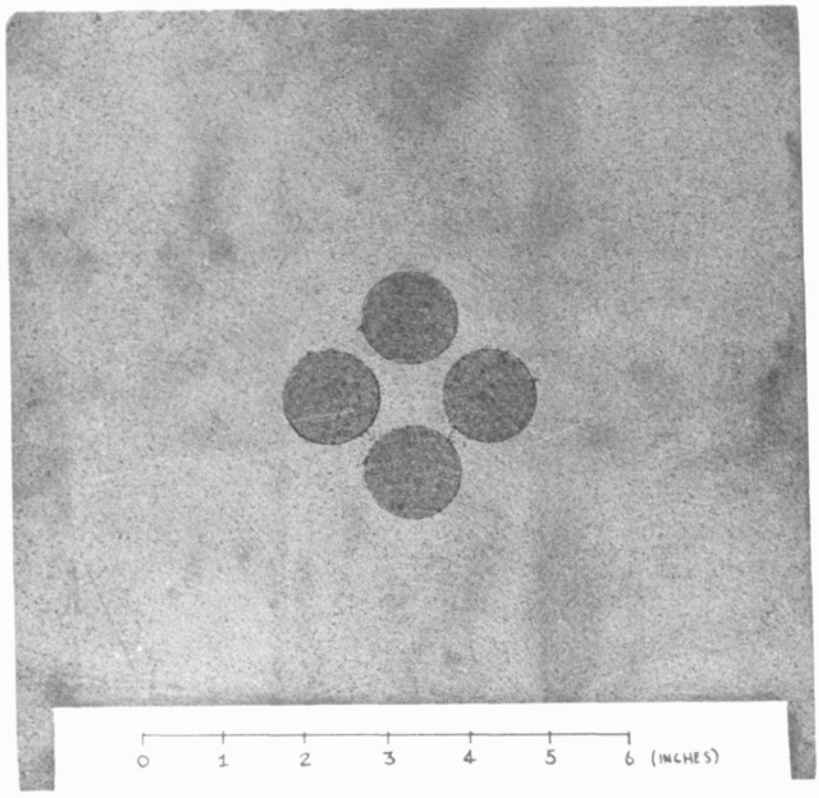
It is unfortunate that Swamy, like Dantu, did not publish any data regarding the distribution of the major and minor principal strains but gave only shear strain values. Therefore, the local mechanisms of fracture, governed certainly to a large part by the distribution of tensile strains[3], were not completely determined by his method.

d) A method allowing the major and minor principal strain distribution to be determined and the crack patterns to be observed on a "slice" of concrete was devised by McCreath[3].

He considered that, in view of the complexity of the problem, certain simplifications were required if the local mechanisms of fracture in concrete were to be investigated to any degree of precision. As a first approximation, he thus considered concrete as a two-phase material consisting of single-sized spherical aggregate particles imbedded in a fine mortar matrix. Plate models (10"x10"x $\frac{3}{4}$" thick), representing thin two dimensional slices of such a gap-graded concrete, were tested in uniaxial compression.

Figure 1-1 shows a typical plate, consisting of four cylindrical aggregate particles in a mortar matrix. Twelve of these plates were tested by McCreath. They all contained the same particle array but the spacing between the particles was varied so that each plate represented a different volume fraction of coarse aggregate.

Each plate was loaded in uniaxial compression and the major and minor principal strain distribution inside the aggregate particle array was determined using a combined photoelastic coating and strain gauge (2 mm) technique. The field strains in the mortar, at points not influenced by the presence of aggregate were also determined. By the use of an experimentally derived fracture initiation envelope



TYPICAL PLATE-MODEL (McCREATH[3])

FIGURE 1-1

for mortar, McCreath then predicted where cracking would start in the mortar matrix and at what level of composite material strain. The plates were then loaded to failure and the process of crack initiation and propagation was studied using the isochromatic patterns photographed during the failure tests. The final crack patterns were observed on the uncoated face of the plates with the use of a fluorescent dyeing technique. It was thus possible to verify the predictions that had previously been made for each model.

The main conclusions from these twelve plate-model tests representing one type of particle array were that cracking always initiated in the mortar matrix and at higher loads progressed towards and around the aggregate particles. The value of the compressive strain of the composite material at fracture initiation was found to decrease with increasing volume fraction of coarse aggregate. This was in good qualitative agreement with the results of a series of tests on cylinders containing various volume fractions of single-sized glass spheres in a mortar matrix where the point of fracture initiation had been determined by the use of the volumetric strain method[13].

McCreath's results were considered by the author as highly significant, but not conclusive since only one series of plates, representing only one type of particle array, had been tested. Especially in view of the fact that the three-dimensional tests were in agreement with the results of the plate-model tests, the mechanism of fracture observed by McCreath on his plates was certainly representative, in some way, of the internal cracking mechanism of concrete. So it was felt by the author that more plate-models tests would give additional valuable information on the initiation and propagation of cracks in concrete.

CHAPTER II

DETERMINATION OF PLATE-MODEL CHARACTERISTICS

Section 1. Introduction

Having decided to do more tests using the method described by McCreath, i.e. the testing of plate-models, the parameters to be varied in this new series of tests were examined. The type, shape, surface texture and grading of aggregate, the mortar matrix characteristics, the loading rate and type, and the geometry of the model system were the most important ones. Obviously, it was impossible to consider all these at this time. But since the aim of these new tests was to make the plate-models more representative of "real" concrete, it was felt that the particle array was the parameter to vary.

McCreath had only tested one series of plates: a single-sized four aggregate particle array (see figure 1-1) with different spacings (representing different volume fractions of coarse aggregate) in uniaxial compression. But even if varying the type of loading was considered of great importance, new models still had to be tested in uniaxial compression to make sure that the result of the first series was not an odd one which would subsequently prove to be vastly different with other aggregate configurations.

Therefore, in order to be able to compare future results with previous ones, all the other parameters mentioned were kept the same. They were all considered by McCreath to be average for a "normal concrete".

Section 2. Aggregate particle arrays

In order to find out which arrays of aggregate particles were most common to concrete, two 6" cubes, containing 50% of glass-spheres

($\frac{3}{4}$" diameter) were cast. They were subsequently sliced in two, one in the direction of the casting, the other perpendicular to it. Then, the aggregate configuration was studied by means of a successive grinding and photographing technique.

The distribution of spheres in every slice and in every direction was found to be completely random (see figure 2-4) although, possibly, certain configurations seemed more common than others.

To make sure that the typical arrays were not due to end effects, or common only to one volume fraction of coarse aggregate, a new series of glass-marble concrete specimens were cast (with $\frac{3}{4}$" diameter spheres) consisting of four 4" cubes, four 6" cubes, four 6"x12" cylinders and four 4"x10" cylinders. For each type of specimen, four different volume fractions of coarse aggregate were used: 20%, 30%, 40% and 50%. Each specimen was sliced in two and examined closely.

The conclusions drawn for this examination were:

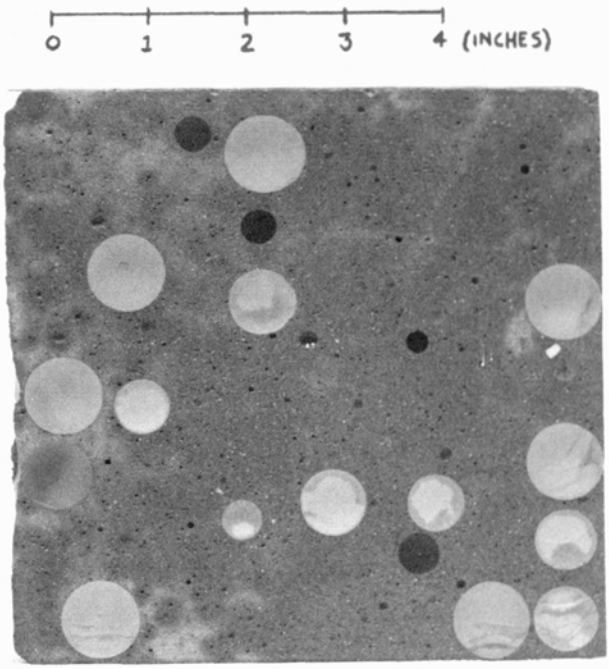
a) The center portion of all specimens seemed free from end effects.

b) The specimen shape and the volume fraction considered did not seem to affect the full randomness of the aggregate distribution. (See figures 2-1, 2-2, 2-3, 2-4).

c) The four configurations shown in figure 2-5 were common to all shapes and volume fractions.

It was therefore decided to consider these four arrays as forming a reasonable representation of concrete, but bearing in mind that to obtain a complete picture, many more models would have to be considered. But a choice had to be made and it was not possible to test a large number of models.

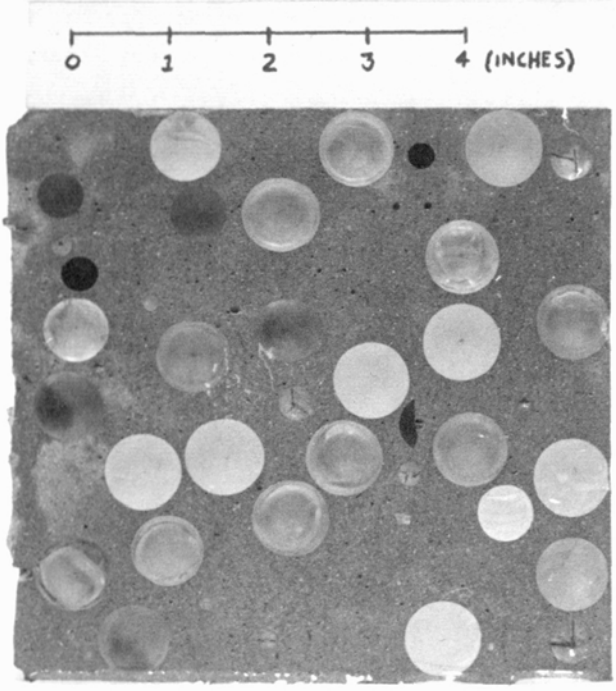
McCreath had already tested array (D) (see figure 2-5). It was felt that if the three other arrays yielded approximately the same



GLASS-MARBLE CONCRETE CUBE

VOLUME FRACTION OF COARSE AGGREGATE = 20%

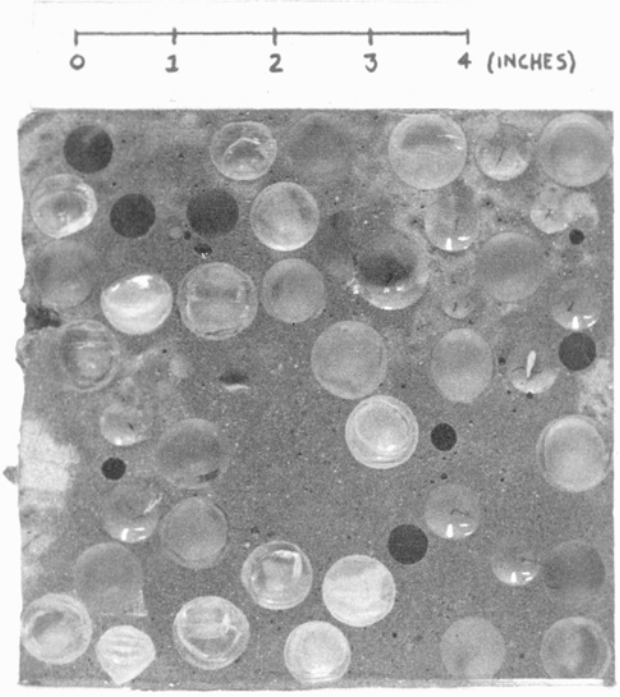
FIGURE 2-1



GLASS-MARBLE CONCRETE CUBE

VOLUME FRACTION OF COARSE AGGREGATE = 30%

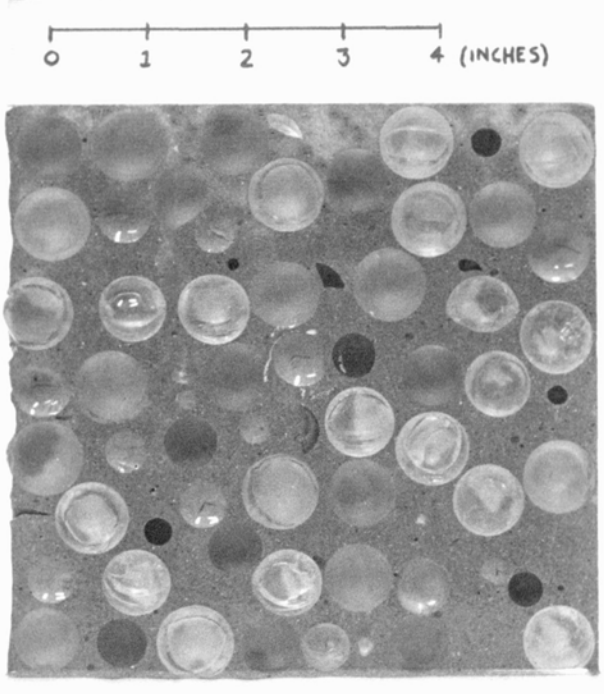
FIGURE 2-2



GLASS-MARBLE CONCRETE CUBE

VOLUME FRACTION OF COARSE AGGREGATE = 40%

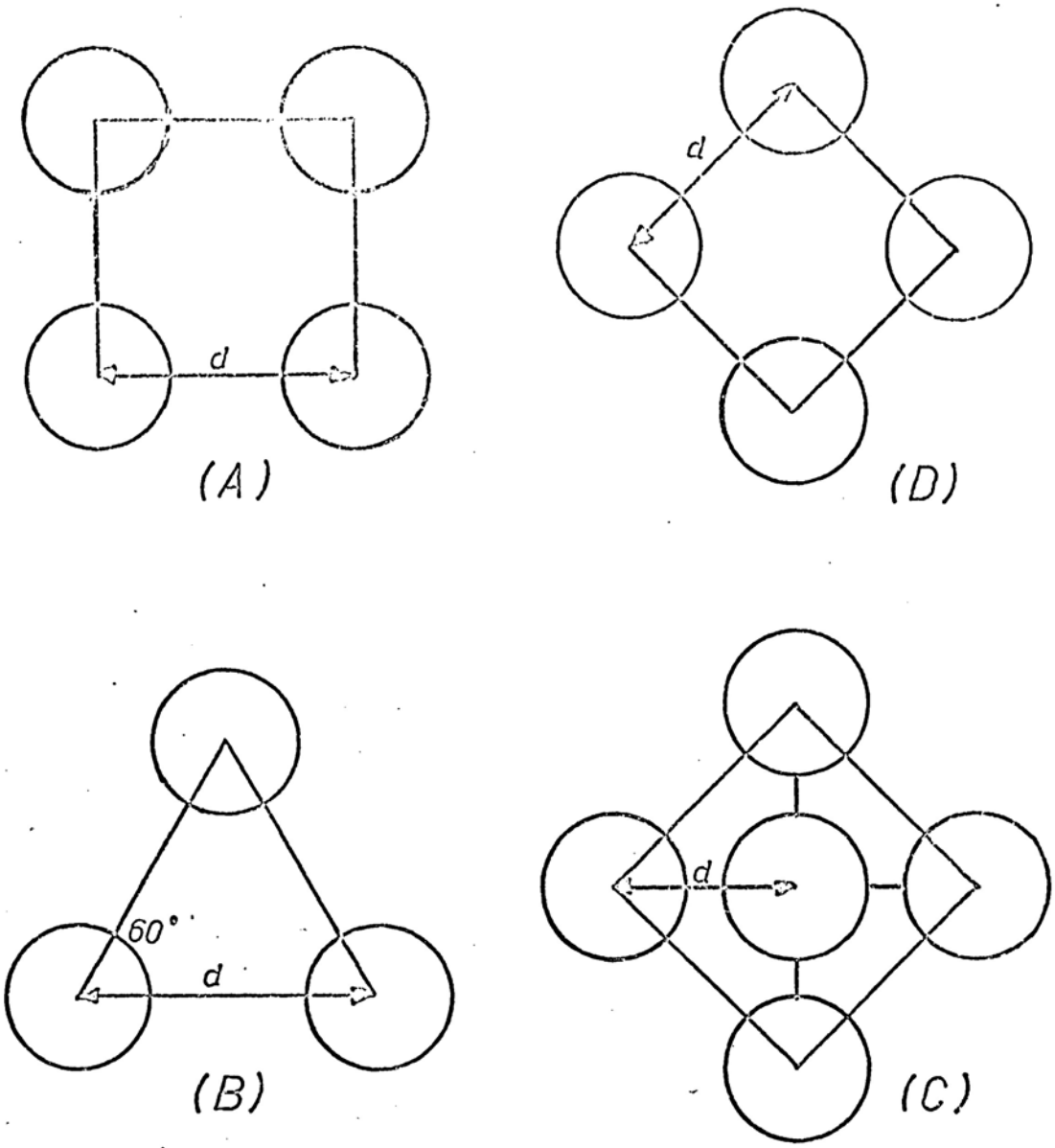
FIGURE 2-3



GLASS-MARBLE CONCRETE CUBE

VOLUME FRACTION OF COARSE AGGREGATE = 50%

FIGURE 2-4



TYPICAL PARTICLE ARRAYS IN GLASS-MARBLE CONCRETE SPECIMENS

fig. 2-5

results possibly no more would have to be considered.

Section 3. Spacing of particles

The aim of the tests being to relate the cracking initiation level to the percentage of aggregate in the concrete, it was decided to cast four plates of each model using different spacings. The ratios of the distance between aggregate (d) (see figure 2-5) to the diameter of the particle (D) used were 1.54, 1.35, 1.23, and 1.14 for each model. Ratios larger than 1.6 were thought of no great importance since they meant a very low percentage of aggregate, and ratios lower than 1.14 meant considerable difficulties in testing because of the length of the strain gauges required.

It is, to say the least, difficult to know exactly what volume fraction of coarse aggregate is represented by a certain d/D ratio. But, according to a theoretical formula derived by McCreath, the ratios chosen represented respectively 20, 30, 40, and 50% volume fraction of coarse aggregate. This range of volume fractions was the one considered to be of importance.

Unfortunately, further consideration of this formula showed that it could lead to errors, because the spacing to volume fraction ratios were measured on only one particular cut of the piece of concrete containing the regular array of spheres, i.e. where the spheres were at full diameter. For the same volume fraction, another cut could be made, not at the full diameter, and another d/D ratio derived. At large spacings, a slice could be taken where there would be no spheres at all.

For these reasons it was felt that another way of correlating the spacings in the plate-models to the volume fraction represented in three-dimensions was needed.

Section 4. Determination of the coarse aggregate content represented by each model

Firstly, on each of the 6" cubes previously cast to study the particle array, the percentage of the total area covered by the coarse aggregate was measured on each face of the cut (each cube had been sliced in two). Since volume fractions of 20-50% had been cast, this allowed the plotting of figure 2-6 which shows the relation between these two parameters.

The measurements, taken on 72 square inches for each volume fraction, were considered to give a good approximation since the diameter of the glass spheres was $\frac{3}{4}$ inch.

Secondly, on each of the four inch cubes, the average spacing (S) divided by the average diameter of the aggregate particles (D) was measured on each face of the cut.

The average spacing was defined as the arithmetical mean of the length of all the possible paths from one particle to another. A path was considered possible if there were no other in the way of the center to center line. These results were also plotted against volume fraction and are shown on figure 2-7.

For the lowest volume fraction, S represented the average of at least 40 distances which was considered sufficient for these purposes.

Then, on each of the twelve plates, the same measurements were taken.

The percentage of the total surface occupied by the aggregate particles was calculated for each plate within the boundaries shown on figure 5-9, which are the ones used later on for composite strain measurements. These simply assume a plate full of aggregate particles

RELATION BETWEEN V_f of C.A. AND PART OF TOTAL SURFACE COVERED BY AGGREGATE

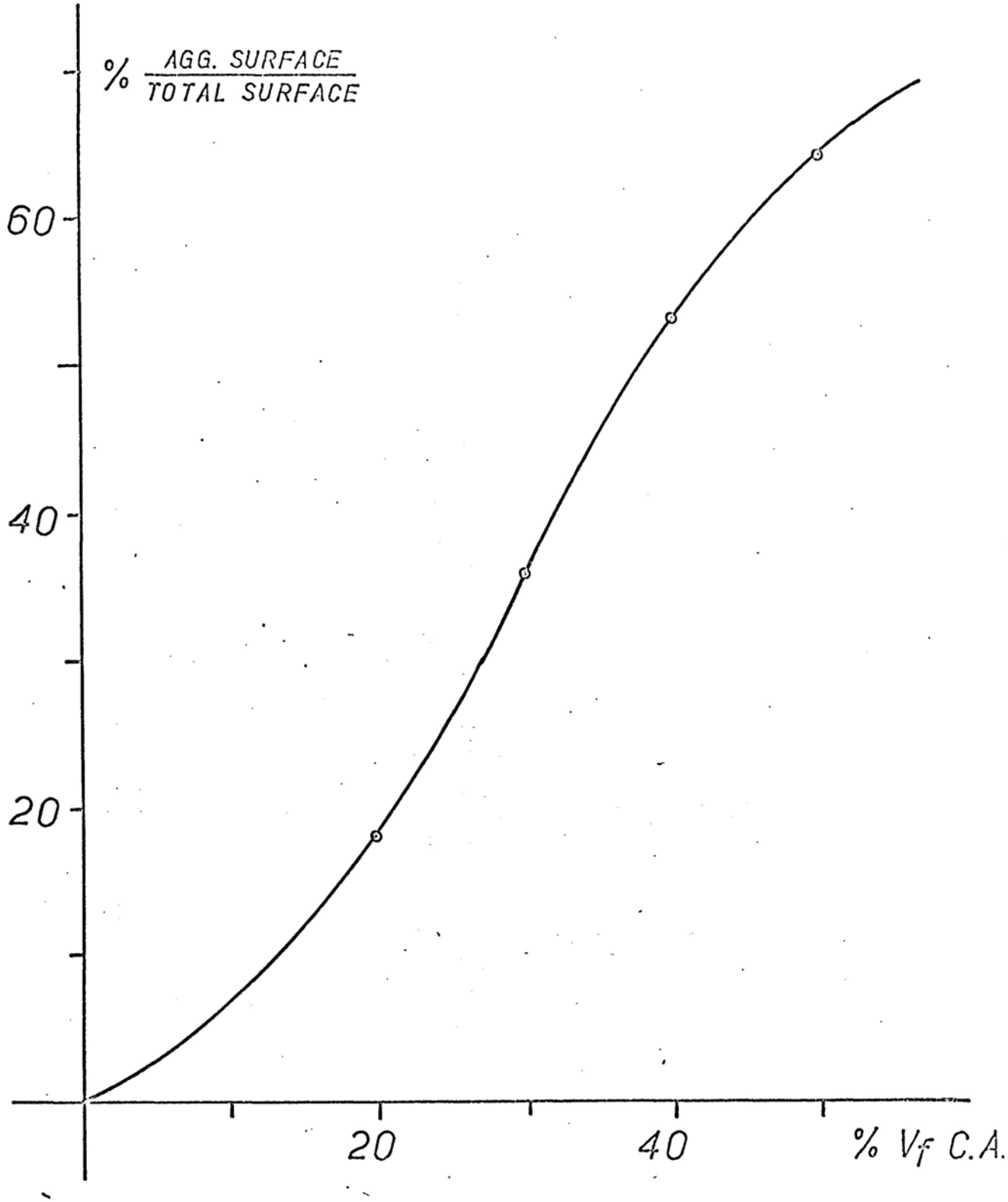


fig. 2-6

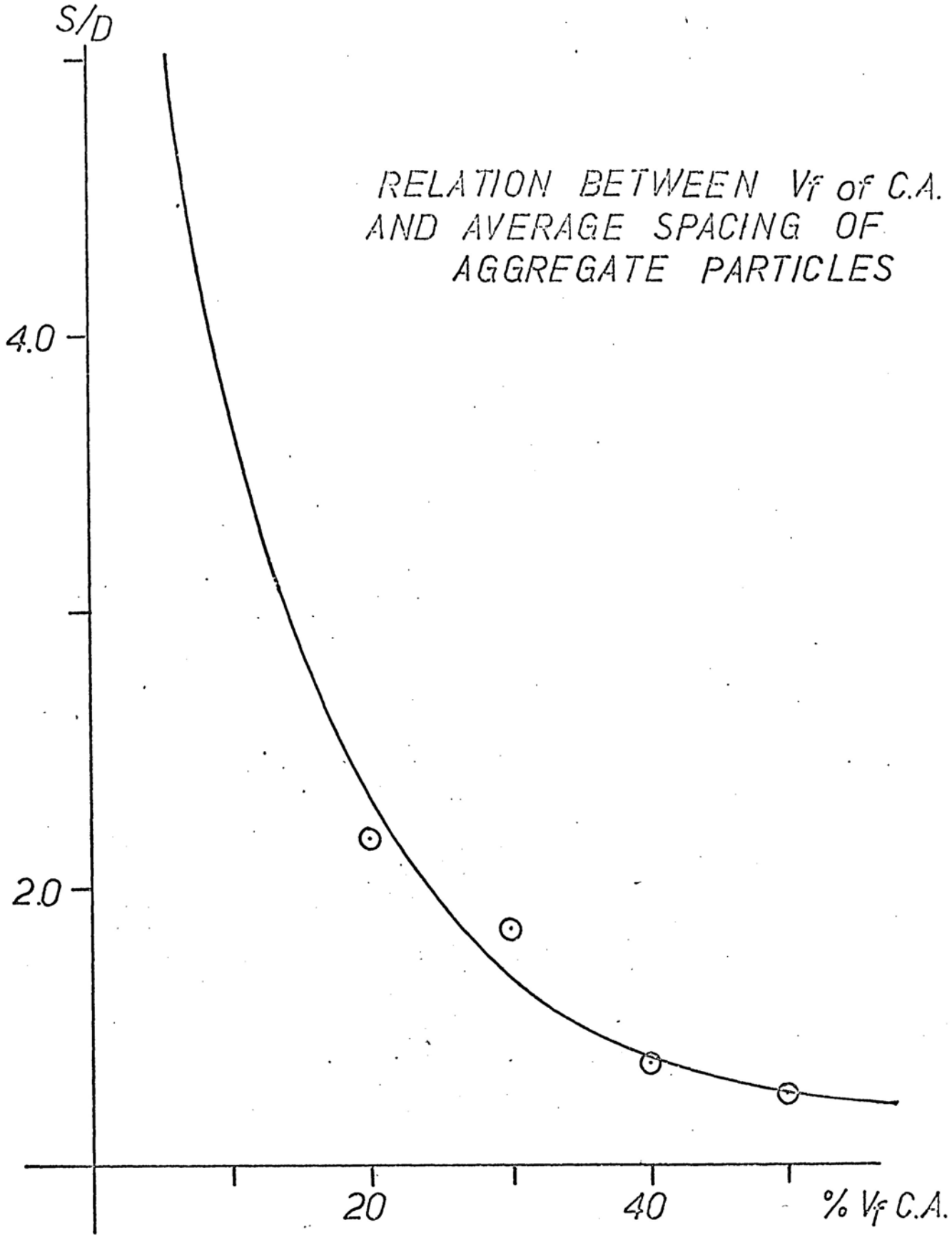

S/D
RELATION BETWEEN Vf of C.A.
AND AVERAGE SPACING OF
AGGREGATE PARTICLES
4.0
2.0
20
40
% Vf C.A.

fig. 2-7

divided into equal elements. Then, from the graph in figure 2-6 the volume fraction represented was determined.

The average spacing divided by the diameter was also computed for each plate, using the definition of possible path cited previously. From figure 2-7 it was possible to determine in that way the volume fraction represented by the different spacings on the plates.

Table 2-A shows the results obtained from the two graphs and their average for each plate. It was found that these two methods of determining the volume fraction represented by each spacing on each plate gave approximately the same results, even though the measurements were made on cuts in the cubes containing more than one apparent diameter size, and the aggregate particles in the plates were all of the same diameter. For the four-particle array and the five-particle array a closer agreement was found than with the 3-particle array. This was to be expected because the average distance is more meaningful as the number of distances used for the average increases.

So it was decided to use the average of the two results to finalize the volume fraction represented by each spacing on each plate. The close agreement of these two very different methods on two sizes of cubes, was considered to be proof of the validity of this method.

TABLE 2-A

CHARACTERISTICS OF PLATE-MODELS

PLATE	d/D	% V_fC.A. (from fig. 2-6)	% V_fC.A. (from fig. 2-7)	% V_fC.A. average
MPA-1	1.54	28.00	28.00	28.00
MPA-2	1.35	33.50	33.50	33.50
MPA-3	1.23	39.50	39.00	39.25
MPA-4	1.14	46.00	47.00	46.50
MPB-1	1.54	31.00	33.50	32.25
MPB-2	1.35	38.00	42.50	40.25
MPB-3	1.23	46.00	52.50	49.25
MPB-4	1.14	55.00	64.00	59.50
MPC-1	1.54	28.00	26.00	27.00
MPC-2	1.35	33.50	30.50	32.00
MPC-3	1.23	39.50	36.00	37.75
MPC-4	1.14	46.00	41.00	43.50

Note: MPA refers to array (A)

MPB refers to array (B)

MPC refers to array (C)

CHAPTER III

EXPERIMENTAL TECHNIQUE

Section 1. Materials

Details of the mortar components of the plate-models were as follows:

Water-Cement ratio, 0.39

Sand-Cement ratio, 1.40

Ordinary Portland Cement,

Sand grading within B.S.S. sieve size range No. 25 - No. 100.

The cylindrical coarse aggregate particles, cored out of a sheet of "Ebony Granite" rock were 30 millimeters in diameter and 25 millimeters thick. This granite was found to have an "elastic" modulus (E) approximately 3.75 times higher than the modulus of the mortar matrix. The smooth surface of the rock cylinders as cores was roughened to the required average surface texture by soaking in a 10% solution of hydrofluoric acid for 20 minutes. The surfaces were then dried and wire brushed carefully to remove all deposits.

Additional information on the properties of these materials can be obtained from McCreath's thesis[3].

Section 2. Casting and Curing

The plates were cast in 10" x 10" x 1.5" steel moulds to the bottom of which the cylindrical coarse aggregate particles had been previously fixed at the position required. To ensure accurate placing of these particles, a grid had been scribed on the base plate of the moulds. Double-sided tape, manufactured by the 3M company, was used to fix the particles to the base plate and it was found that this tape successfully ensured their stability throughout the compaction process.

Casting was carried out in three equal layers. Each layer was compacted separately on a vibrating table until an insignificant number of air bubbles were left on the surface of the mix.

A standard method of curing (described by McCreath) was used as follows: after casting, the specimens were stored under damp sacking for one day, then demoulded and cured in water at 68°F for 27 days. After being removed from the water, they were cured in air under laboratory ambient temperature conditions (68°F., 60% humidity) until the testing date which was approximately four months later.

The plates were ground to the required size (10" x 10" x $\frac{3}{4}$") using an Abwood grinding machine with a diamond impregnated polishing wheel. Opposite sides were made parallel, adjacent sides perpendicular, and all sides perpendicular to the face of the plate. A precision of $^1/_{1000}{}^{th}$ of an inch was obtained during these operations. Grinding was carried out immediately after the plates were removed from the water because the use of the diamond wheel requires water as a coolant.

Section 3. Photoelastic Technique

a) Birefringent Coatings

The birefringent photoelastic coatings used (manufactured by Photoelastic Inc.) were 10" x 10" and $\frac{1}{8}{}^{th}$ of an inch thick. Their fringe sensitivity was approximately 600 micro-strains (600/1,000,000^{ths} of inch per inch) per fringe. They were cut to the required size and shape (9" x 9", 45 degree edges), in the manner described by McCreath, and attached to the face of the plates at fourteen days after the plates had been ground. To allow moisture-equilibrium to be reached throughout the thickness of the coating, testing was not commenced until at least six weeks after attaching the coatings.

b) Optical Instruments

Only normal incidence photoelastic measurements were made during the tests. A reflection type polariscope, model 030, manufactured by Photoelastic Inc., was used together with a telemicroscope attachment (model 037) allowing readings to be taken at precise points on the coatings.

c) Use of Coatings

Under normal incidence, the value of the shear-strain and the direction of the principal strains at each point can be determined. The lines joining the points of equal shear strain (isochromatics) are each represented by a different colour. The colour indicates which fringe (or part thereof) has been reached and therefore the value of the shear strain can be determined since a fringe represents a known value of shear-strain. Lines joining points of equal direction of principal strains are termed isoclinics. They appear as black zones on the coating and the angle to which the analyser has to be rotated to bring a black zone to the point under consideration indicates the direction of the principal strains with respect to the axis of reference.

The isoclinics are superimposed on the isochromatics, but quarter-wave plates are used to eliminate the isoclinic pattern when isochromatic measurements are being made.

In addition, abrupt changes in the isochromatic pattern provide qualitative information regarding the cracking processes in the model being studied. Successful application of this method has been reported by McCreath[3] and Navaratnarajah[15].

d) Validity of Measurements

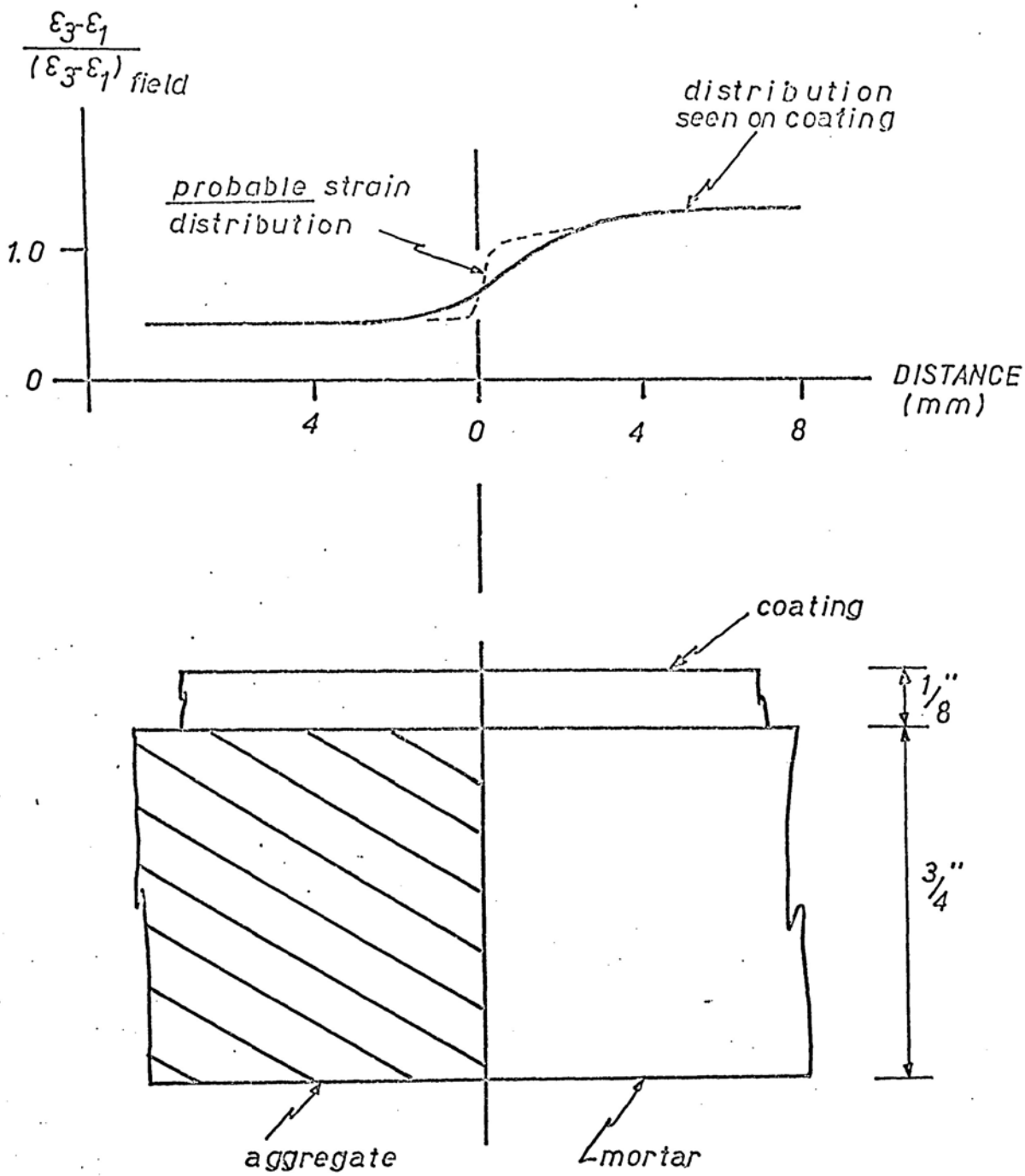
The reinforcing and thickness effects of the birefringent coatings must be considered before any valid strain information can

be obtained. Although these two effects have little or no influence on the determination of the isoclinics[16], the measurement of the shear-strain value can be affected significantly.

Considering the thickness and the elastic modulus of the plate-models and of the coatings, together with information given in "Experimental Stress Analysis"[14], it was found that a correction of less than 3% was needed to cover reinforcing effects. This correction is included for the present tests within the "face correction factor" devised by McCreath. This factor will be further discussed in chapter V.

Works by Duffy and associates[17-18] on the thickness effects of the coatings have been reported by Dally and Riley[14]. Duffy assumed a certain strain gradient at a point on the surface of a material coated with a birefringent coating. He then calculated the elastic distribution of strain across the coating from the material to the free surface of the coating and thus derived correction coefficients for the use of coatings at points of known strain gradients.

In the plate-models, high strain gradients probably exist at certain points at the aggregate-mortar interface[20] (see figure 3-1) and a correction would certainly be needed at these points[19]. But since the application of this correction requires prior knowledge of the value of the gradient which is attempted to be measured, a long process of assuming a gradient and calculating the correction factor successively many times would be required. This was not considered necessary since the present analysis was limited to the mortar matrix. It was simply decided not to consider any measurements made close to the aggregate particle surface. Comparison between theoretical solutions and experimental values obtained by McCreath for plates



STRAIN DISTRIBUTION AT AGGREGATE-MORTAR INTERFACE IN PLATE-MODELS

fig. 3-1

containing a single aggregate particle have shown that, practically, no correction factors are needed for the mortar matrix deformations.

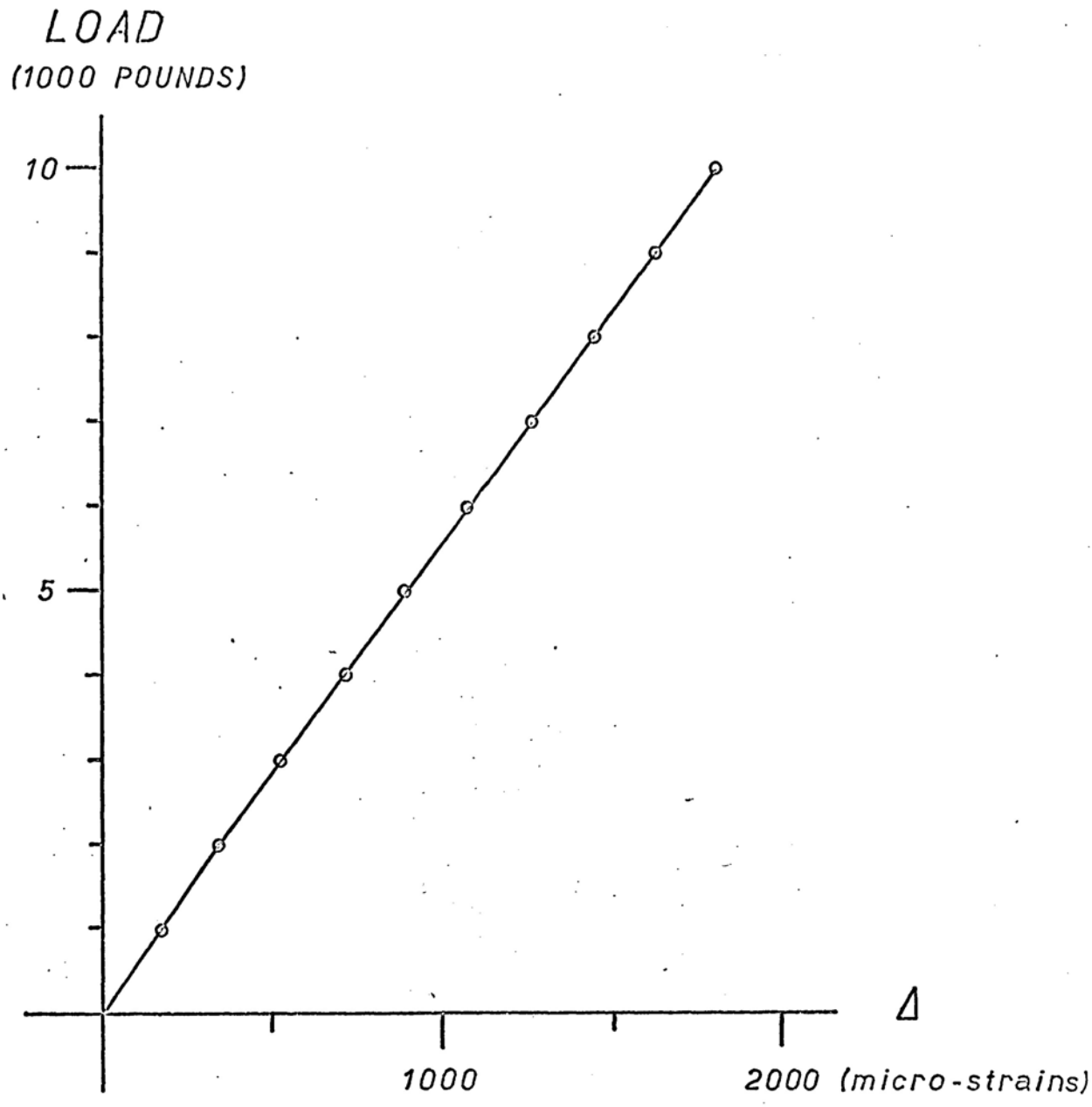
Section 4. Loading System

In the testing procedure discussed by McCreath, it was stated that loads of approximately 1000 p.s.i. were required for the strain distribution analysis in the 'elastic' range. A value of 1100 p.s.i. was adopted as safe for the present test series since it was considered that fracture initiation would probably not occur until at least 1500 p.s.i. This fact was later confirmed by the results of the investigation.

Instead of the excessively large and inconvenient 175 ton force testing frame used by McCreath, a small load frame with a five ton force capacity was adopted and used to apply the required loads to the plate-models. Precise load measurement and control was obtained with the use of a load cell placed between the moving piston and the screw-jack applying the load.

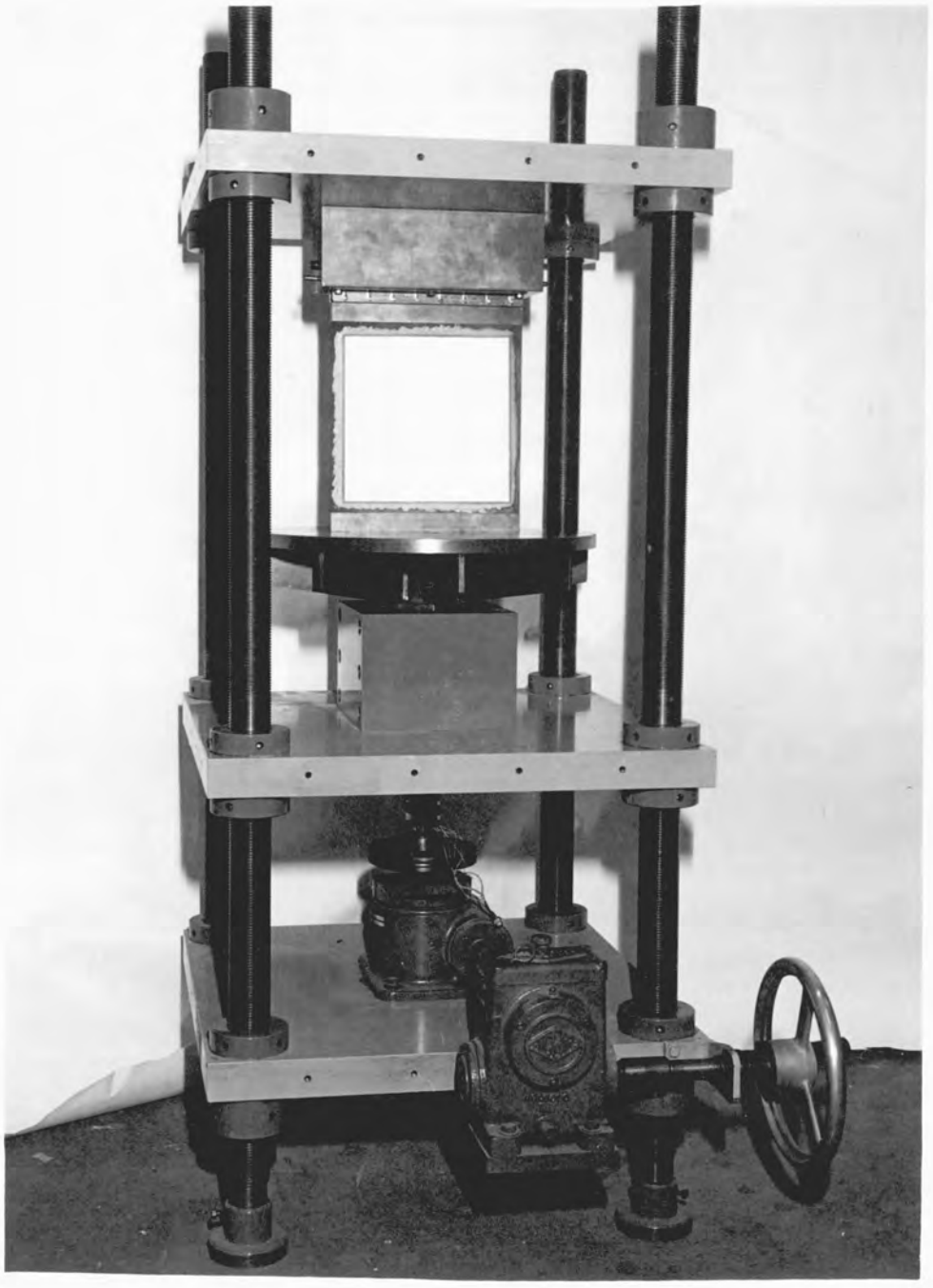
The load cell consisted of a mild steel cylinder on which two axial and two transverse electrical resistance strain gauges (PL-10) were fixed at it's mid-section at equal distances from each other. By aligning two opposite gauges axially and two others perpendicular to these, and by connecting these gauges to form a four-arm Wheatstone bridge circuit, it was possible to obtain a strain response from the cell of the order of one micro-strain per p.s.i. on a specimen. Figure 3-2 shows the calibration of the load cell which was made using a five-ton force proving ring.

Figure 3-3 shows a typical plate-model in the small load frame. It should be noted that use was made of McCreath's piston platen to ensure an even distribution of applied load on the plates.



CALIBRATION OF LOAD-CELL

fig. 3-2



TYPICAL PLATE-MODEL IN

5 TON-f LOAD FRAME

FIGURE 3-3

CHAPTER IV

THE FRACTURE INITIATION ENVELOPE FOR MORTAR

Section 1. Introduction

As the title of the present thesis states, the main purpose of this series of tests is to obtain more information on the cracking process in concrete under uniaxial load. Evidently, the most important stage is the one at which cracking initiates because it is a point of no return, when permanent changes have occurred in the structure of the material.

Many investigators have tried to find that point from measurements taken on concrete specimens under increasing load. Of all these methods, discussed in chapter III of McCreath's thesis, only one seems to give valid and consistent results. It is the one devised by Newman[13].

The term "discontinuity", first stated by Newman[21], has been further defined by Newman[13] as that point on the longitudinal strain against volumetric strain graph where there is a marked deviation from linearity. Tests done by Newman[13] have shown that this method is applicable to almost every case. On almost every sample tested, the pattern of this graph is as follows: first, there is a small non-linear portion of the curve due to "bedding down" effects, then there is a very linear portion which terminates suddenly.

As will be shown in section 2 of the present chapter, the method derived by Newman enables the investigator to pin-point very exactly this discontinuity point. Furthermore, the method shows that in most cases, the strain variation in the linear portion of the curve is contained within a band plus or minus two micro-strains wide for uniaxial tests, which is a very good degree of precision.

This evidence makes it reasonable to assume that this point really marks the start of micro-cracking in concrete, since it represents a sudden increase in volume. This increase can only be explained by the formation of cracks which allows the volumetric strain response of the material to vary.

Using this hypothesis, the fracture initiation envelope for the plate-model mortar was derived by McCreath (figure 4-1).

This envelope represents all the combinations of the major (ε_1) and minor (ε_3) principal strains required to initiate cracking in the mortar considered. Discontinuity (now termed "fracture initiation") points obtained from uniaxial tension and compression tests, and from triaxial tests at different confining pressures, are plotted in the ε_1-ε_3 plan. The resulting line is then the fracture initiation envelope. Strain combinations inside the envelope are considered safe, and those outside it, likely to initiate fracture.

The envelope is used to assess the most critical point in the mortar matrix in each plate model, and also to predict the composite strain level at which cracking will start at this point. This procedure is fully explained in the quoted reference[3], and an example of its use will be given in chapter V of the present thesis.

Section 2. Uniaxial tests on mortar

Even if the mortar used for the present series of tests (which properties are given in chapter III) was of the same composition as the one used by McCreath, it was felt that a few tests were needed to verify the discontinuity strain levels in uniaxial tension and uniaxial compression.

FRACTURE INITIATION ENVELOPE FOR PLATE-MODEL MORTAR

FROM McCREATH [3]

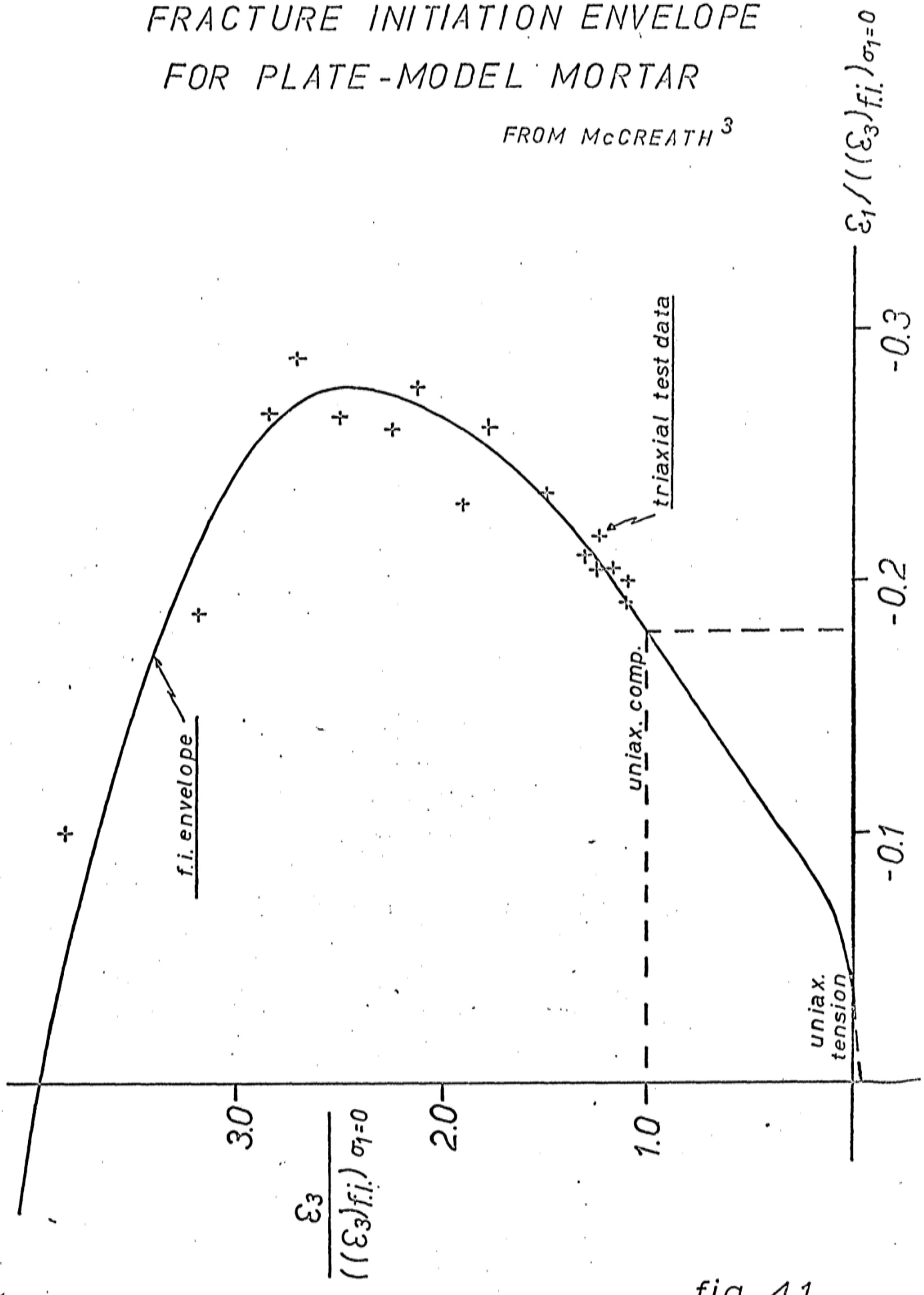


fig. 4-1

For this purpose, three uniaxial tension specimens and two 4" x 10" cylinders were cast at the same time as the two first series of plates. They were cast in three layers, compacted in the same manner as the plates, and cured in the same manner. (see chapter III).

The procedure for these tests was as follows:

Uniaxial tension tests -

These tests were carried out in a special frame designed by Ward[22], which applies a direct tension to a specimen 4"x4"x20" which middle section is reduced to 3"x4"; (see figure 4-2).

First, the surface of the specimens was carefully scraped to remove all latence and then four 60 mm electrical resistance strain gauges were attached to the surface of each specimen in its center section using P.S. adhesive. Two gauges were fixed on two opposite sides of each specimen, one in the direction of loading, the other perpendicular to it.

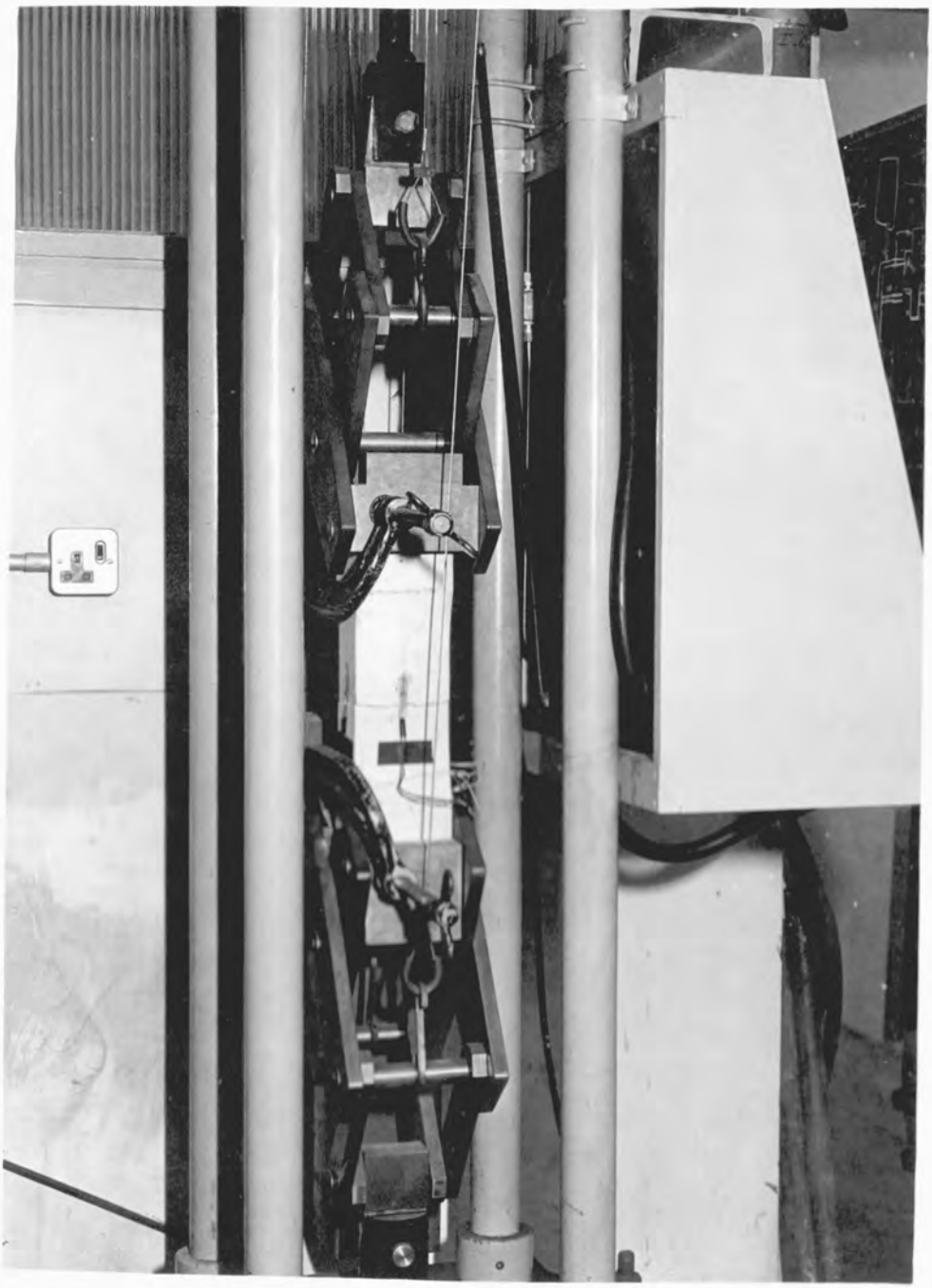
The tension force was applied through a hydraulic jack connected to an Amsler pressure control cabinet, to ensure a precise control of load.

A step by step loading procedure was used with sufficient intervals (about 10 seconds) between steps to enable the Peekel data logger to register the strains.

Uniaxial compression tests -

These were prepared and carried out following the procedure outlined in chapter VII, except that 30 mm strain gauges were used and that, as in the tension tests, a step by step loading sequence was used.

The results of all these tests for the strain combinations at discontinuity are given below:



TYPICAL SPECIMEN (FAILED) IN

TENSILE FRAME

FIGURE 4-2

Uniaxial compression

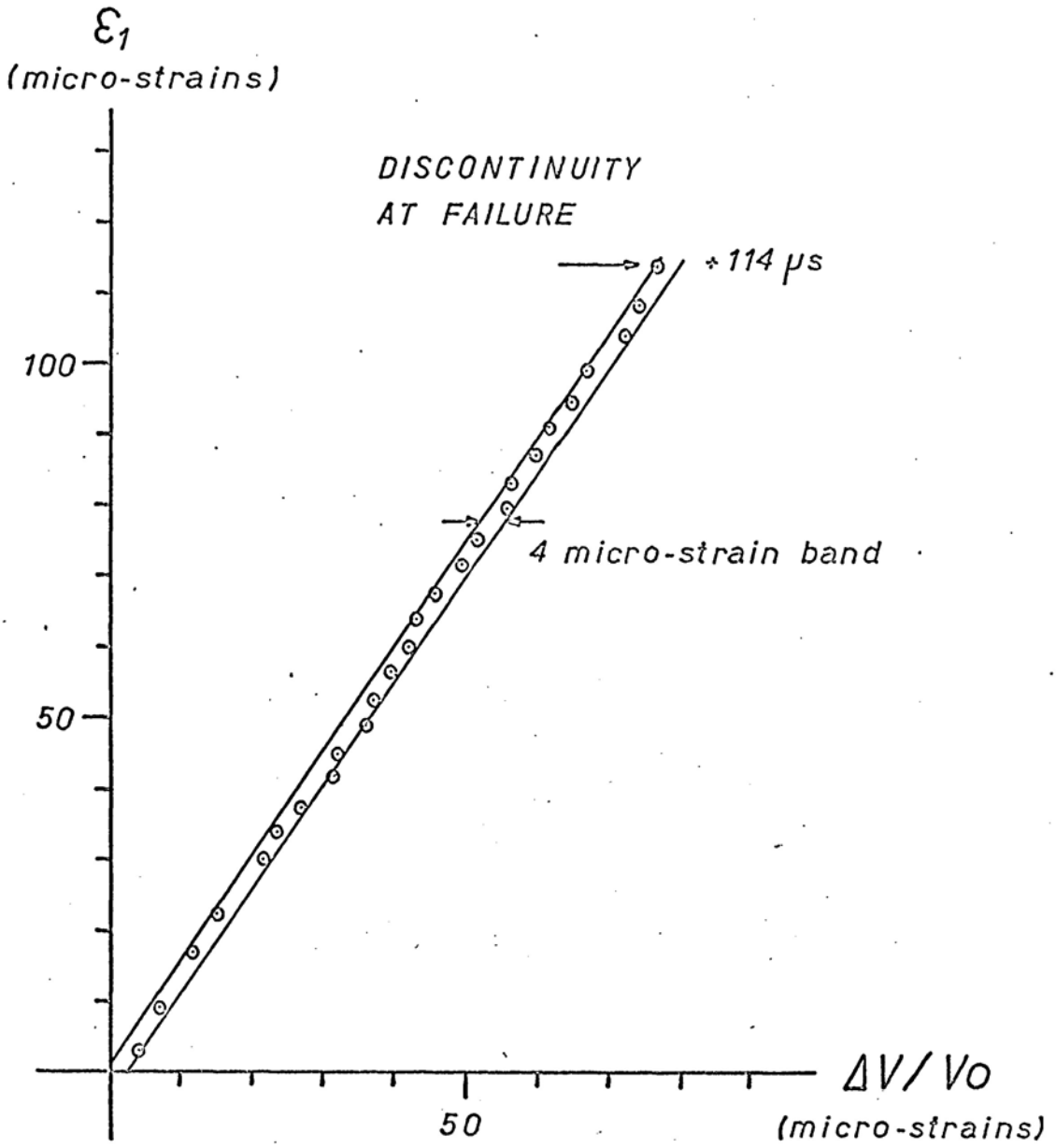
Test No.	(ε_3)f.i. (micro-strains)	(ε_1)f.i. (micro-strains)
1	-1072	+186
2	-1142	+222
AVERAGE	-1107	+204

Uniaxial tension

Test No.	(ε_3)f.i. (micro-strains)	(ε_1)f.i. (micro-strains)
1	-18	+119
2	-16	+108
3	-15	+102
AVERAGE	-14	+108

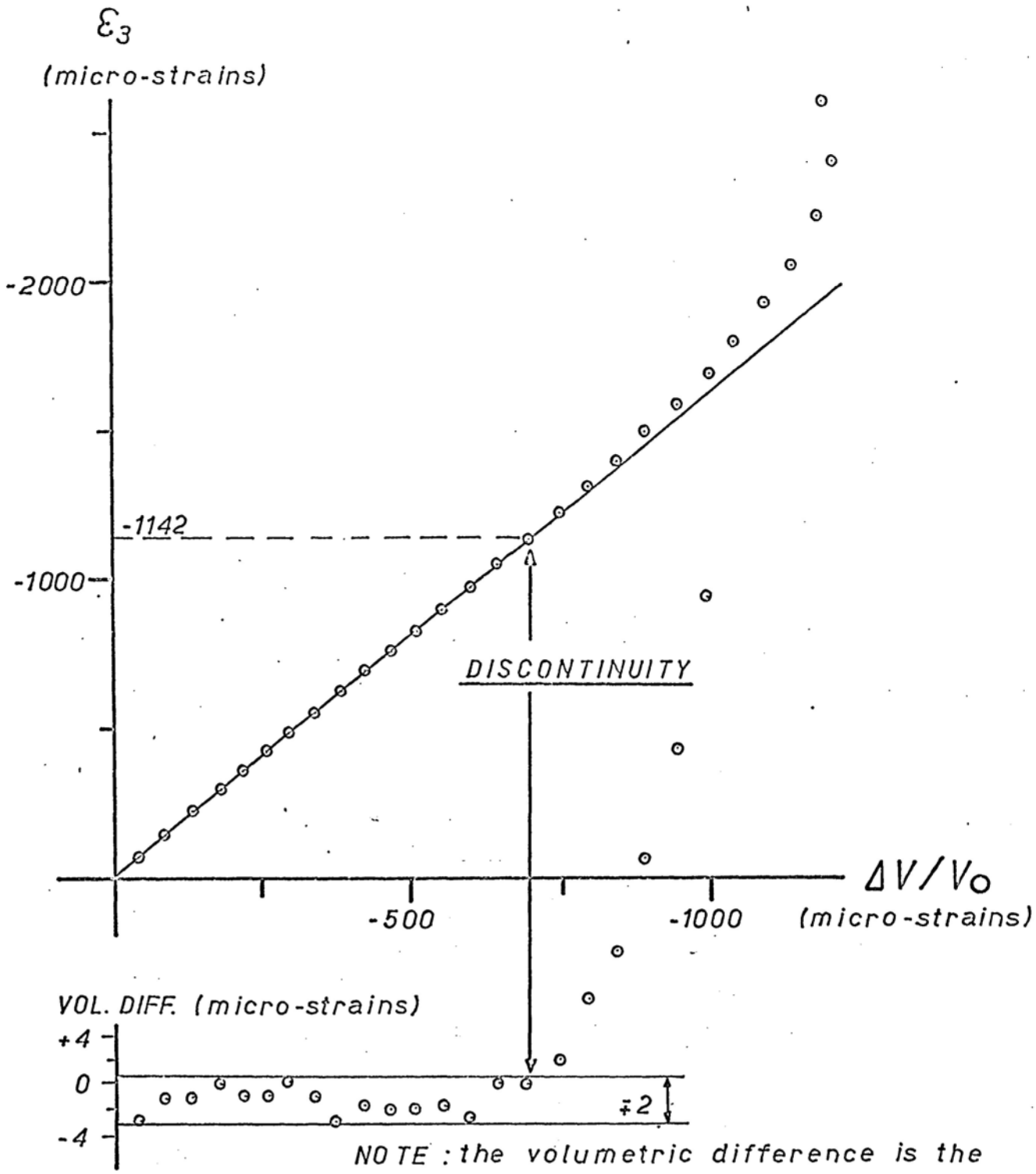
The relation between the longitudinal strain (ε_1) and the volumetric strain ($\Delta V/V_0 = \varepsilon_1 + \varepsilon_2 + \varepsilon_3$) is given in figure 4-3 for one of the tension tests. As for all the other tests, this curve stayed linear up to failure within a band 4 micro-strains wide (as shown on the graph). Therefore, in all cases, discontinuity was found to occur at failure. This was to be expected because in a fine mortar, when a crack significant enough to affect the volumetric strain response of the material is formed, there is nothing to prevent its propagation since in this type of test the load is maintained while the strain gauge readings are recorded.

Figure 4-4 shows the volumetric strain against longitudinal strain plot for one of the compression tests, as well as the volumetric difference between the points on the graph and the chosen



UNIAXIAL TENSION TEST ON
PLATE-MODEL MORTAR

fig. 4-3



NOTE : the volumetric difference is the difference between the chosen straight line and the points on the graph.

UNIAXIAL COMPRESSION TEST ON PLATE-MODEL MORTAR

fig. 4-4

straight line. This difference is calculated using a computer programme derived by Newman[13]. The plot shows that until discontinuity the strains remain linear within the plus or minus 2 micro-strain band mentioned previously.

The use of this programme yields a very high degree of precision in pin-pointing discontinuity, much greater than when discontinuity is obtained just by examining the volumetric strain against longitudinal strain graph. Errors up to 200 micro-strains in assessing ε_3 at fracture initiation could be made without the use of this programme.

Section 3. Changes in the fracture initiation envelope

As will be seen in chapter V, the portion of the fracture initiation envelope that was of practical use for the plate model tests was the part lying between the uniaxial tension point and the uniaxial compression point. Unfortunately, no data was available for this part of the curve (see figure 4-1). Therefore the uniaxial points became of great importance.

So the discontinuity points obtained from the tests were compared to the ones obtained by McCreath.

Taking into account the fact that the loading system used for this new series of uniaxial tension tests was much less liable to fluctuation and much more stable than previously (pressure control came from the Amsler cabinet instead of the system previously used[22]), it was considered that a tension strain at discontinuity of +108 micro-strains was a much more realistic figure than the +62 micro-strains obtained by McCreath. It should be noted as well that all the three new test results agreed very closely.

The uniaxial compression discontinuity value at -1107 micro-

strains was low compared with -1653 (McCreath's value). It was felt it was better to use -1107 micro-strains because the cylinders used to determine this value were cast at the same time as one of the new series of plates and out of the same batch.

The fracture initiation envelope was therefore replotted with these new figures and using McCreath's triaxial test results (non-dimensionalized with respect to the value for discontinuity under uniaxial compression, -1653 micro-strains). A straight line was drawn between the uniaxial tension point and the uniaxial compression point. This was considered valid since there were no data available between these two points which bound a zone of compression-tension, and because the prolongation of this straight line lay within the scatter of McCreath's triaxial test points. The bend in the curve, required for it to pass through the uniaxial tension point on the ε_3 axis on the minus side, was considered likely to happen under the ε_1 axis in the zone of tension-tension. As can be seen in figure 4-5 these changes did not alter significantly the overall pattern of the fracture initiation envelope as given by McCreath.

FRACTURE INITIATION ENVELOPE FOR PLATE-MODEL MORTAR

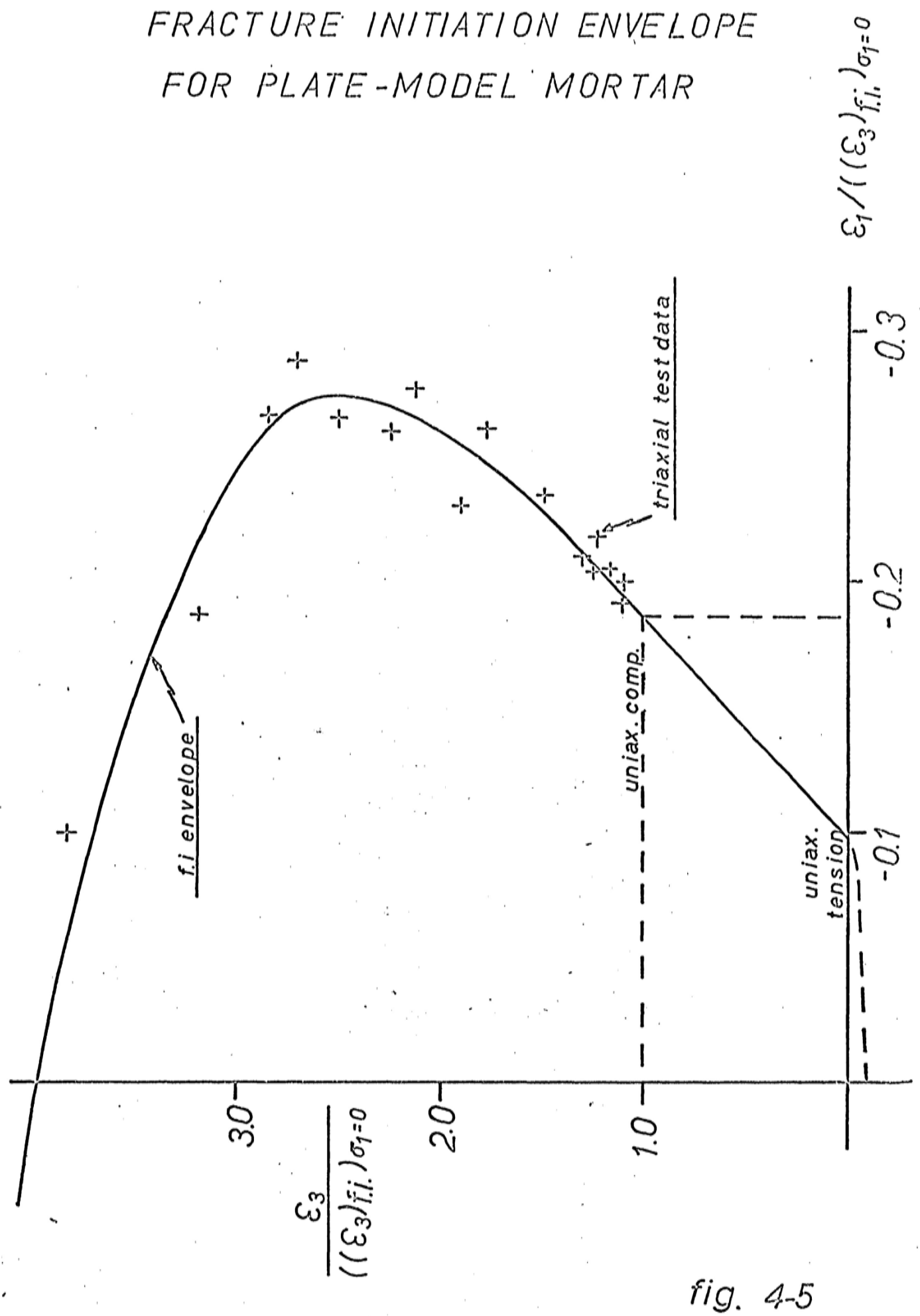


fig. 4-5

CHAPTER V

STRAIN DISTRIBUTION ANALYSIS IN PLATE-MODELS

Section 1. Introduction

The procedure followed for the strain analysis in the plate-models was that used by McCreath. An example of this method of testing will be given in this chapter. Plate MPB-1 is used for this purpose. Each step in the procedure followed for the analysis is described and when changes in the method given by McCreath are made they are fully explained and discussed.

The results for the eleven remaining plates are given at the end of this chapter in the form of graphs (four for each plate) and the significance of each graph is explained in the description of the step-by-step procedure. The last section of this chapter will explain the meaning of the results of the strain analysis for each series of plates. A more comprehensive discussion is given in chapter VI, following the description of the loading tests to failure of the plates.

It must be mentioned again that the testing of the plates in the elastic range is used to study the strain distribution prior to microcracking in the plate-models and also, and most important, to predict the onset of cracking in the mortar matrix. The basic assumption that cracking will in fact initiate in the matrix and not at the aggregate-mortar interface will also be discussed in the next chapter. This assumption is of course of great importance because, as mentioned previously, the analysis of strain is limited to the mortar matrix for the purposes of this investigation.

Section 2. Testing Procedure

a) Grid Scribed.

When a plate was ready for testing, a grid was scribed on the coated face using a sharp needle. Figure 5-1 shows that grid for the plate under consideration. This particular grid consists of a set of polar coordinates (necessary to enable the operator to take readings at precise points) and outlines the cylindrical aggregate particles. Marks were also made on each plate in each corner, at two inches away from the sides, where field strains were to be read.

b) Load Cycling

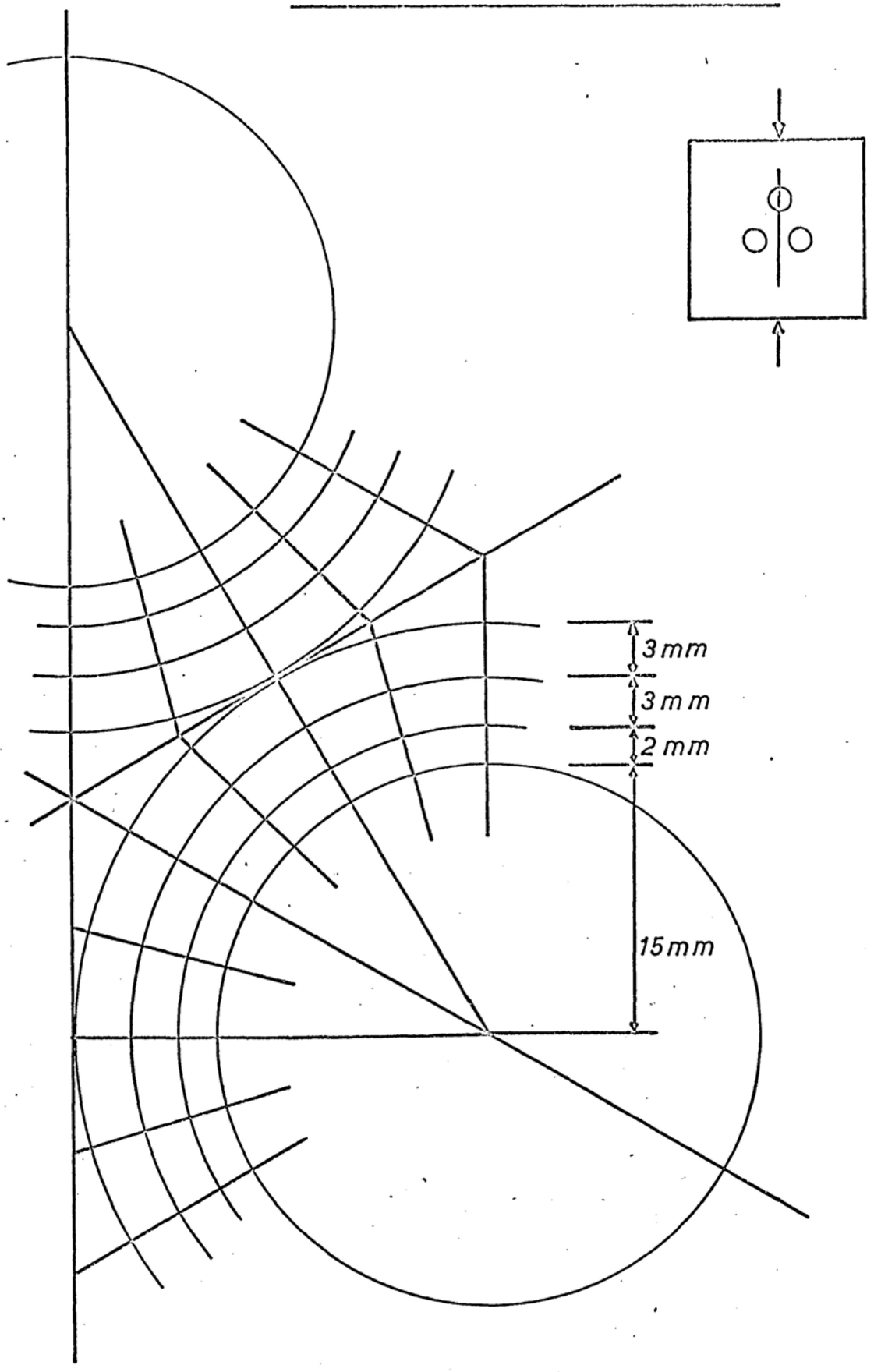
Before any measurements were taken under load, each specimen was cycled six times to a level of 1100 p.s.i. in the small load-frame. This level was that at which the isochromatic readings were to be made. The load cycling was done to ensure the stability of these readings. It was considered that any loading and unloading of the plate would not cause significant variations in the isochromatic and strain gauge readings after such a number of load cycles.

c) Determination of Isoclinic Values

Each plate was then loaded to approximately 1000 p.s.i. and the value of the isoclinic (direction of principal strains) at each point on the grid was determined. A slightly lower level of load than for the isochromatic readings was used because at the higher level the first fringe was generally reached at some points and therefore the isoclinics (black zones) became hard to differentiate from the isochromatics (dark colour at the first fringe) on which they were superimposed.

At each point the isoclinic value was read three times and a variation of three degrees at the most was usually found. It

PLATE MPB - 1 -



SCRIBED REFERENCE GRID

fig. 5-1

was considered that the use of the average of these three readings enabled the determination of the isoclinics to be made within one degree.

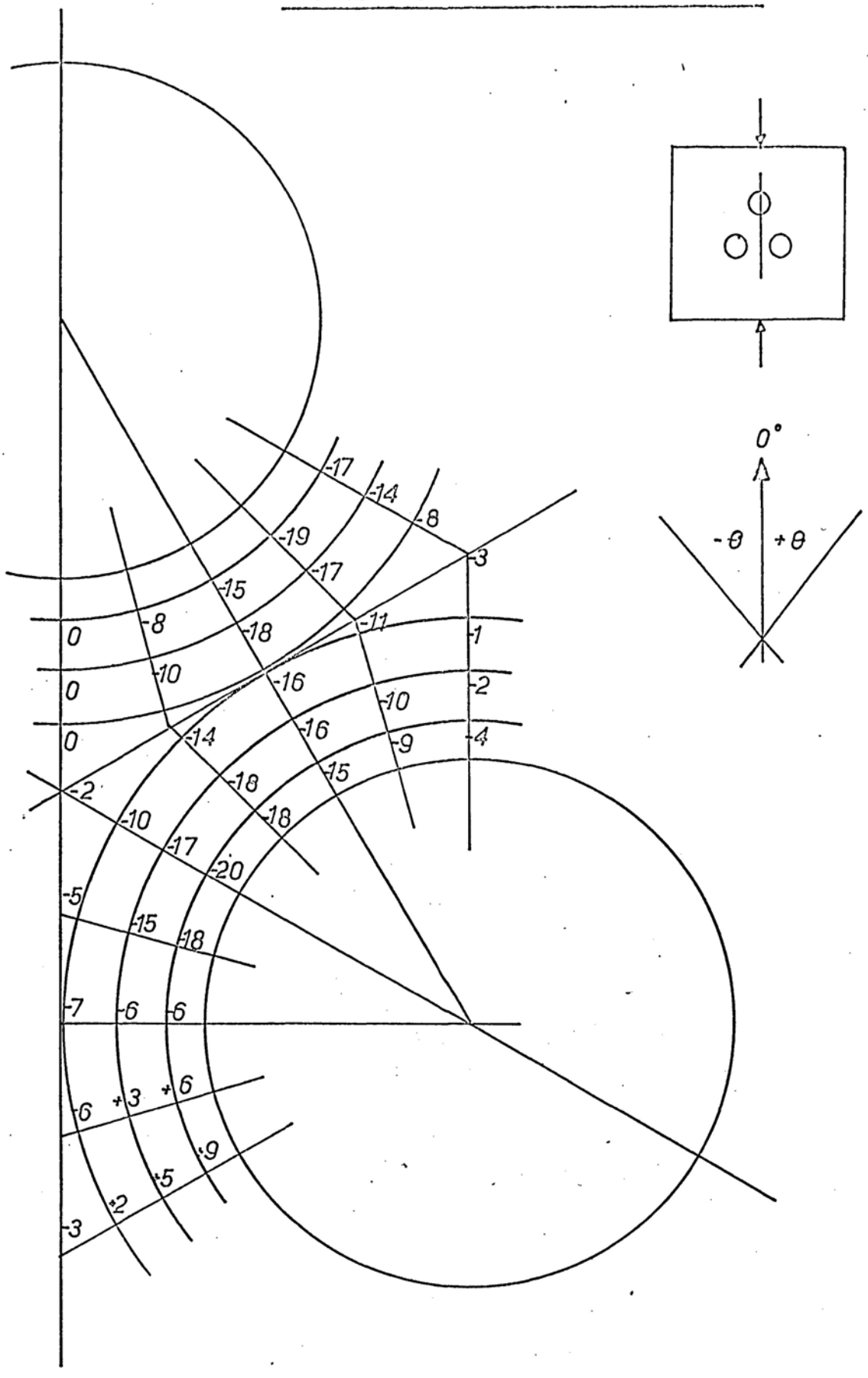
It should be mentioned that on some plates, at a few points where the isochromatic pattern due to shrinkage (which will be fully discussed in sub-section "h") interfered with the load pattern in such a way as to cause zones of low shear strain on the coating, the isoclinics were not as sharp. Therefore, in some cases a variation of 6 or 7 degrees was found between the three readings. It was considered that using the average in such cases gave isoclinic readings to within ± 2 degrees approximately.

The average isoclinic value at each point for plate MPB-1 is given in figure 5-2. For this particular case, the variation in the reading at each point was never more than 3 degrees. Simple consideration of these values allows the plotting of the isoclinic lines (shown on figure 5-3), but this process is best performed by the person who has seen the actual pattern on the plate.

Theoretically, on a perfect plate one might expect the isoclinics along the symmetryline to be always at zero degrees, which is not the case here. But considering that the actual position of the aggregate particles was not perfect, that the mortar matrix might contain air voids at certain spots and that the actual loading system was not exactly perfect, it was felt that a small variation was normal for such a concrete plate.

Photograph B on figure 5-4 shows the zero degree isoclinic due to shrinkage only and Photograph D on the same figure, the one that appears on the plate under load. Both of them are roughly symmetrical, but detailed analysis of the plate under load showed that

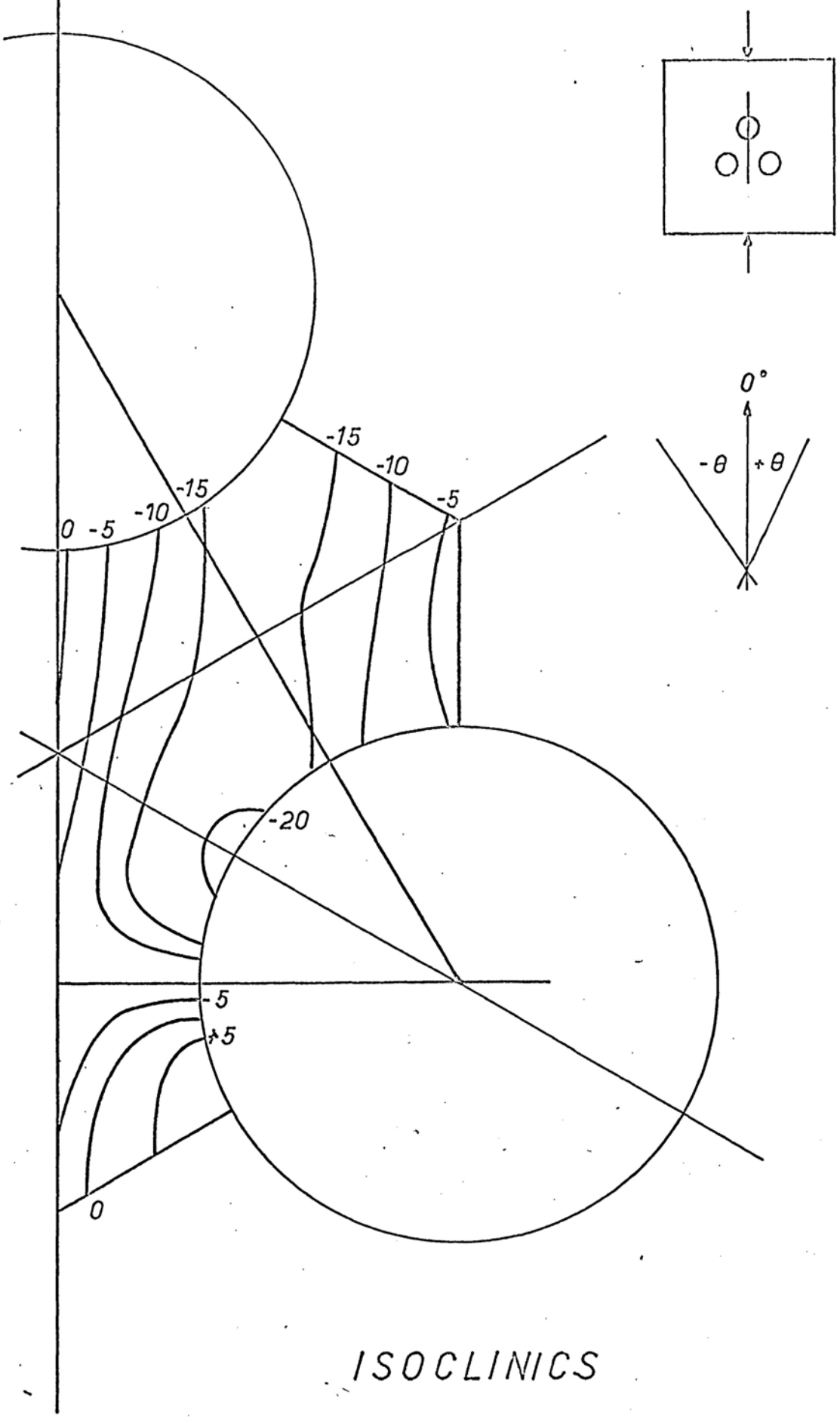
PLATE MPB -1-



ISOCLINIC VALUES
TO NEAREST DEGREE

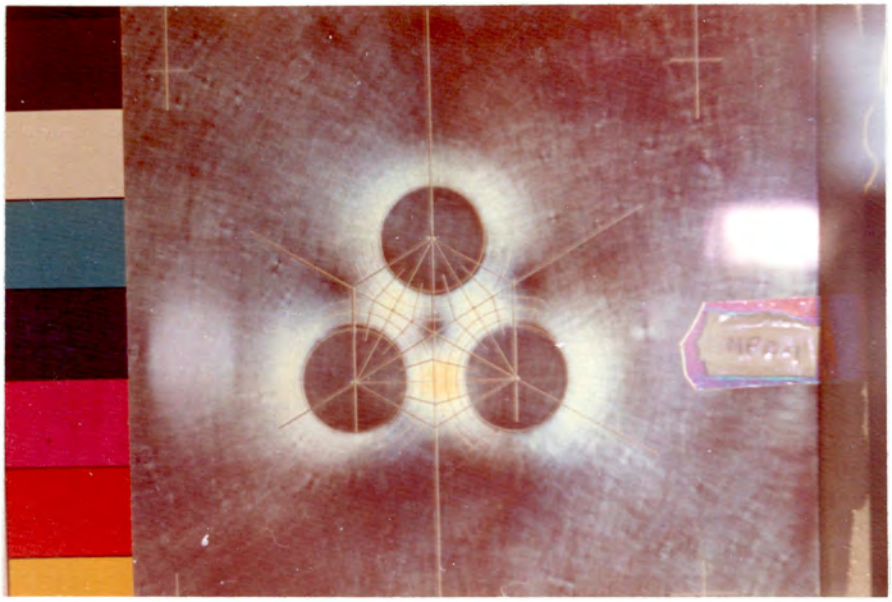
fig. 5-2

PLATE MPB - 1 -

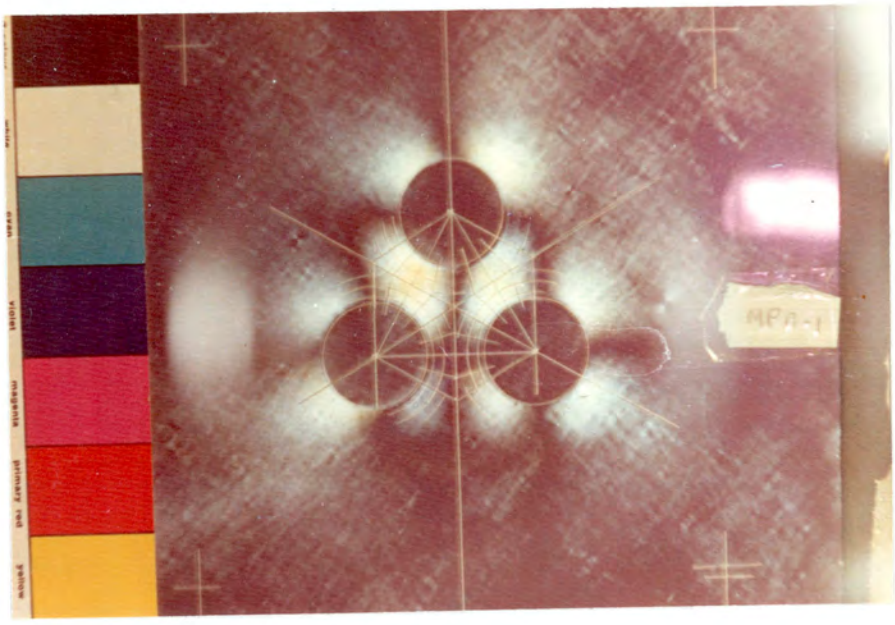


ISOCLINICS

fig. 5-3

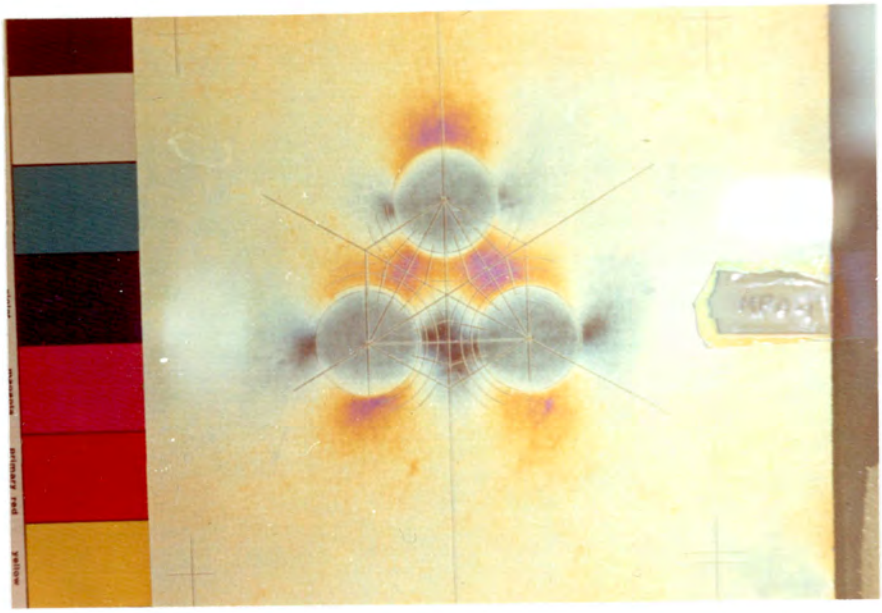


(A) Shrinkage Isochromatics (MPB-1)

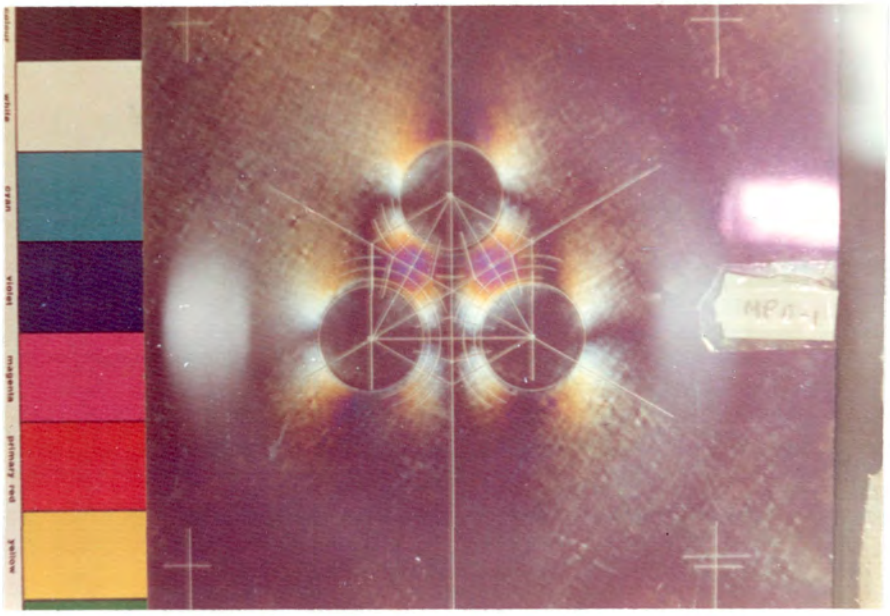


(B) Shrinkage Isoclinics (MPB-1) (0°)

Figure 5-4



(C) Isochromatics - 1100 p.s.i.-(MPB-1)



(D) Isoclinics - 1000 p.s.i.-(MPB-1) (0°)

Figure 5-4 (Cont'd)

this isoclinic was slightly bent towards the left side.

d) Placing of Strain Gauges

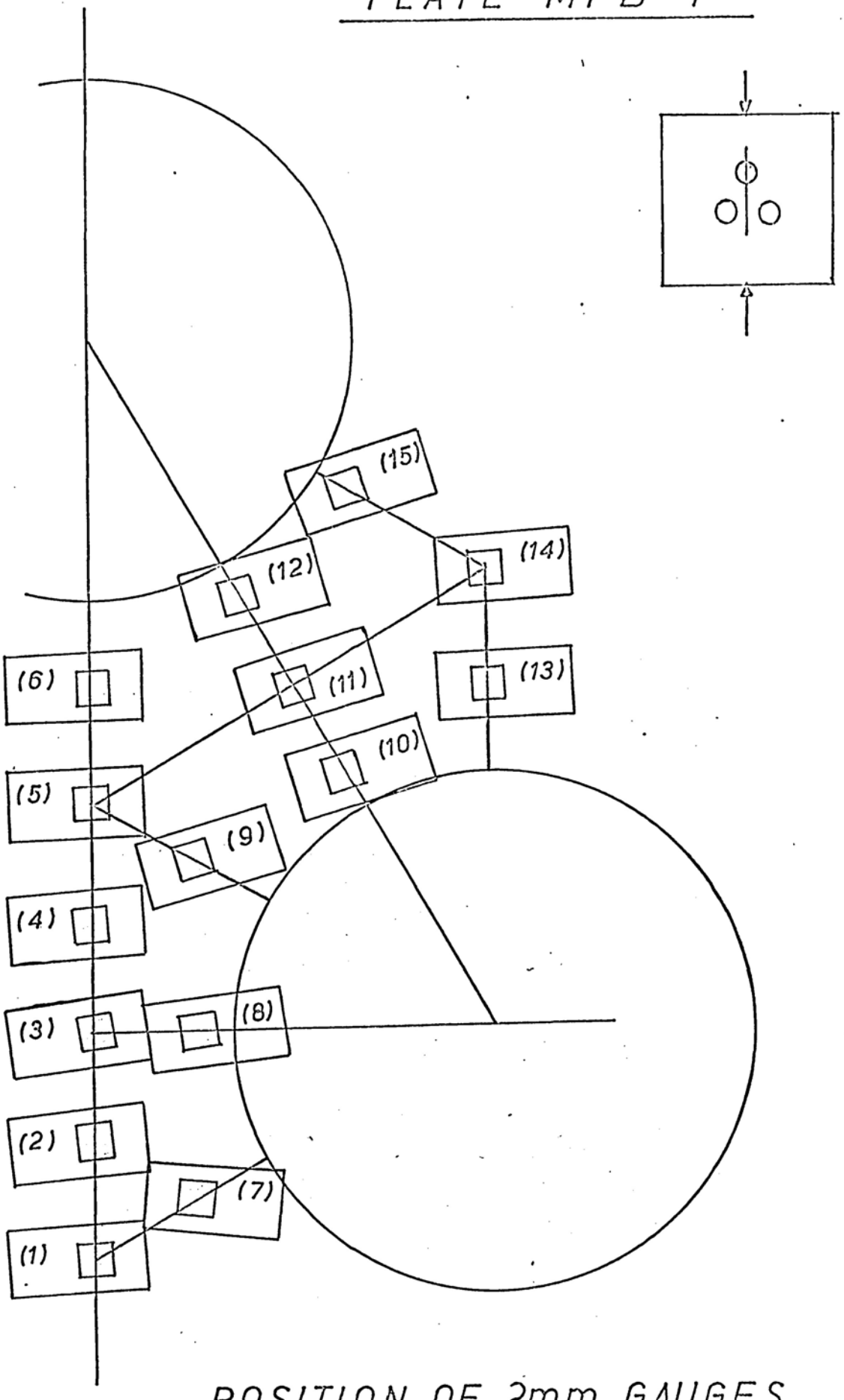
In order to obtain values of the principal tensile strain, 2 mm foil strain gauges (FB-2) were subsequently fixed (using P.S. adhesive) at various points on the plate inside the particle array, aligned in the direction of the isoclinics measured at these points. Since the values shown on figure 5-2 are for the direction of the minor principal strain (ε_3), 90 degrees were added to that value to obtain the direction of the major, most tensile, principal strain (ε_1).

A grid similar to the one scribed on the photoelastic coating and the isoclinic values obtained for each of the points to be gauged were drawn in pencil on the uncoated face of the plate. This allowed the gauges to be placed with a precision of $\pm$ 1/2 degree (the precision to which the isoclinics were measured) and $\pm$ 1/2 mm ($\frac{1}{4}$ of the active length of the gauge) approximately, which was considered sufficient.

Figure 5-5 shows the gauges placed on plate MPB-1. For this plate, it would have been difficult to use more than 15 gauges without reducing the necessary working space between gauges.

Obviously, the most important criterion in choosing the position of the gauges was the need to cover as many points as possible, but giving priority to those points adjudged to be critical. The plate with the largest spacing of the series was tested before other plates in the series were gauged because it was possible to use more gauges on that one and make sure that no critical zones were missed. The results of this first plate were then used for judging the optimum gauge positions on the other plates, the more

PLATE MPB -1-



POSITION OF 2mm GAUGES

fig. 5-5

important critical zones being known. For example, only 7 gauges were used on plate MPB-4 compared with the 15 used on MPB-1.

• • •

The field gauges, placed as previously mentioned, at a distance of 2" from the sides in each corner, consisted of cross-pairs of 5 mm gauges, aligned in vertical and horizontal positions because the isoclinics were always zero at these points on the plates.

As stated in McCreath's thesis, it was considered that at these points, the strains in the mortar matrix were not significantly affected by the aggregate particles and therefore could be said to represent the strains in a pure mortar plate. These strains thus served as a basis for comparing the strains inside the packing, disturbed by the particles, to those in a pure mortar plate.

e) Shrinkage Pattern Readings

Before the plate was reloaded for isochromatic and strain gauge readings, the value of the isoclinic and the isochromatic from the pattern due to shrinkage were read at each of the gauged points. These values for plate MPB-1 are given in table 5-A.

f) Isochromatic and Strain Gauge Readings

A load of approximately 1100 p.s.i. was then applied to the plate. The gauges were read using a Peekel data logger and at the same time the isochromatics were measured at every gauged point and in the four corners. From the strain gauge readings, no creep was noticeable during the length of the tests.

For each gauged point on plate MPB-1, the isochromatic reading is given in table 5-A, together with the corresponding strain gauge reading and the shrinkage pattern reading mentioned previously.

Each isochromatic reading represents the average of two measurements.

Point	Shrinkage Isoclinic (degrees)	Shrinkage Isochromatic (micro-strains)	Load Isochromatic (micro-strains)	ε_1 (micro-strains)
1	+12	+62	-226	+13
2	+5	+124	-192	+59
3	+1	+157	-166	+62
4	+2	+142	-194	+73
5	0	+12	-281	+41
6	-6	-59	-390	+35
7	-7	+65	-246	+15
8	+5	+130	-160	+32
9	+12	+89	-311	+46
10	-40	-68	-385	+52
11	-33	-136	-463	+30
12	-32	-112	-440	-8
13	-16	-56	-410	+42
14	-33	-42	-376	+43
15	-56	-71	-341	+43

Table 5-A

It should be noted that the value of the isochromatic represents $\varepsilon_X - \varepsilon_Y$, X being the isoclinic value at the point considered, and ε_X and ε_Y being either one of the principal strains. This value thus represents $\underline{\varepsilon_3 - \varepsilon_1}$ in some cases (yielding a <u>minus</u> sign for the isochromatic value) and $\underline{\varepsilon_1 - \varepsilon_3}$ in others (yielding a <u>positive</u> sign).

The field strains, as measured by the isochromatics and by the field gauges were:

	$(\varepsilon_3 - \varepsilon_1)_f$ (gauges) (micro-strains)	$(\varepsilon_3 - \varepsilon_1)_f$ (coating) (micro-strains)
Top left corner	-231	-359
Top right corner	-220	-320
Bottom left corner	-254	-291
Bottom right corner	-239	-270
Average value	-236	-310

The shear-strain value in micro-strains from the coating is obtained by multiplying the number of fringes measured by the sensitivity of the coating. For plate MPB-1, the sensitivity of the coating used was 593 micro-strains per fringe.

It is difficult to assess the precision with which the isochromatic readings are taken because the determination of the value depends on judging the tint of passage from one fringe to another. Even if each operator does a sample test using a coated aluminium beam to calibrate with a known value of shear strain, errors of up to 3/100 of a fringe (approximately 20 micro-strains) are still likely. Comparing the results from the values obtained from gauge readings and isochromatic readings for field strains gives a rough idea of this precision. Gauge readings varied by 34 micro-strains at most from one corner to another and coating readings by 89.

But, as will be pointed out later, this possible isochromatic error is not large if we consider that it rests solely on the minor principal strain (of the order of -200 to -300 micro-strains). When the principal strains are determined, the gauge readings, yielding a precision of ± 2 microstrains, are used to assess the major principal strains.

g) Face Correction Factor

The difference in strains from one side of a plate to the other (from field strain measurements) was corrected by use of the following factor.

$$\text{Face Correction Factor} = \frac{(\varepsilon_3 - \varepsilon_1) \quad \text{(gauges)}}{(\varepsilon_3 - \varepsilon_1) \quad \text{(coating)}}$$

This factor was applied to all the isochromatic values obtained from the coating so that the tensile strains measured could be compared to the shear-strain value at each point.

For plate MPB-1, the face correction factor was:

$$\text{F.C.F.} = \frac{-236}{-310} = 0.761$$

It is fully realized that applying a factor obtained from readings in the corners of the plate to isochromatic values measured within the particle array must be viewed with suspicion, but nevertheless it's use certainly decreases the possibility of error by a large margin.

A list of all the face correction factors used is given in table 5-C.

h) Determination of the Principal Strains

As can be seen on photograph A in figure 5-4, the isochromatic pattern due to the shrinkage strains between the aggregate particles sometimes reached one quarter of the first fringe (approximately -150 micro-strains, pale yellow). Since field strains due to loading alone amounted to about -300 micro-strains, this pattern had to be taken into account especially since in every case large shrinkage strains were found to occur in the critical zones, which was <u>not</u>

the case for the plates tested by McCreath. It was not possible simply to use a higher load because the plates had to be tested in the "elastic" range before the formation of the first crack; loads higher than 1100 p.s.i. were thought unsafe considering the results obtained by MCcreath for the strain levels at fracture initiation for his plates.

Photograph C in figure 5-4 shows the isochromatic pattern on plate MPB-1 under load. This pattern represents the cumulative effect of the shrinkage pattern and of the pattern due to load only. At points where the isochromatic values due to these two patterns were of different signs, a zone of low shear strain appeared (in between the two bottom particles of the array for instance).

Since the shrinkage isoclinics and the load isoclinics were not significantly different (less than 15 degrees generally), the value of the isochromatic due to shrinkage was subtracted directly from the one obtained under load in order to obtain the value due to the loading only. It was felt that a variation of 15 degrees did not have a significant influence in the amount of shear strain $(\varepsilon_3 - \varepsilon_1)$ although it would change significantly each principal strain. A strain analysis based on more precise computations was not necessary because of the degree of precision of the other operations involved (face correction factor, measurements of isochromatics etc.). In zones where the isoclinics differed by more than 15 degrees the shrinkage pattern represented $\frac{1}{6}^{th}$ of a fringe or less, so that large errors were not possible.

The same considerations apply to the isoclinic values used to align the 2 mm gauges in the direction of the major principal strain. Obviously, it was not possible to isolate easily the isoclinic due

to load only, so the isoclinics read when the plate was under load were used even if they were known to be influenced by the shrinkage pattern. But, since in zones of high shear-strain due to shrinkage the isoclinics agreed approximately, it was felt that only minor errors were introduced in this way. So, for all plates, the graph of the isoclinics shows the direct values obtained under load as all the other graphs (isochromatics and isotenics) represent the values due to load only, separated from shrinkage effects.

The value of the shear strain from the loading only being known at each point, it was then multiplied by the face correction factor and the value of the principal tensile strain ε_1 (obtained from the two millimeter gauges) was added to it yielding the value of ε_3. It is in this way that the principal strains at each point were determined. Therefore all the values obtained were related to the uncoated face of the plate so that the average compressive field strain $(\varepsilon_3)_f$ measured by the field gauges could be used to non-dimensionalize the value for each point.

For plate MPB-1, the non-dimensionalized value of each of the principal strains for each point is given in table 5-B.

Point	$\varepsilon_3/(\varepsilon_3)_f$	$\varepsilon_1/(\varepsilon_3)_f$
1	0.995	-0.063
2	0.879	-0.285
3	0.888	-0.299
4	0.883	-0.353
5	0,879	-0.198
6	1.043	-0.169
7	1.068	-0.072
8	0.913	-0.155
9	1.247	-0.222
10	0.908	-0.251
11	1.053	-0.145
12	1.237	+0.030
13	1.095	-0.203
14	1.019	-0.208
15	0.777	-0.208

Table 5-B

Figure 5-6 shows the $\varepsilon_1/(\varepsilon_3)_f$ value at each point on the plate together with the isotenic lines. The ε_3 isotenics and the isochromatics are given in figures 5-7 and 5-8. The use of the average field strain to non-dimensionalize each value helps to give a good picture of how the aggregate particles affect the strain distribution.

i) Composite Strains

Having removed all the 2 mm gauges, 30 mm and 60 mm gauges were then placed vertically across the particle array to measure the composite strains. These strains are used to represent the average compressive deformation of a plate full of aggregate particles arranged in the same manner and with the same spacing as the particles in the plate-model considered. They are necessary for later comparison of the plate-models with real concrete. These composite strains were measured at the value of the field strain attained in the tests to determine the isochromatic values.

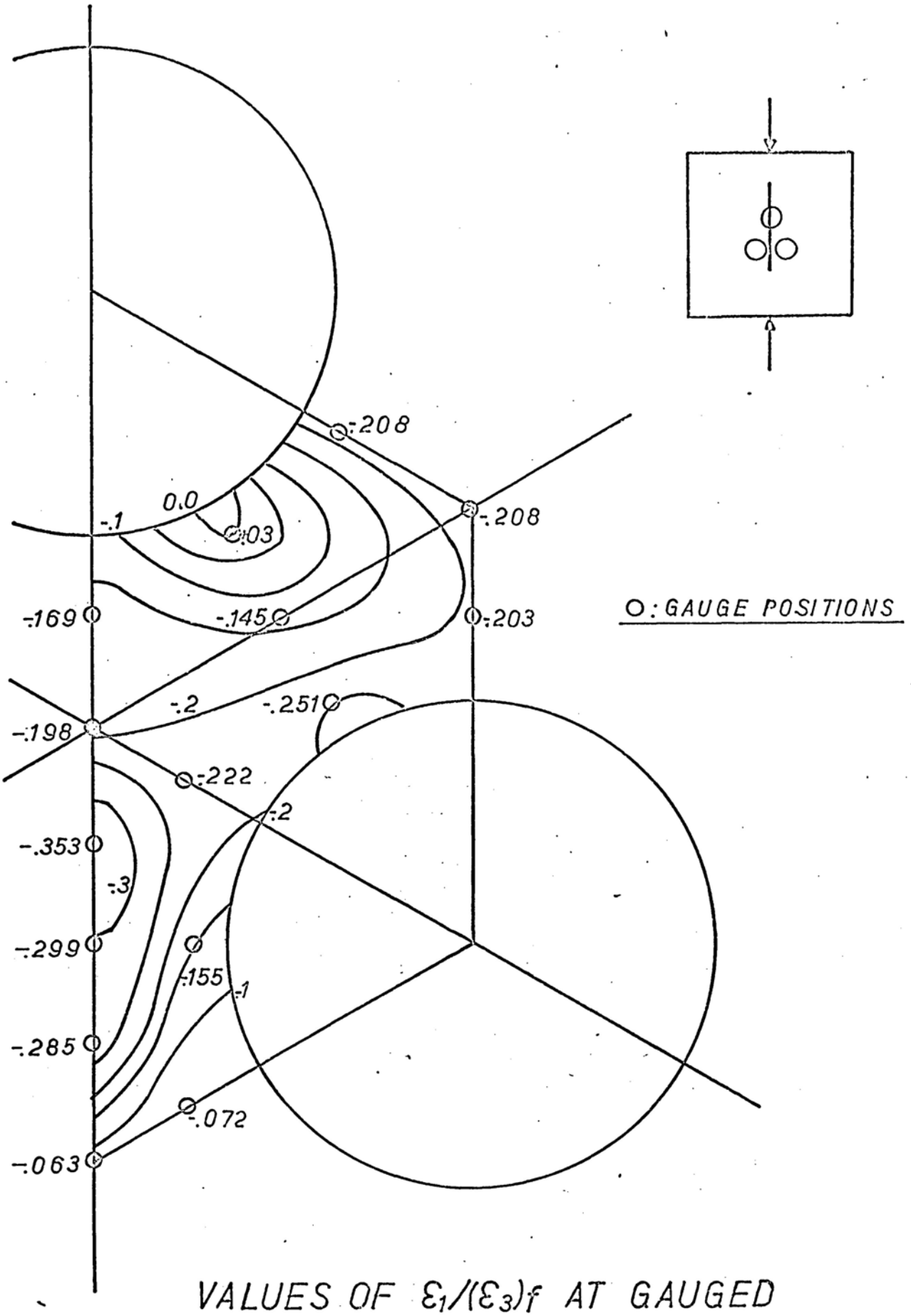
The boundaries of the elements considered for the above measurements are shown on figure 5-9. Figure 5-10 shows the actual positions of the gauges used. These positions were defined with the aim of representing the <u>average</u> vertical deformation of the element under load.

For plate MPB-1 the ratio of the average of these composite strain gauge readings to the field strains was:

$$\frac{(\varepsilon_3)_{\text{comp.}}}{(\varepsilon_3)_{\text{field}}} = 0.857$$

Ratios of all plates are given in table 5-C. They were found to decrease with increasing volume fraction of coarse aggregate in

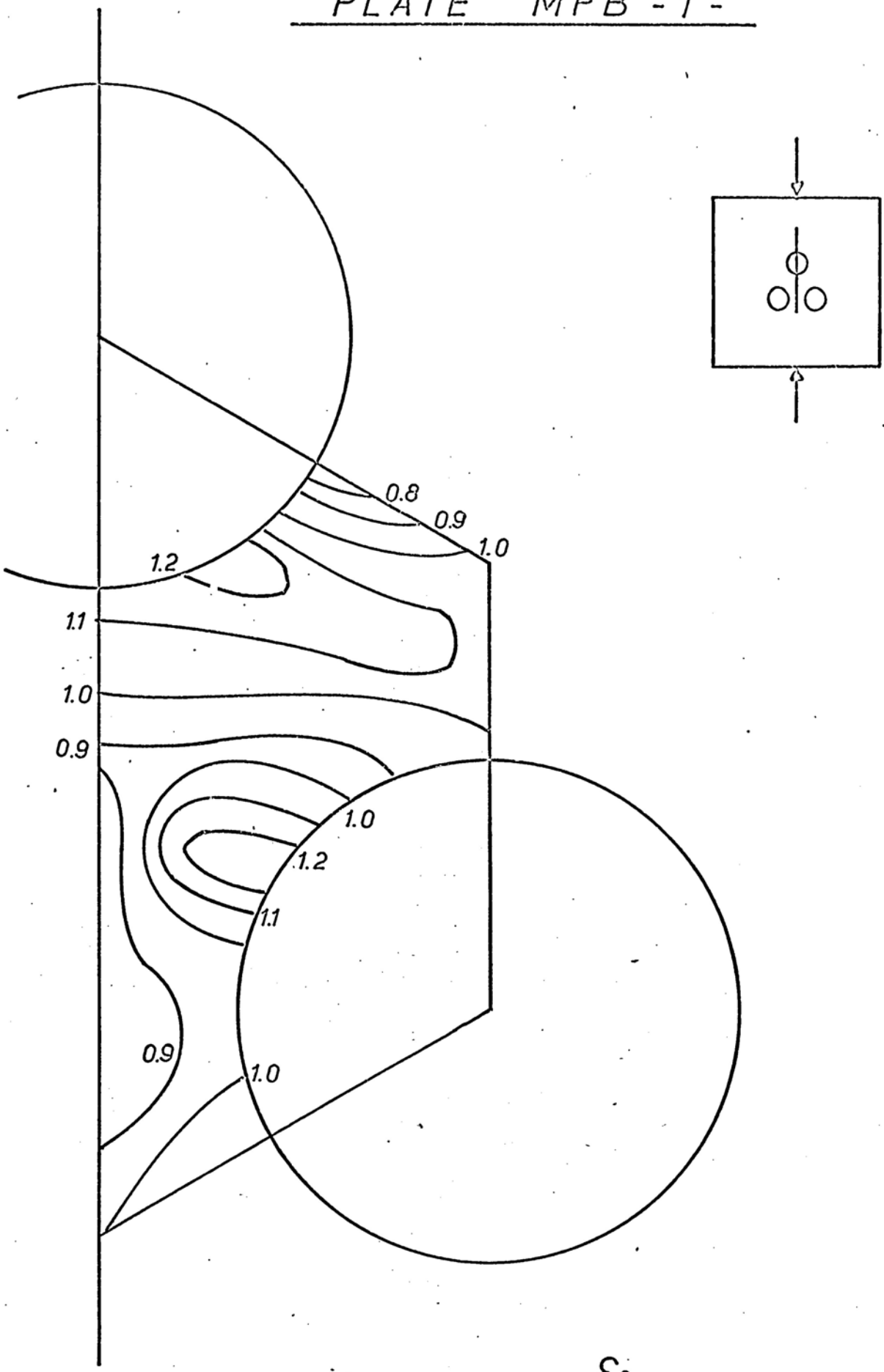
PLATE MPB -1-



VALUES OF $\varepsilon_1/(\varepsilon_3)_f$ AT GAUGED POINTS AND ISOTENICS AT EVERY 0.05

fig. 5-6

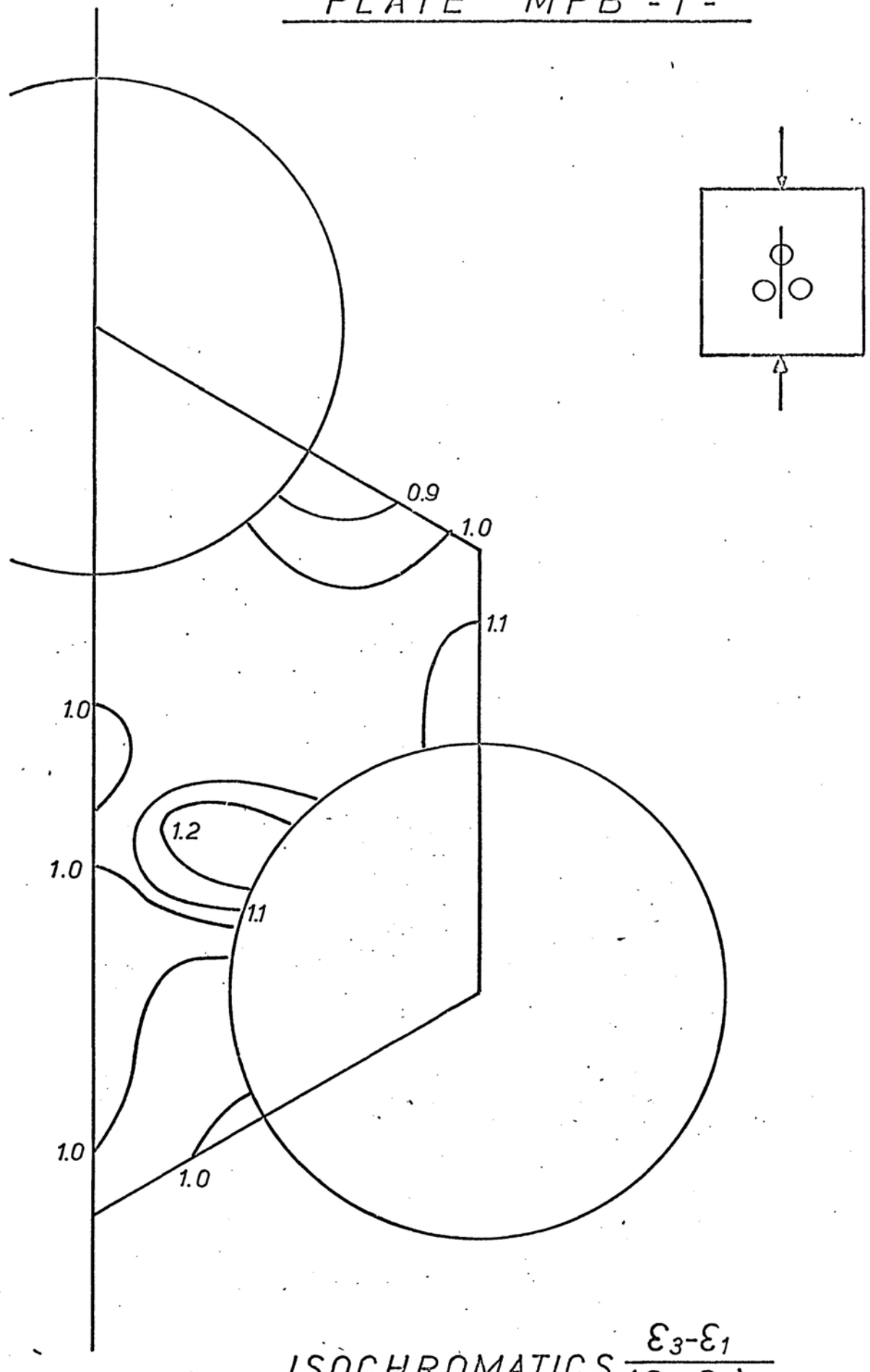
PLATE MPB -1-



ISOTENICS $\frac{\varepsilon_3}{(\varepsilon_3)_f}$

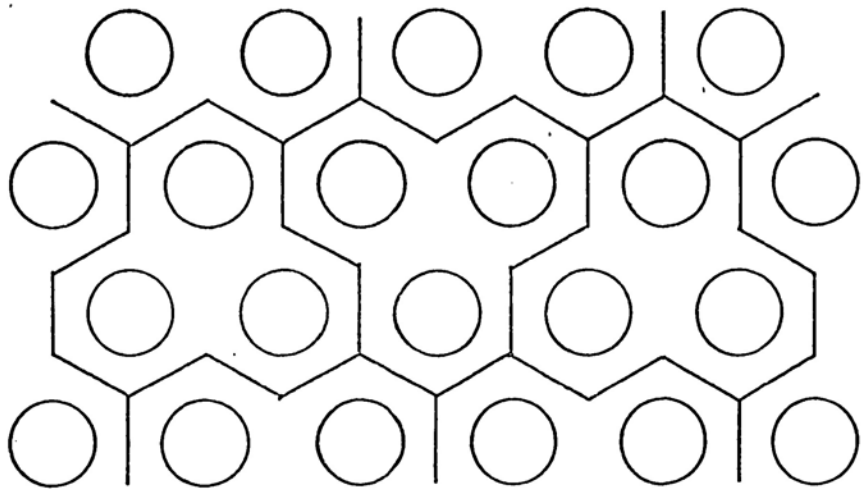
fig. 5-7

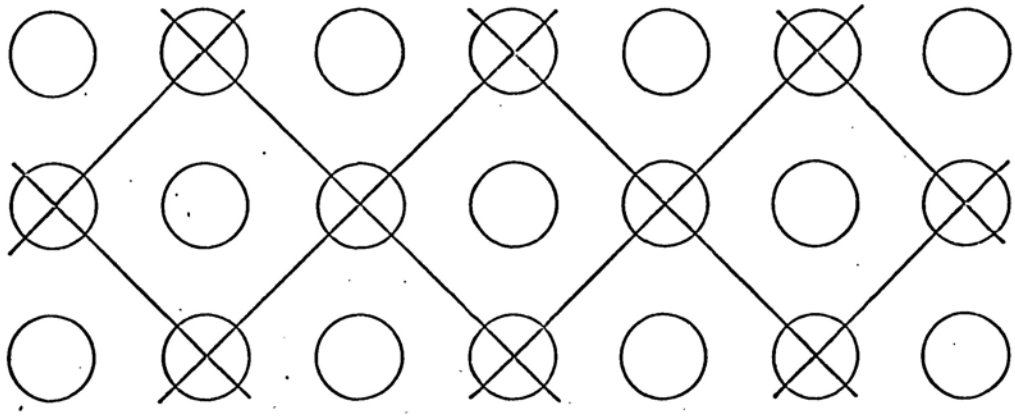
PLATE MPB -1-

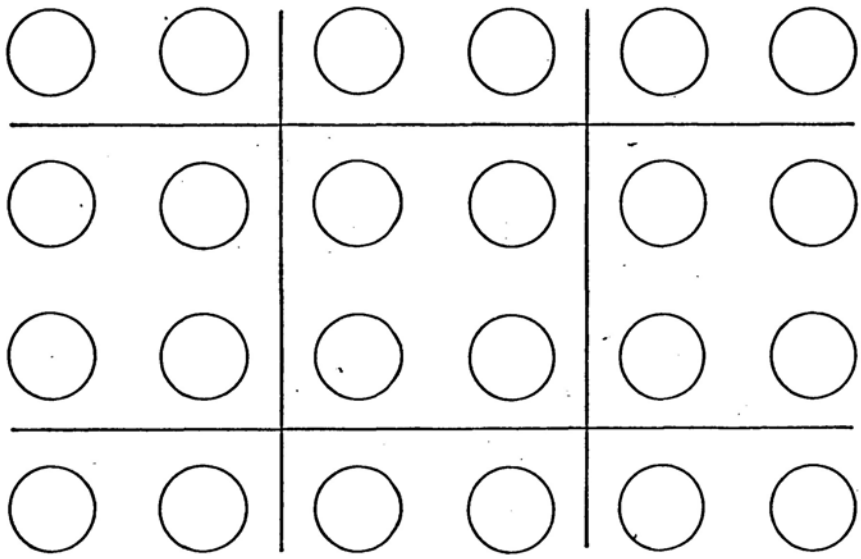


ISOCHROMATICS $\frac{\varepsilon_3-\varepsilon_1}{(\varepsilon_3-\varepsilon_1)_f}$

fig. 5-8

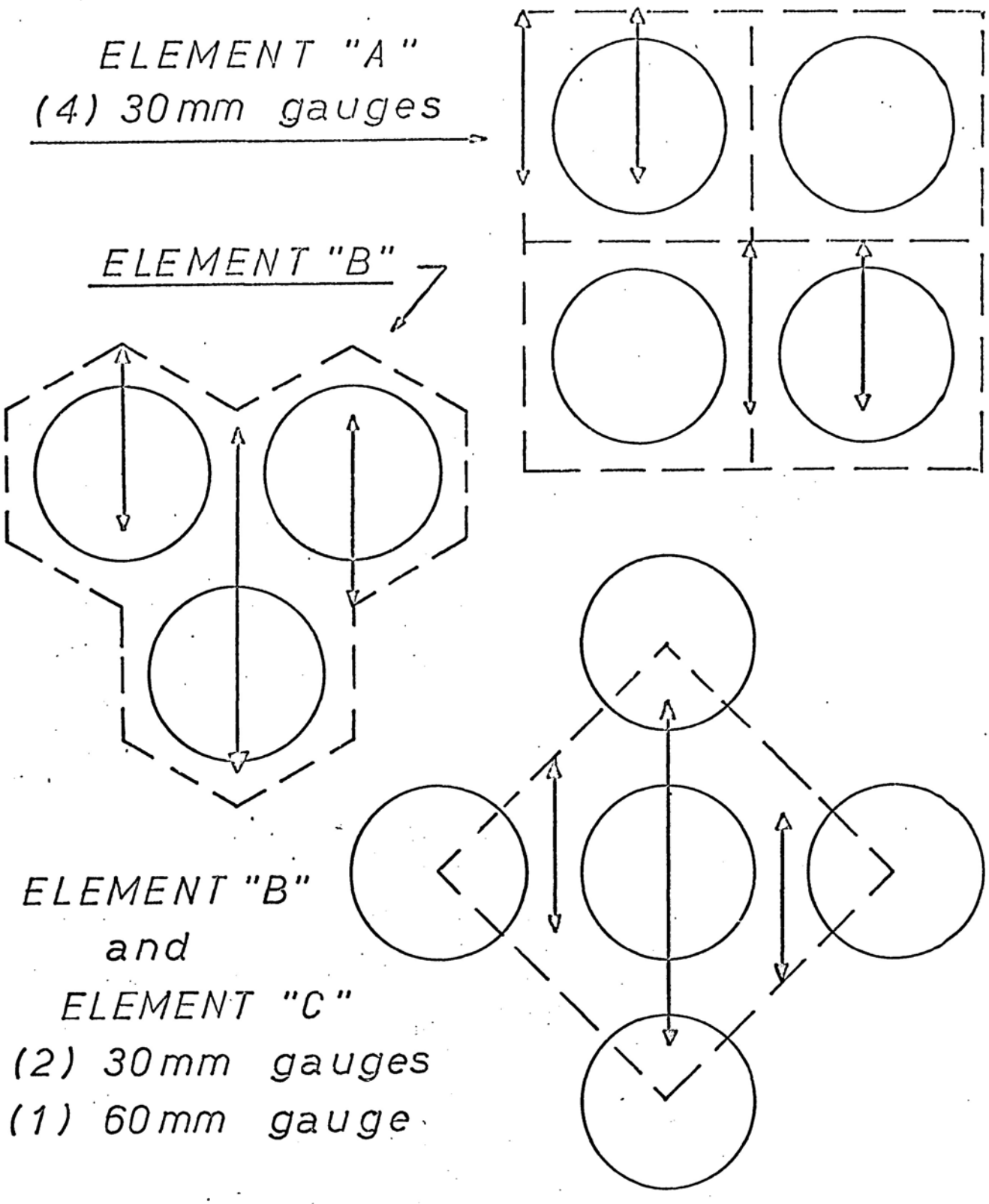






ELEMENTS CONSIDERED FOR
COMPOSITE STRAIN MEASUREMENTS

fig. 5-9



POSITION OF GAUGES FOR
COMPOSITE STRAIN MEASUREMENTS

fig. 5-10

each series which was considered normal since the value of "modulus of elasticity" for a given concrete usually increases with increasing percentage of aggregate because the aggregate particles are more rigid.

j) Critical Point Analysis

Following the procedure outlined by McCreath all the non-dimensionalized values of the principal strains at each point were plotted on the graph containing the fracture initiation envelope. The points lying outside the envelope were considered critical, i.e. likely to influence the cracking process at some stage. The point where the ratio A/L as shown on figure 5-11 was the largest was termed the most critical point. It was concluded by McCreath that cracking would start at this point, at a level of strain indicated by the point where the line from the origin to the most critical point crossed the envelope.

For plate MPB-1 Point no. 4 was found to be the most critical and, as shown on the graph, cracking was predicted at a level of strain of

$$((\varepsilon_3)_{f.i.})\ \text{most crit. point} = 0.310 \times ((\varepsilon_3)_{f.i.}\ \text{pure mortar}\ \sigma_1=0)$$

The ratio of composite strain to field strain being known, it was then possible to calculate in the following way the level of composite strain at which fracture would initiate, to be compared with values obtained for real concrete.

$$\frac{(\varepsilon_3)_{comp.}}{(\varepsilon_3)_{field}} = .857 \; ; \quad \frac{\varepsilon_3}{(\varepsilon_3)_f} = 0.883 \text{ at most critical point, hence}$$

$$\frac{(\varepsilon_3)_{comp.}}{(\varepsilon_3)_{m.c.p.}} = \frac{(\varepsilon_3)_{comp.}}{(\varepsilon_3)_{field}} \times \frac{(\varepsilon_3)_{field}}{(\varepsilon_3)_{m.c.p.}} = \frac{0.857}{0.883} = 0.963$$

PLATE MPB -1-
CRITICAL POINT ANALYSIS

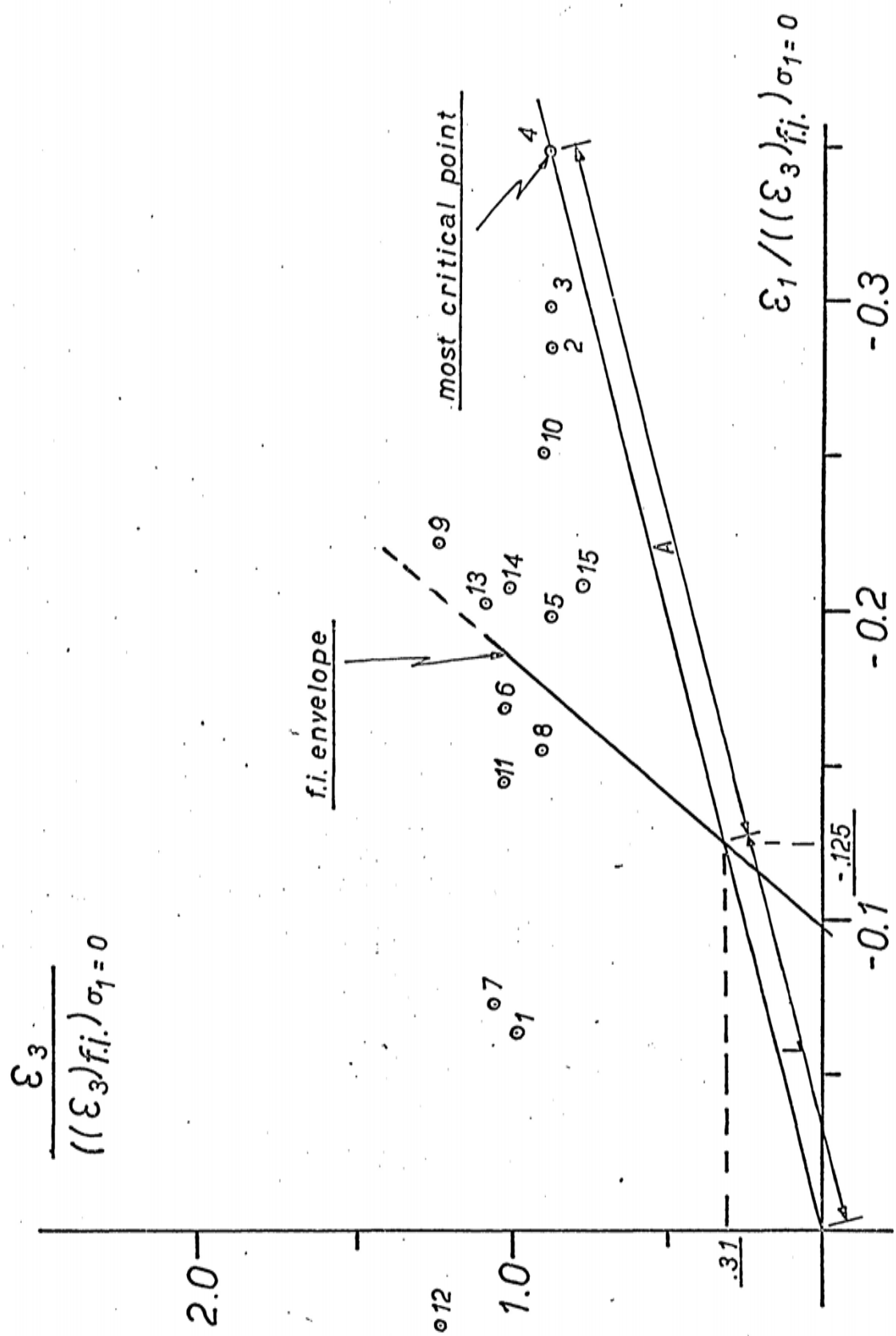


fig. 5-11

This value of 0.963 was assumed to stay constant up to fracture initiation, so

$$\frac{((\varepsilon_3)\ \text{comp.})\ \text{f.i.}}{((\varepsilon_3)\ \text{m.c.p.})\ \text{f.i.}} = 0.963$$

But since $((\varepsilon_3)\text{m.c.p.})\text{f.i.} = 0.310 \times ((\varepsilon_3)\ \text{pure mortar})\ \text{f.i.}$

$$\frac{((\varepsilon_3)\ \text{comp.})\text{f.i.}}{((\varepsilon_3)\ \text{pure mortar})\ \text{f.i.}} = 0.299$$

So for this particular plate, cracking was predicted at a level of strain much lower than the one for mortar under uniaxial compression. This shows that the introduction of aggregate reduced significantly the composite strains required to initiate fracture.

Table 5-C gives this particular ratio and the strain ratios at the most critical point for all the plates.

Section 3. Discussion of Results

a) Results

For each plate model, there are two sets of results. Firstly, quantitative results predicting the onset of cracking at a certain strain level and at a certain point, and secondly, the overall strain distribution under load in the elastic range.

Table 5-C gives the first set of results. Since these were verified upon loading to failure with a method described in chapter VI no comments are necessary here.

Figures 5-12 to 5-55 give information regarding the strain distribution under load for the various models. The isoclinics, the isochromatics, the major principal strain isotenics and the minor principal strain isotenics are shown for each plate.

PLATE-MODELS TEST RESULTS

Plate	% V_f C.A.	Face Correction Factor	$\frac{(\varepsilon_3)_{COMP}}{(\varepsilon_3)_{field}}$	at most critical point		$\left(\frac{(\varepsilon_3)_{COMP}}{(\varepsilon_3)_{pure\ mortar}}\right)_{f.i.}$
				$\varepsilon_1/(\varepsilon_3)_f$	$\varepsilon_3/(\varepsilon_3)_f$	
MPA-1	28.00	0.606	0.836	-0.385	1.180	0.287
MPA-2	33.50	0.854	0.794	-0.338	1.530	0.375
MPA-3	39.25	0.786	0.775	-0.339	1.250	0.327
MPA-4	46.50	0.939	0.745	-0.381	1.095	0.253
MPB-1	32.25	0.761	0.851	-0.353	0.883	0.299
MPB-2	40.25	1.038	0.723	-0.241	0.735	0.395
MPB-3	49.25	0.865	0.632	-0.251	0.545	0.300
MPB-4	59.50	0.833	0.569	-0.263	0.950	0.305
MPC-1	27.00	1.338	1.022	-0.326	1.235	0.452
MPC-2	32.00	1.091	0.887	-0.260	0.823	0.457
MPC-3	37.75	0.814	0.828	-0.317	1.074	0.358
MPC-4	43.50	1.043	0.793	-0.250	0.877	0.442

Table 5-C

b) Validity of Results

The strain analysis was considered to give a fairly good degree of precision. Measurements were made in one quarter or one half of the aggregate particle array, depending on the symmetry of the array. Certain points were duplicated to check out possible errors, especially in zones of low shear strain where the isoclinics were difficult to read. These verifications showed that strain gauge readings, for example, did not vary by more than 10 micro-strains in 50 when the alignment of the gauge was varied to the extreme of the possible error. This is confirmed by a Mohr circle analysis for a typical state of strain of $\varepsilon_1 = +50$ and $\varepsilon_3 = -250$. A variation of 10 micro-strains would require at least a 10° change in alignment in such a case.

It can be safely assumed therefore, that testing errors do not significantly affect the overall patterns shown on the graphs, especially since these are shown not to vary much from one plate to another in the same series.

It was felt desirable to present all the information in the form of graphs to facilitate observation of the strain disturbances caused by the aggregate particles. But since plotting these lines is subjective, as can be seen in figure 5-6, no direct measurements should be made on the graphs to obtain precise values.

The variation in the strain levels from one plate to another in the same series was felt to be due both to variations in the material itself and to possible errors in the testing method. As regards the material, it is easy to see that the mortar matrix in the small gauged areas could be subject to variations from one zone to another, due to differences in air content and water content for instance.

c) Critical Zones

MPA Series:

For this type of packing, the area directly between two particles aligned in the direction of loading was always found to be critical, with the most critical point approximately in the mid-section. Although the compressive strains were relatively undisturbed, very high tensile strains occurred in this zone.

A secondary crtitical zone of very small extent was found in-between two particles aligned perpendicular to the direction of loading; this was mostly due to the value of the compressive strain which was low at that point, the tensile strains being only slightly above normal ($\varepsilon_1/(\varepsilon_3)_f = 0.18$). At the centre of symmetry of the packing, a tensile strain of approximately zero was always found, therefore that portion of the specimen was considered very safe.

It should be noted in addition that as the spacing between the aggregate particles became smaller, the strain disturbances stayed of the same order. This experimental result will be of great importance when, in the next chapter, the effect of varying the volume fraction upon the composite strain levels at discontinuity is discussed.

MPB Series

For the first three plates in this series, the most critical point was found to lie between the two aggregate particles aligned perpendicular to the direction of loading. A zone extending roughly a quarter of a diameter on each side of this point in a vertical direction was found to be critical. It is a zone of low compressive strain generally and fairly high tensile strain. The strain disturbances were not very significant in the zones between the particles

aligned at 30 degrees to the direction of load.

In plate number 4, where the same effects should have occurred, no critical points were found inside the packing and measurements made above the upper aggregate particle showed the most critical point to be situated in this zone. Special 1 mm foil strain gauges were used inside the packing because of the close proximity between the particles. These yielded the same results.

MPC Series

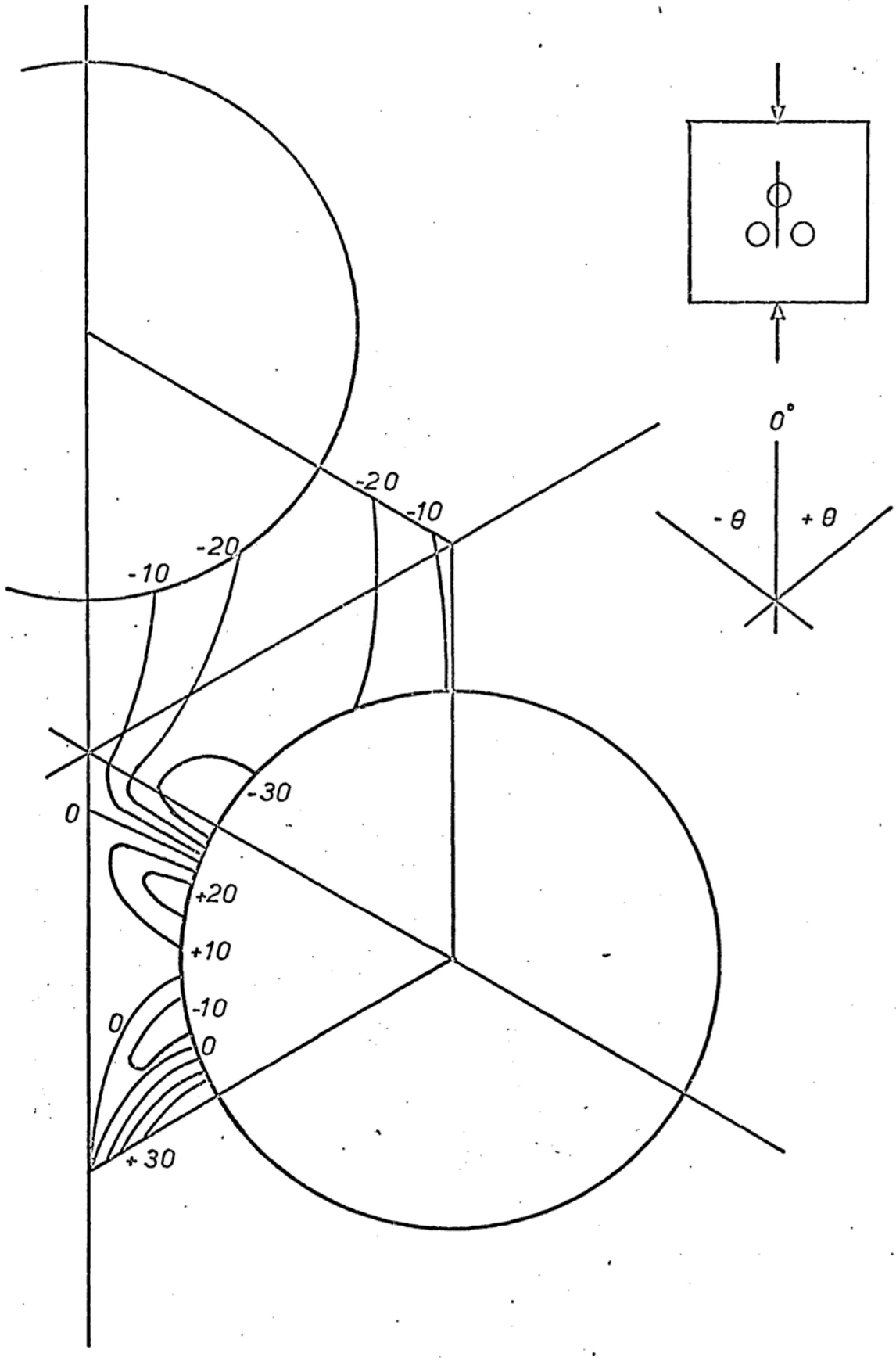
As in the first series, results from this set of plates showed that the proximity of two particles in the direction of loading caused a high tensile strain disturbance in the mortar between. The most critical point was found in this zone. The area between the particles placed horizontally was found to have low compressive strains but normal tensile strains and therefore, was only slightly, if at all, critical.

Plate MPB-2 had the most critical point at some distance from the line of symmetry but it was only slightly more critical than the one along the symmetry line, due to a lower compressive strain and not to a higher tensile strain.

The strain distribution in plate MPB-4 was probably affected by an air void or a shrinkage crack and this effect will be studied in chapter VI.

As in the first series, the strain disturbances did not vary significantly from one plate to another.

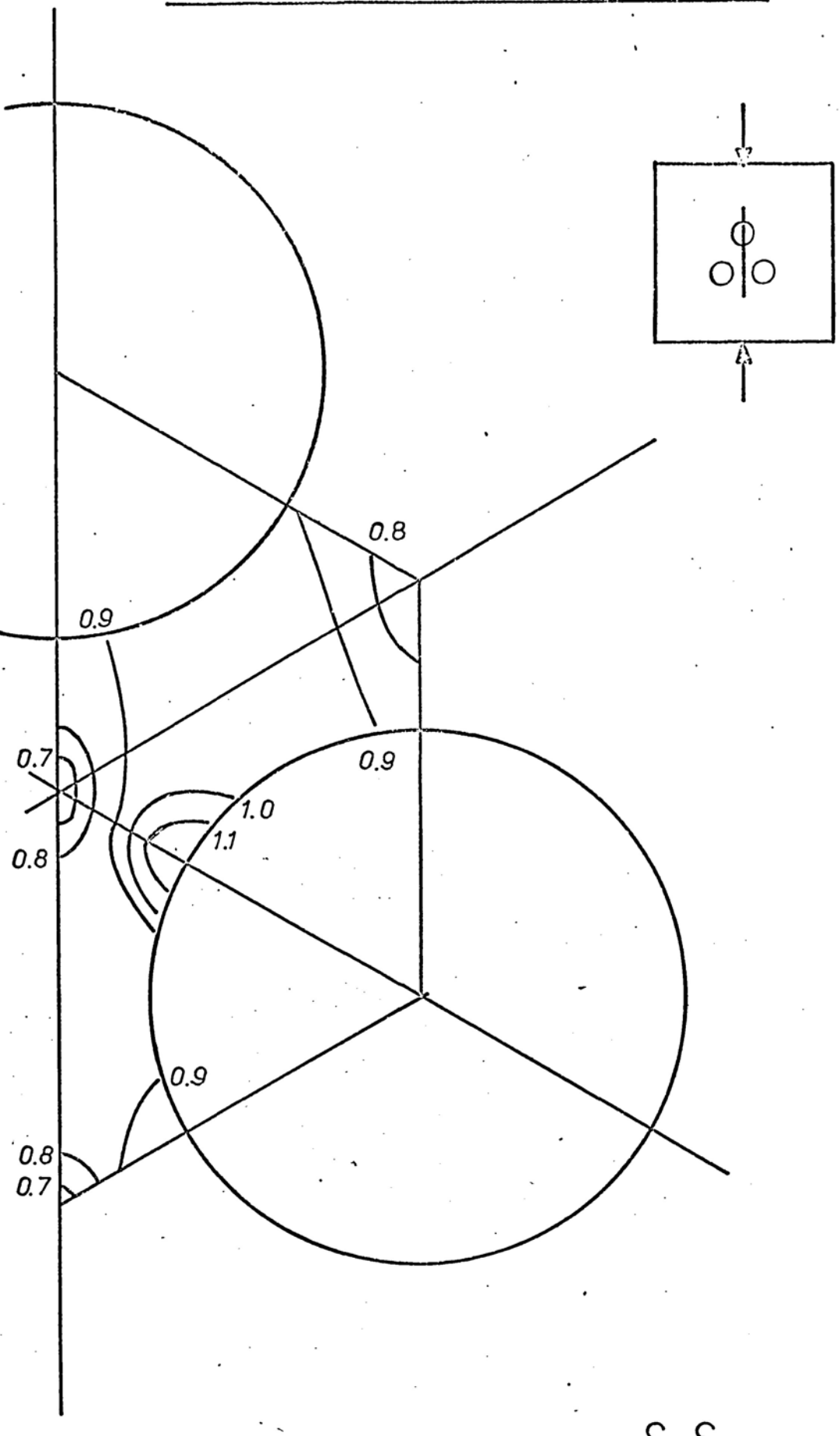
MPB-2- V_f = 40.25 %



ISOCLINICS

fig. 5-12

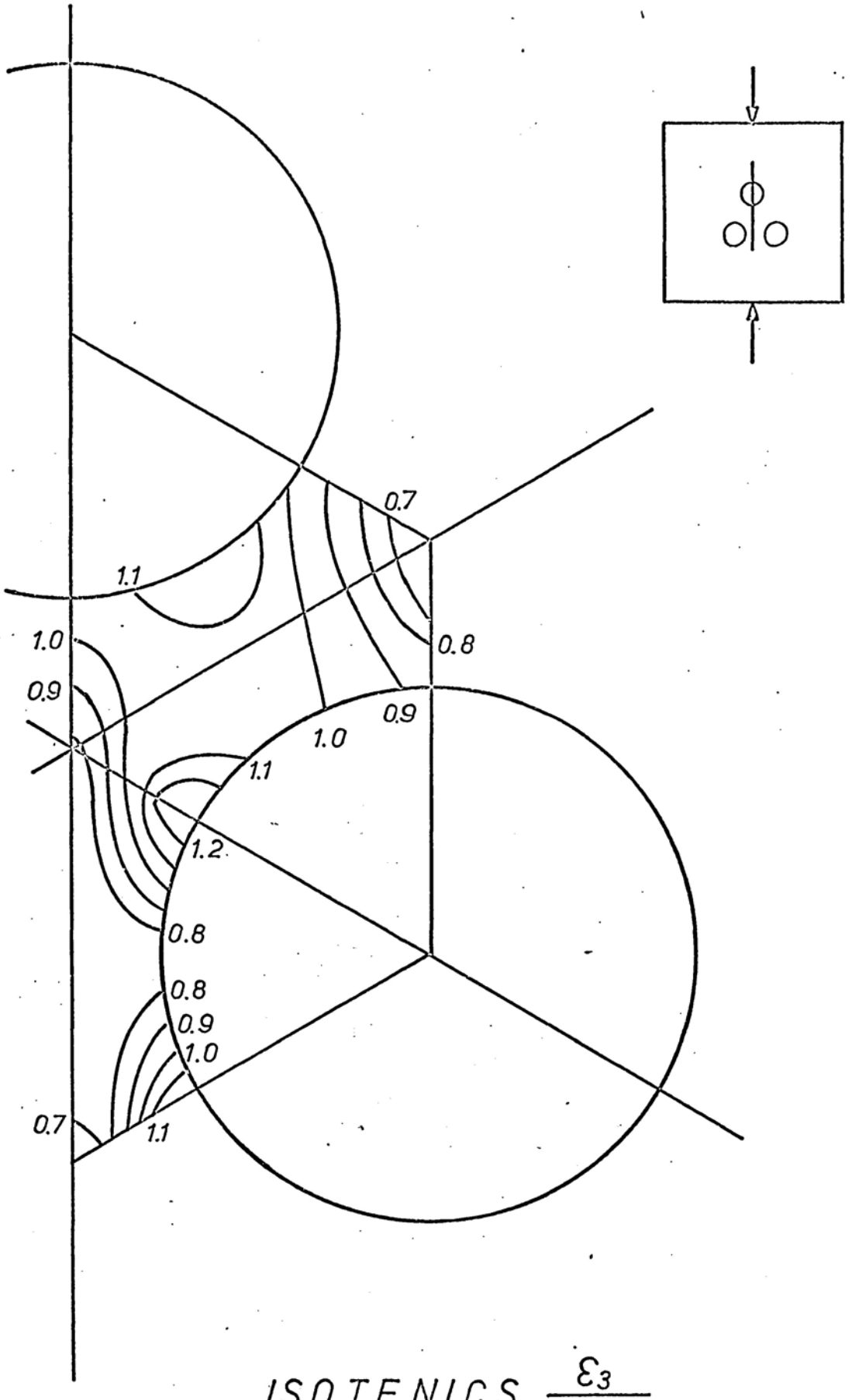
MPB-2- $V_f = 40.25\%$



ISOCHROMATICS $\frac{\varepsilon_3-\varepsilon_1}{(\varepsilon_3-\varepsilon_1)_f}$

fig. 5-13

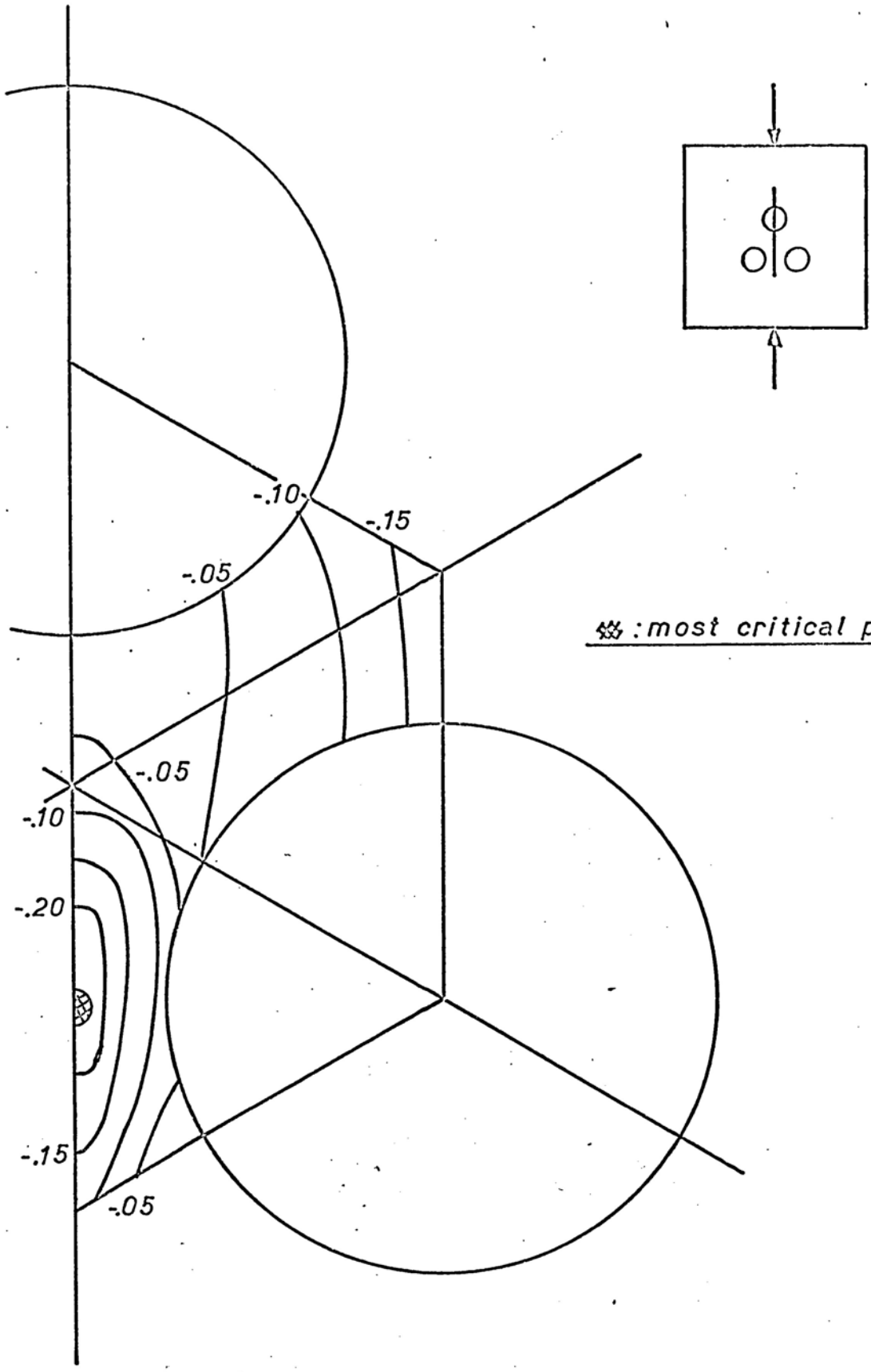
MPB -2- V_f = 40.25%



ISOTENICS $\frac{\varepsilon_3}{(\varepsilon_3)_f}$

fig. 5-14

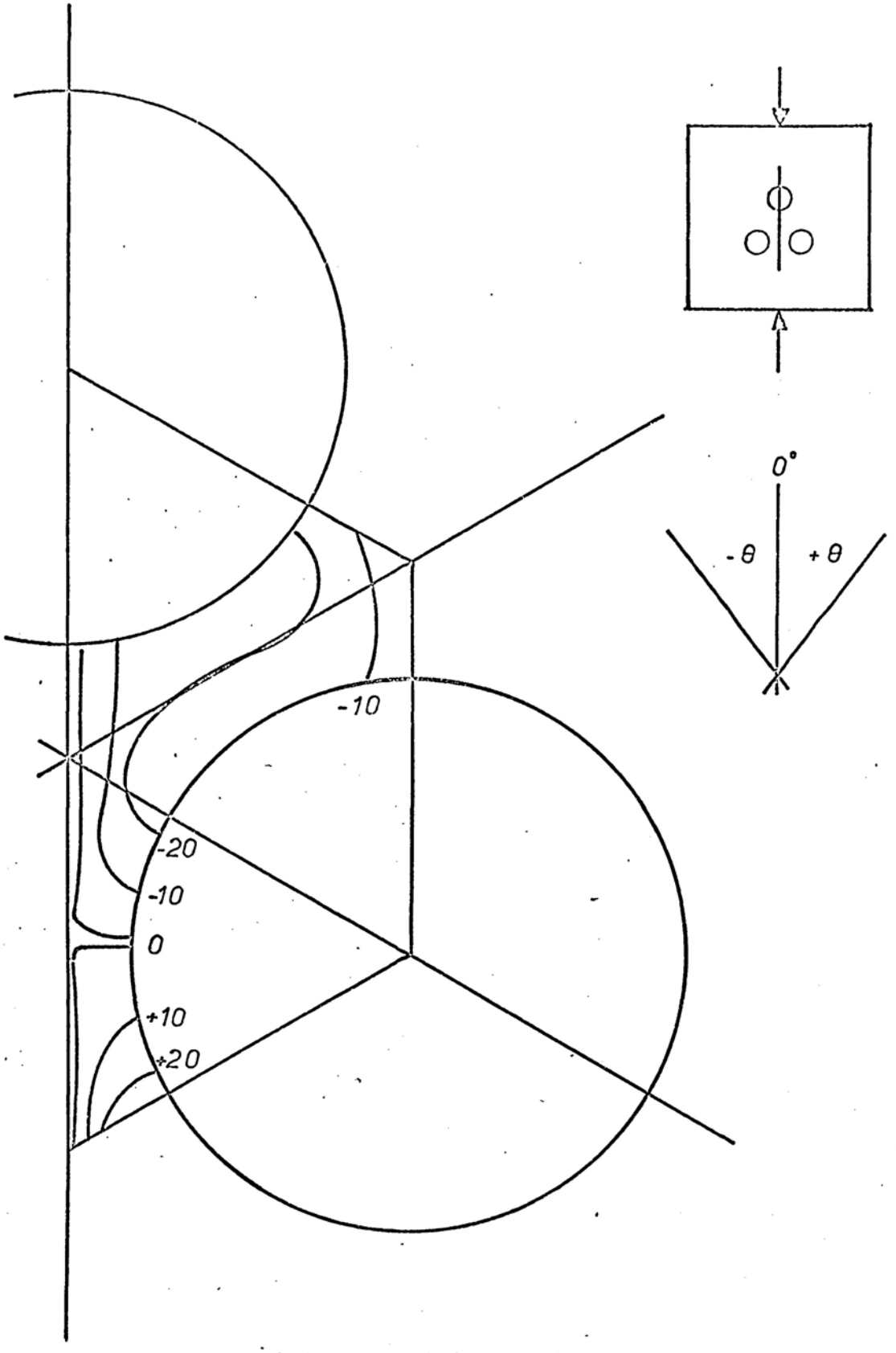
MPB - 2 - $V_f = 40.25\%$



ISOTENICS $\frac{\varepsilon_1}{(\varepsilon_3)_f}$

fig. -5-15

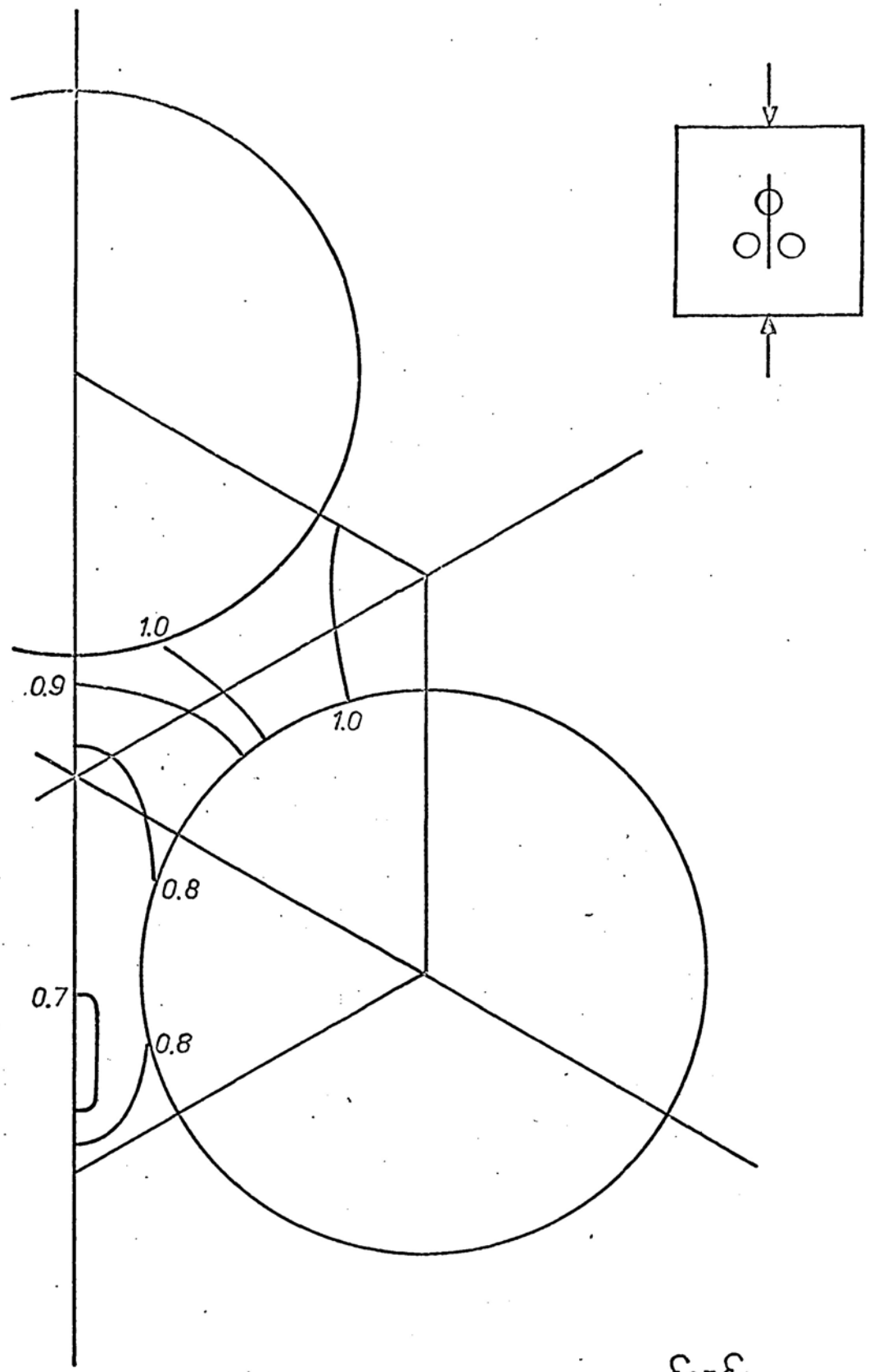
MPB -3- $V_f = 49.25\%$



ISOCLINICS

fig. 5-16

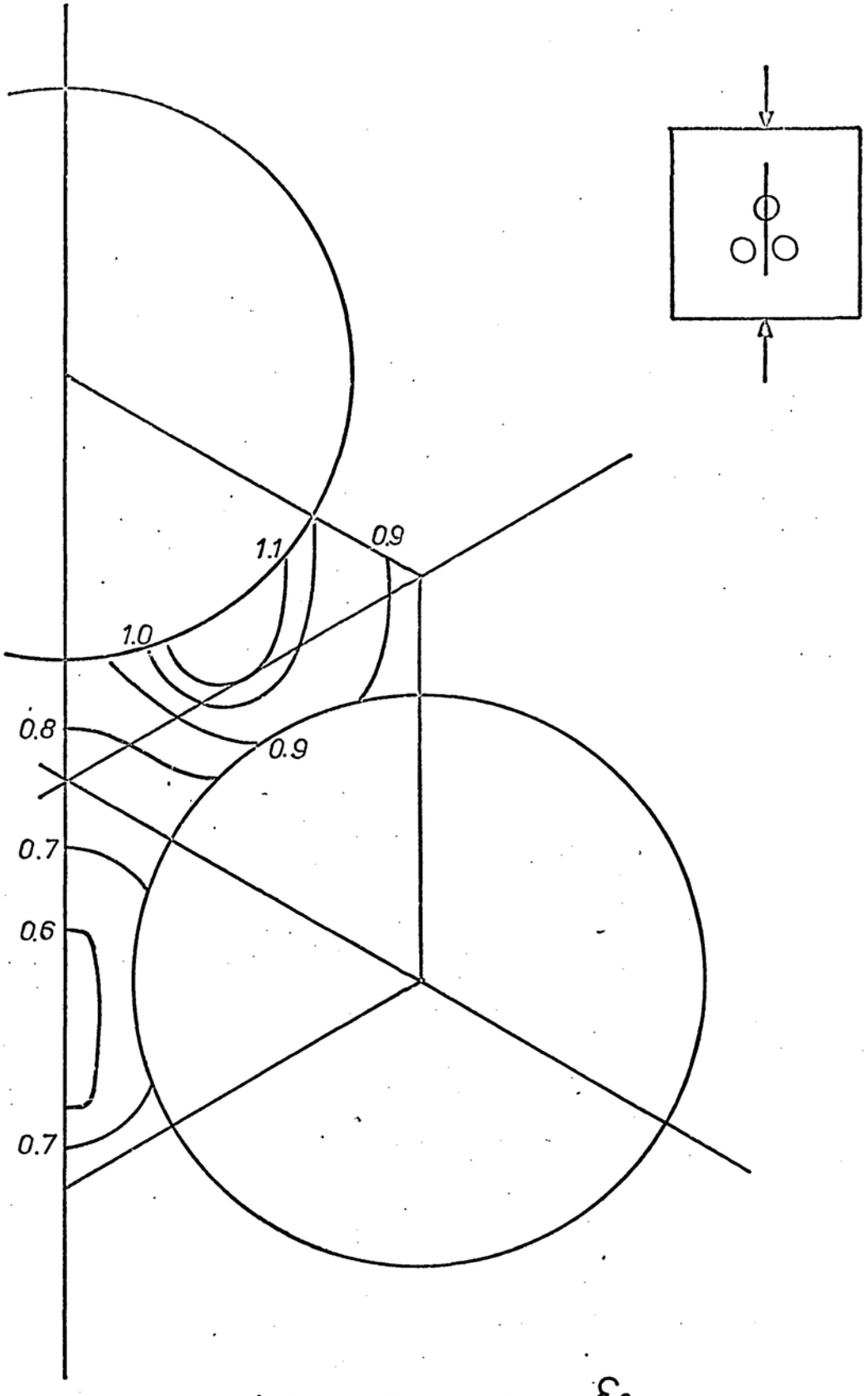
MPB -3- $V_f = 49.25\ \%$



ISOCHROMATICS $\frac{\varepsilon_3 - \varepsilon_1}{(\varepsilon_3 - \varepsilon_1)_f}$

fig. 5-17

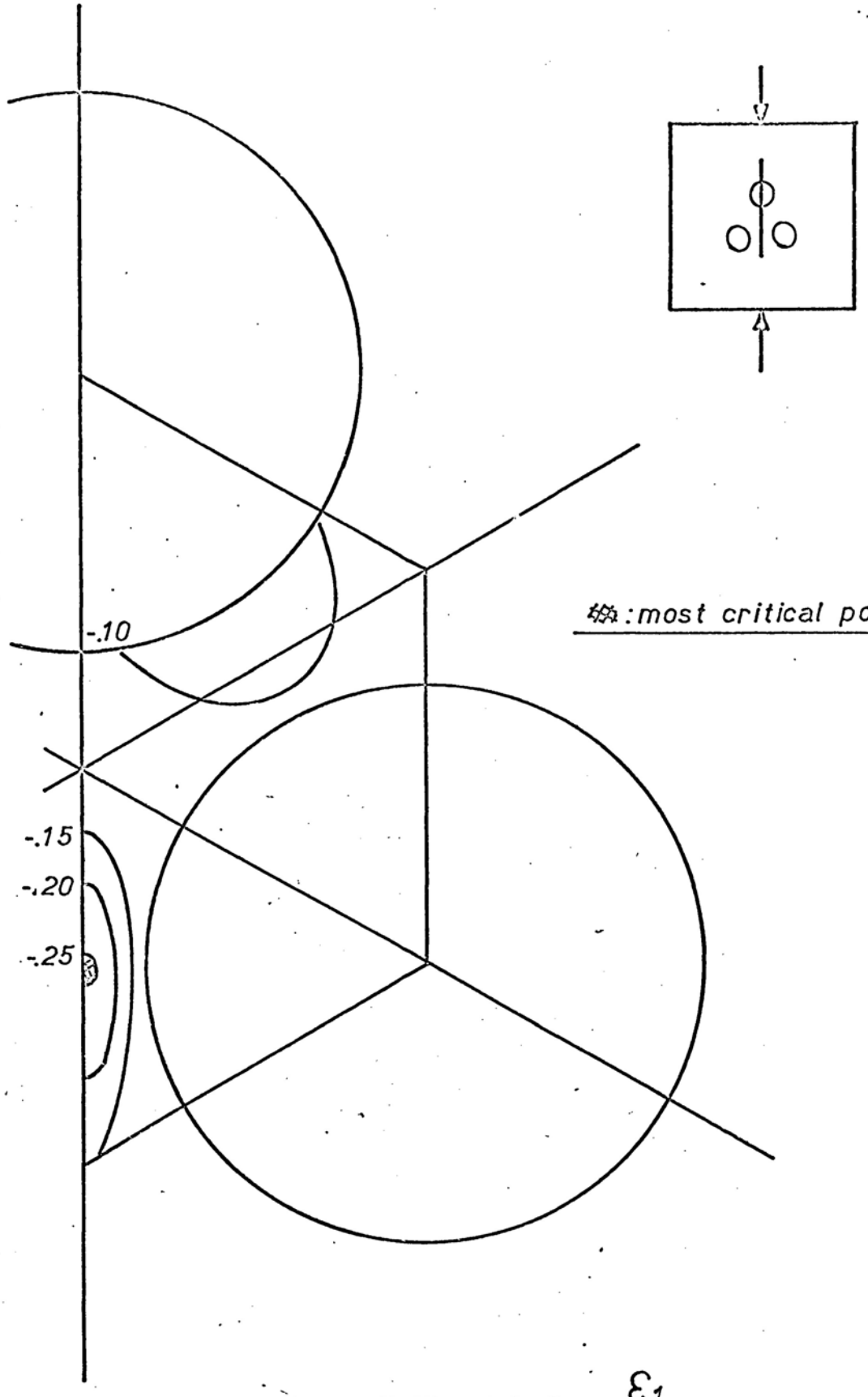
MPB -3- $V_f = 49.25\%$



ISOTENICS $\frac{\varepsilon_3}{(\varepsilon_3)_f}$

fig. 5-18

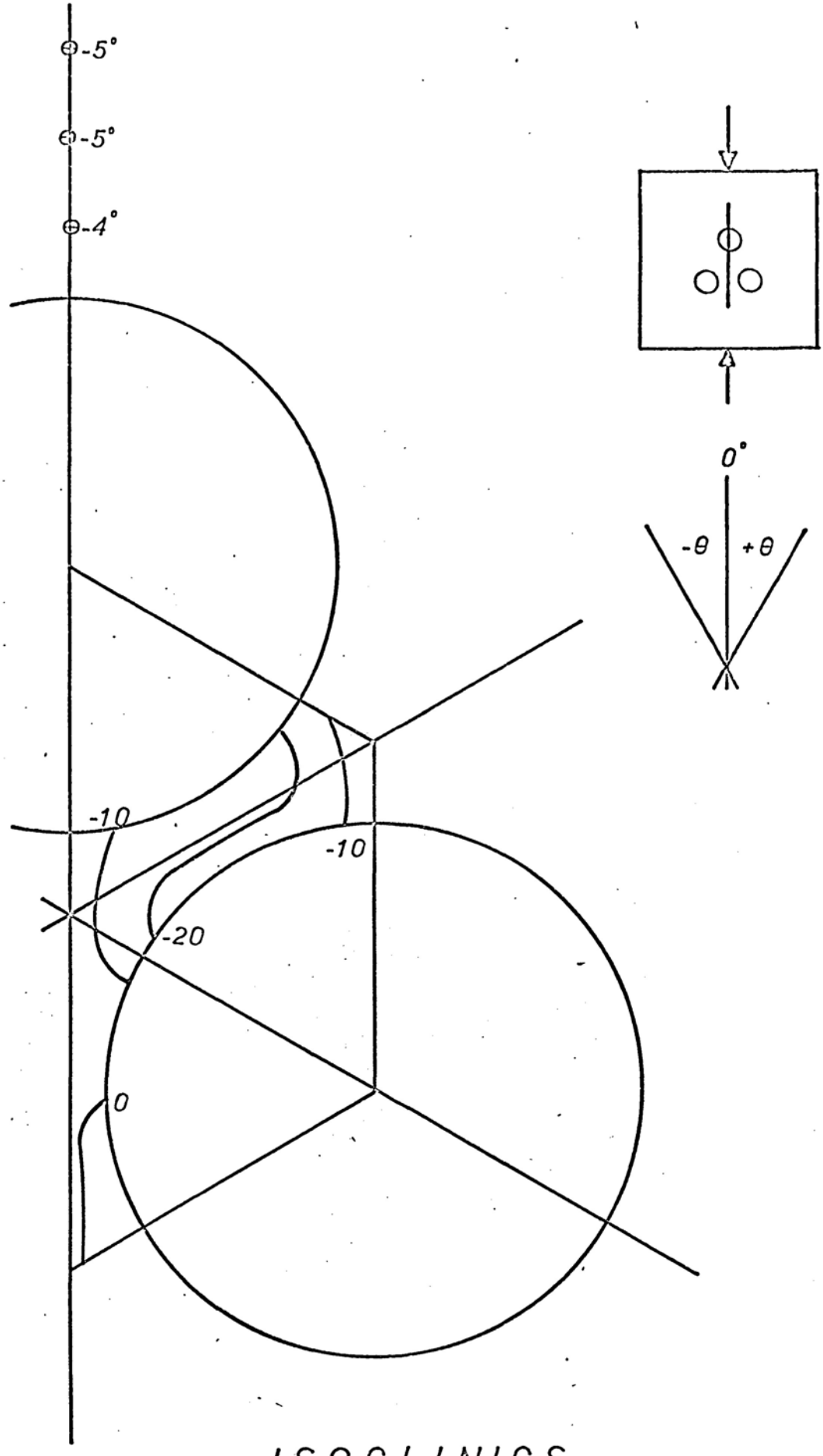
MPB -3- $V_f = 49.25\%$



ISOTENICS $\frac{\varepsilon_1}{(\varepsilon_3)_f}$

fig. 5-19

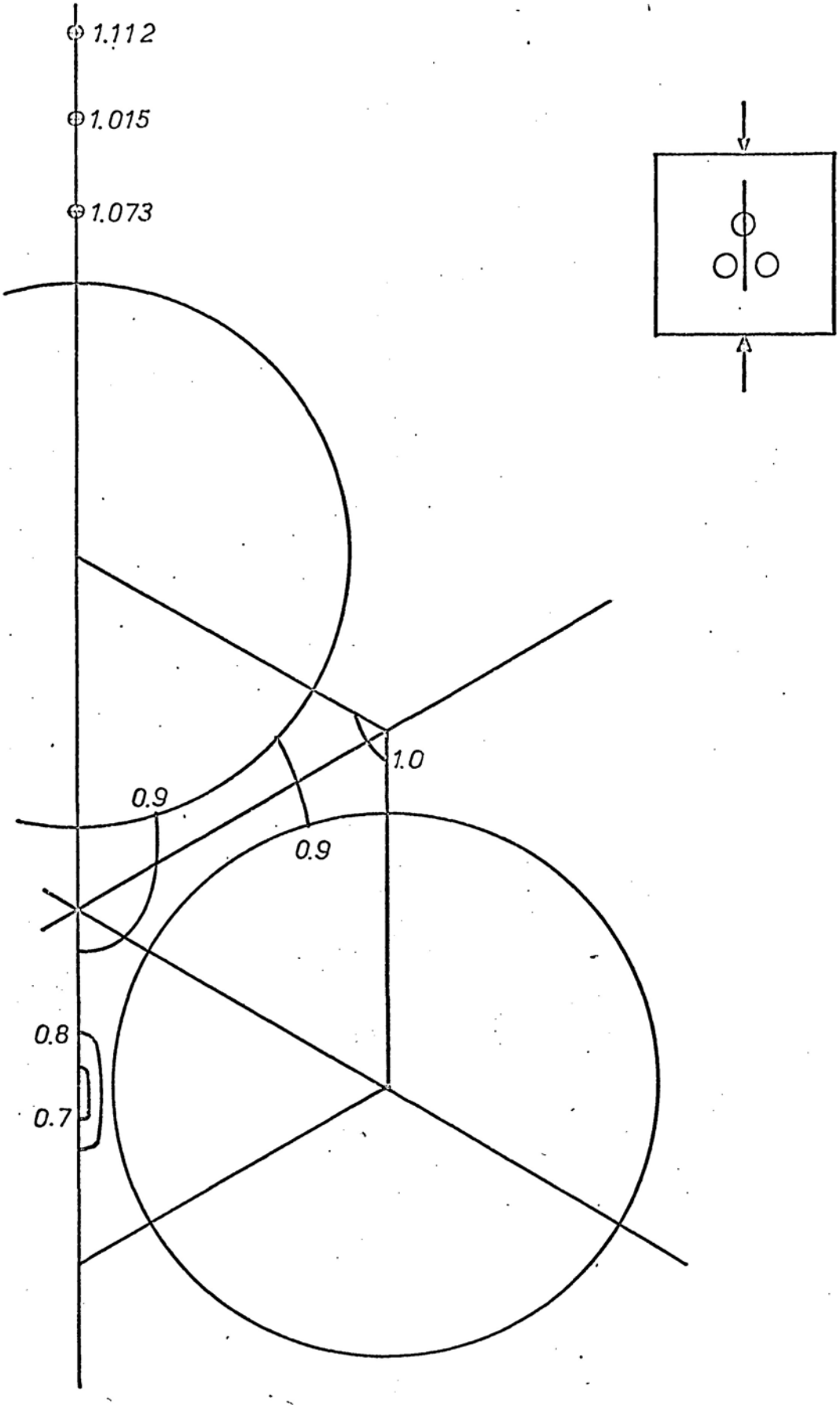
MPB -4- V_f = 59.5 %



ISOCLINICS

fig. 5-20

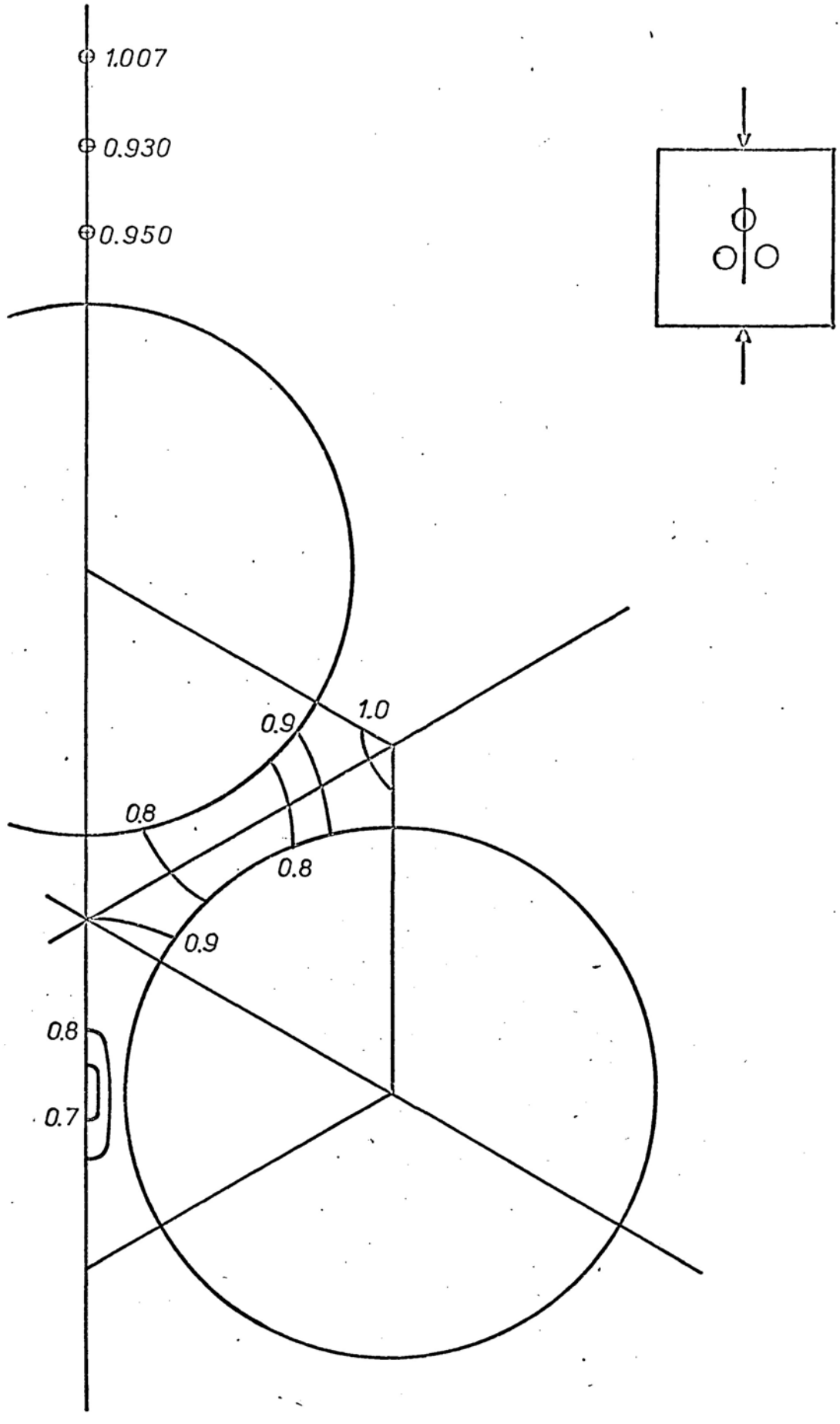
MPB -4- $V_f = 59.5\%$



ISOCHROMATICS $\frac{\varepsilon_3-\varepsilon_1}{(\varepsilon_3-\varepsilon_1)_f}$

fig. 5-21

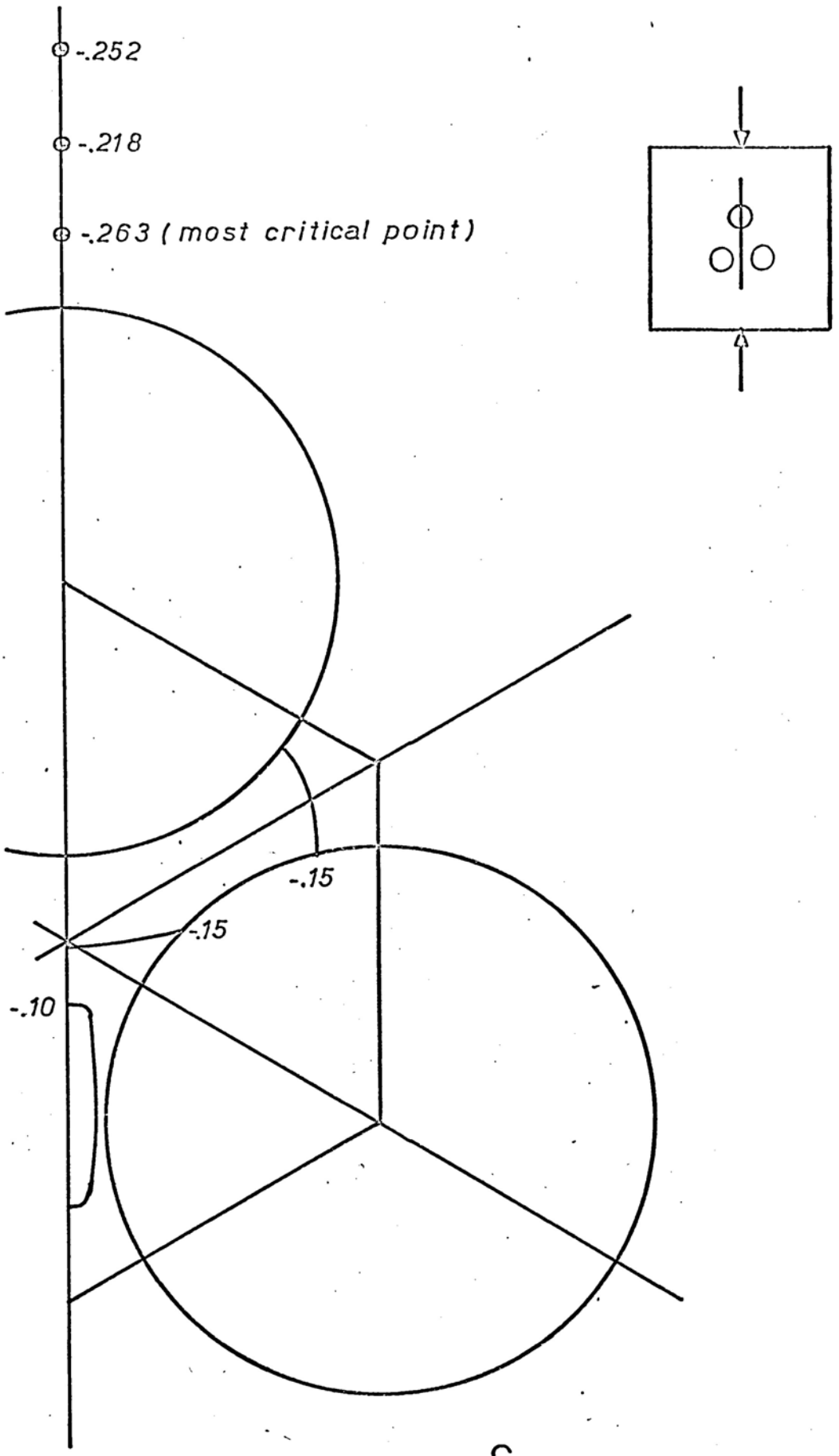
MPB-4- $V_f = 59.5\%$



ISOTENICS $\frac{\varepsilon_3}{(\varepsilon_3)_f}$

fig. 5-22

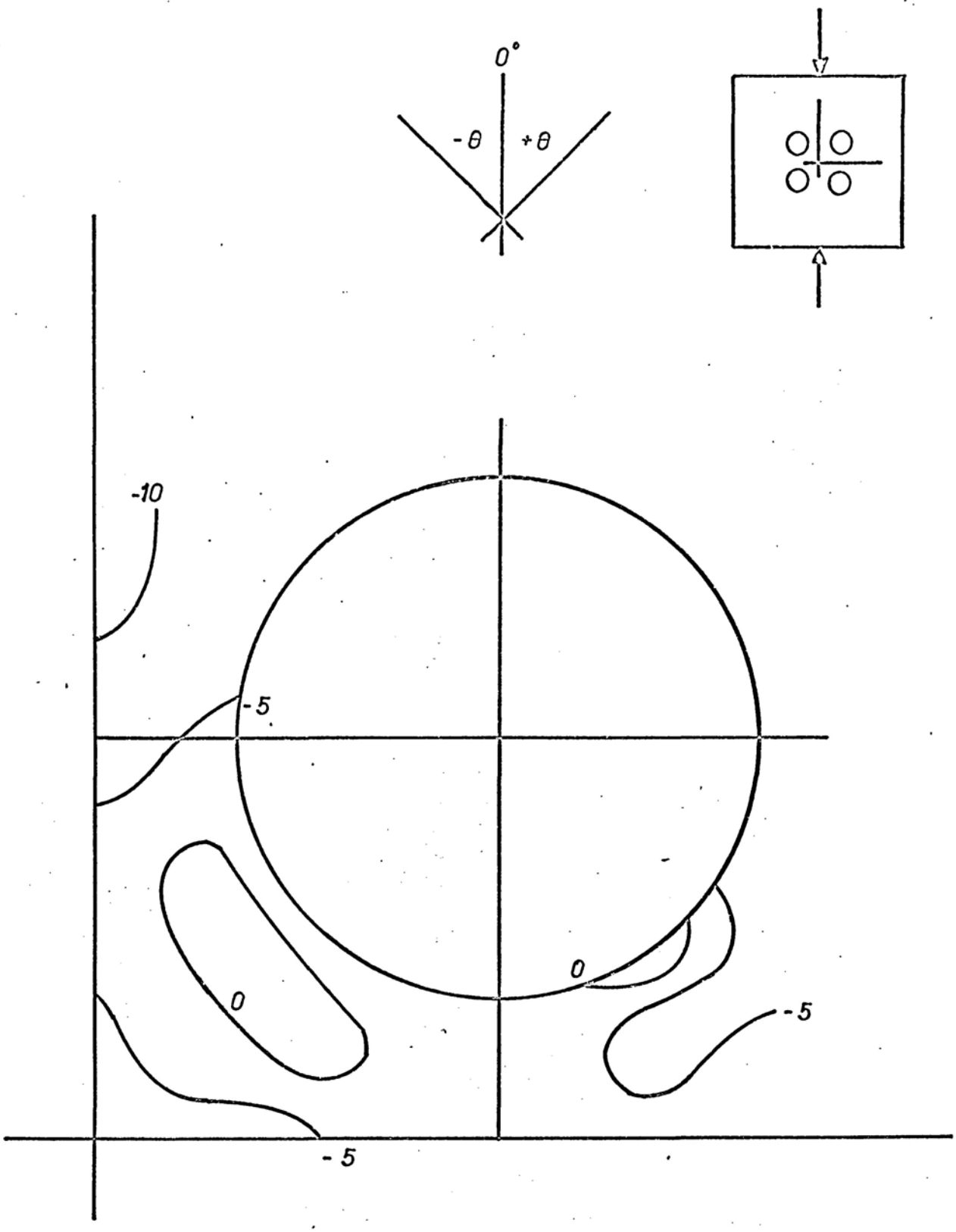
MPB-4- $V_f = 59.5\%$



ISOTENICS $\frac{\varepsilon_1}{(\varepsilon_3)_f}$

fig. 5-23

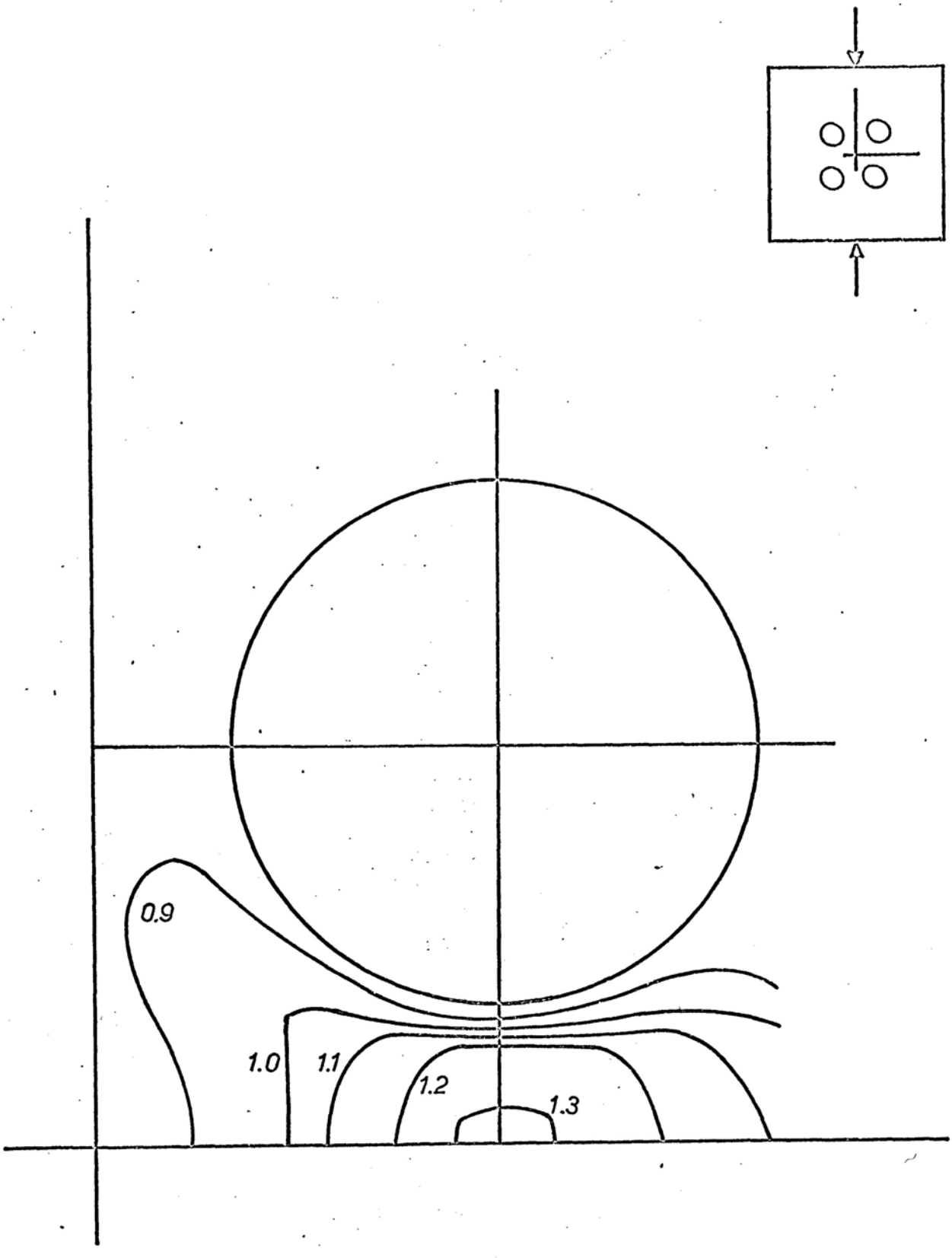
MPA-1 - V_f = 28 %



ISOCLINICS

fig. 5-24

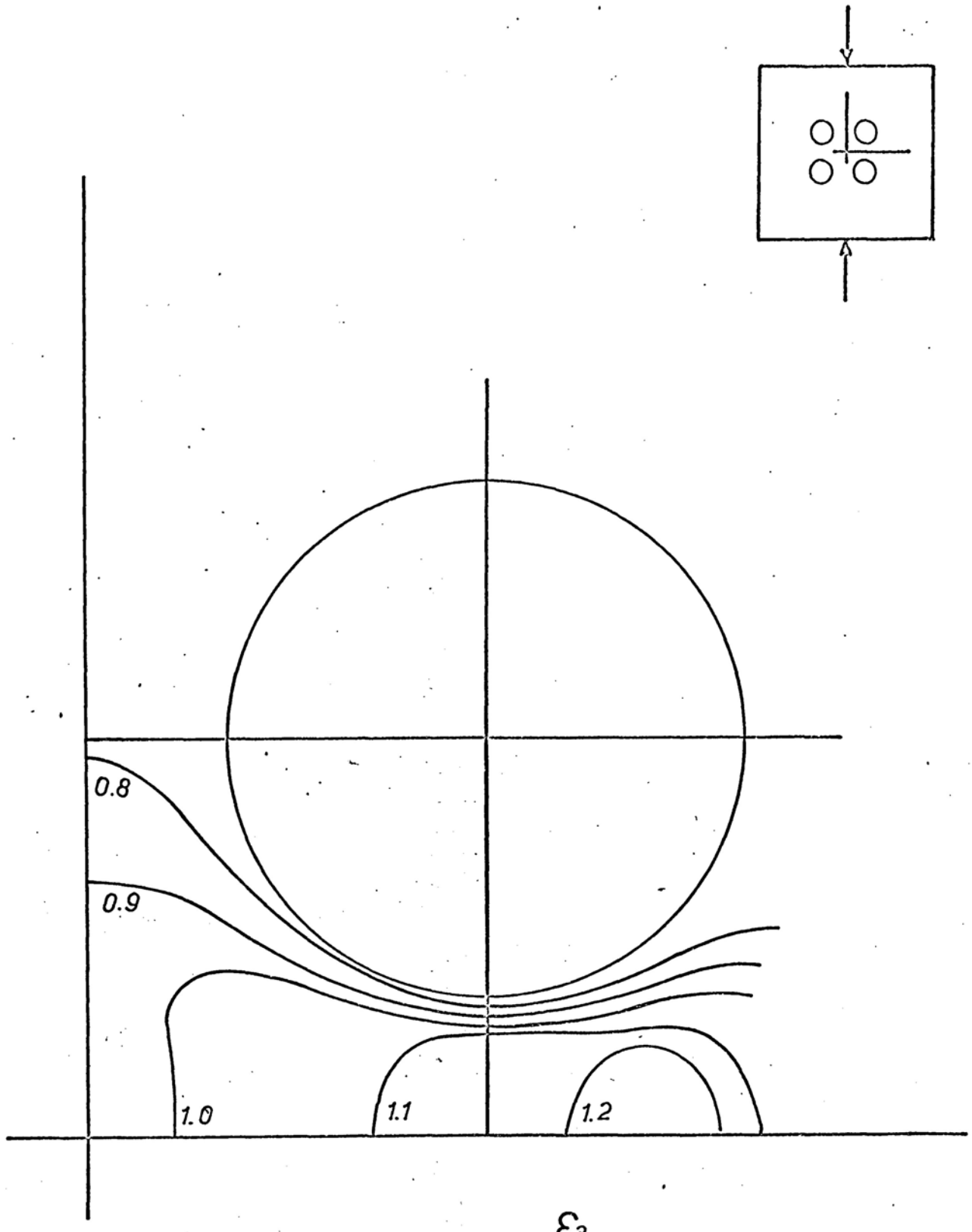
MPA-1 - $V_f = 28\ \%$



ISOCHROMATICS $\frac{\varepsilon_3 - \varepsilon_1}{(\varepsilon_3 - \varepsilon_1)_f}$

fig. 5-25

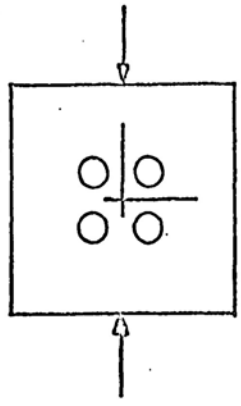
MPA -1- $V_f = 28\ \%$

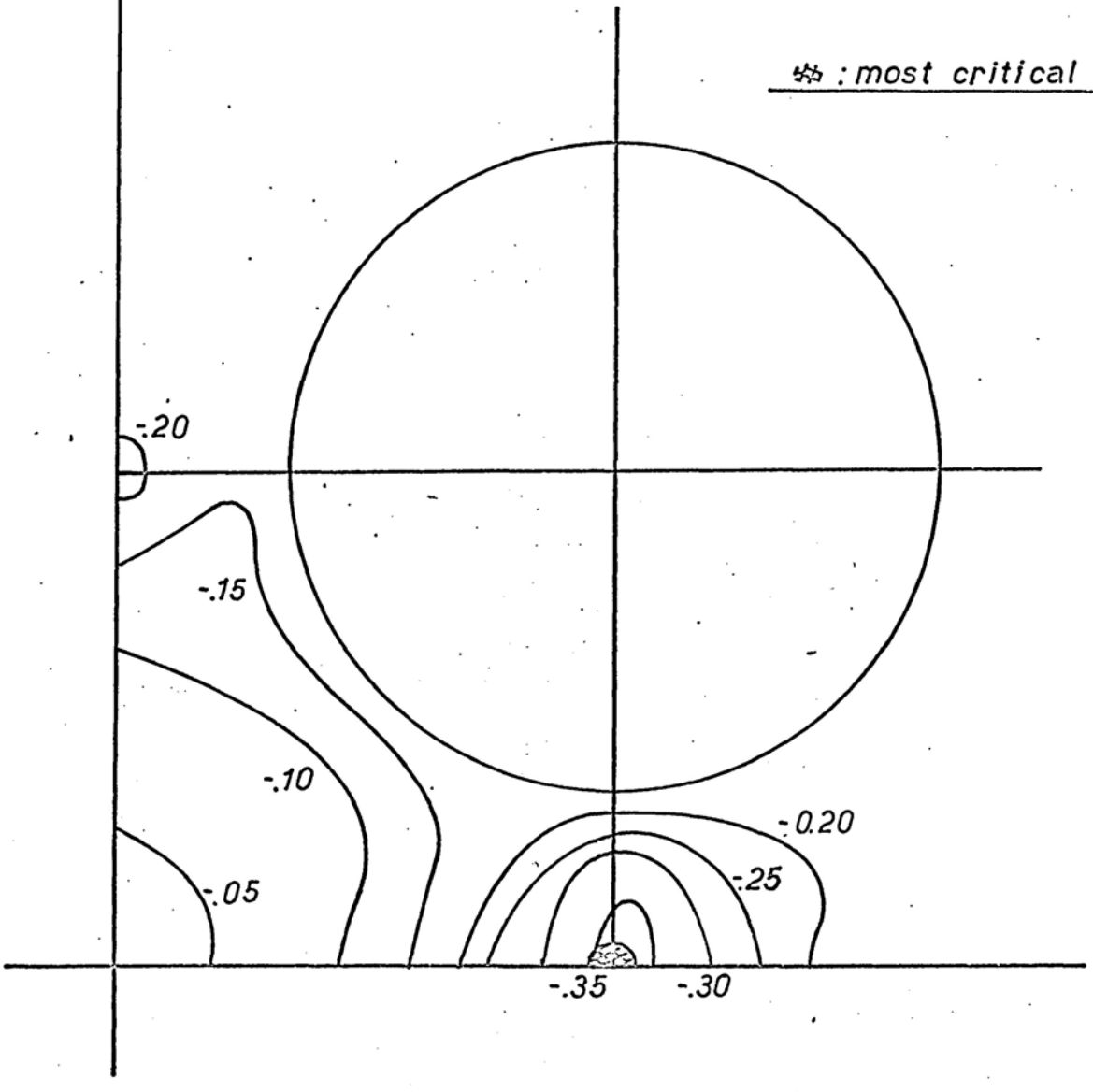


ISOTENICS $\frac{\varepsilon_3}{(\varepsilon_3)_f}$

fig. 5-26

MPA - 1 - V_f = 28 %

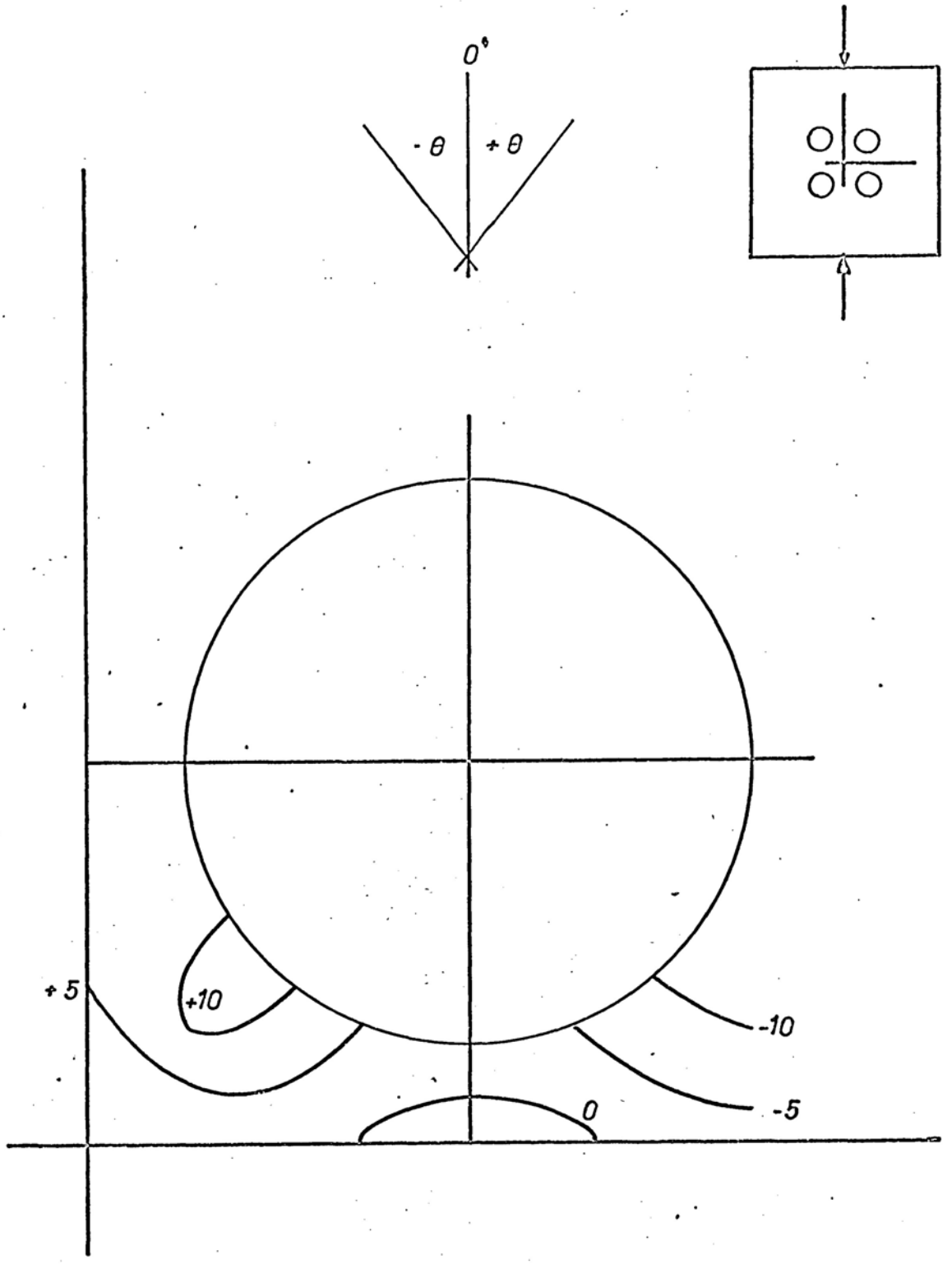




ISOTENICS $\frac{\varepsilon_1}{(\varepsilon_3)_f}$

fig. 5-27

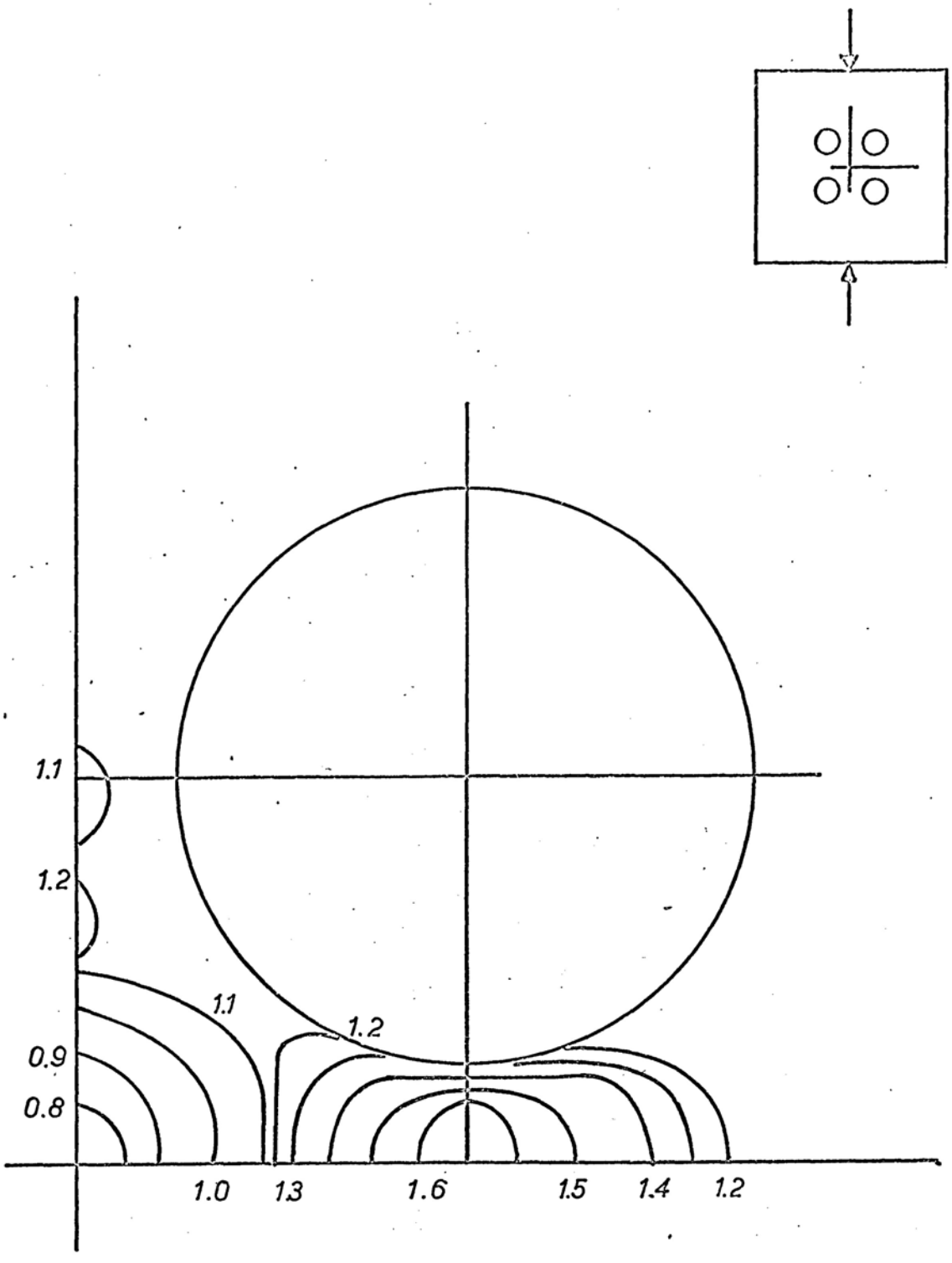
MPA -2- $V_f = 33.5\ \%$



ISOCLINICS

fig. 5-28

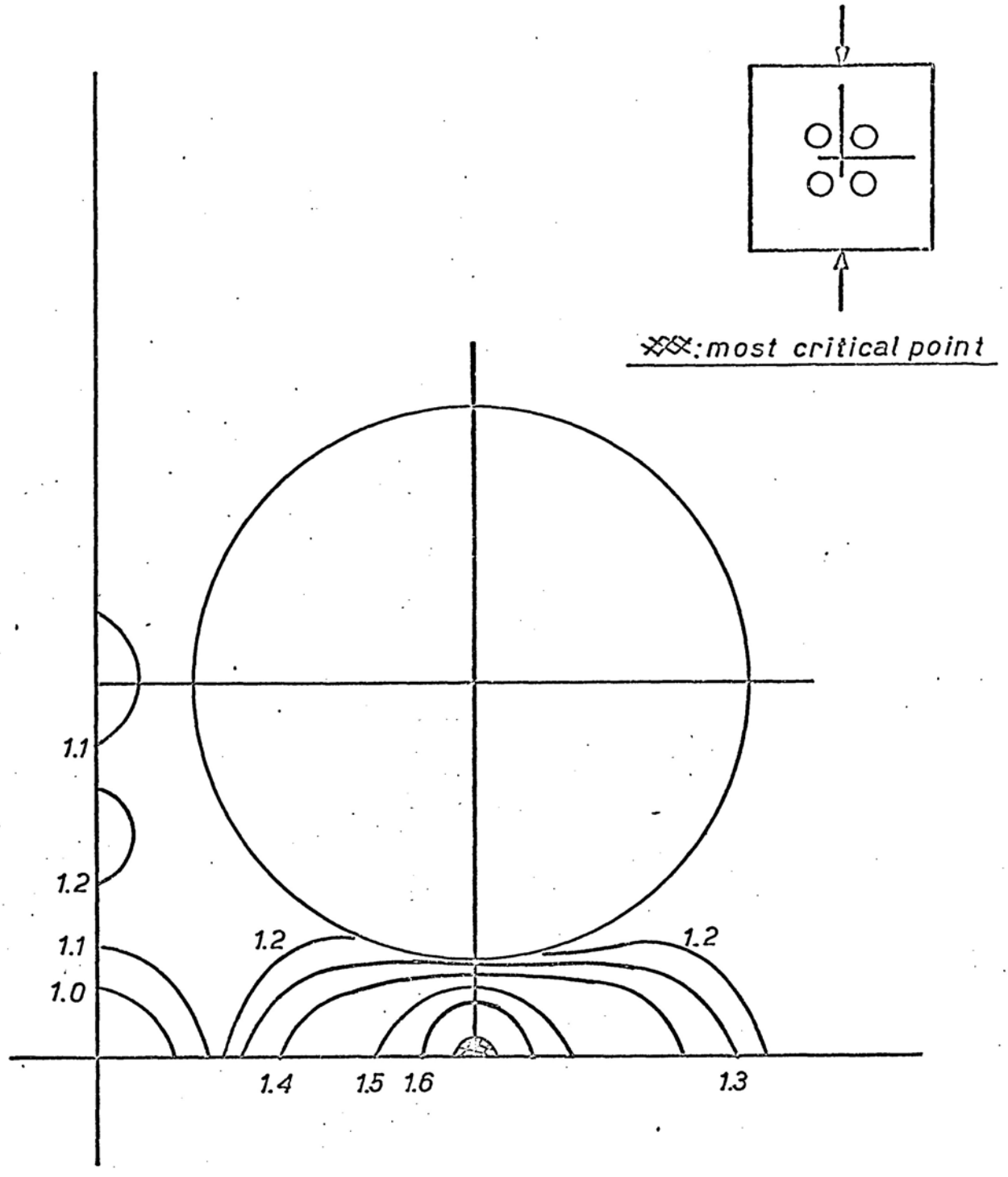
MPA - 2 - $V_f = 33.5\%$



ISOCHROMATICS $\frac{\varepsilon_3 - \varepsilon_1}{(\varepsilon_3 - \varepsilon_1)_f}$

fig. 5-29

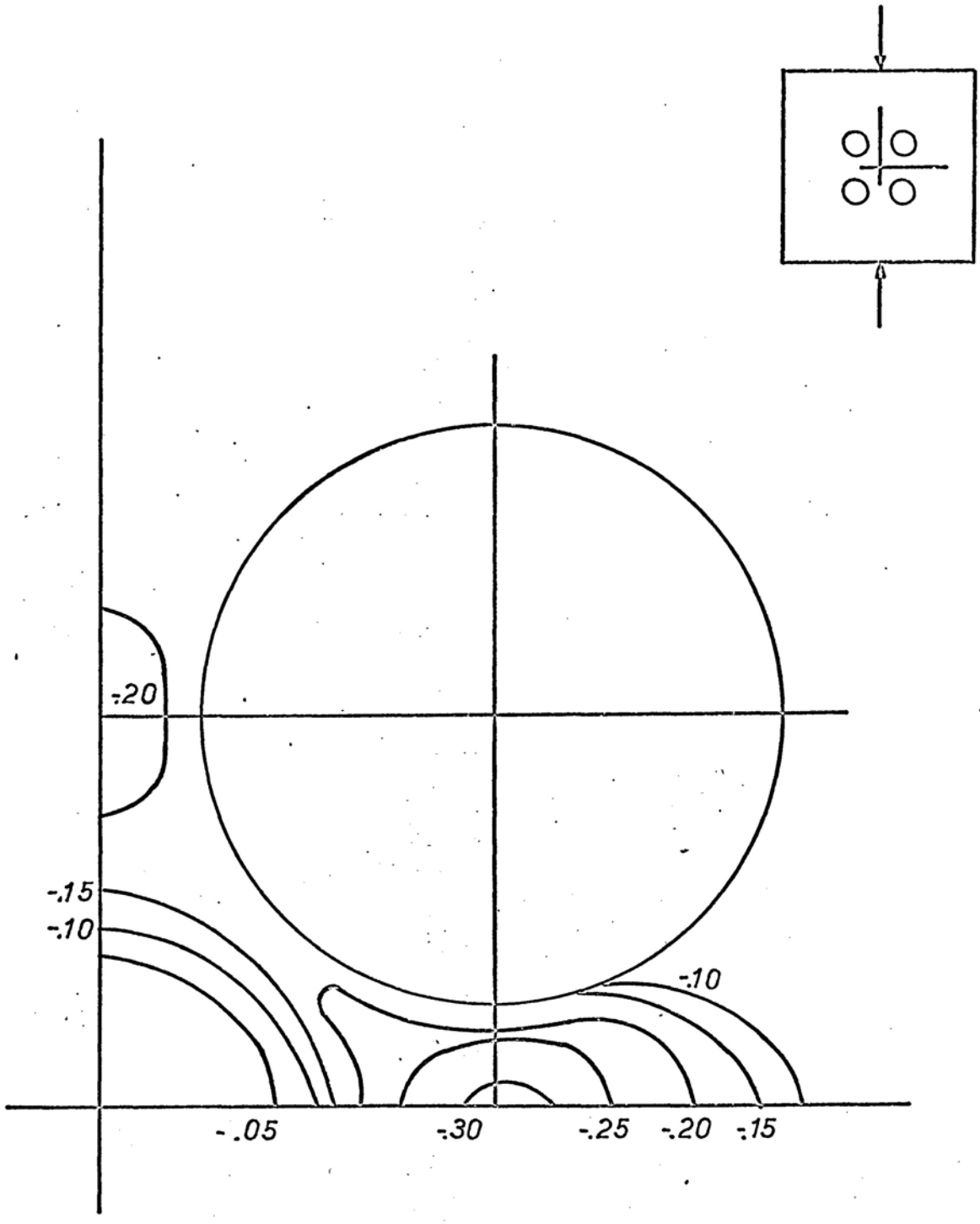
MPA - 2 - $V_f = 33.5\ \%$



ISOTENICS $\frac{\varepsilon_3}{(\varepsilon_3)_f}$

fig. 5-30

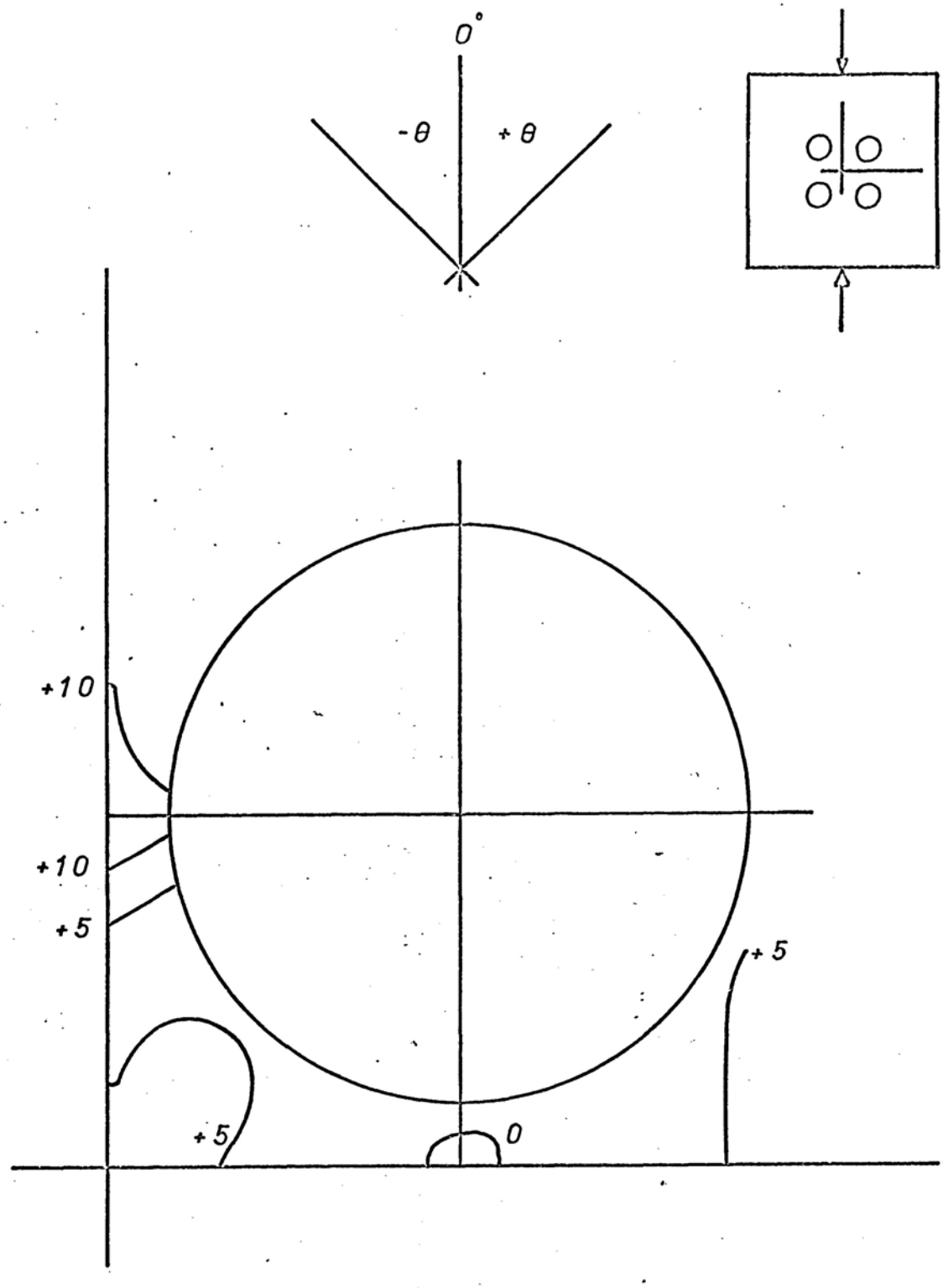
MPA - 2 - $V_f = 33.5\ \%$



ISOTENICS $\frac{\varepsilon_1}{(\varepsilon_3)_f}$

fig. 5-31

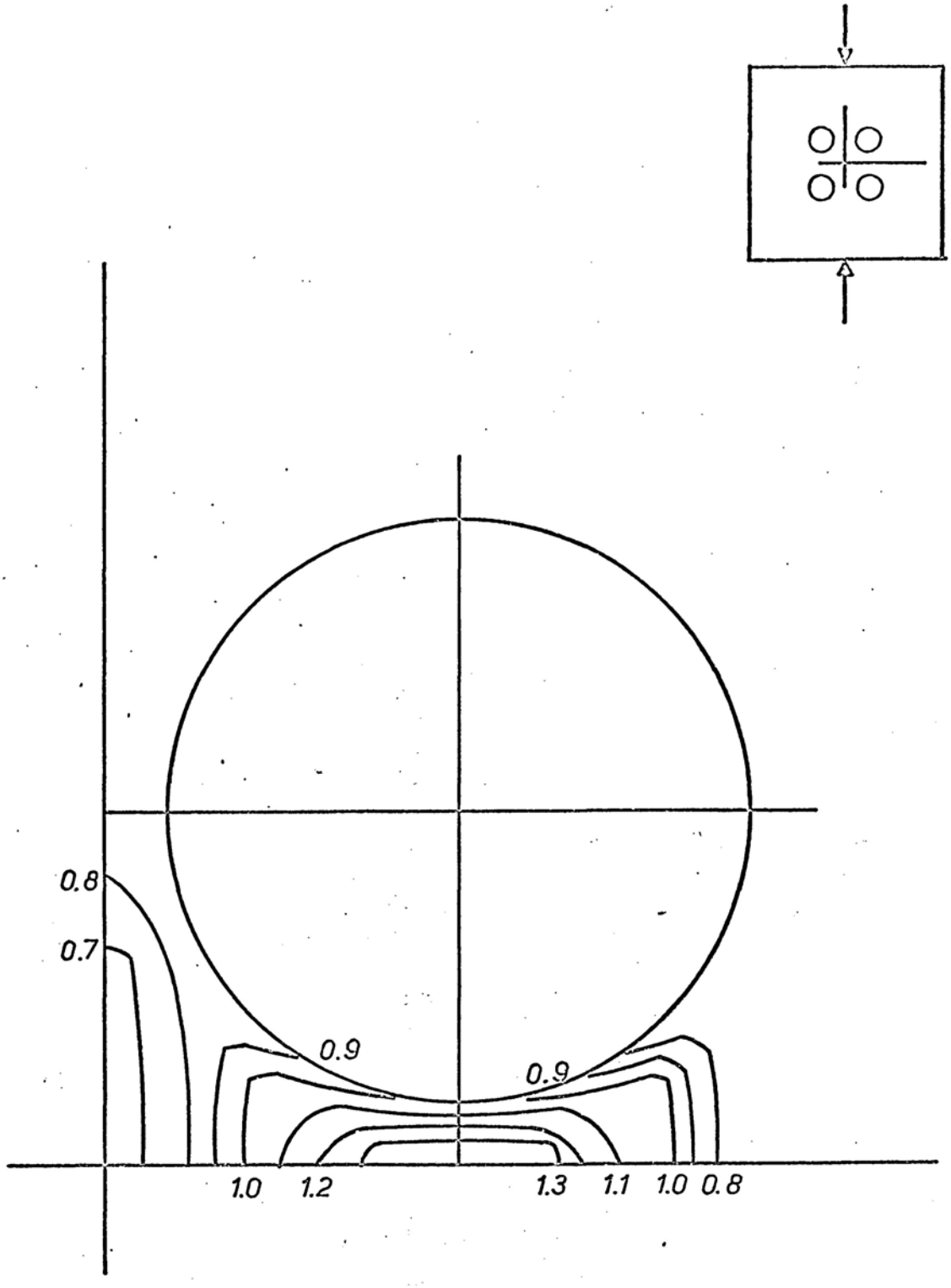
MPA - 3 - $V_f = 39.25\%$



ISOCLINICS

fig. 5-32

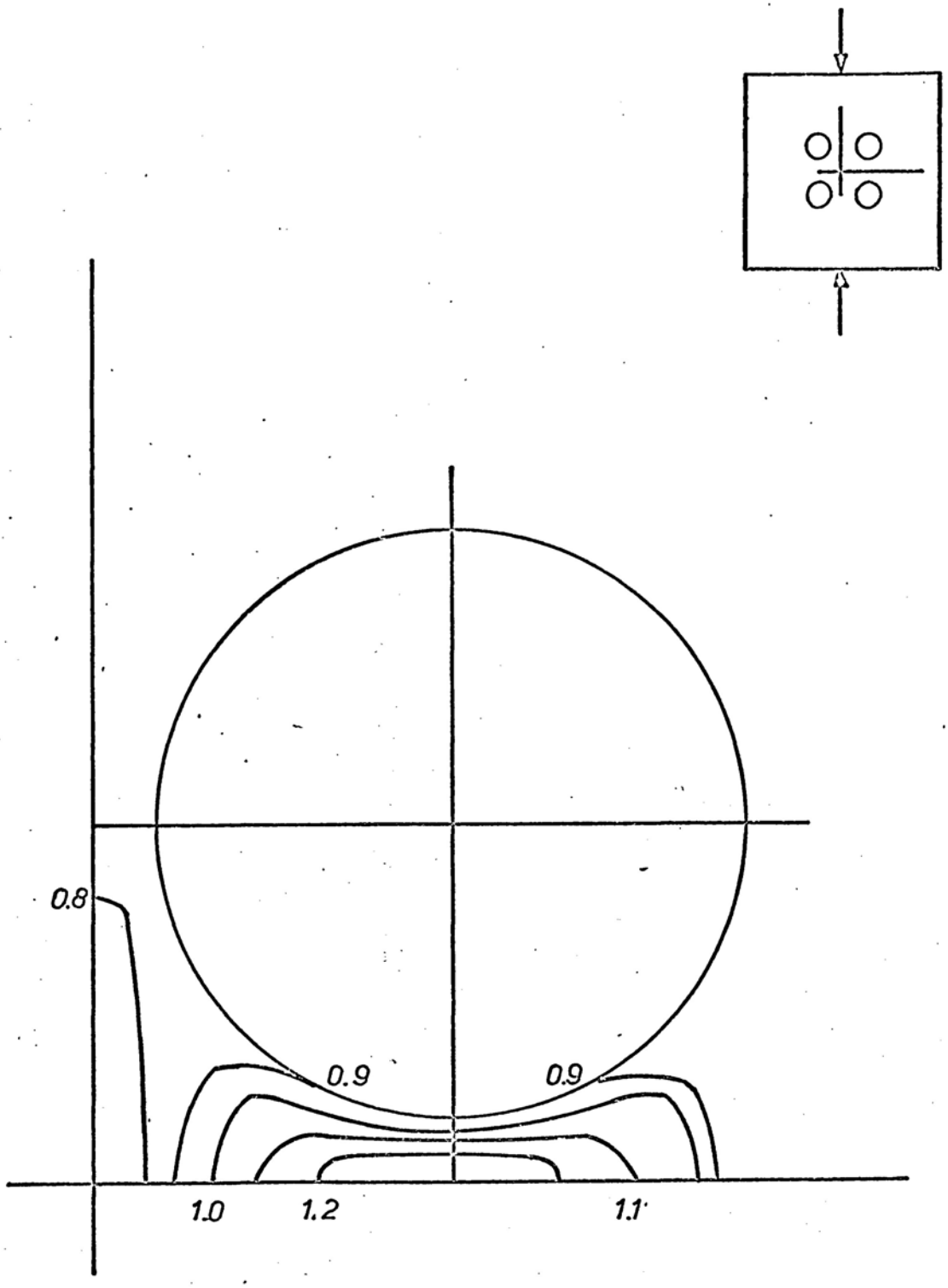
MPA - 3 - $V_f = 39.25\ \%$



ISOCHROMATICS $\frac{\varepsilon_3 - \varepsilon_1}{(\varepsilon_3 - \varepsilon_1)_f}$

fig. 5-33

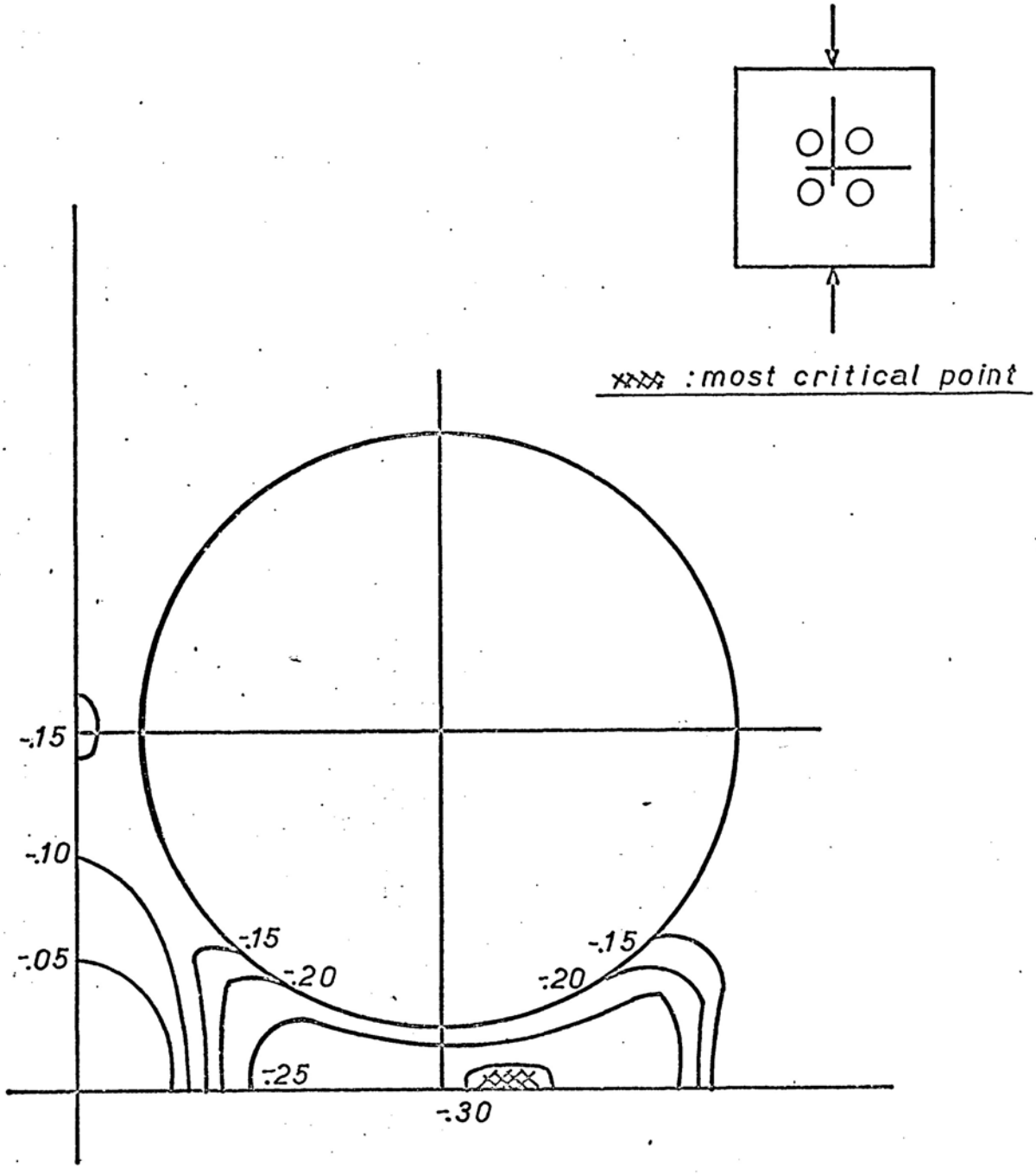
MPA - 3 - $V_f = 39.25\ \%$



ISOTENICS $\frac{\varepsilon_3}{(\varepsilon_3)_f}$

fig. 5-34

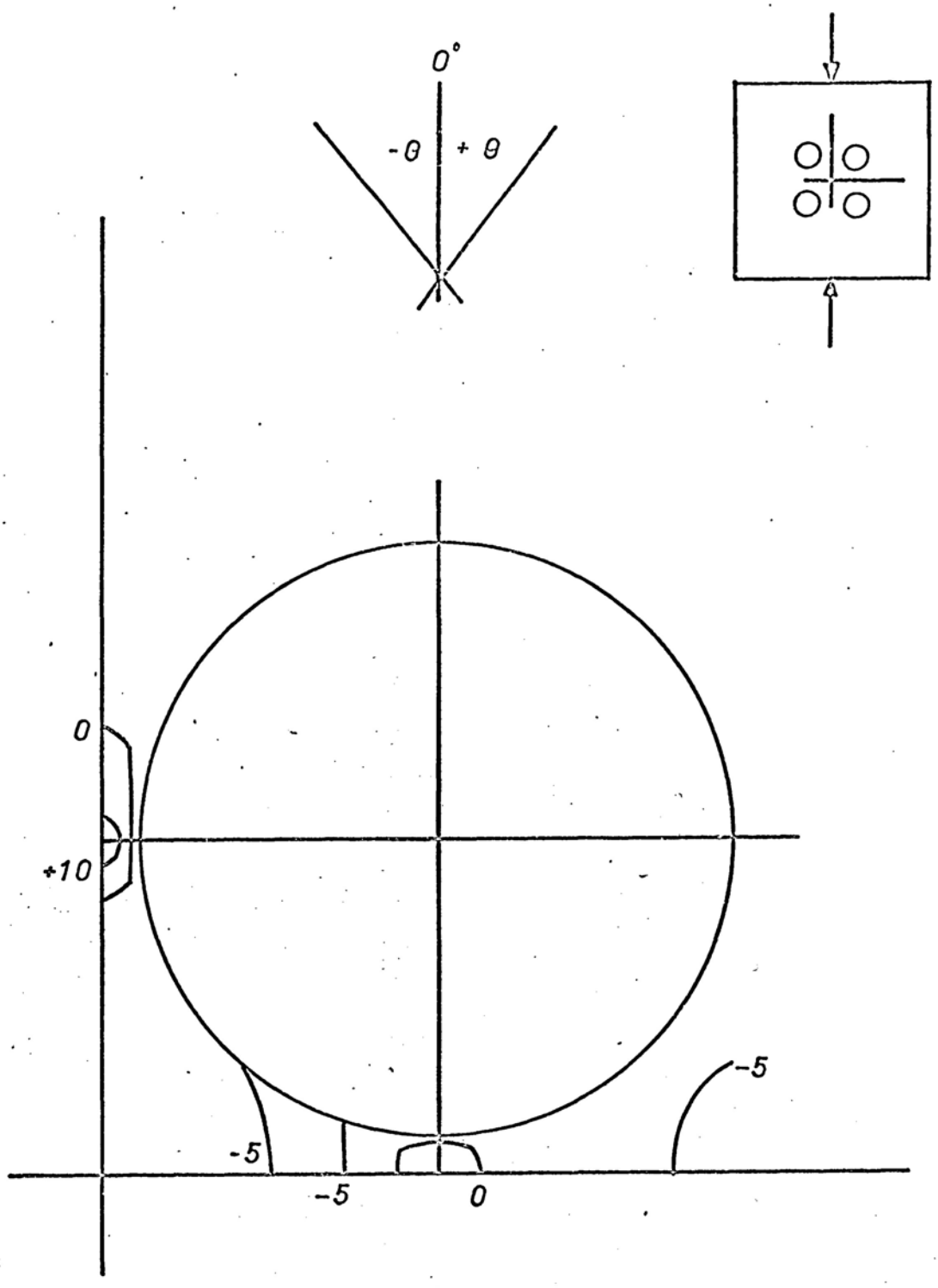
MPA - 3 - V_f = 39.25 %



ISOTENICS $\frac{\varepsilon_1}{(\varepsilon_3)_f}$

fig. 5-35

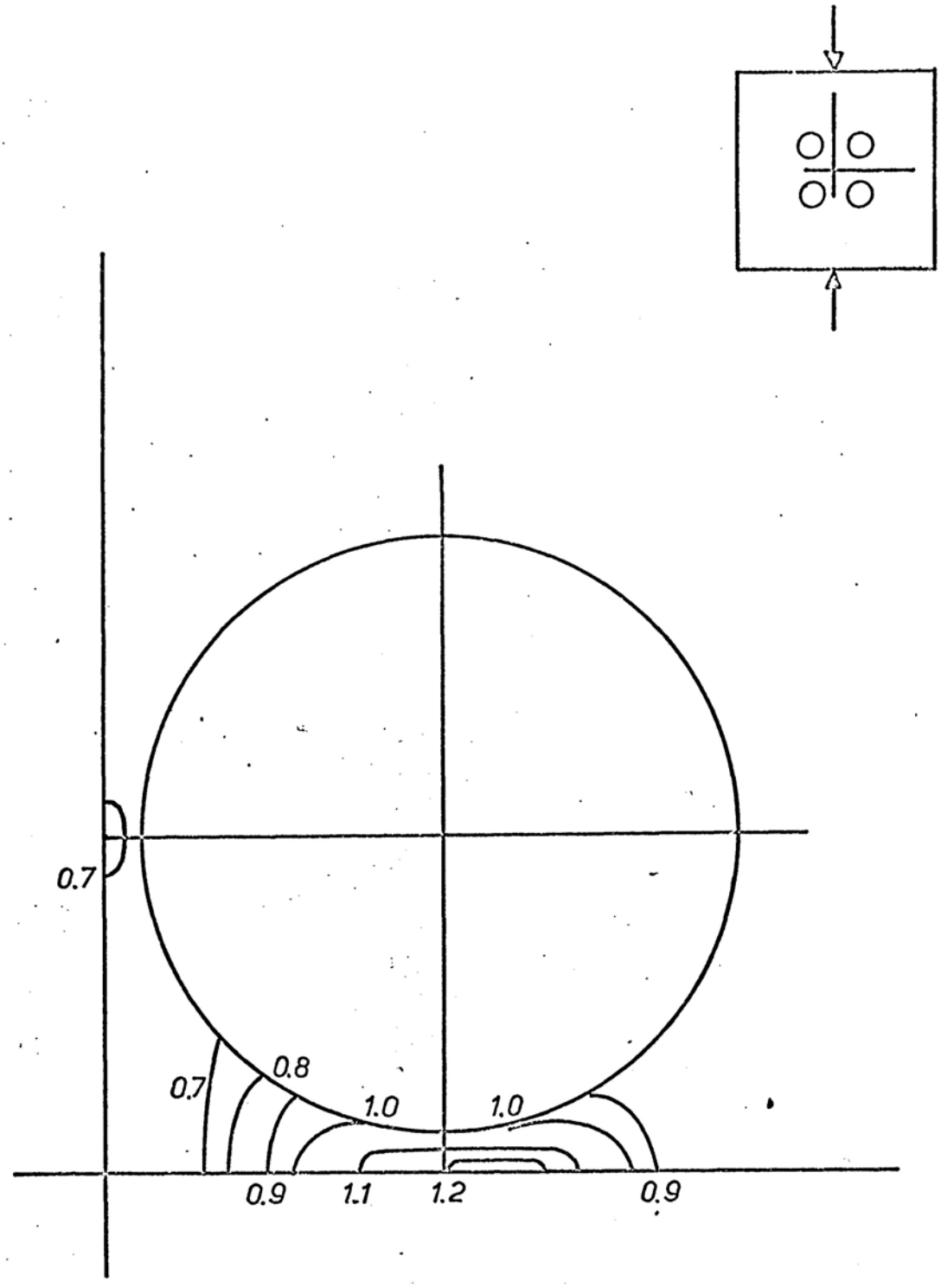
MPA-4- V_f = 46.5 %



ISOCLINICS

fig. 5-36

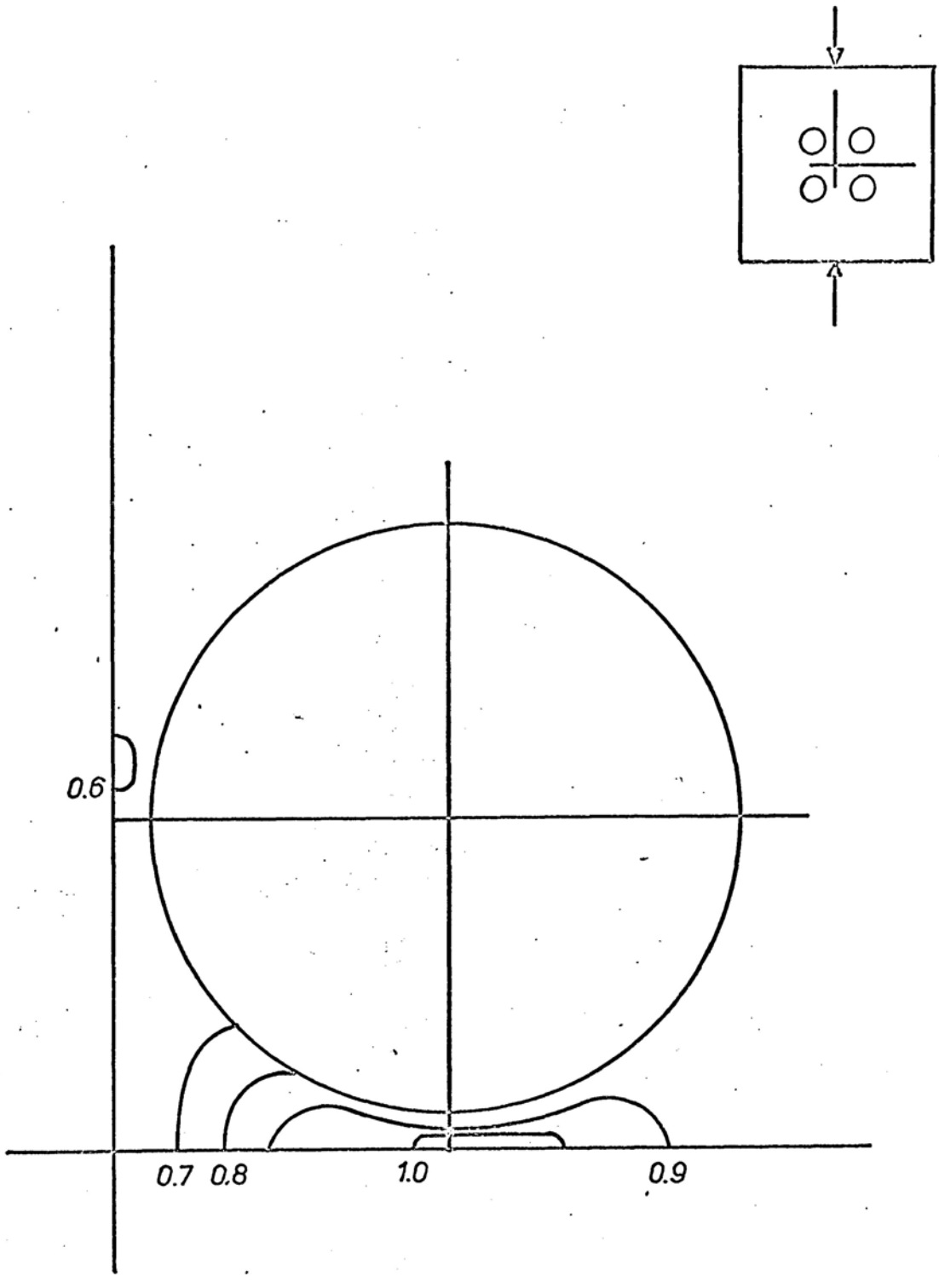
MPA - 4 - $V_f = 46.5\ \%$



ISOCHROMATICS $\frac{\varepsilon_3 - \varepsilon_1}{(\varepsilon_3 - \varepsilon_1)_f}$

fig. 5-37

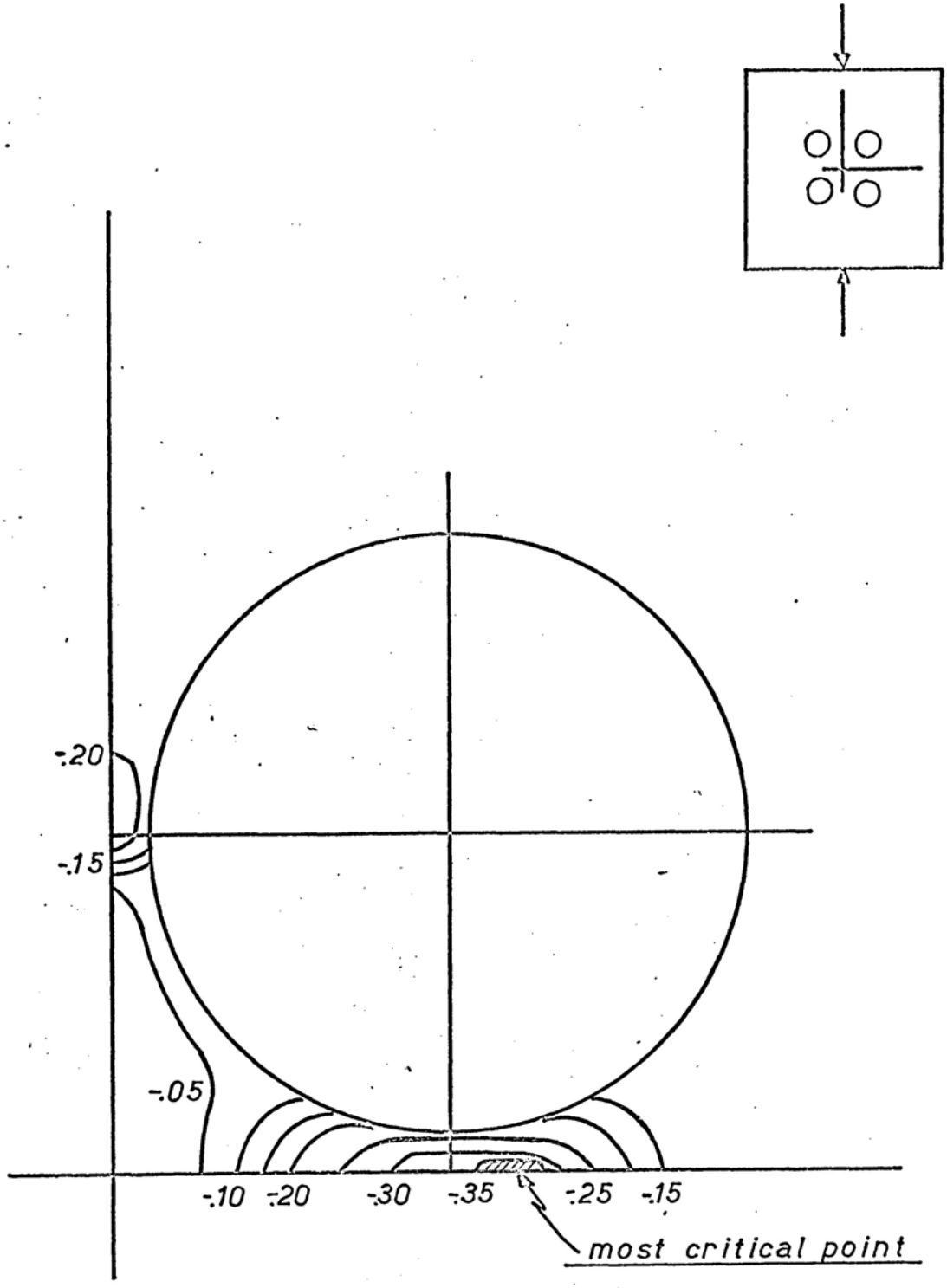
MPA - 4 - $V_f = 46.5\ \%$



ISOTENICS $\frac{\varepsilon_3}{(\varepsilon_3)_f}$

fig. 5-38

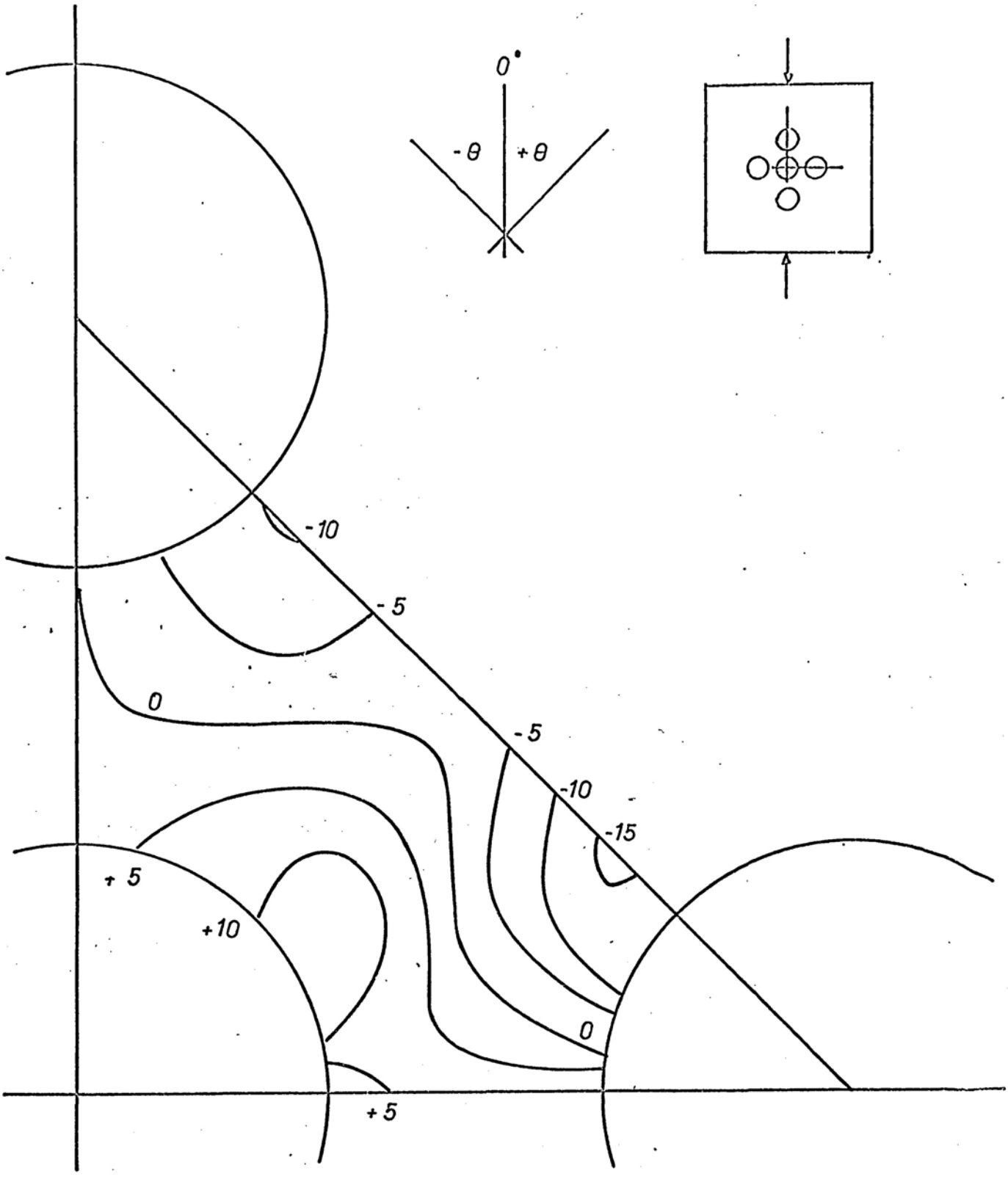
MPA - 4 - $V_f = 46.5\%$



ISOTENICS $\frac{\varepsilon_1}{(\varepsilon_3)_f}$

fig. 5-39

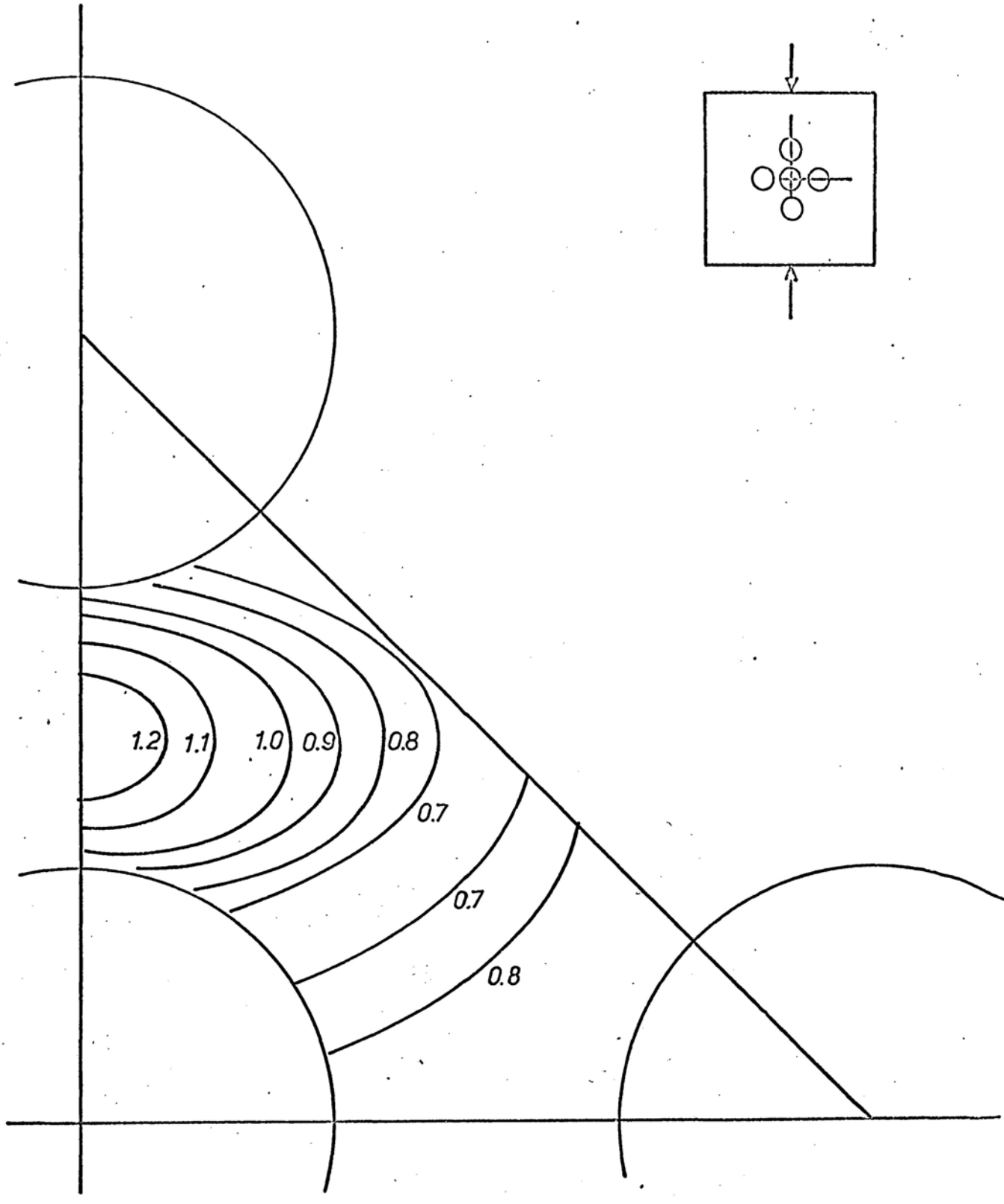
MPC -1- V_f = 27 %



ISOCLINICS

fig. 5-40

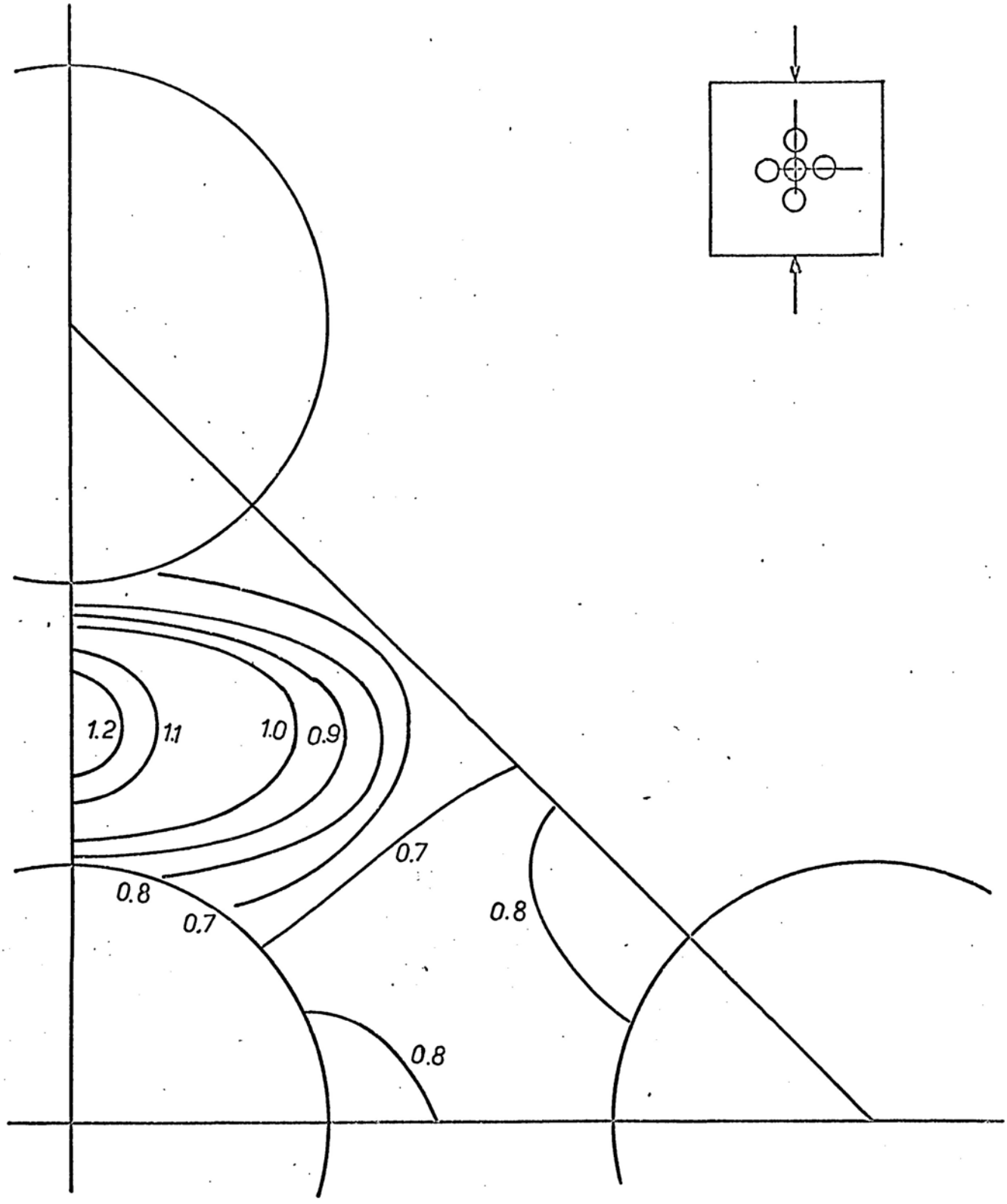
MPC-1 - V_f =27%



ISOCHROMATICS $\frac{\varepsilon_3-\varepsilon_1}{(\varepsilon_3-\varepsilon_1)_f}$

fig. 5-41

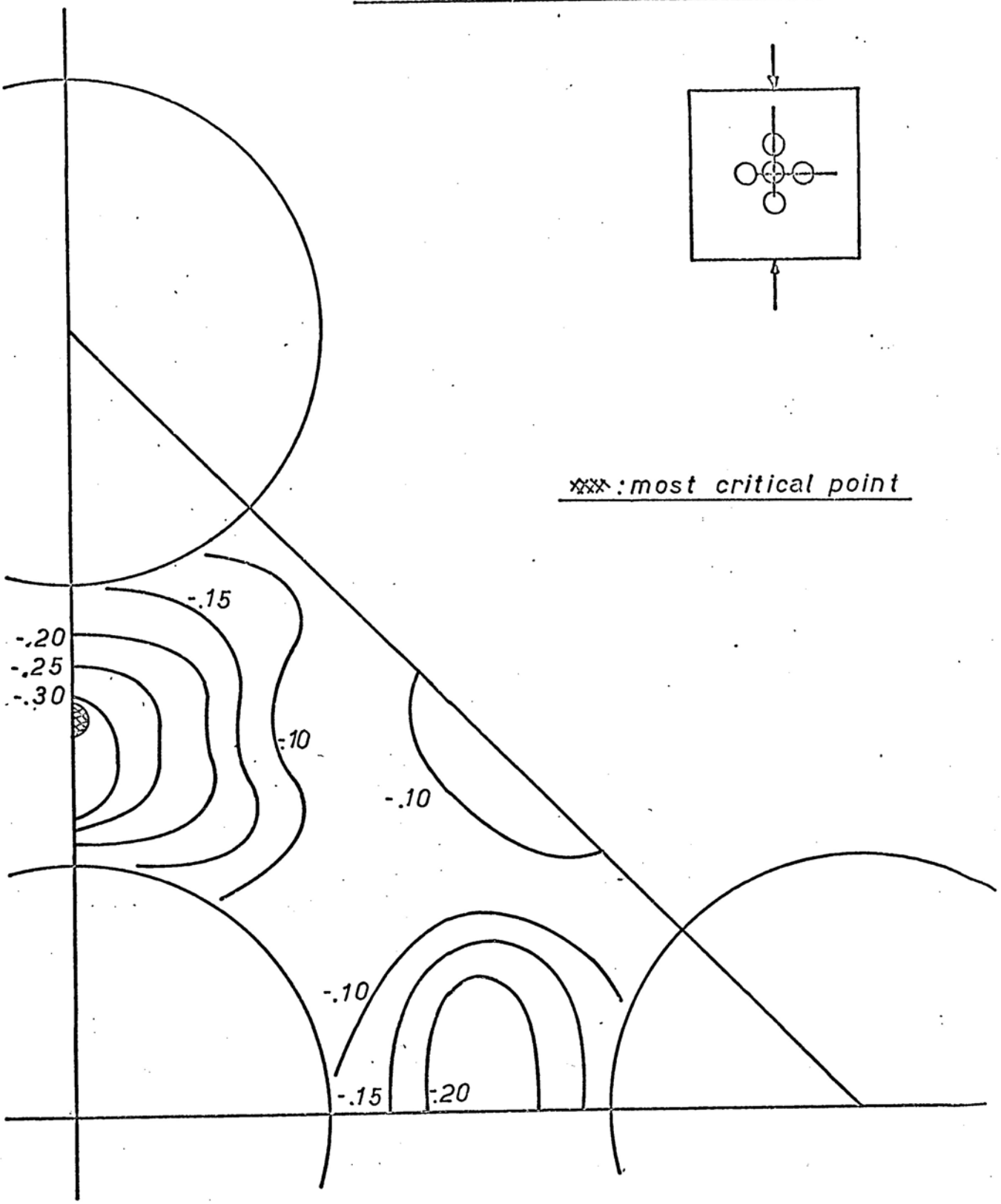
MPC - 1 - $V_f = 27\ \%$



ISOTENICS $\frac{\varepsilon_3}{(\varepsilon_3)_f}$

fig. 5-42

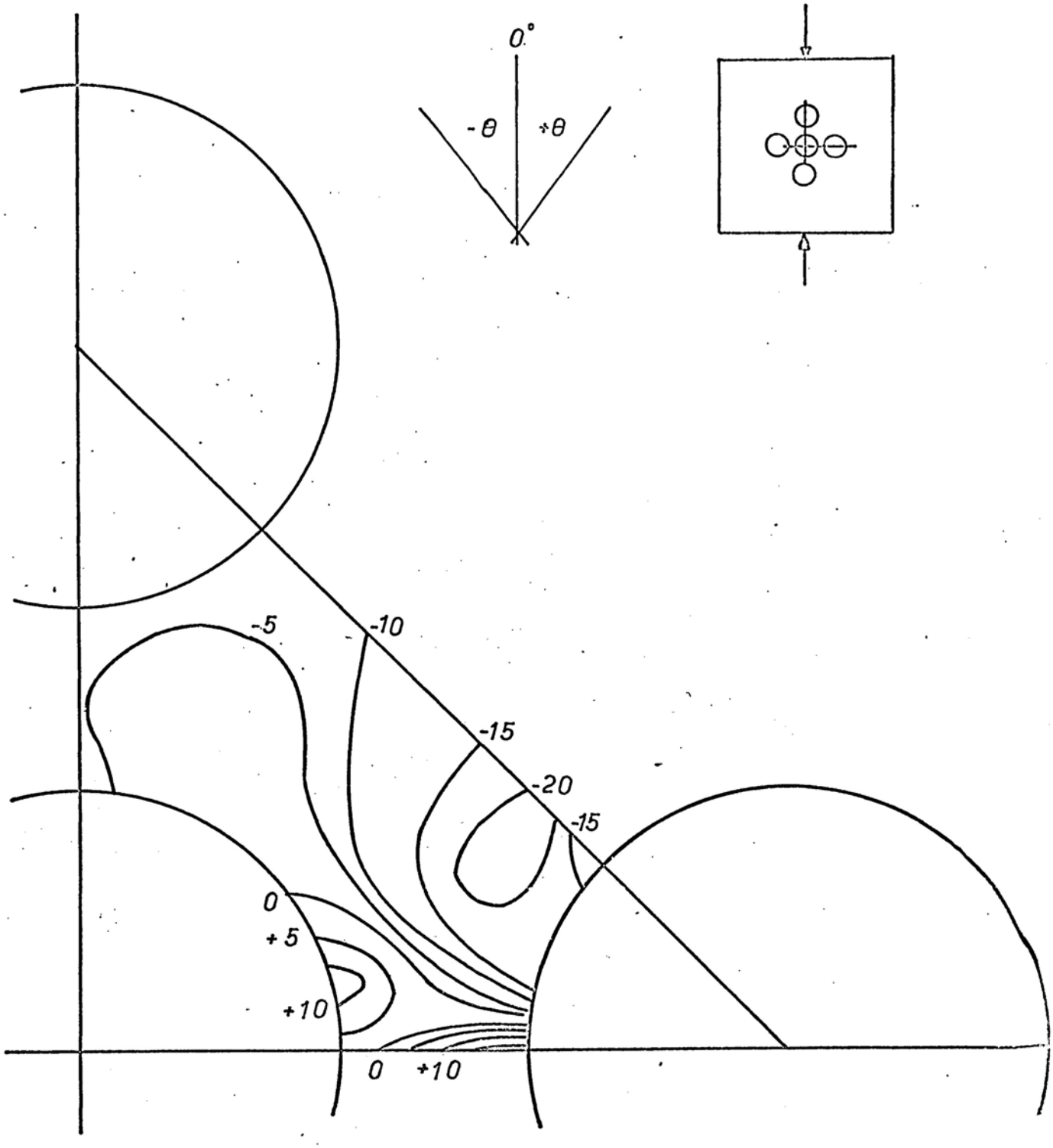
MPC -1- V_f = 27 %



ISOTENICS $\frac{\varepsilon_1}{(\varepsilon_3)_f}$

fig. 5-43

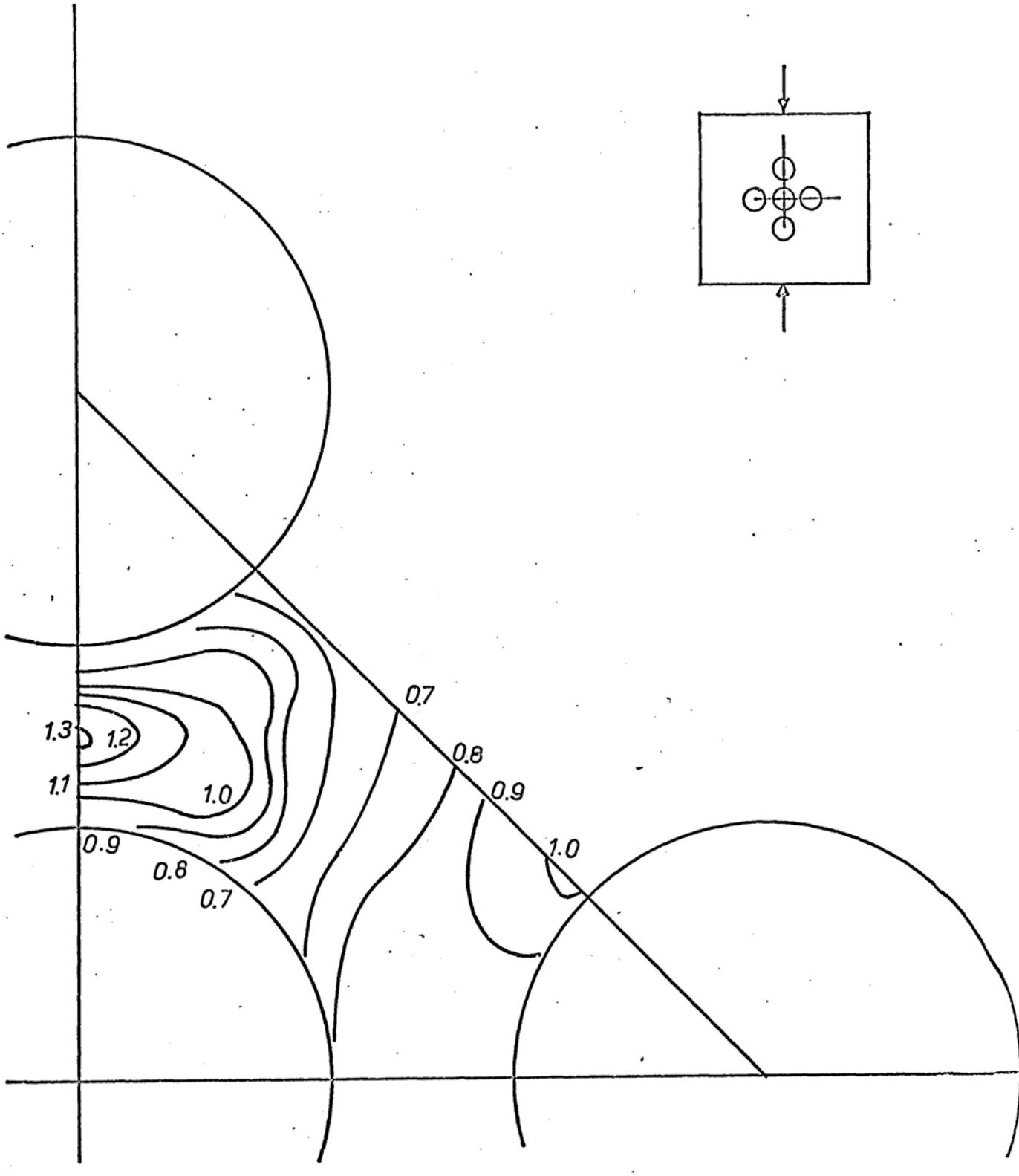
MPC -2- V_f = 32 %



ISOCLINICS

fig. 5-44

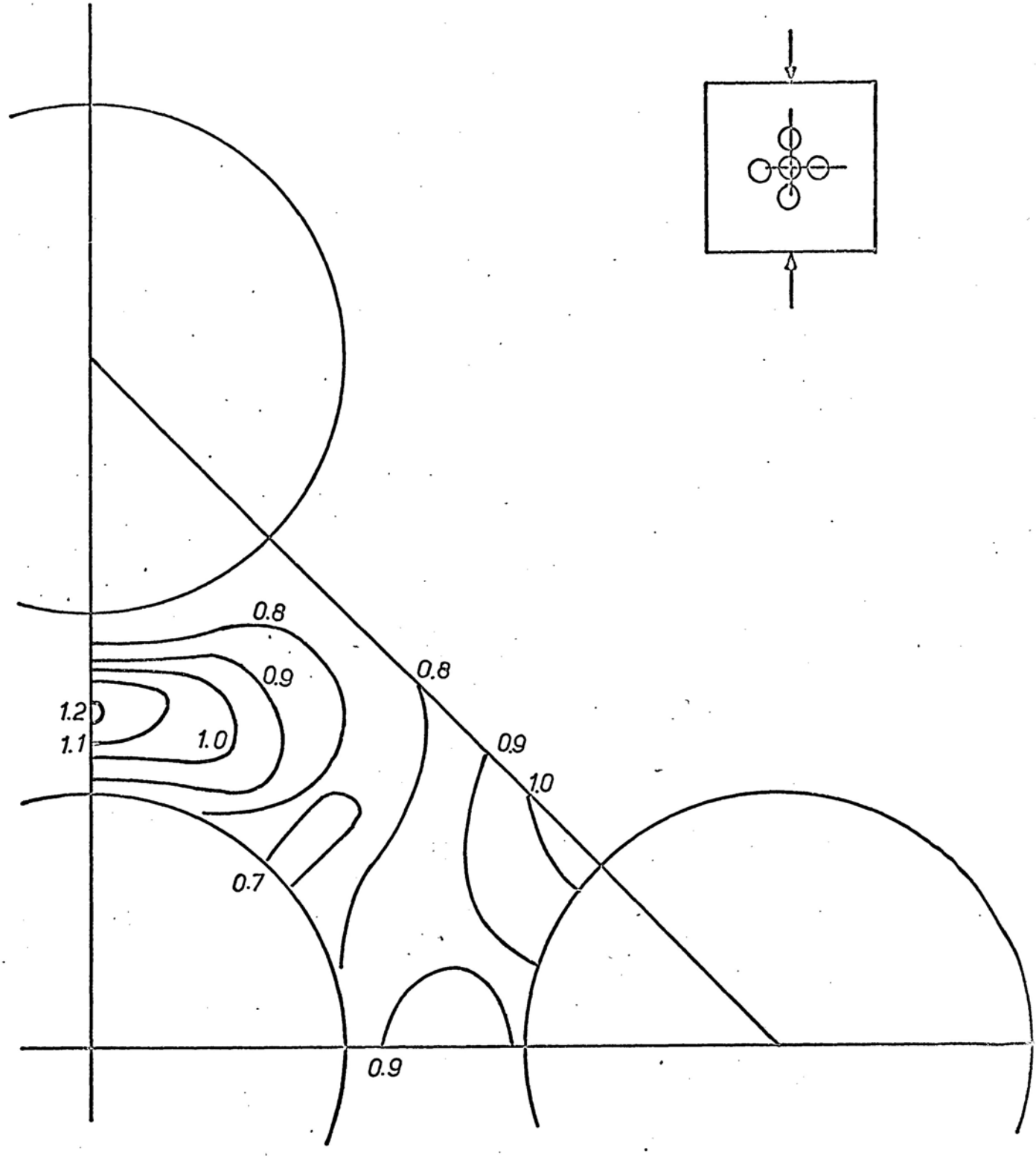
MPC -2- $V_f = 32\ \%$



ISOCHROMATICS $\frac{\varepsilon_3-\varepsilon_1}{(\varepsilon_3-\varepsilon_1)_f}$

fig. 5-45

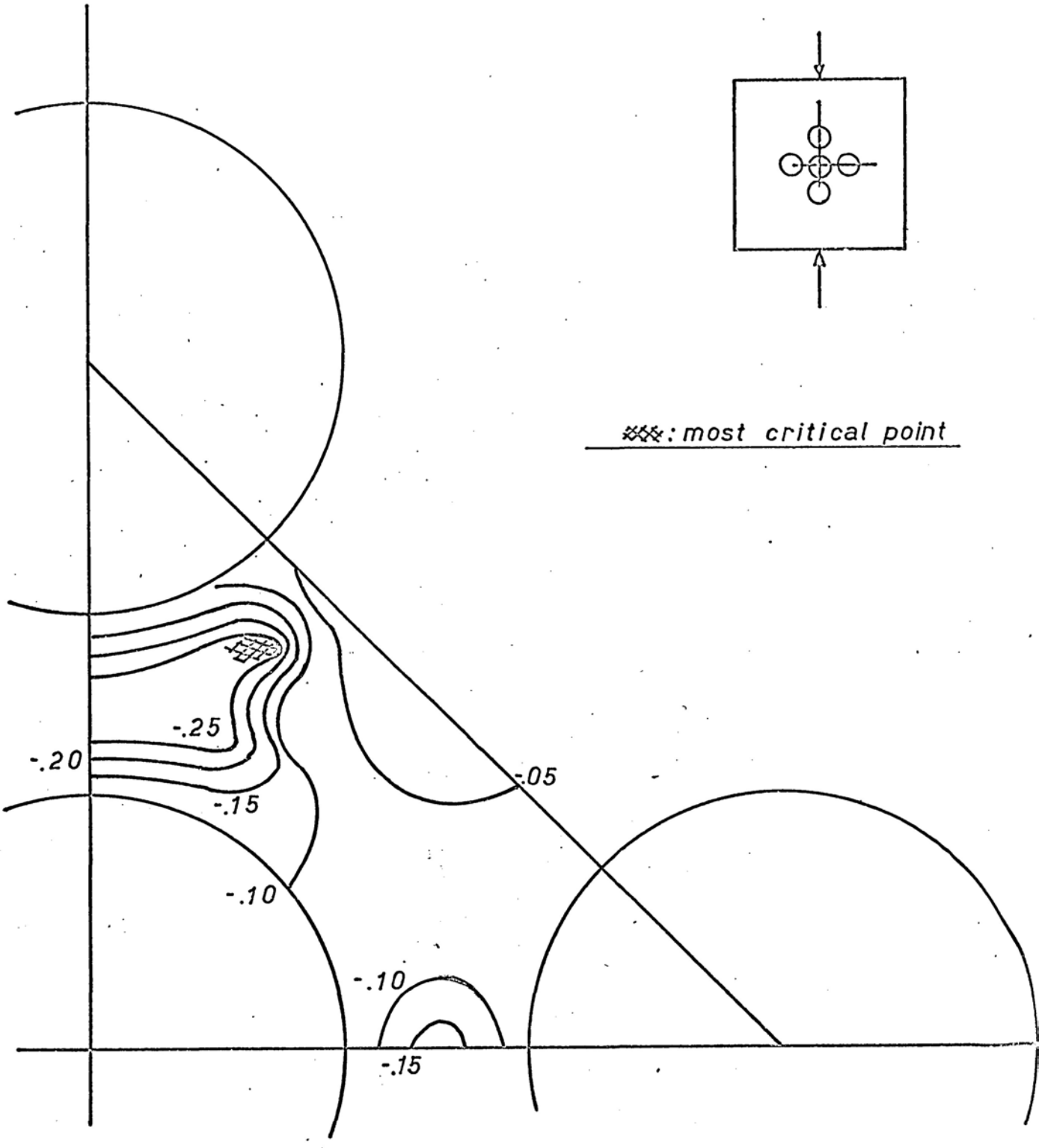
MPC-2- V_f = 32 %



ISOTENICS $\frac{\varepsilon_3}{(\varepsilon_3)_f}$

fig. 5-46

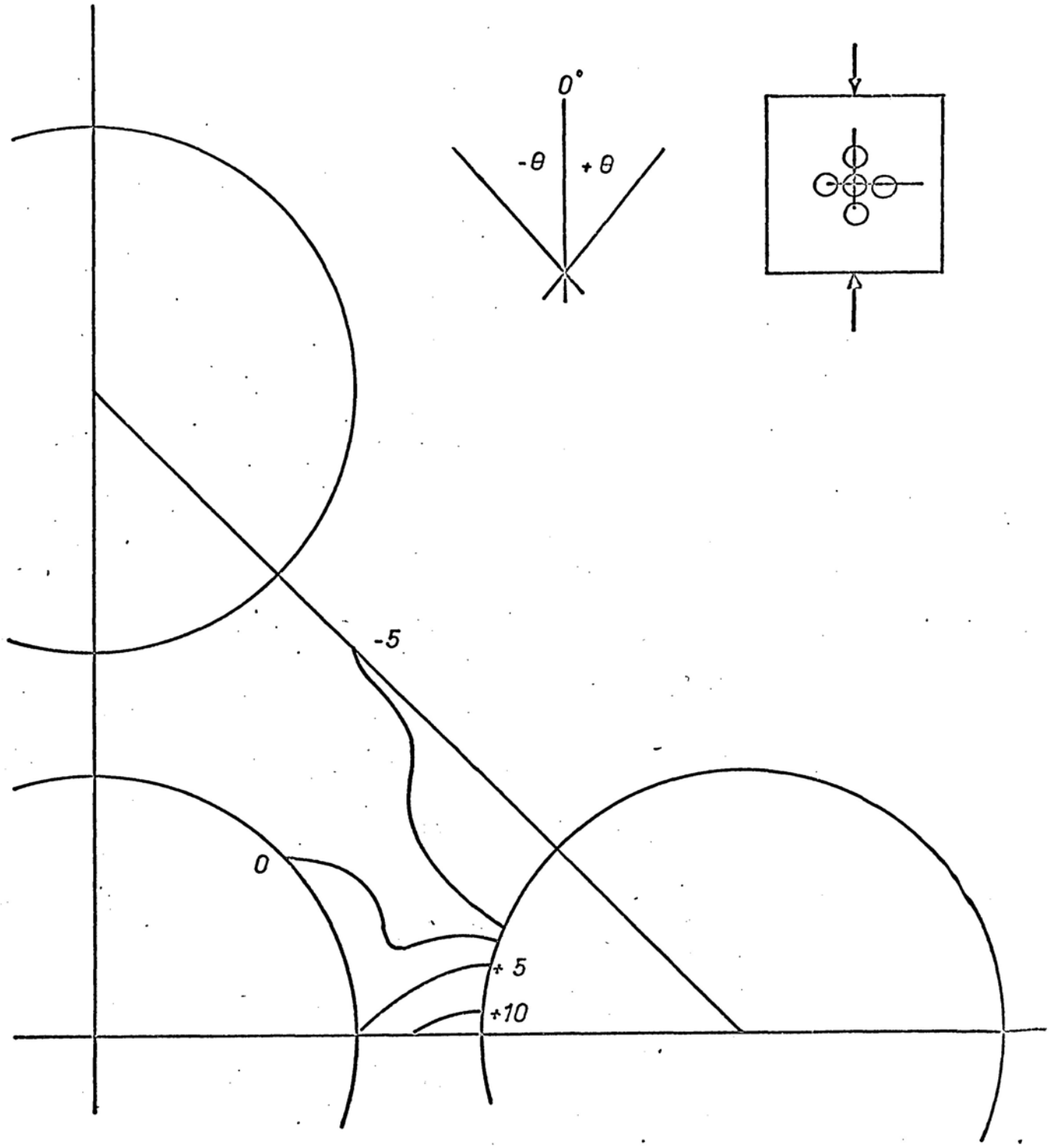
MPC - 2 - V_f = 32 %



ISOTENICS $\frac{\varepsilon_1}{(\varepsilon_3)_f}$

fig. 5-47

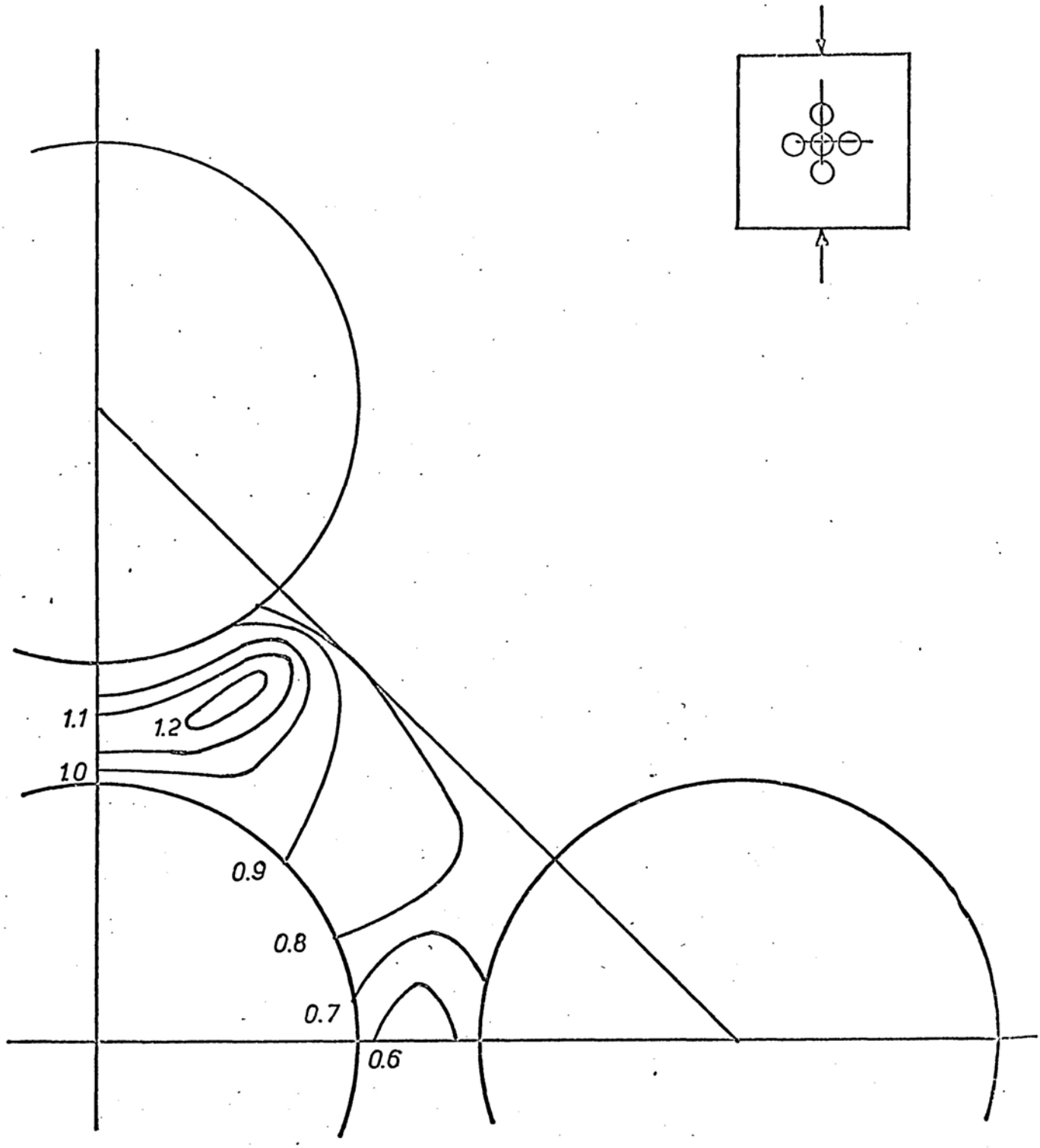
MPC - 3 - V_f = 37.75 %



ISOCLINICS

fig. 5-48

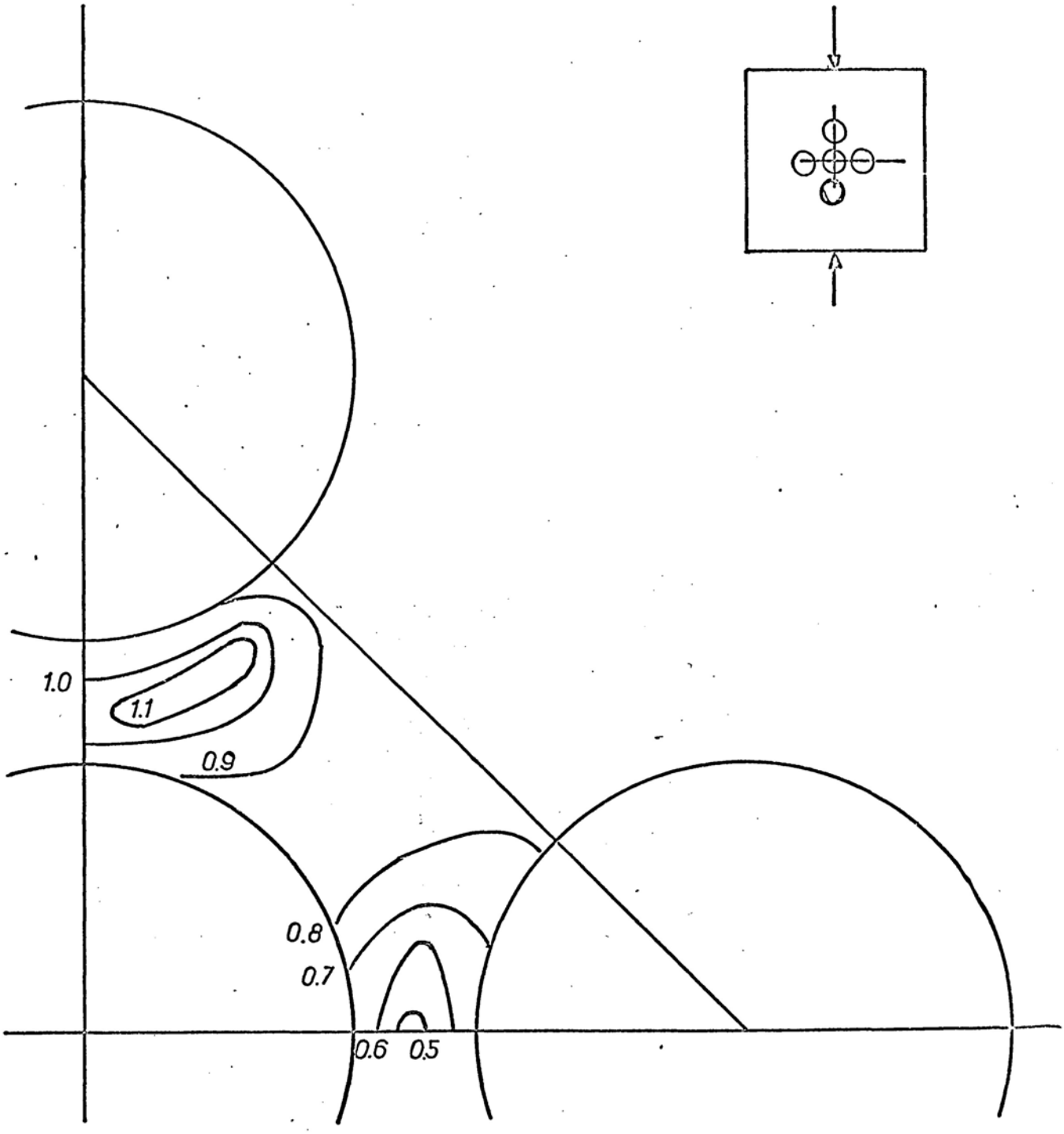
MPC - 3 - V_f = 37.75 %



ISOCHROMATICS $\frac{\varepsilon_3-\varepsilon_1}{(\varepsilon_3-\varepsilon_1)_f}$

fig. 5-49

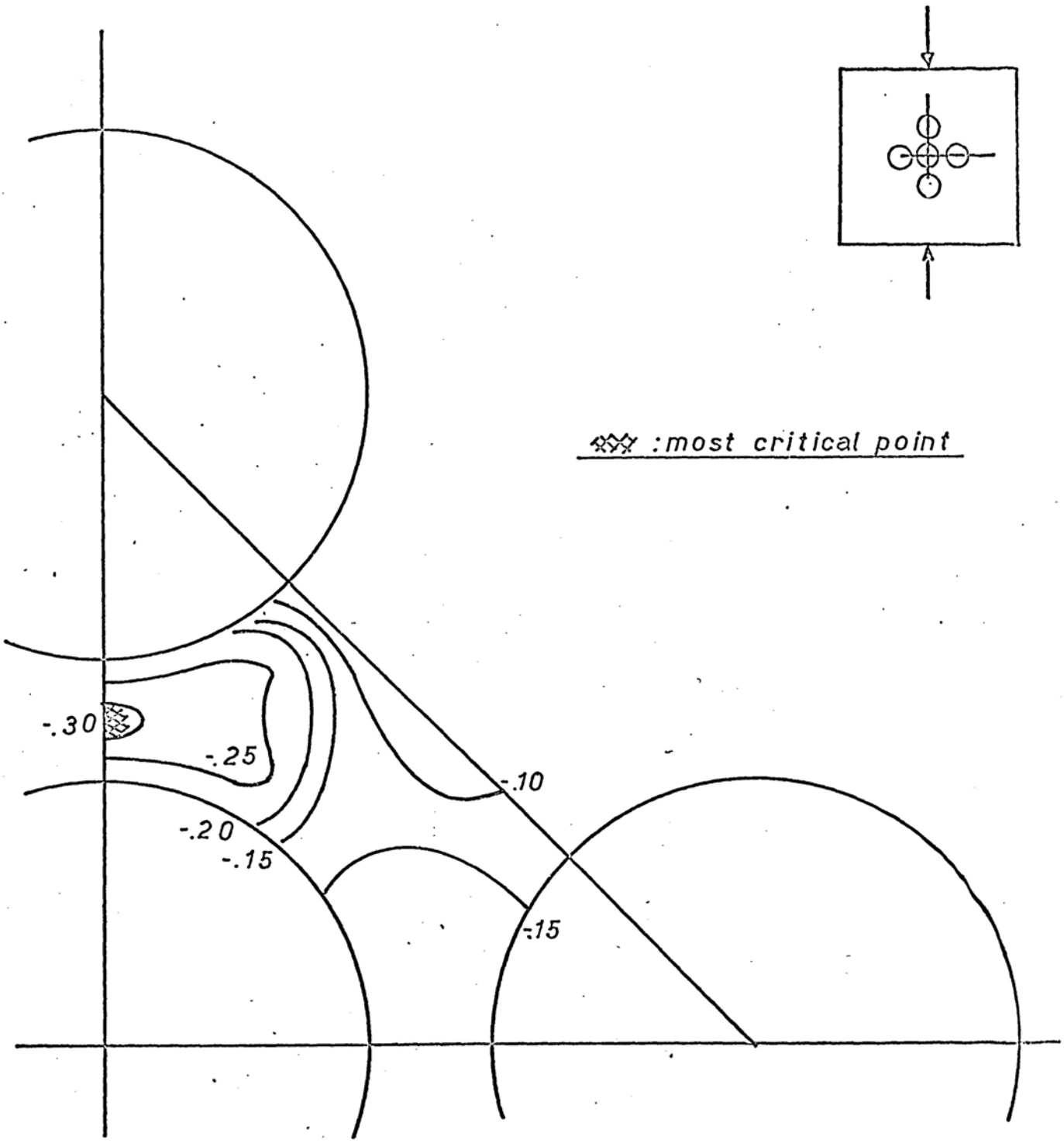
MPC-3- $V_f = 37.75\ \%$



ISOTENICS $\frac{\varepsilon_3}{(\varepsilon_3)_f}$

fig. 5-50

MPC-3- V_f = 37.75 %

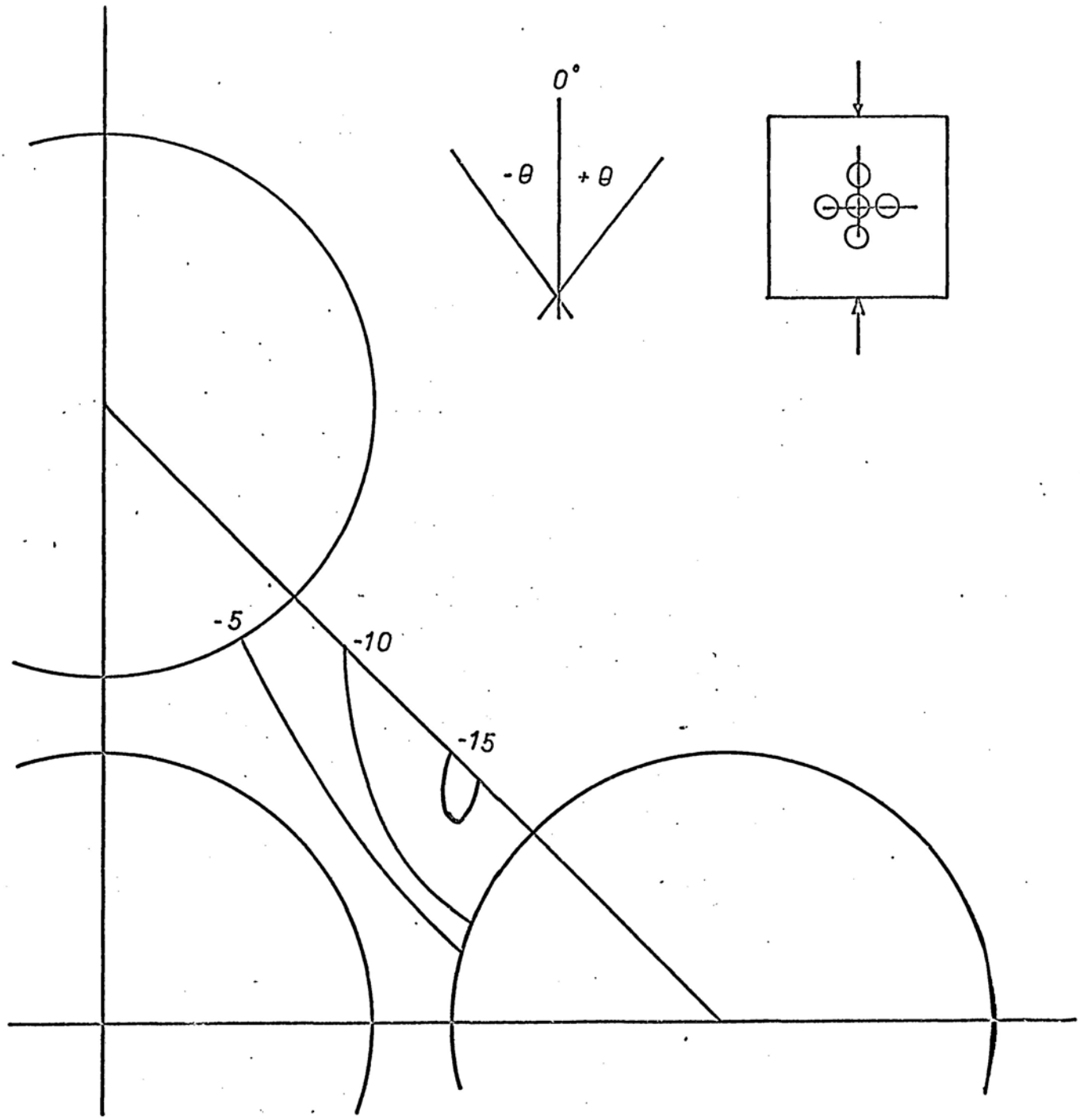


⁂ : most critical point

ISOTENICS $\frac{\varepsilon_1}{(\varepsilon_3)_f}$

fig. 5-51

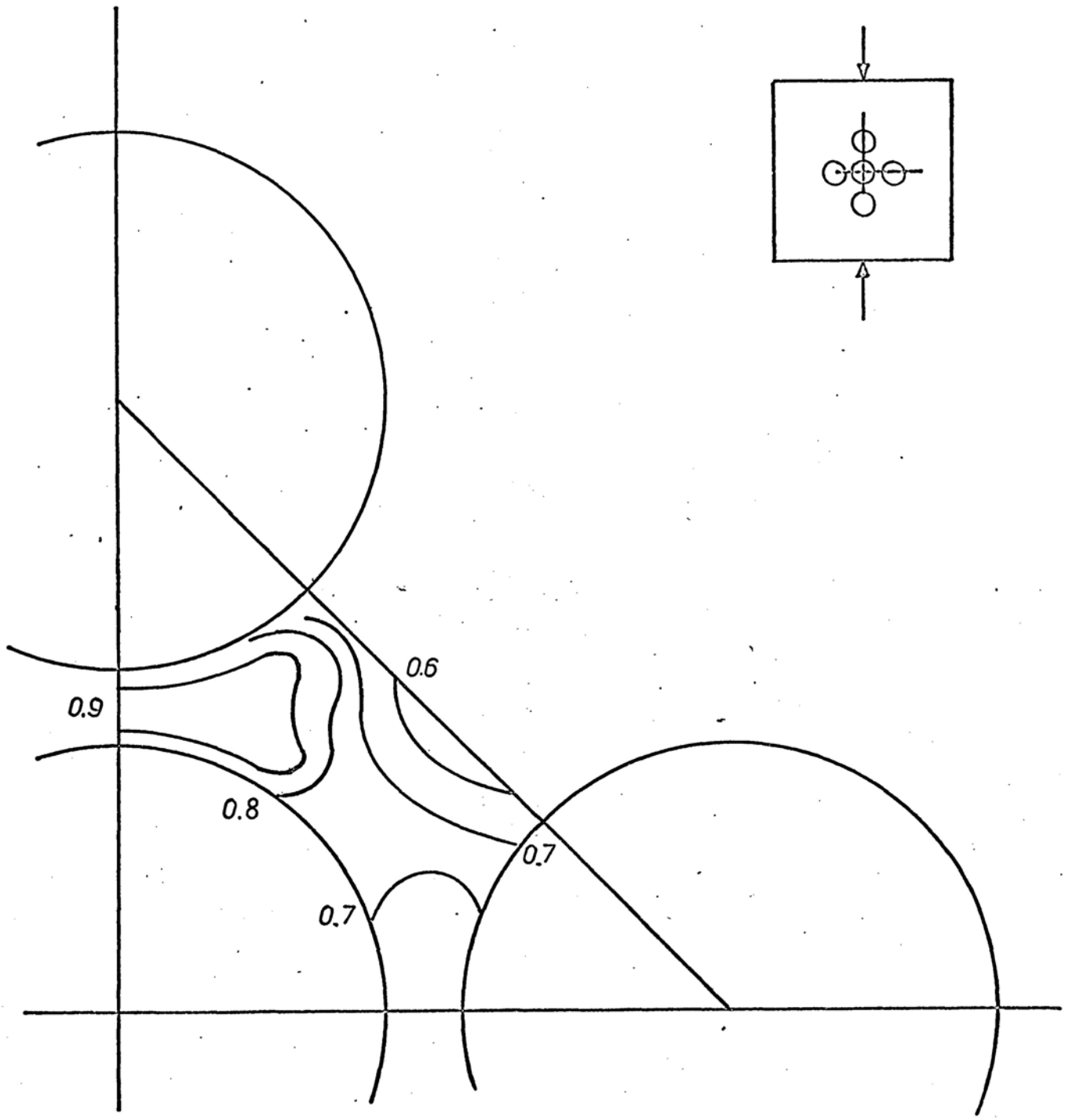
MPC - 4 - V_f = 43.5 %



ISOCLINICS

fig. 5-52

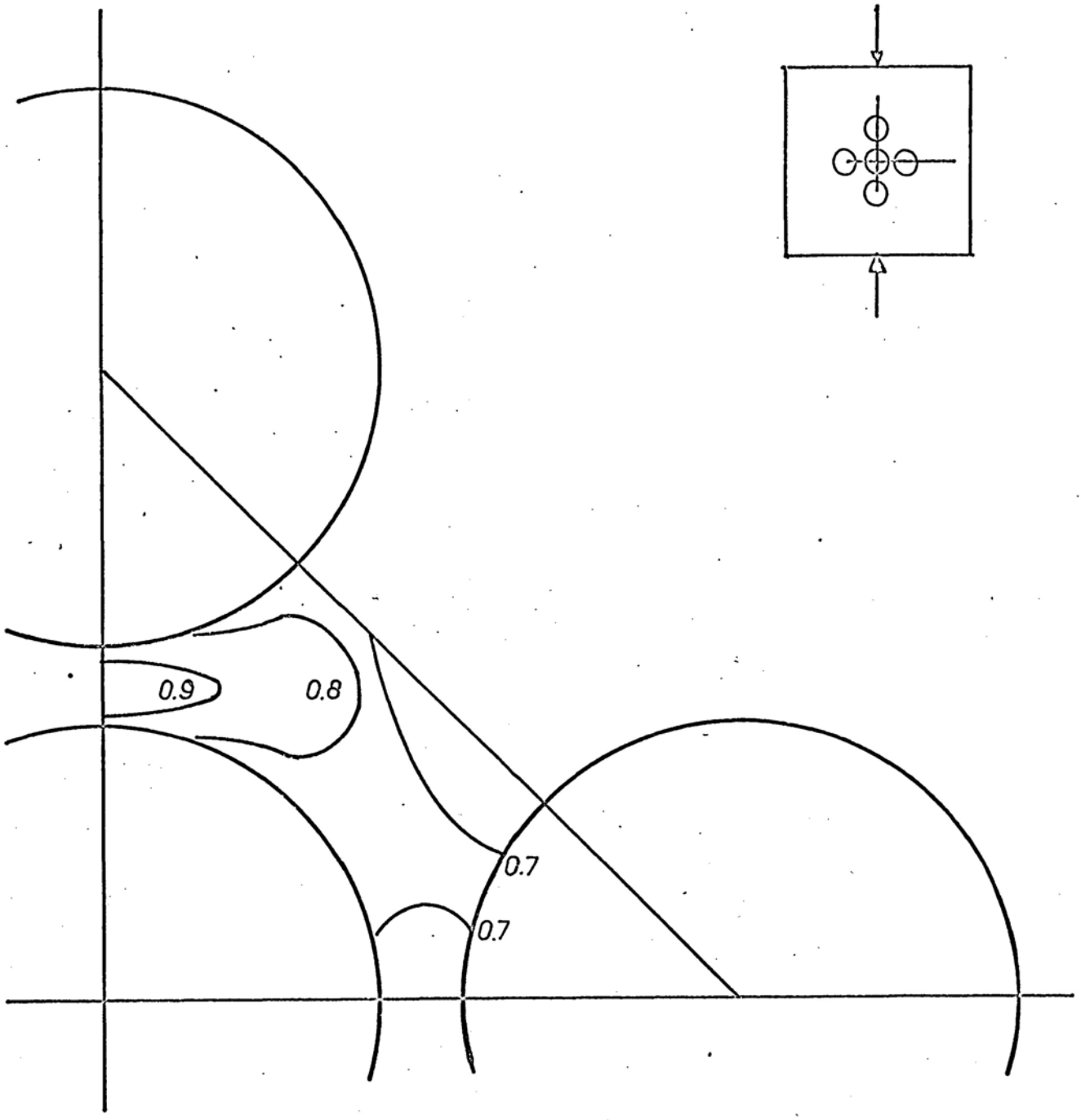
MPC-4- V_f = 43.5 %



ISOCHROMATICS $\frac{\varepsilon_3-\varepsilon_1}{(\varepsilon_3-\varepsilon_1)_f}$

fig. 5-53

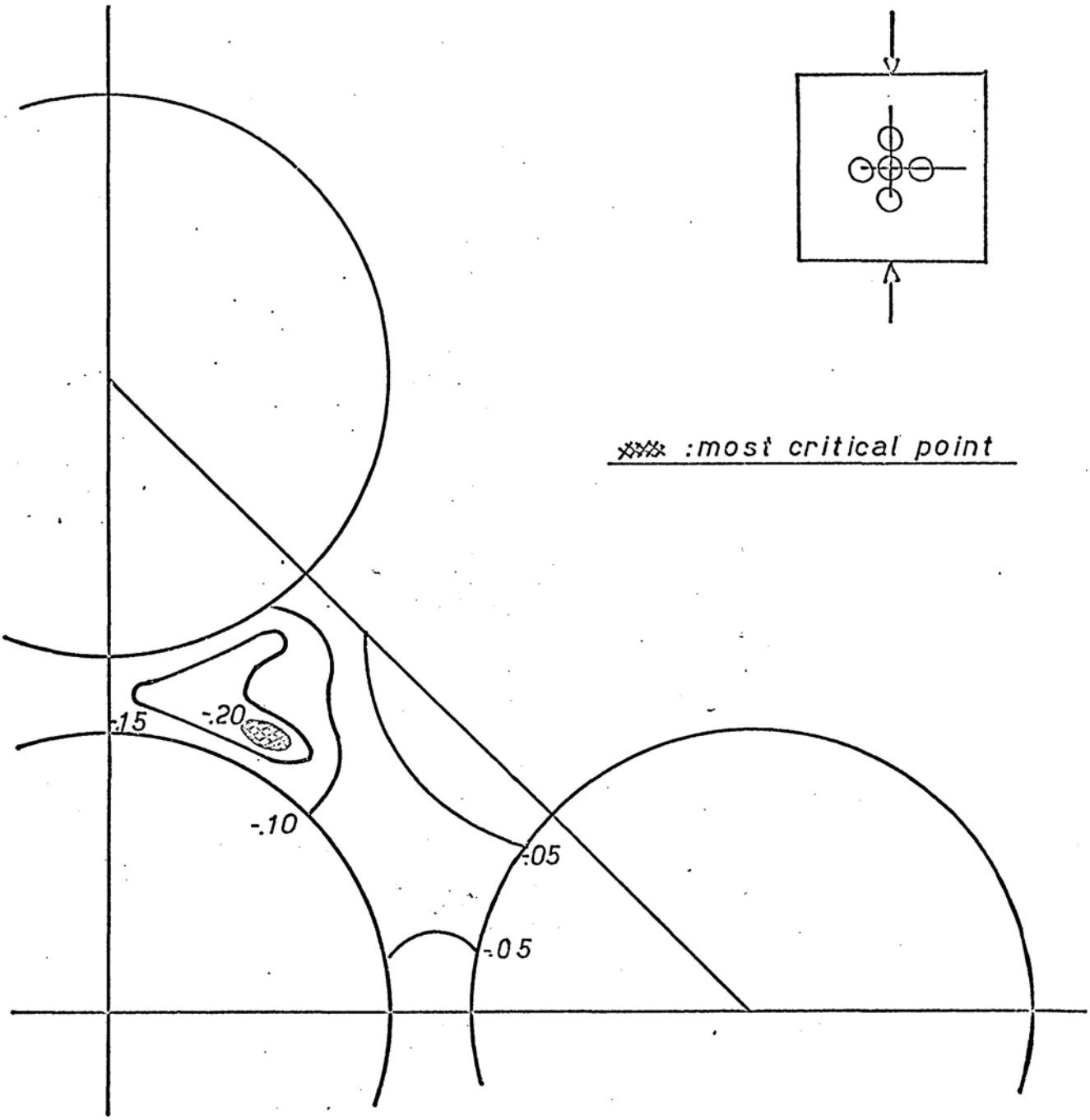
MPC -4- V_f = 43.5 %



ISOTENICS $\frac{\varepsilon_3}{(\varepsilon_3)_f}$

fig. 5-54

MPC-4- $V_f = 43.5\ \%$



ISOTENICS $\frac{\varepsilon_1}{(\varepsilon_3)_f}$

fig. 5-55

CHAPTER VI

LOADING TESTS TO FAILURE OF THE PLATE-MODELS

Section 1. Introduction

To allow verification of the composite strains at fracture initiation which had been obtained from the strain analysis discussed in chapter V, a continuous recording of the principal tensile strain at the most critical points on the plates was made during these failure tests. It was felt that the formation of the first crack at these points would be indicated by a sudden sharp increase in the recorded strain[23].

The other aim of these tests was to obtain information on the phenomenon of crack propagation in the plates by examination of the crack patterns on the plates at the end of the tests. Additional information was also obtained from photographs taken during the tests of the isochromatic patterns on the photo-elastic coatings.

Section 2. Testing Procedure

a) Position of Strain Gauges

All the strain gauges previously used for the strain analysis were removed from the uncoated face of each plate-model, and replaced by a new array of gauges.

On each of the twelve plates, two 30 mm strain gauges were used to measure the principal compressive strain in the mortar field ($(\varepsilon_3)_f$). They were placed on each side of the aggregate particle array, at two inches from the sides of the plate, aligned in the direction of loading and at exactly mid-way between the top and bottom of the plate.

Only two strain gauges were used to measure the field strains (instead of the four used previously) because, as will be seen

later, the data-logger used for the strain recording could only cope with one reading every second. Had there been four field gauges, the successive readings of the tensile strain at the most critical point would have been too far apart in time. Also, it was felt better to use gauges with an active length longer than previously (5 mm field gauges were used for the "elastic" strain analysis in chapter V) to ensure more realistic readings through each test up to failure.

MPA Series

On each of the four plates in this series, there were two "most critical points" because of the symmetry of the array of particles. So two 2 mm gauges were fixed on each of these plates. The strain analysis having shown that the "most critical point" was always at, or very near, the center of each critical zone (Cf Chapter V section 3), this is where the gauges were placed, aligned in the direction of the principal tensile strain. It was considered that very small variations of the most critical points from the above position should be disregarded and the gauges placed at the critical zone center on all plates in the series. The strain distribution had been analysed only in one of these critical zones on each plate, so the position of the gauge in the other zone had to be decided upon using results from the series as a whole. These results, together with considerations of symmetry indicated that the most critical point was in the middle of the center-to-center line joining the two particles aligned in the direction of loading.

MPB Series

On each of the plates in this series there was only one "most critical point". Therefore one 2 mm gauge was fixed at that point on each plate, aligned in the direction of the principal tensile strain.

MPC Series

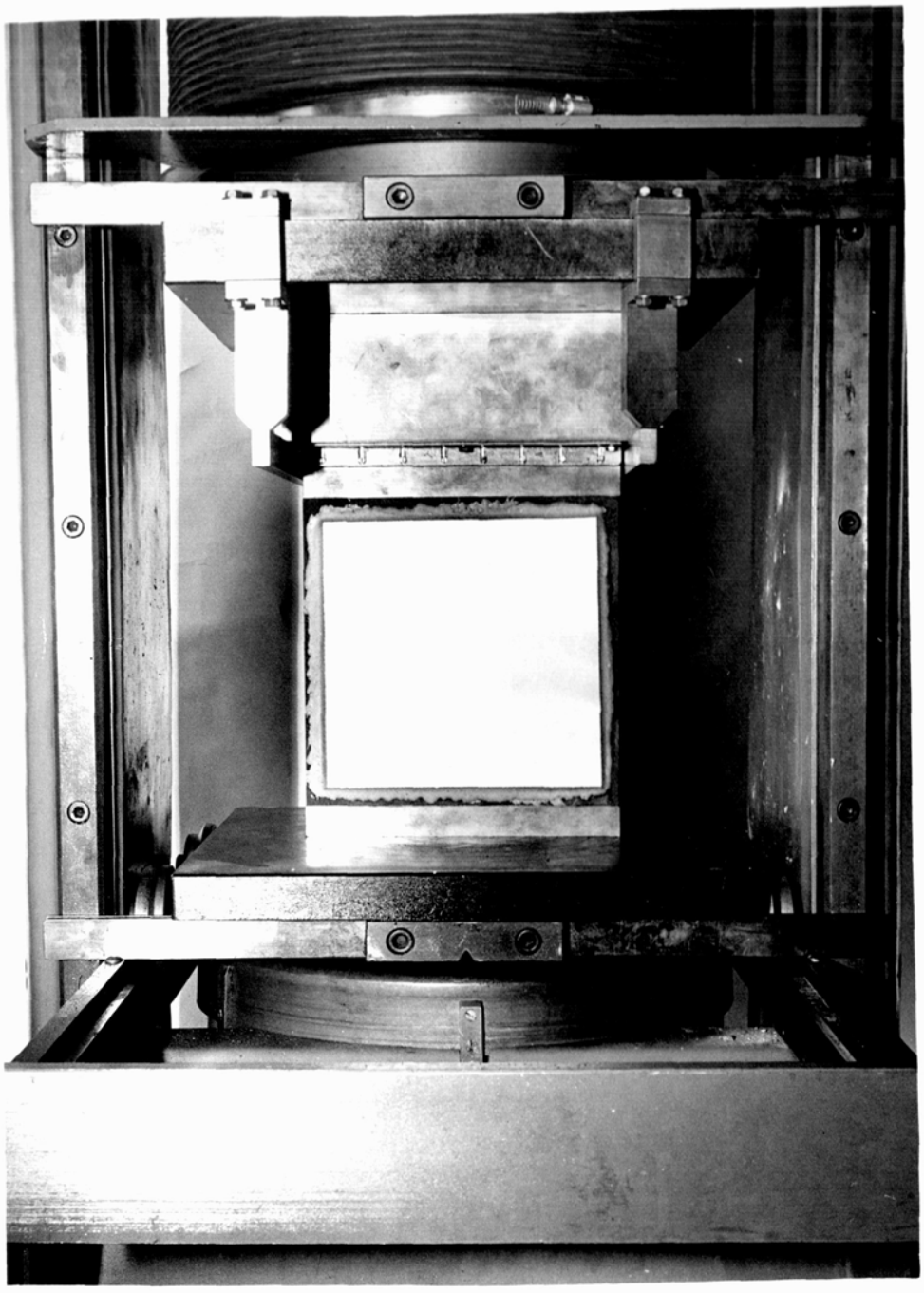
The same considerations apply to this as to the MPA Series. There were two equally critical zones due to the symmetry of the aggregate particle array (CF Chapter V section 3) and so two 2 mm gauges were used on each plate. They were placed at the mid-sections of the critical zones in all cases except one gauge on plate MPC-4. On that particular plate, the most critical point in the zone where strain measurements had been made was not only offset by a significant distance from the symmetry line but also much more critical than the point on that line. This could not be disregarded.

b) Loading Arrangements

The piston platen previously used in the small load frame to ensure an even distribution of applied load was also used in these tests. It was attached to the top platen of an Amsler 300 Ton-force testing frame. Each plate in turn was placed in this frame (see figure 6-1) and a constant vertical compressive strain rate of approximately 300 micro-strains per minute was applied to it until the Amsler dial showed that maximum load had been reached. At this point which was termed "failure" the load was taken off rapidly in an attempt to avoid complete breakdown and disruption of the specimen. In seven cases out of twelve, this was achieved and it was then possible to grind the back face of each plate to examine closely the crack patterns.

c) Recording of Strains and Applied Load

During the tests, a Peekel data-logger continuously recorded the strains from the gauges on the plates and also from a pressure transducer connected to the Amsler pressure control cabinet. A load of approximately 2 ton-force (600 p.s.i. on the plate) was needed to ensure the operation of the Hydro-Pacer controlling the vertical strain rate, so strain readings taken below



TYPICAL PLATE-MODEL IN

300 TON-f AMSLER TESTING FRAME

FIGURE 6-1

this load were disregarded. As mentioned previously, a speed of one strain reading every second was used.

The order in which the strain readings were taken on the plates with four gauges was as follows: the first field gauge, the first 2 mm gauge, the pressure transducer, the second 2 mm gauge and the second field gauge. For the plates with only three gauges, the same order was kept but the second 2 mm gauge reading was omitted.

d) Photographs

The isochromatic pattern on the photoelastic coating on each plate was photographed every 30 seconds using a Leica camera and an electronic flash unit. The camera was placed at about three feet from the plate, behind the analyser unit of a polariscope. The light source was placed behind the polarizer unit of another polariscope at a certain distance to the side of the camera so that the light would not be reflected directly into it. Trial tests had been conducted previously to determine the exact setting of the camera and the optimum position of the flash unit.

The first picture was usually taken at a load level of approximately 2 Ton-force. The applied load was noted every time a photograph was taken. In these tests which lasted approximately 15 minutes, 30 photographs were generally taken. The shrinkage pattern on the plates (i.e. at zero load) had been photographed previously.

Section 3. Determination of Fracture Initiation Point

a) Results

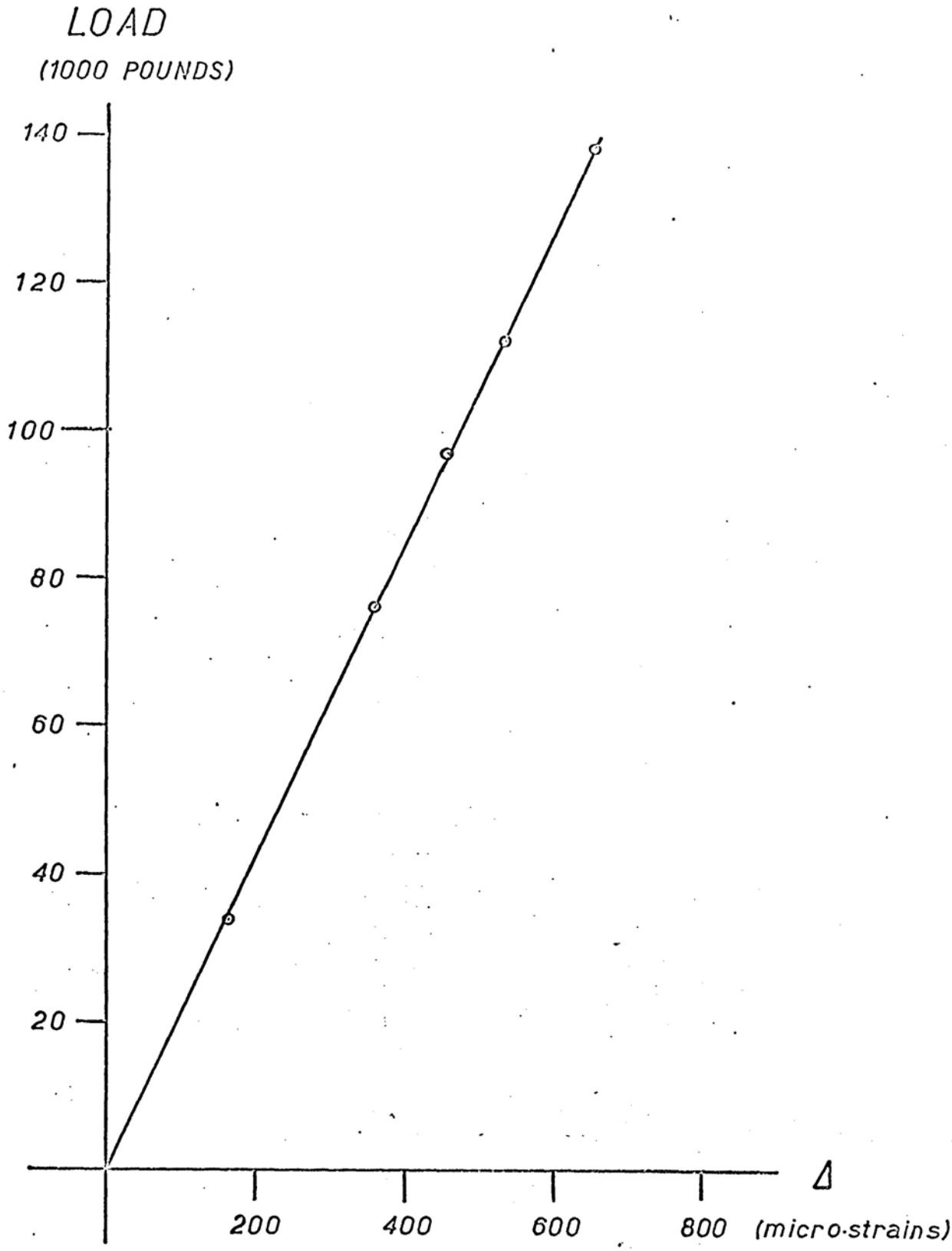
The readings of the tensile strain at the most critical points on each plate were plotted directly against the load measured by the pressure transducer. The relation between these two variables for a typical plate (MPB-1) is shown on figure 6-3 for the first 12 Tons

of load (approximately 3600 p.s.i. on the plate). The calibration of the pressure transducer (shown on figure 6-2) had shown that the relation between the applied pressure and the transducer reading in micro-strains was linear so, for simplicity reasons, direct micro-strain readings were plotted.

On the graph in figure 6-3, as on those for all other plates (figures 6-4 and 6-5 show two more of these graphs), it was noted that the relation remained linear within a four micro-strain band in which the data points were randomly distributed (shown on figure 6-3). After a certain point, significant deviation from linearity occurred. It was considered that this point marked the onset of micro-cracking in the mortar matrix at the corresponding gauge positions. At this low level of strain, in a short term test, only the formation of microcracks can explain such a marked change in the rate of increase of the tensile strain.

Knowing the value of the tensile strain at which microcracking had initiated, it was then possible to obtain from the recorded data the corresponding field strains and to calculate the compressive composite strain at fracture initiation as shown on figure 6-3. The average field strain was corrected for gauge factor and the ratio $((\varepsilon_3 \text{COMP.})\text{f.i.}/(\varepsilon_3 \text{pure mortar})\text{f.i.})$ was calculated using the ratio of the composite strain to field strain measured during the strain distribution analysis, this ratio being constant up to fracture initiation.

For every 2 mm gauge on every plate, the $(\varepsilon_3 \text{comp})\text{f.i.}/(\varepsilon_3 \text{pure mortar})\text{f.i.}$ ratio was calculated. In one case only (MPC-4) it was impossible to do this because no linear portion of the curve was evident. On table 6-4, all these ratios are shown. Where a plate had two gauges, the average result is given together with the predicted



CALIBRATION OF PRESSURE TRANSDUCER

fig. 6-2

DETERMINATION OF FRACTURE INITIATION POINT ON PLATE MPB -1-

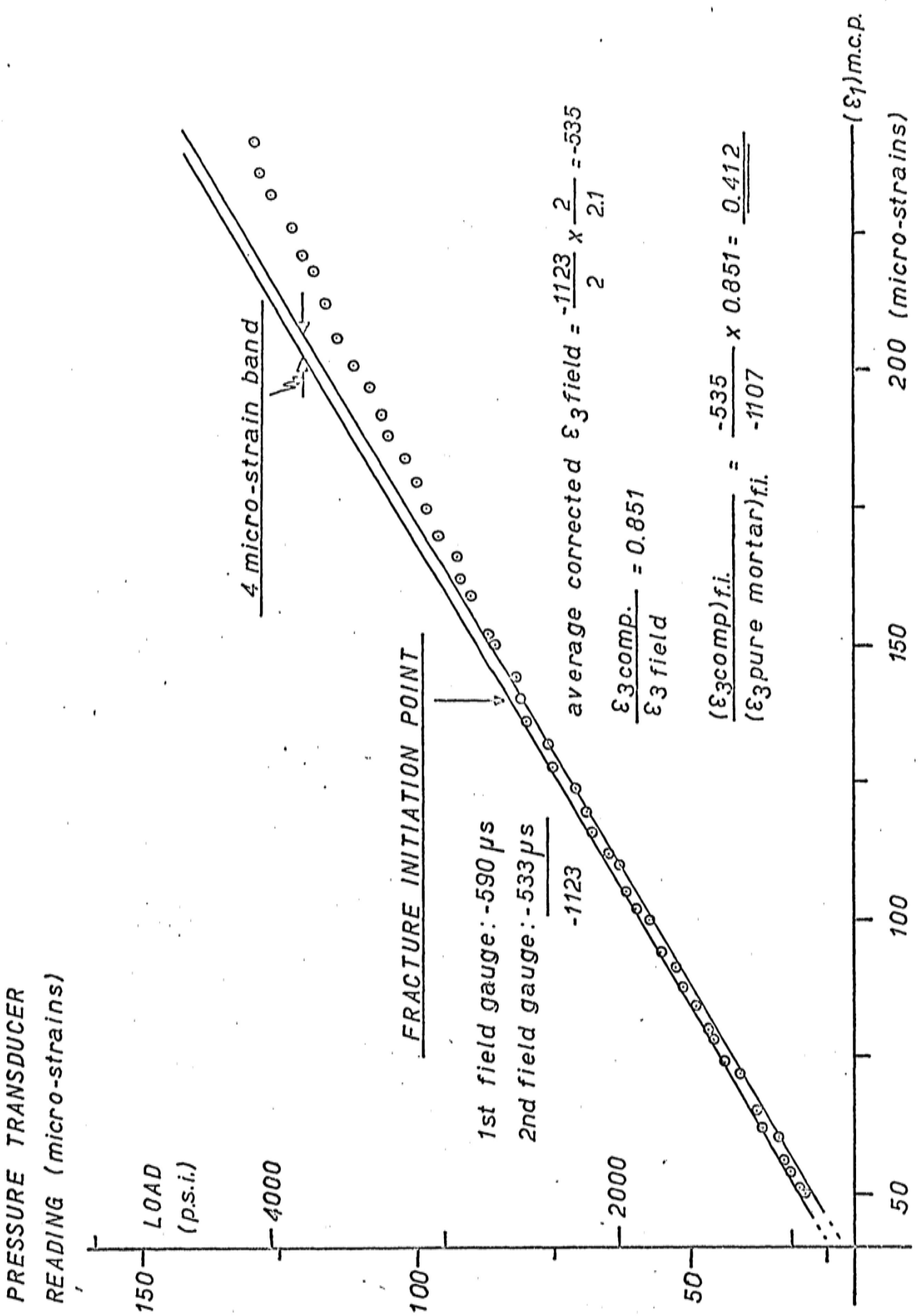


fig. 6-3

DETERMINATION OF FRACTURE INITIATION POINT ON PLATE MPA-3

(1st 2mm gauge)

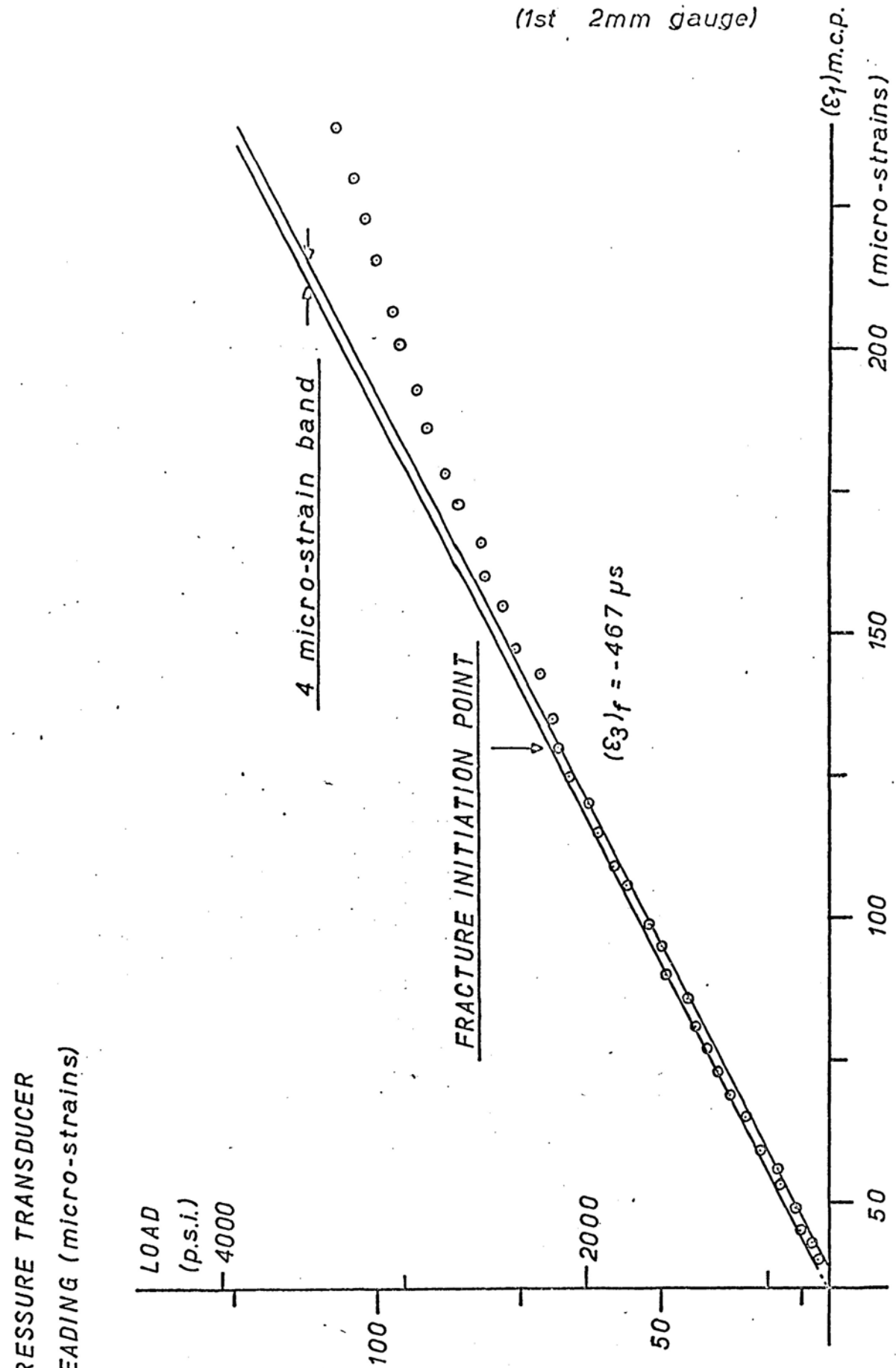


fig. 6-4

DETERMINATION OF FRACTURE INITIATION POINT ON PLATE MPA-3

(2nd 2mm gauge)

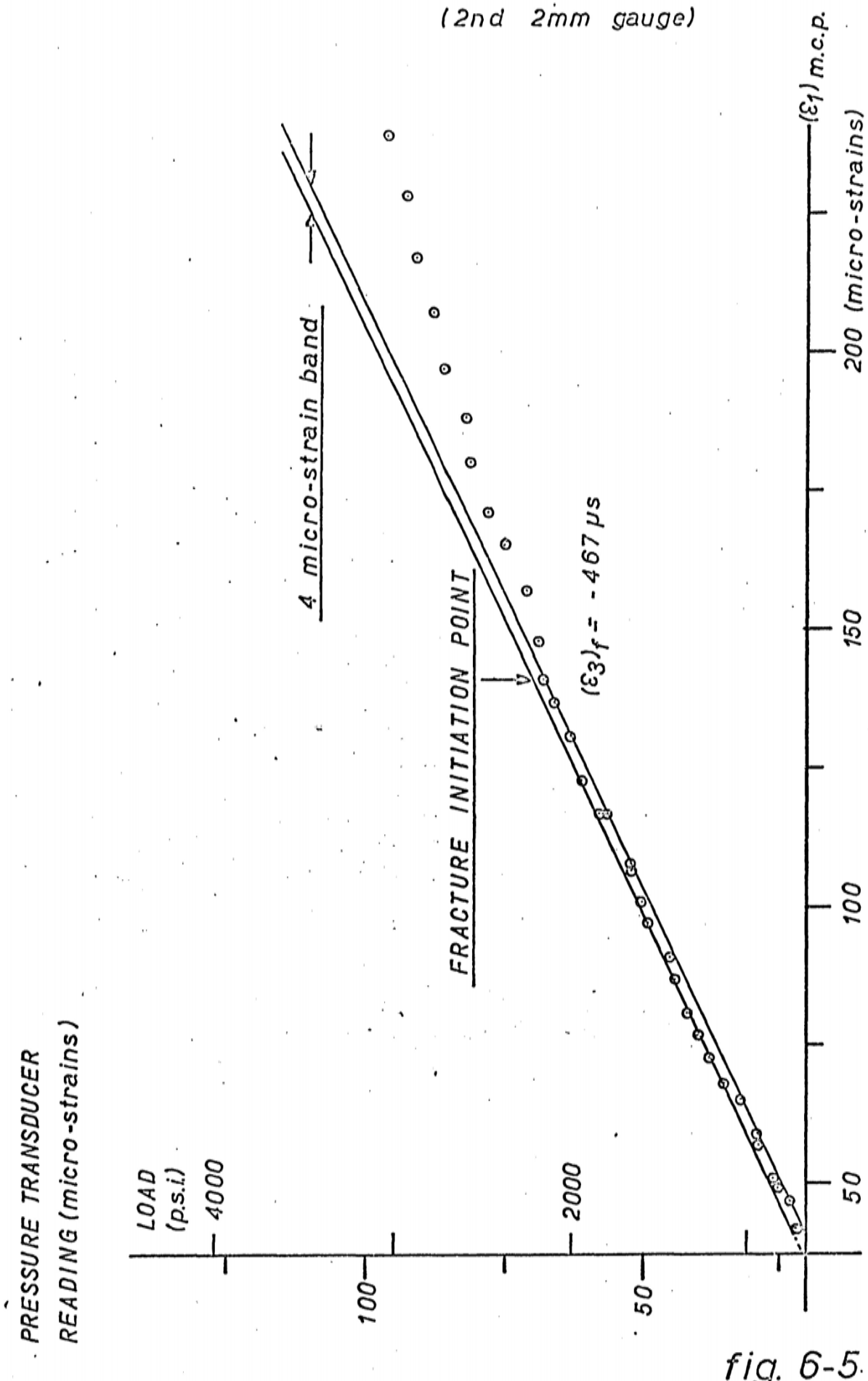


fig. 6-5

PLATE MODEL FAILURE TESTS RESULTS

$$\frac{((\varepsilon_3 \text{COMP})_{f.i.} / (\varepsilon_3 \text{ P.M.})_{f.i.})}{}$$

PLATE	RESULTS FROM FAILURE TESTS		AVERAGE ("REAL") RESULT	PREDICTED RESULT
MPA-1	.406	.418	.412	.287
MPA-2	.250	.493	.371	.375
MPA-3	.327	.327	.327	.327
MPA-4	.302	.241	.271	.253
MPB-1	.412	-	.412	.299
MPB-2	.355	-	.355	.395
MPB-3	.239	-	.239	.300
MPB-4	.215	-	.215	.305
MPC-1	.400	.492	.446	.452
MPC-2	.347	.347	.347	.457
MPC-3	.257	.325	.291	.358
MPC-4	.332	-	.332	.442

Table 6-A

ratios from the strain analysis in Chapter V. In this way, comparison with the average value shown can be made.

The variation between the two results on a single plate was found generally to be low. The agreement between the predicted ratios and the so-called "real" ones, obtained during the present failure tests, will be discussed in the following sub-section.

b) Relation Between Composite Strain at Fracture Initiation and Coarse Aggregate Content.

It was mentioned in chapter II that for each aggregate particle array considered four plates were cast. Different spacings between particles had been used to study the variation in the plate-model properties with varying volume fraction of coarse aggregate. In that chapter it was also explained how the volume fraction of coarse aggregate, represented by each spacing on each plate,had been determined. The quantitative result obtained through the testing of the plate-models being the value of the minor principal composite strain at fracture initiation for each plate (table 6-A), three graphs were plotted (one for each series) to study the relation between the $(\varepsilon_3 \text{comp})_{\text{f.i.}}/(\varepsilon_3 \text{pure mortar})_{\text{f.i.}}$ ratio and the volume fraction of coarse aggregate. To enable a valid comparison of the values of the predicted ratios with the "real" ones, both these values were plotted on each graph at each point.

It was found on each of these graphs that the relation between the minor principal composite strain at fracture initiation and the volume fraction of coarse aggregate was approximately the same whether the predicted results or the "real" results only were considered. But the scatter of the data points was found to be much smaller for the "real" results than for the predicted ones. On the graphs in figures 6-6, 6-7 and 6-8, where both these two sets of results are

MPA SERIES RESULTS

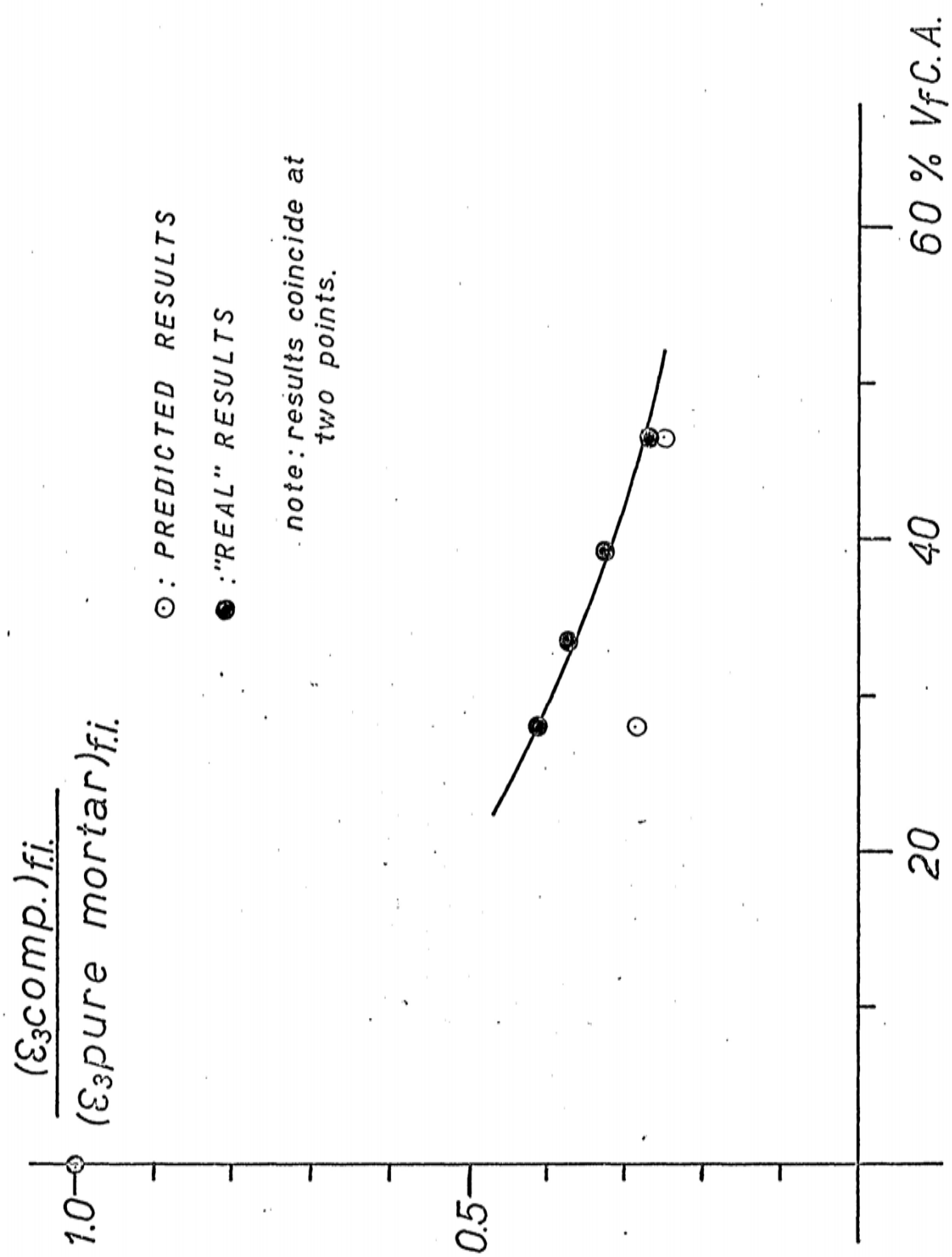


fig. 6-6

MPB SERIES RESULTS

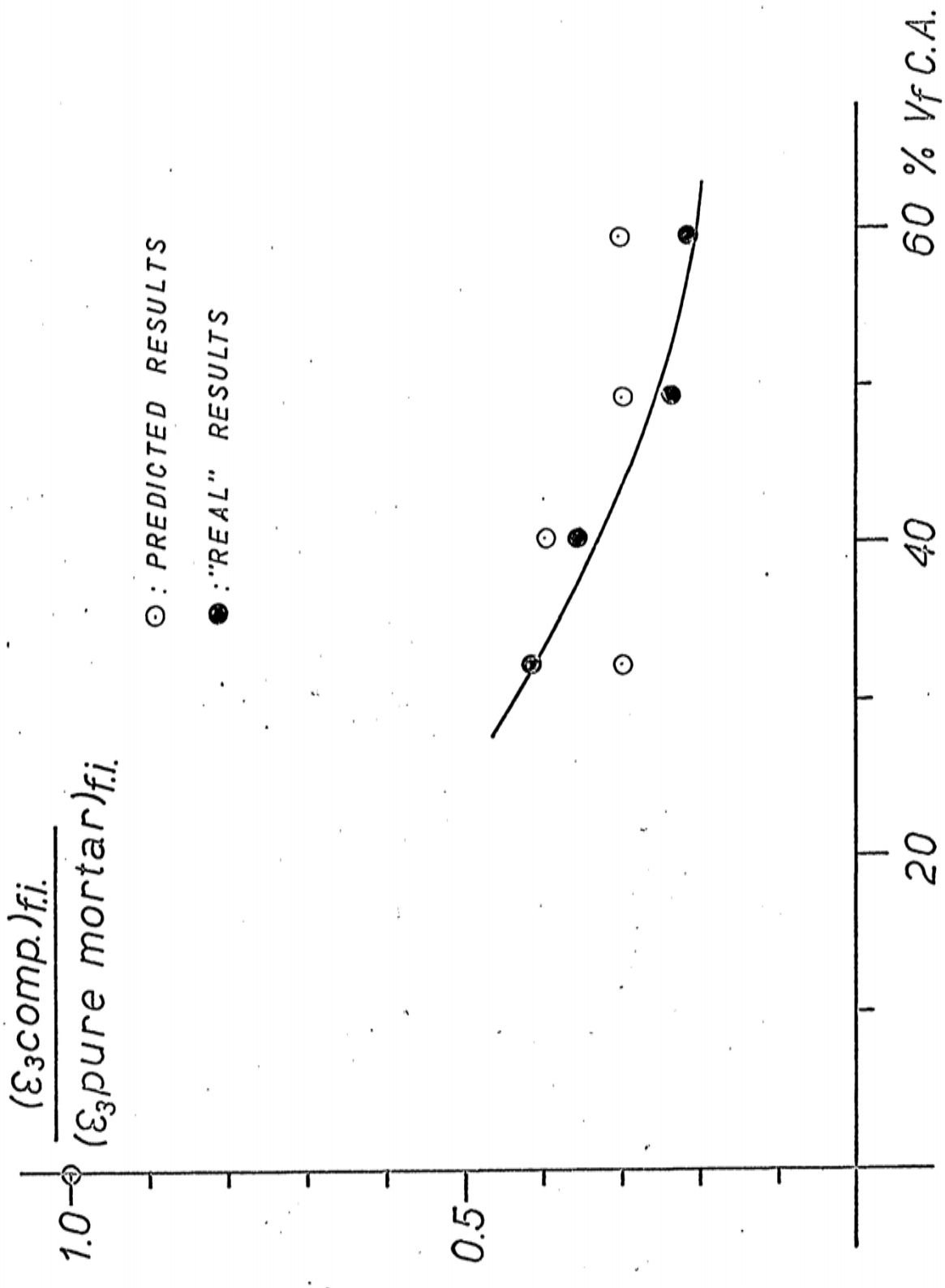


fig. 6-7

MPC SERIES RESULTS

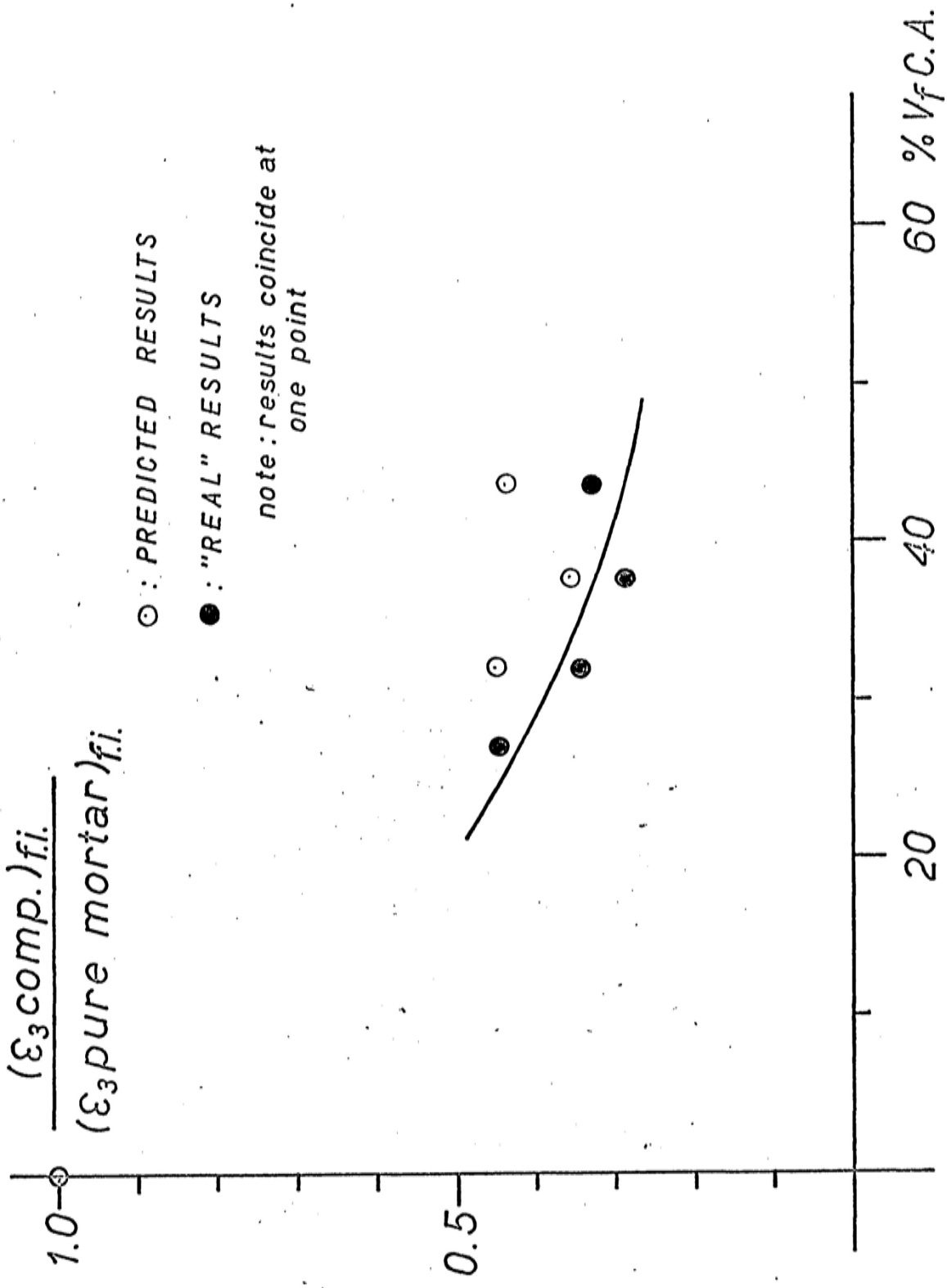


fig. 6-8

plotted against volume fraction of coarse aggregate (V_f C.A.), the average curve through the "real" points is shown. It can be seen that only a small deviation about this line occurs. Therefore it was considered that this method of obtaining the "real" composite strains at fracture initiation was not only valid but gave more precise results than those obtained using the method described by McCreath. Since it was found, considering all twelve plates, that the predicted ratios were neither consistently higher or lower than the "real" ones, it was thus considered that the hypothesis of linearity from zero load to the formation of the first micro-crack, on which the McCreath method is based, was justified.

For the three particle arrays considered, the relation between the volume fraction of coarse aggregate and the minor principal composite strain at fracture initiation appeared similar : a rapid decrease in strains from V_f C.A. = 0% (pure mortar) to approximately V_f C.A. = 30%, and then a slower decrease up to and over 50%. It was decided to compare the results from the three series of tests by plotting them on a single graph. As shown in figure 6-9, these results are contained within a small band thus yielding a single well-defined relation between the volume fraction of coarse aggregate and the composite compressive strains at fracture initiation for all the particle arrays. All the data points were found to lie at random in this band and although small differences between models might have been expected, the testing errors were larger and these differences were not seen.

c) Comparison with McCreath's Results

McCreath[3] had tested twelve plates using the particle array (D) shown on figure 2-5. As mentioned in chapter II, the formula he had used to determine the volume fraction of coarse aggregate represented by each of the various spacings on the plates he had tested was

PLATE-MODEL TEST RESULTS

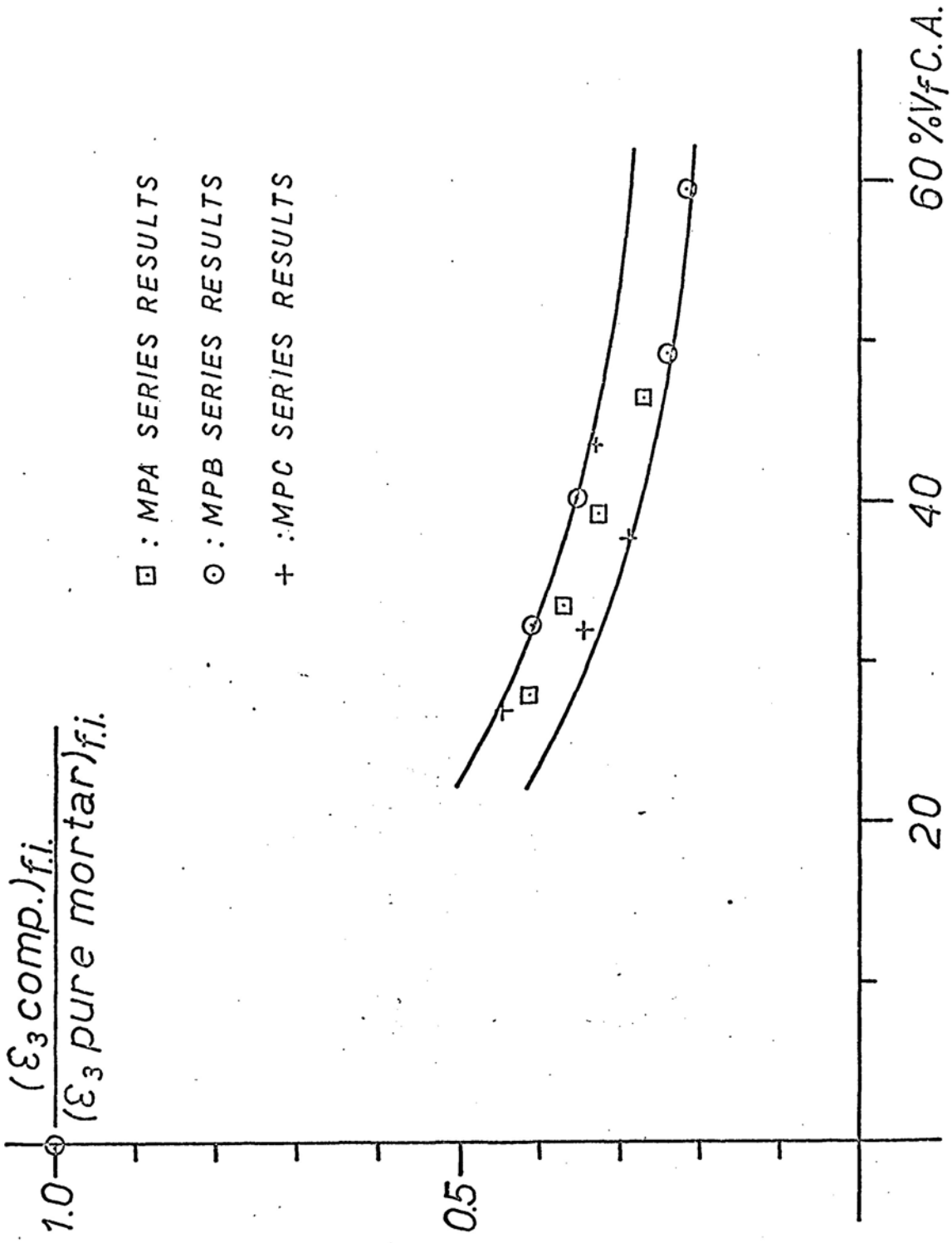


fig. 6-9

considered erroneous. So the percentage of coarse aggregate represented was recalculated for each plate using the method described in chapter II. In table 6-B, McCreath's results are given. The spacing between particles for each plate and the volume fraction of coarse aggregate as given by McCreath and as recalculated are also shown.

On a graph similar to that on figure 6-9 McCreath's results were then plotted (see figure 6-10). They were found to have a larger scatter than the present "real" results obtained during the failure tests. This had been expected since they represented only predicted composite strains at fracture initiation. But the trends exhibited by both series of twelve plates were seen to be similar although McCreath's results were lower (more critical) than the present ones.

It was nevertheless concluded that the relation shown on figure 6-9 could be safely used to represent the general trend exhibited by the results of the four arrays tested. It was considered that the differences between the present series of test results and McCreath's results were not significant because of the degree of scatter of the test results involved.

d) Comparison with Tests on Three-Dimensional Concrete

It was considered necessary to compare one basic property of the plate-models with the same property measured on three-dimensional concrete specimens, in order to show that the plate-models were representative of three-dimensional concrete. The information obtained from the tests on the plates in the "elastic" range, i.e. the extent of the critical and non critical zones, the position of the most critical points, and the study of the propagation of micro-cracking in the plates up to failure would be meaningless otherwise.

Test results from concrete cylinders with the same characteristics

McCreath's Results

(Plates tested with array 'D' (see fig. 2-5))

$\frac{d}{D}$	% V_fC.A. (McCreath)	% V_fC.A. (recalculated)	$\frac{(\varepsilon_3 COMP)_{f.i.}}{(\varepsilon_3 pure\ mortar)_{f.i.}}$
2.46	5	16.0	.504
1.77	13.4	24.0	.381
1.54	20.0	28.5	.373
1.41	26.3	32.0	.219
1.34	30.6	34.5	.224
1.29	34.9	36.5	.318
1.24	39.2	39.0	.149
1.17	46.9	44.5	.185
1.14	50.0	46.0	.102
1.11	54.6	49.0	.246
1.03	67.2	58.0	.196
1.00	72.2	64.0	.140

Table 6-B

PLATE-MODEL TEST RESULTS

(including McCreath's)

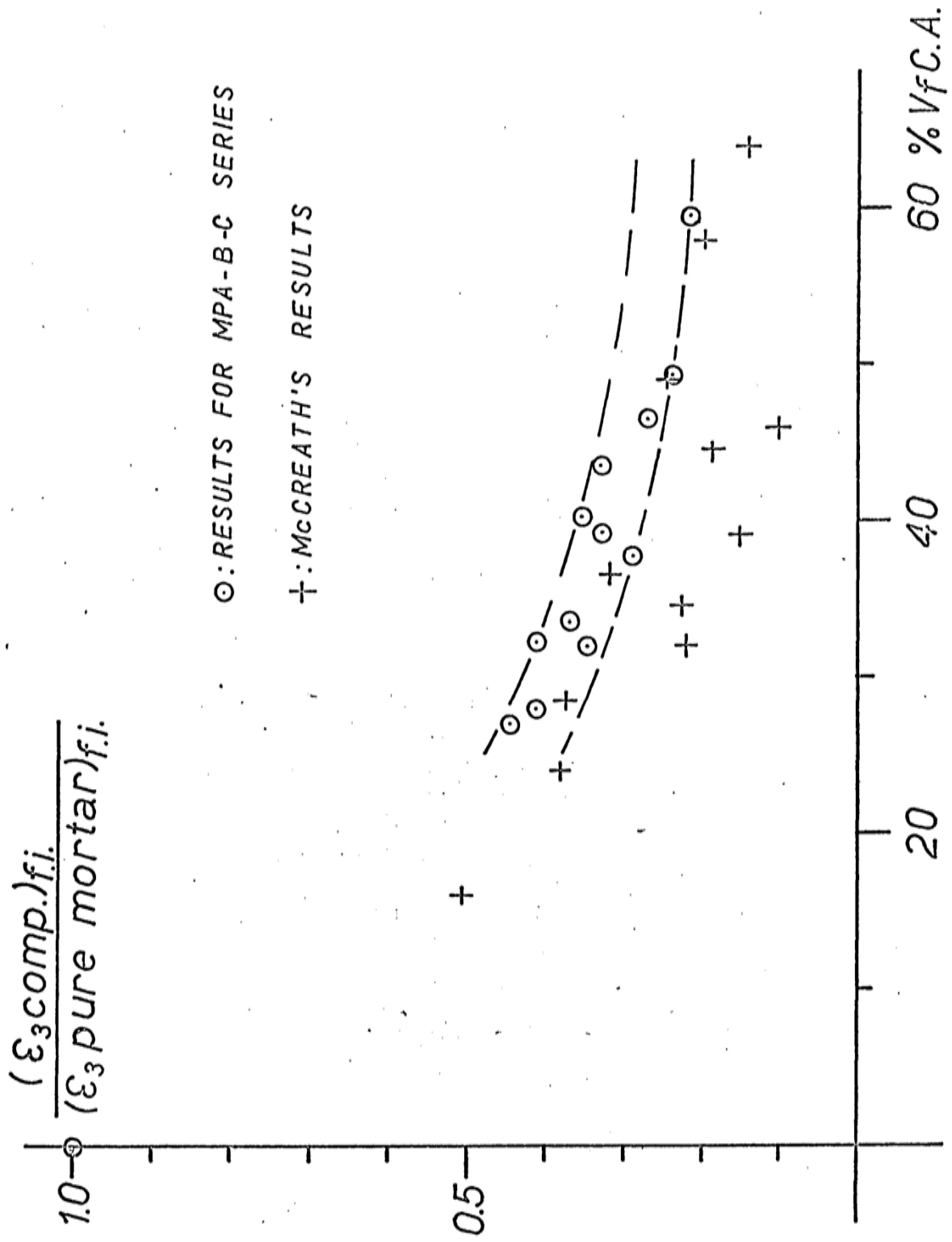


fig. 6-10

as the plate-models were available. McCreath[3] had tested in uniaxial compression a series of concrete cylinders (10" long x 4" diameter) containing various volume fractions of single-sized glass spheres in a mortar matrix similar to that of the plate-models. The glass-spheres had a surface texture equivalent to the one on the coarse aggregate used in the plate-models and the specimens had been cured in the standard way described in chapter III. Newman[13] had also tested in uniaxial compression a series of cylinders having the above characteristics, as part of a program of triaxial tests.

Figure 6-11 shows the relation between the minor principal composite strain at fracture initiation and the volume fraction of coarse aggregate for the cylinders tested by McCreath. On figure 6-12, the same relation for Newman's specimens is shown. As Newman's results yielded a more precise and well defined trend, it was decided to compare the levels of composite strain at fracture initiation measured in the plate-models with the ones measured on Newman's specimens. It should be noted that these results are similar to McCreath's, but are more critical for the same volume fraction of coarse aggregate. The main reason for this is most probably the more precise method used by Newman to determine the point of discontinuity (Cf chapter IV).

The proposed comparison was made by plotting Newman's results on a graph similar to the one on figure 6-9. From this, it was seen that the behaviour of the plate-models coincided with the behaviour of the glass-marble concretes in the region of volume fractions covered by the plates tested. Only minor differences between the measured composite strain to pure mortar strain ratios at fracture initiation for both series of tests were found (see figure 6-13).

GLASS - MARBLE CONCRETE TEST RESULTS

FROM McCREATH [3]

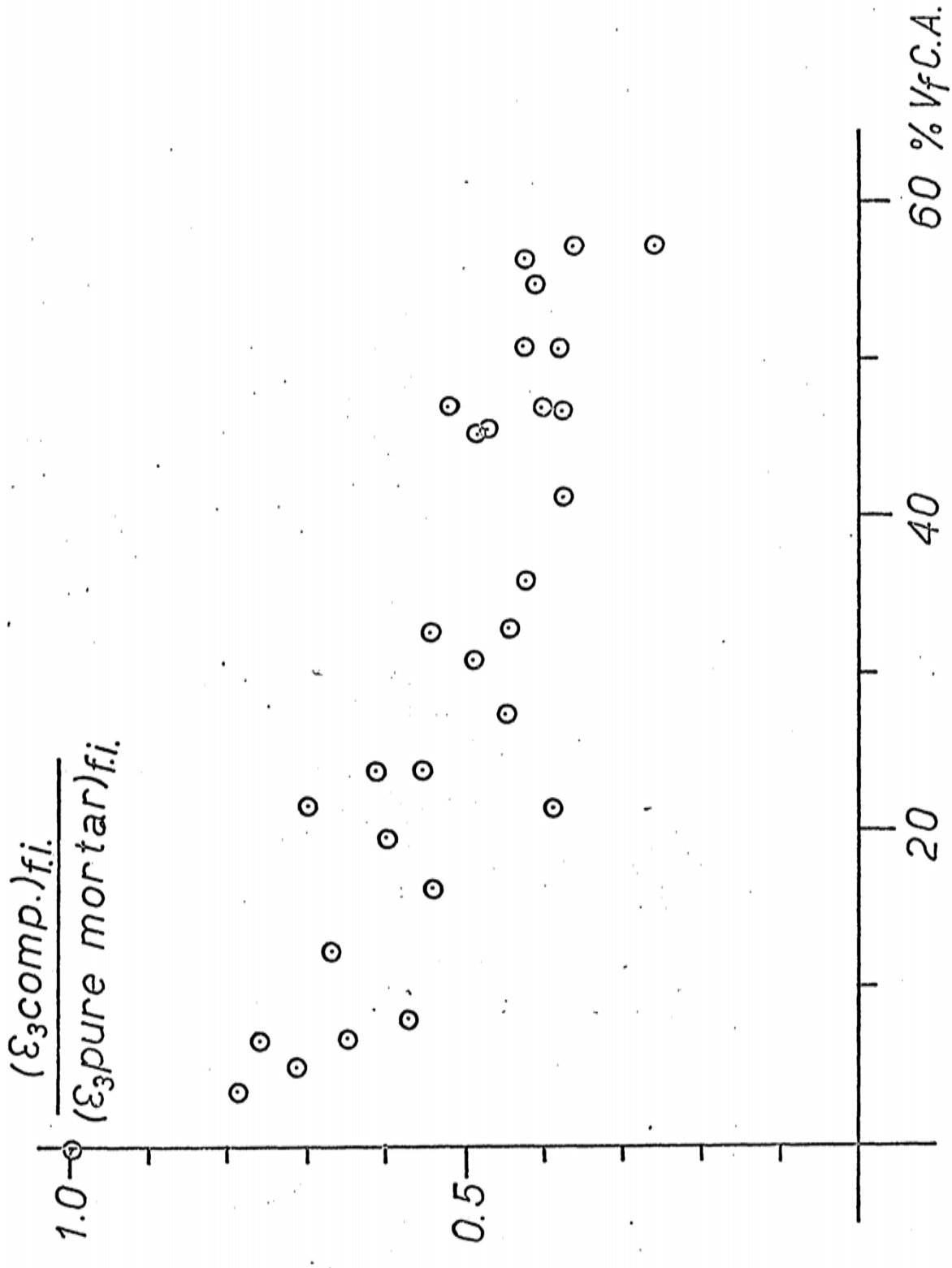


fig. 6-11

GLASS - MARBLE CONCRETE TEST RESULTS

FROM NEWMAN[13]

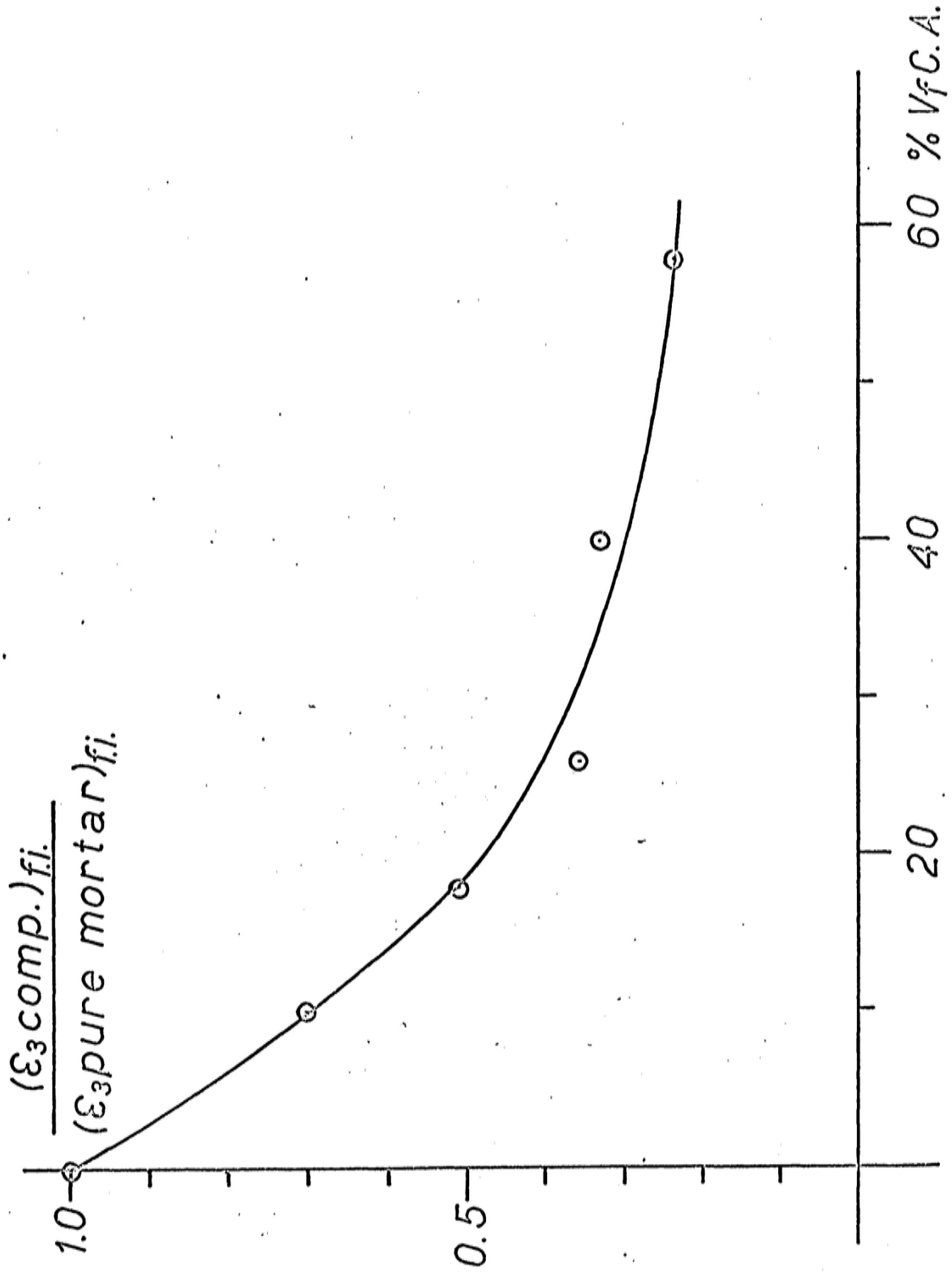


fig. 6-12

GLASS-MARBLE CONCRETE AND PLATE-MODEL TEST RESULTS

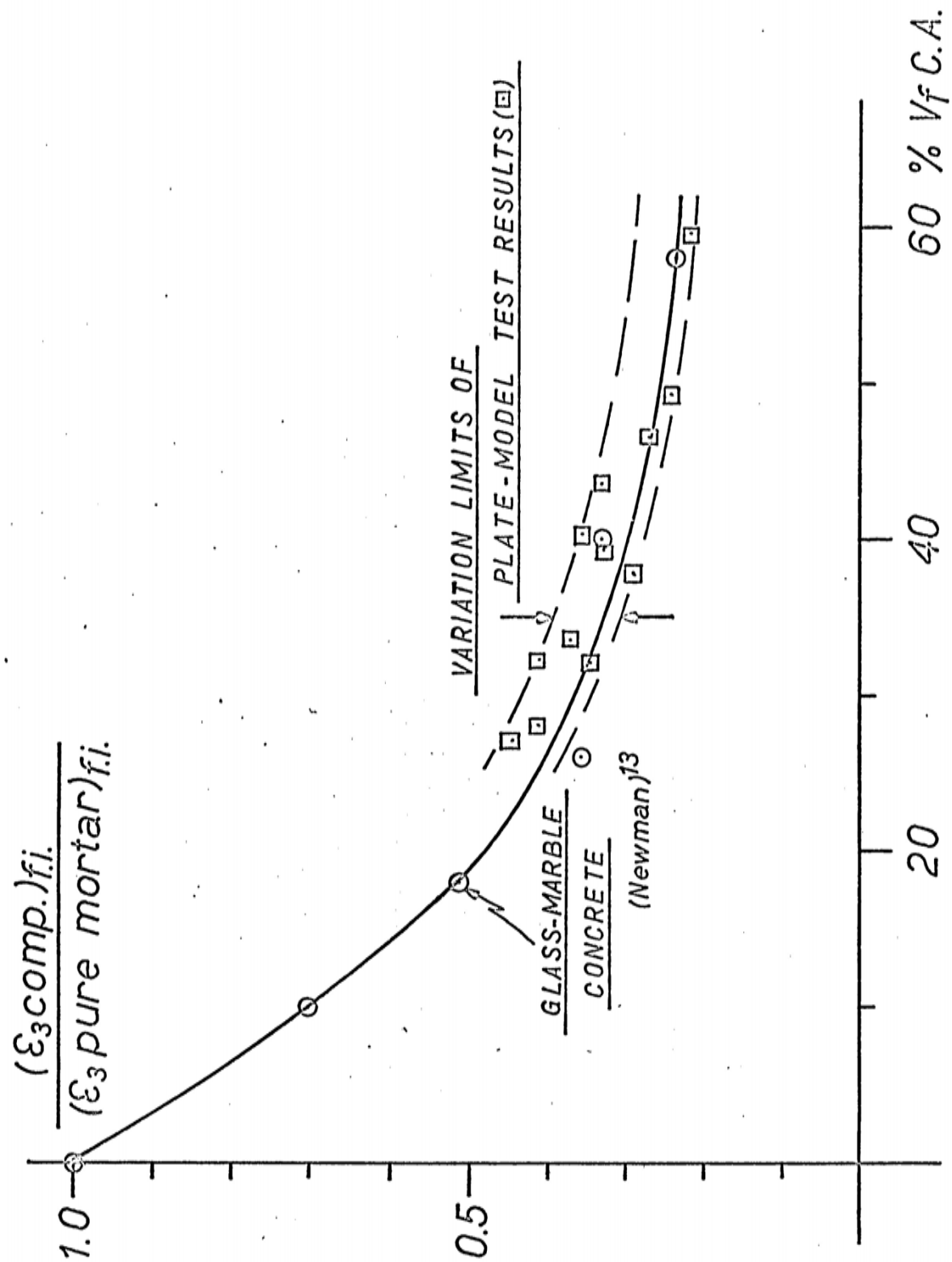


fig. 6-13

It was considered that this close agreement was especially significant since a direct method had been used to pin-point fracture initiation in the plate-models and an indirect overall strain measurement method had been used for the glass-marble concretes. It was therefore concluded that the plates were a valid two-dimensional representation of such gap-graded concretes and that the phenomena observed in the plates were probably a good representation of those occurring inside the glass-marble concretes. So it was felt that the plates could be safely used to explain the process of crack initiation and propagation in these concretes.

Section 4. Strains up to Failure

After the composite strains required to initiate micro-cracking in the mortar matrix in the plate-models had been obtained by determination of the point at which the load to tensile strain (measured at the most critical point) relation ceased to be linear, a study of the tensile strains from that point onwards and up to failure was conducted.

In the first series of plates (MPA) the relation between the measured compressive field strains ($(\xi_3)_f$) and the tensile strains at the most critical points after the onset of micro-cracking was found to be approximately the same for the four plates and so independent of the spacing of the aggregate particles. After fracture initiation, the tensile strains increased with respect to the field strains at a very rapid rate up to failure. In certain cases, more than 6000 micro-strains were recorded. The average relation between these tensile and field strains is shown on the graph in figure 6-14 as a single curve for the four plates.

In the MPB series, the recorded tensile strains on the first

three plates varied with the field strains in approximately the same way. After fracture initiation, the rate of increase of the tensile strains became somewhat larger than previously but at a certain point was seen to decrease. On plate MPB-4, the field strain to tensile strain relation was seen to be vastly different and was plotted individually on figure 6-14. For the other three plates, an average curve is shown on that figure.

In the last series of plates (MPC) the strain response was also found to be approximately the same for all plates after crack initiation, and somewhat similar to the behaviour of the MPA plates. An average curve representing the relation between the measured tensile strains at the most critical points and the field strains is shown on figure 6-14.

Examination of figure 6-14 showed that for all plates the tensile strain at the most critical point at any value of the field strain was greater than that for pure mortar. For plates MPB-1-2-3, this increase in tensile strain was found to be much smaller than for all other plates. It was concluded that in these MPB plates, the onset of micro-cracking had somehow allowed a certain redistribution of the stresses which prevented a large increase in the tensile strain at the most critical point. In the other plates, the onset of micro-cracking was considered to have simply weakened the material without altering the applied stress state and that therefore large increases in the tensile strain had occurred due to extensive micro-cracking.

It is difficult to determine the manner in which a stress redistribution has occurred without a comprehensive stress analysis, but however, consideration of the position of the most critical points on the plates is of assistance in understanding their behaviour. On

RELATION BETWEEN FIELD STRAIN AND TENSILE STRAIN AT MOST CRITICAL POINTS

fig. 6-14

plates MPB-4, MPA-1-2-3-4 and MPC-1-2-3-4, the most critical point was either on top of one aggregate particle (MPB-4) or in-between two particles which were aligned in the direction of loading (MPA, MPC). It is reasonable to assume that at such points, cracking could not alter the applied stress state because there were no other possible stress paths.

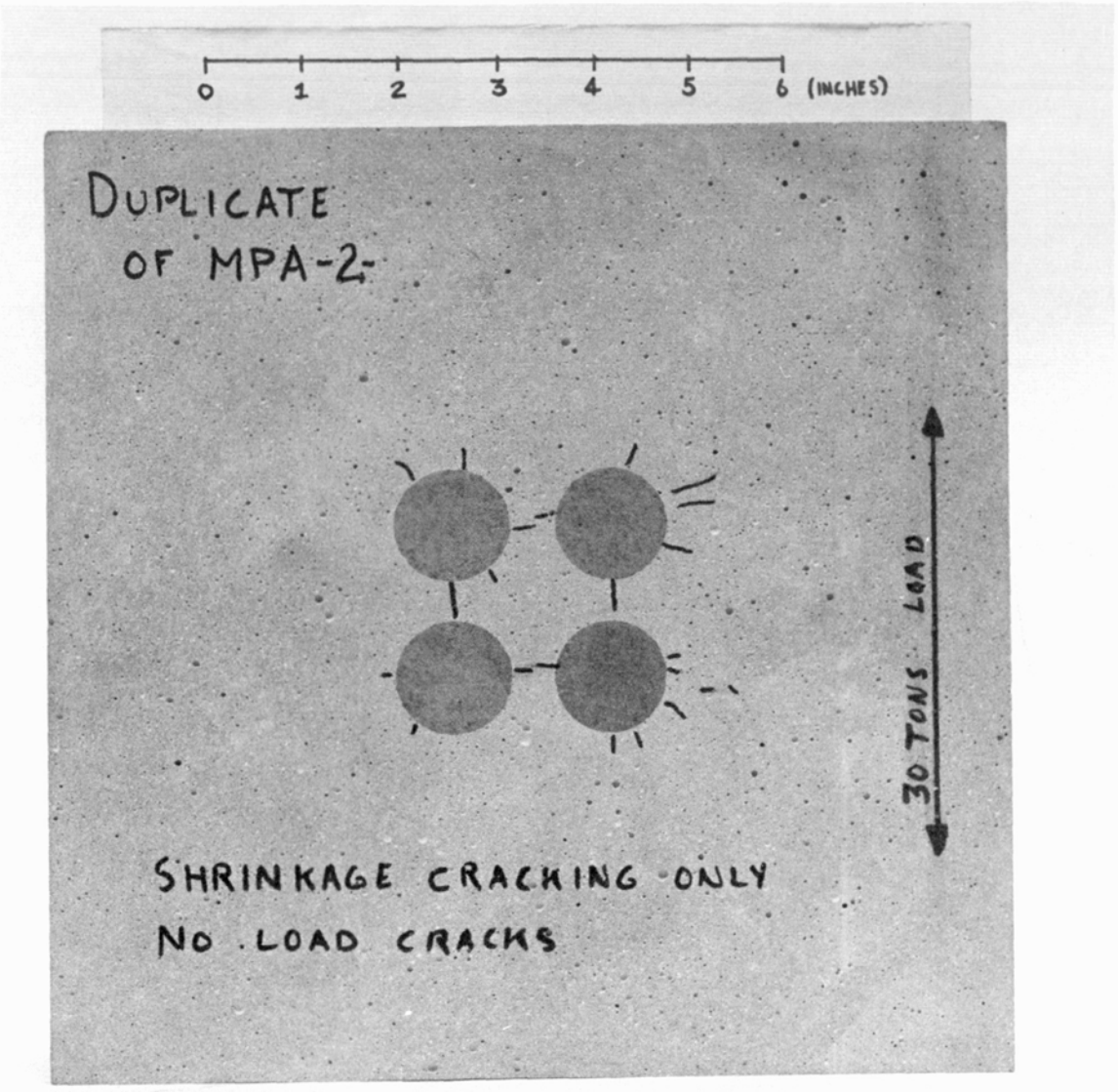
Section 5. Crack Patterns

a) Crack Patterns prior to Loading

Two different methods were used to detect the cracks due to drying shrinkage of the plates. Before loading, the plates were examined using a stereo-microscope (90 x magnification). Use was also made of a fluorescent dyeing technique described by McCreath[3]. In this method, plates are sprayed with a special "flaw detecting ink" and viewed under ultraviolet light which indicates flaws as fluorescent lines.

The pattern of shrinkage cracks thus detected was found to be the same for all plates, whatever particle array was considered. A number of cracks (of no more than $\frac{1}{4}$ to $\frac{1}{2}$ of a diameter in length) were seen to radiate from the cylindrical aggregate inclusions. The dyeing technique indicated that cracks directly between two particles close to each other were usually larger than all others. It should be noted in addition that these large cracks were the only ones visible through the microscope.

A typical pattern of shrinkage cracks is shown on figure 6-15. It should be noted that the zones where the cracks appeared larger coincide with the zones of high shear-strain on the photoelastic coating when no load was applied to the plate (see frame 'a', figure 6-21). The other cracks are found in zones of low shear strain due



TYPICAL SHRINKAGE CRACK PATTERN

FIGURE 6-15

to shrinkage.

b) Influence of Shrinkage Cracks

Due to the various aggregate particle arrays tested, the alignment of the shrinkage cracks in the critical zones with respect to the direction of the principal strains was not always the same. In models A and C, the shrinkage cracks were aligned in the direction of the minor principal strain and in the first three MPB plates, in the direction of the major principal strain. In the model tested by McCreath[3], there were no cracks at all in the critical zones.

It was felt that the possible influence of these shrinkage cracks upon the analysis of the strain distribution in the plate-models would have been to cause high tensile strains at certain points where the cracks were aligned in the direction of loading (plates MPA, MPC, and MPB-4). This in turn would have caused lower composite strain levels at fracture initiation to be predicted.

It was therefore considered unlikely that the shrinkage cracks had influenced the strain distribution since it was not thought likely that the shrinkage cracks would have thus caused the predicted composite strains at fracture initiation in models A and C to be approximately the same as in model B and as in McCreath's model. It should also be noted that the distribution of tensile strain in the plate-models always showed a gradual strain increase from a safe zone to a critical zone and to the most critical point. It is probable that large strain differences from one point to another would have been noticed if a crack had opened up under load at a gauge point. Only in one case was the strain distribution affected in such a way as to suggest the possible influence of a crack (plate MPC-4).

Since the composite strains at fracture initiation obtained during the loading tests to failure of the plates coincided generally

with the predicted ones, it was also considered unlikely that fracture had suddenly been initiated by the extension of a shrinkage crack under one of the 2 mm gauges placed at the most critical points on the plates.

It was therefore concluded that the shrinkage cracks were probably only surface cracks not having a significant influence in the present analysis of the plate-models.

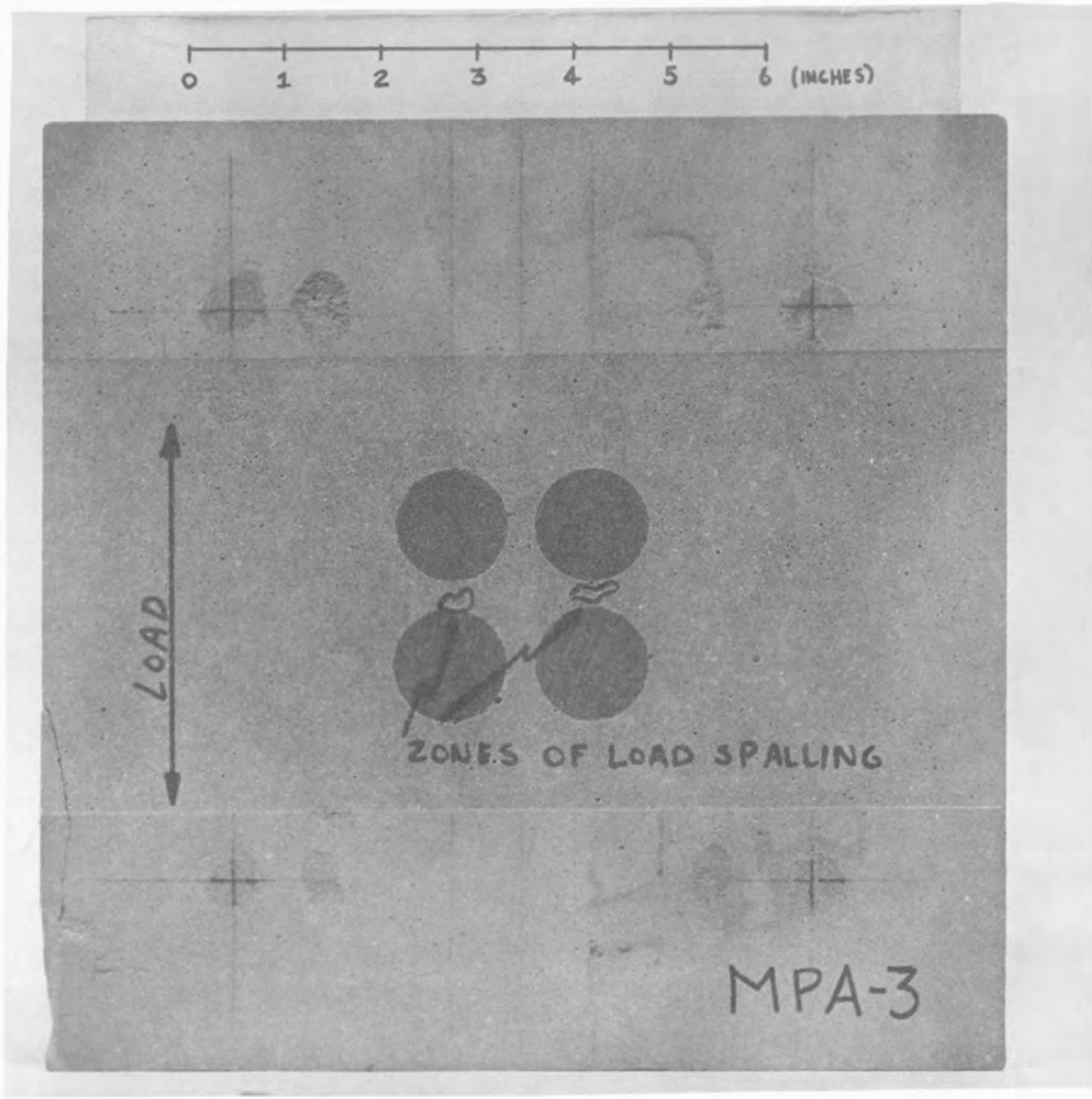
Finally, it should be mentioned that the discontinuity strains measured on glass-marble concrete cylinders being similar to the ones measured on the plate-models for the same volume fractions of coarse aggregate, any general influence of shrinkage cracks upon the behaviour of the plate-models must have been the same as on the three-dimensional concrete specimens.

c) Crack Patterns Observed after Failure

MPA Series

In this series, two plates out of four remained fairly intact after failure. It was possible to grind the uncoated face of these using the Abwood grinding machine, taking away barely one hundredth of an inch, to remove the adhesive used for fixing the strain gauges. In this way, smooth surfaces were obtained which were sprayed with the "flaw detecting ink" and viewed under ultraviolet light.

On each of these two plates, only shrinkage cracks were observed in the mortar matrix outside the critical zones. In these critical zones however, the mortar seemed to be completely disrupted and had spalled off in certain places. In figure 6-16, plate MPA-3 is shown. The zones of spalling of the mortar under load are outlined but the shrinkage cracks are not showed since they remained unaffected by the load as far as could be seen and they exhibited a



CRACK PATTERN AFTER FAILURE

FOR PLATE MPA-3

FIGURE 6-16

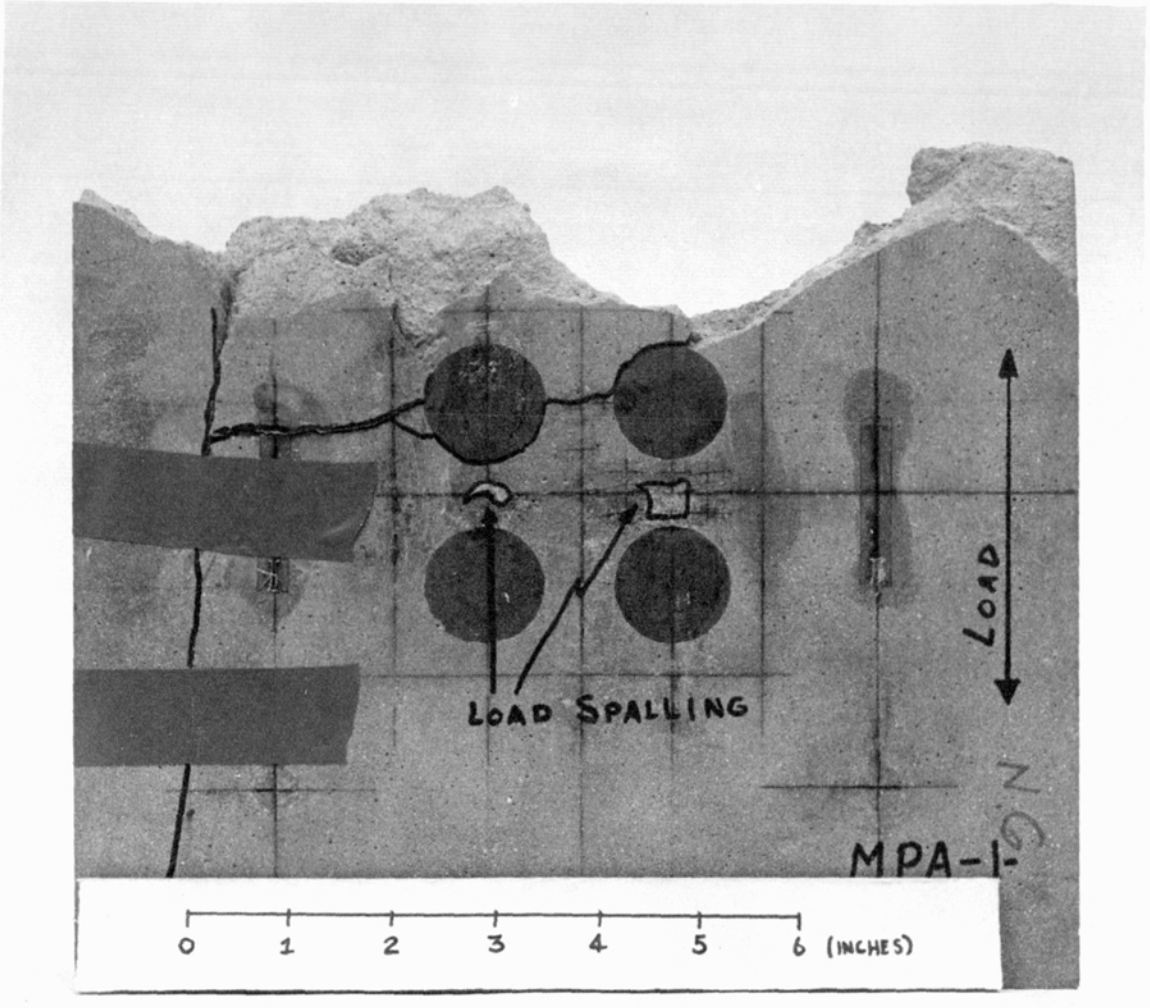
pattern similar to the one shown on figure 6-15.

One of the plates that it was not possible to grind is shown on figure 6-17. On this plate, and on the last one in this series, zones of spalling of the mortar in the predicted critical zones were observed although they were not as well defined as in the ground plates. A large crack perpendicular to the direction of load was observed on the plate shown in figure 6-17. It was considered this was due to the sudden unloading of the plate when it failed causing a rebound of the vertical strain and therefore putting the plate in tension.

Finally, it should be noted that not only had fracture initiation been predicted in these zones of spalling seen on the plates but that very large tensile strains of up to 10000 micro-strains had been measured at the center of these zones.

MPB Series

In this series also, two plates remained in a condition which allowed grinding after failure. Apart from the major cracks (visible to the naked eye) due to the overall breakdown of one of these plates, no cracking under load was observed. The use of the ultra-violet light and the "flaw detecting ink" revealed the usual pattern of shrinkage cracks, but in the zones where the onset of micro-cracking had been determined by the continuous recording of the tensile strain (as mentioned in the previous sections) no cracks were observed. This was not surprising since the recording of the tensile strain had shown that micro-cracking had not progressed to a large degree in that zone possibly due to stress relieving. It simply showed that a larger amount of micro-cracking was needed before a crack of sufficient length to be detected by the ultra-violet light method could develop. If one considers that a micro-crack in mortar might



CRACK PATTERN AFTER FAILURE

FOR PLATE MPA-1

FIGURE 6-17

be only a small proportion of the spacing between two grains of sand, this is hardly surprising. A photograph of the plate exhibiting large failure cracks is shown on figure 6-18.

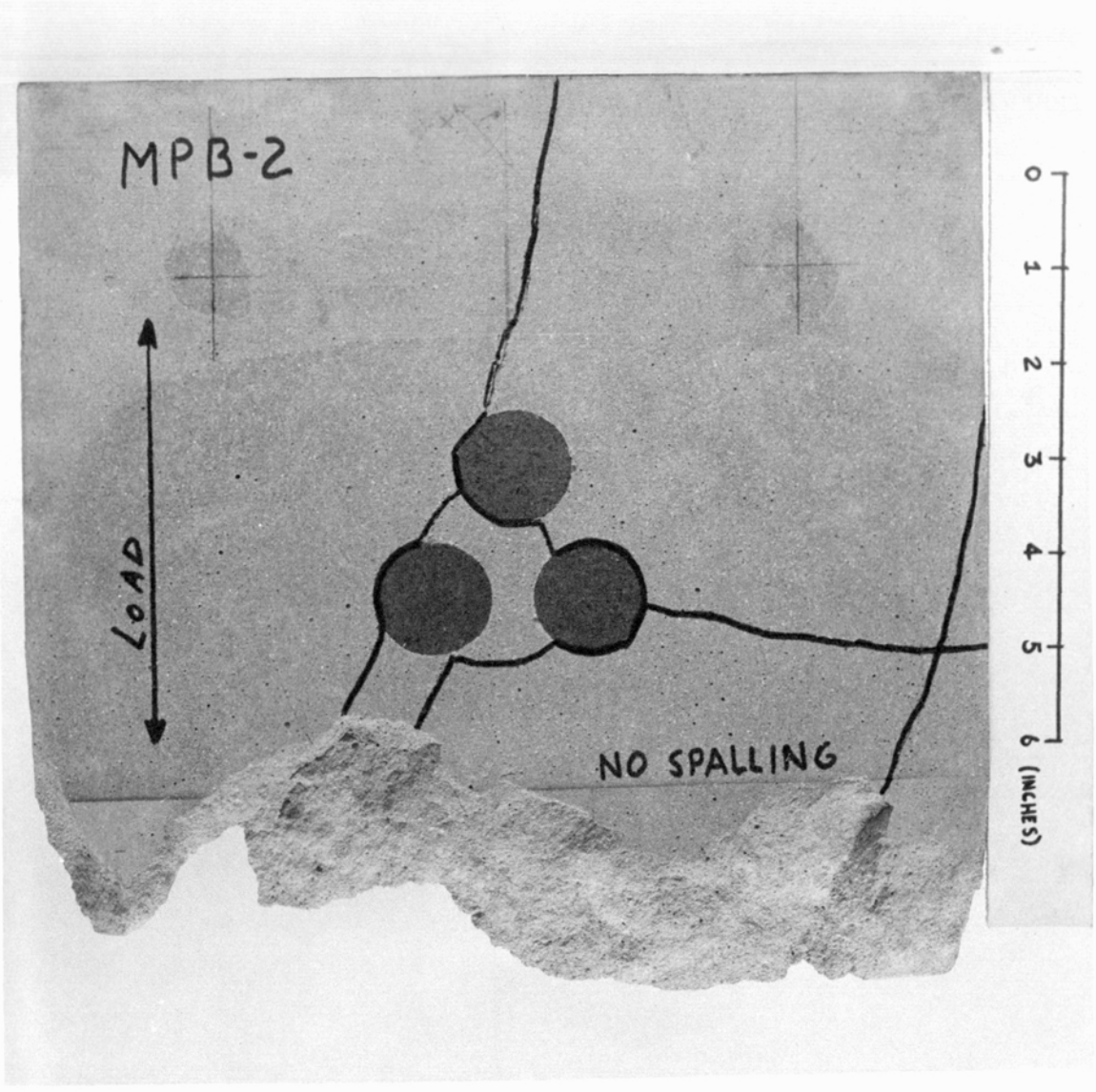
The last plate in the series, MPB-4 was also photographed and can be seen on figure 6-19. Even if grinding was not possible, evidence of load spalling was seen on top of the middle particle in the array. Large tensile strains had been measured at that point which had been predicted to be the most critical.

It was therefore evident from the overall crack patterns in these two plates photographed that the onset of micro-cracking at the most critical point inside the array had little or no influence on the final failure of the plates. These two patterns were seen to be similar but in one case the zone between the two bottom particles had been found to be critical and in the other case, safe.

MPC Series

In the last series, three plates out of four remained intact after failure. Their uncoated face was ground to obtain a smooth surface and they were sprayed with the "flaw detecting ink". On examination under ultra-violet light, the usual pattern of shrinkage cracks appeared on each of them but cracks due to load were only seen on one plate (in the critical zone). On the other plates, there was either no signs of cracking, or in many cases zones of spalling of the mortar in the predicted critical zones.

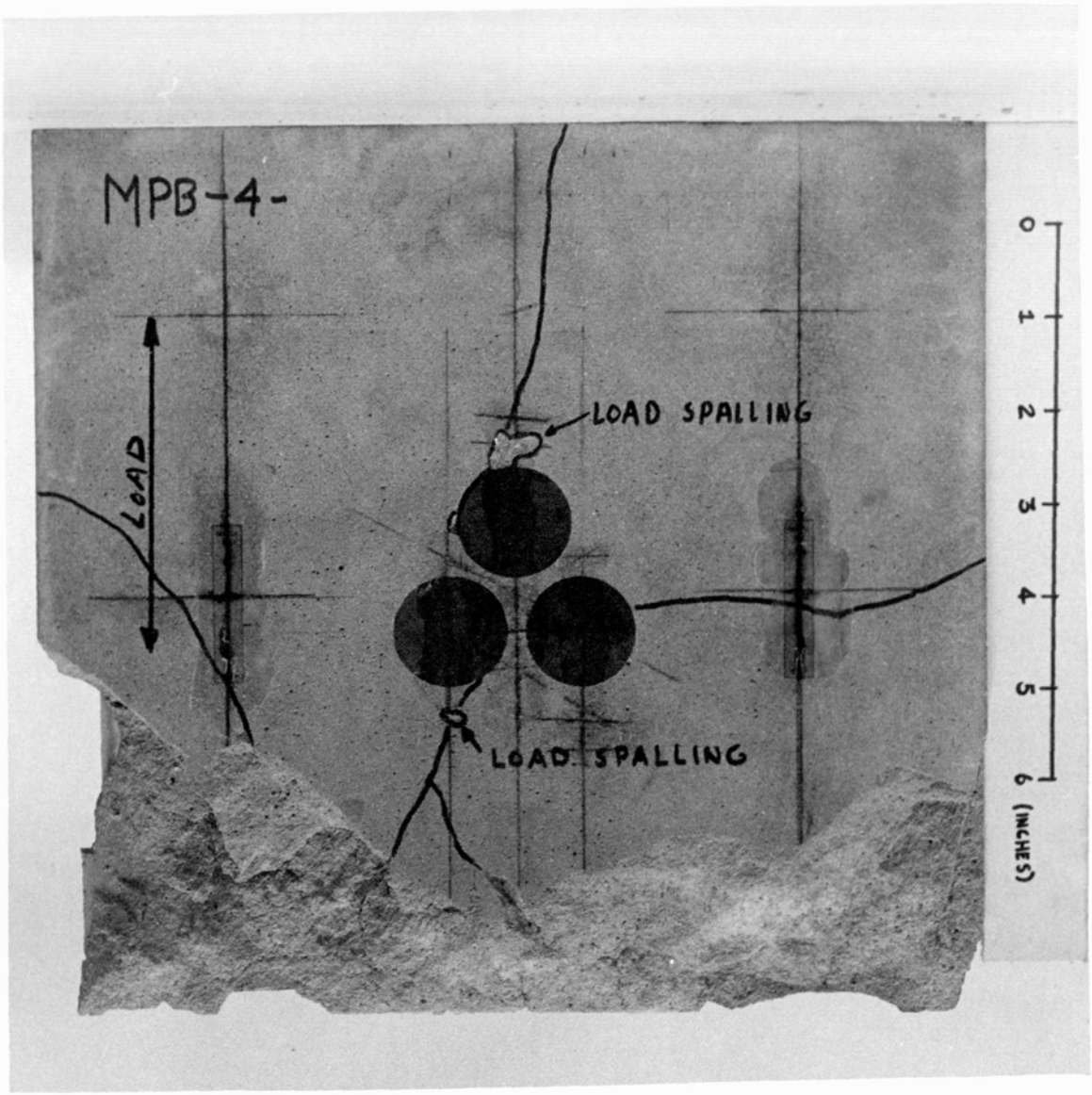
Large tensile strains at failure had generally been measured at the most critical points and the zones where the load spalling was seen usually coincided with the ones where the largest tensile strains had been recorded. It must be concluded therefore that in some critical zones, micro-cracking had not progressed to an extent large enough to be detected by the ultra-violet light method



CRACK PATTERN AFTER FAILURE

FOR PLATE MPB-2

FIGURE 6-18



CRACK PATTERN AFTER FAILURE

FOR PLATE MPB-4

FIGURE 6-19

(except in one case) or to cause spalling of the mortar.

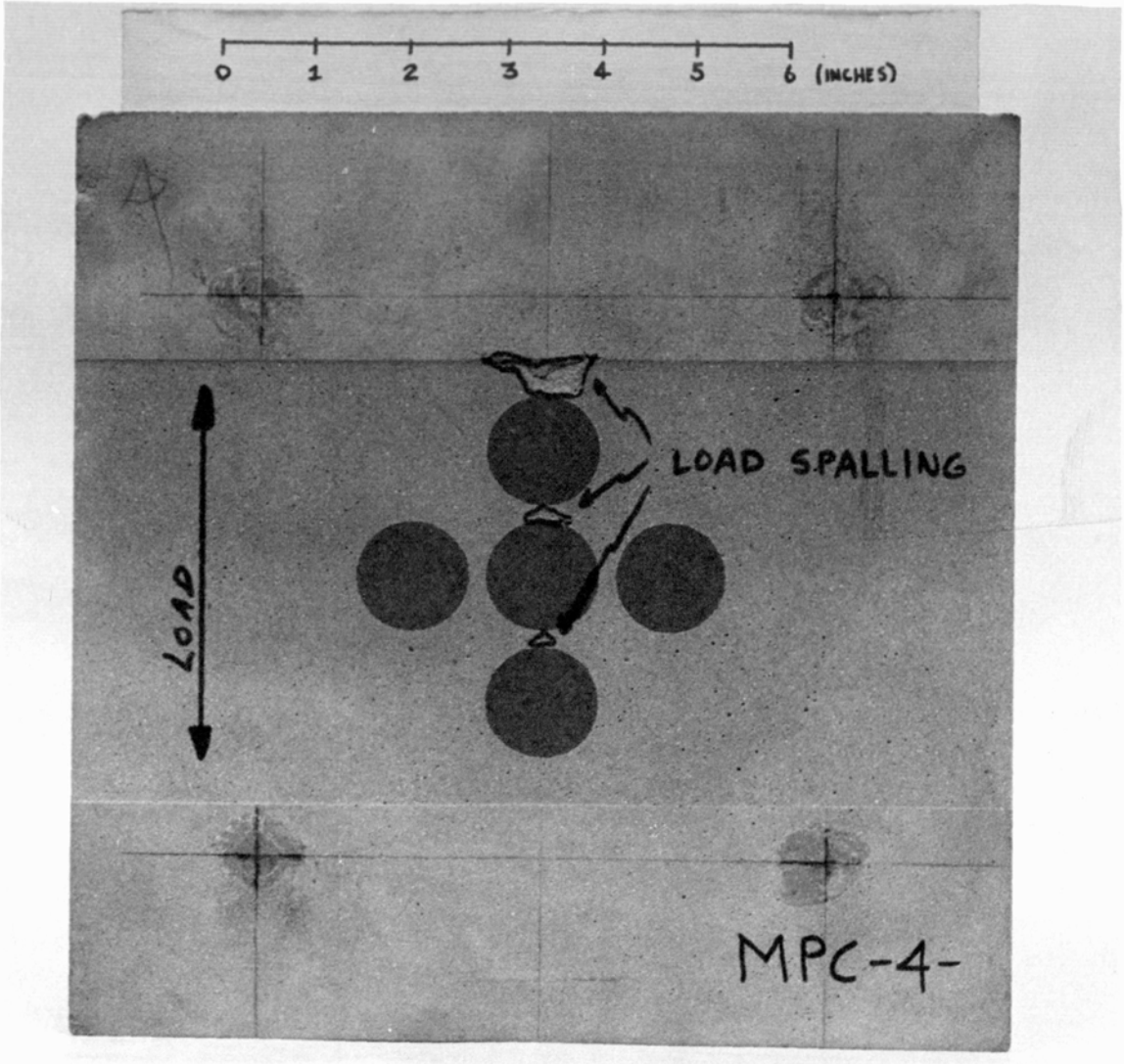
On figure 6-20, a photograph of plate MPC-4 is shown and the zones of spalling of the mortar under load are outlined.

Section 6. Photographs of Isochromatic Patterns

As mentioned previously, the isochromatic pattern on the photo-elastic coating on each plate was photographed every 30 seconds during the loading tests to failure. Examination of each set of photographs and comparison with the sets for the other plates in the series revealed similar behaviour. It was therefore decided that only the description of the photographs taken on one plate in each series would be given in the present chapter. It was not considered necessary to show all the pictures from each chosen typical plate (about 30), so eight frames in each film were selected.

It must be emphasized that the fringes that appear on the photoelastic coating represent a value of shear strain $(\varepsilon_3 - \varepsilon_1)$. As the shear strain increases in the coating, the colour moves from black, to white, to yellow and to red. After red, the first fringe is said to be reached (a shear strain of approximately 600 micro-strains). As the strain increases further, the colour then changes to blue, to green, to yellow and to pink. Now the second fringe is reached (approximately 1200 micro-strains). From that point onwards, the colour only changes from pink to green, to pink etc. and every time the pink colour appears, a new fringe is reached. It should be noted that on the photographs, the pink colour might appear more like mauve due to technical difficulties of reproduction.

Finally, it must be mentioned again that because of the thickness effects of the coating, the strain gradient at certain points is probably much steeper than apparant on the coating.



CRACK PATTERN AFTER FAILURE

FOR PLATE MPC-4

FIGURE 6-20

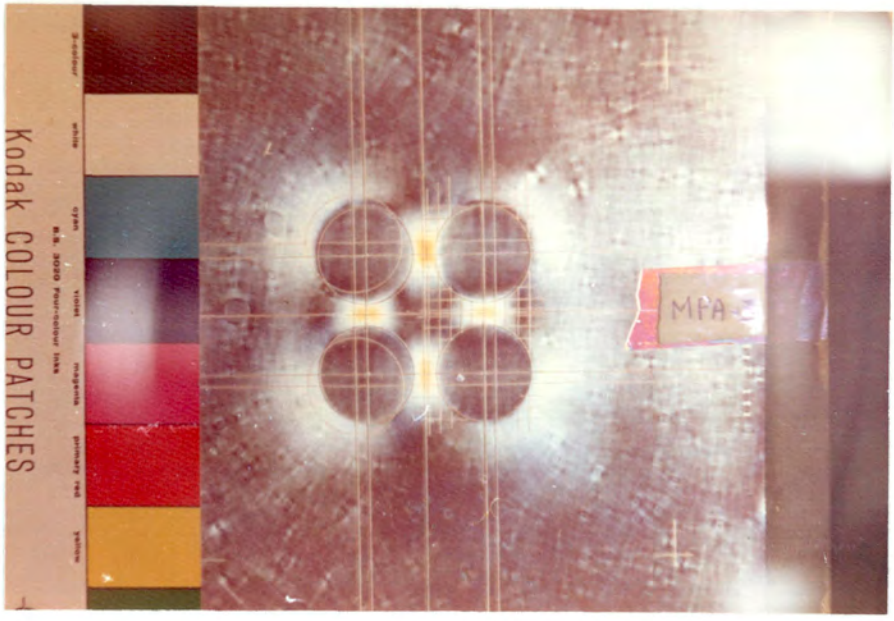
Plate MPA-3 (Photographs on figure 6-21)

The isochromatic pattern due to shrinkage only is shown on the first photograph (frame 'a'). It must be remembered that this pattern has to be "subtracted" from the ones seen on the other pictures to obtain the strains due to the applied load only.

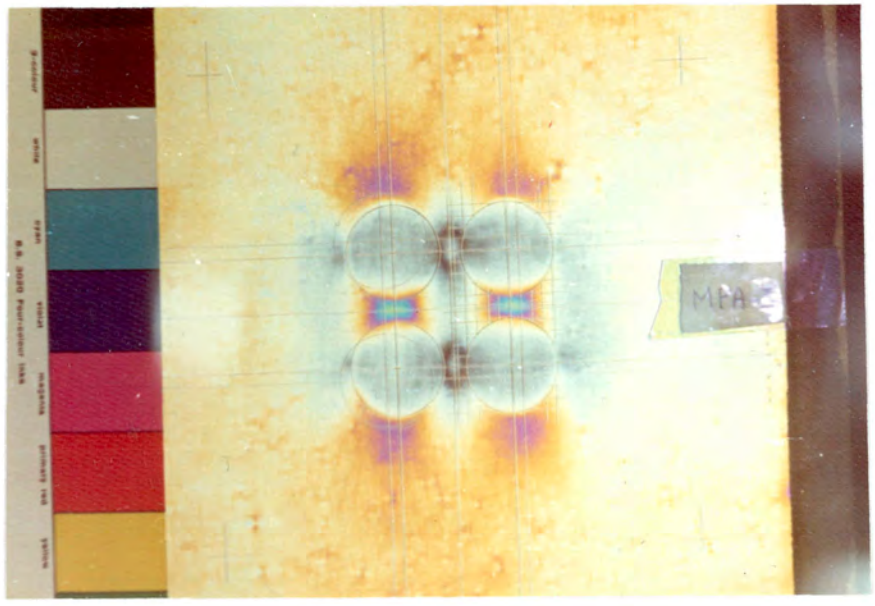
At a load level of 1800 p.s.i. (frame 'b') and then at a load of 3240 p.s.i. (frame 'c') only the mid-sections of the two predicted critical zones seemed to be straining at a higher rate than the mortar in the "field". But at 5100 p.s.i. (frame 'd') high strain concentrations were seen to start moving from the center of the critical zones up to, and around, the aggregate inclusions. Further load increments (frames 'e', 'f', 'g') only served to emphasize this effect.

The last photograph, frame 'h', shows the isochromatic pattern after failure upon removal of the applied load. High residual strains were seen in the critical zones (i.e. between two particles aligned in the direction of load), around the aggregate inclusions and also on top of them. It was considered that these residual strains were certainly due in a large part to the development of micro-cracking. As the sequence of the photographs strongly suggests, micro-cracking had initiated at the mid-section of the critical zones and later had progressed around the aggregate inclusions. On the uncoated face of the plate, evidence of a very high degree of micro-cracking (spalling of the mortar) had been noted, but only in the critical zones. This, therefore, suggested that around the aggregate inclusions and on top of them, micro-cracking had not progressed to such a high degree as to cause spalling.

In the mortar "field", only a relatively small amount of permanent disruption seemed to have been caused and at the center



(a)
0 p.s.i.

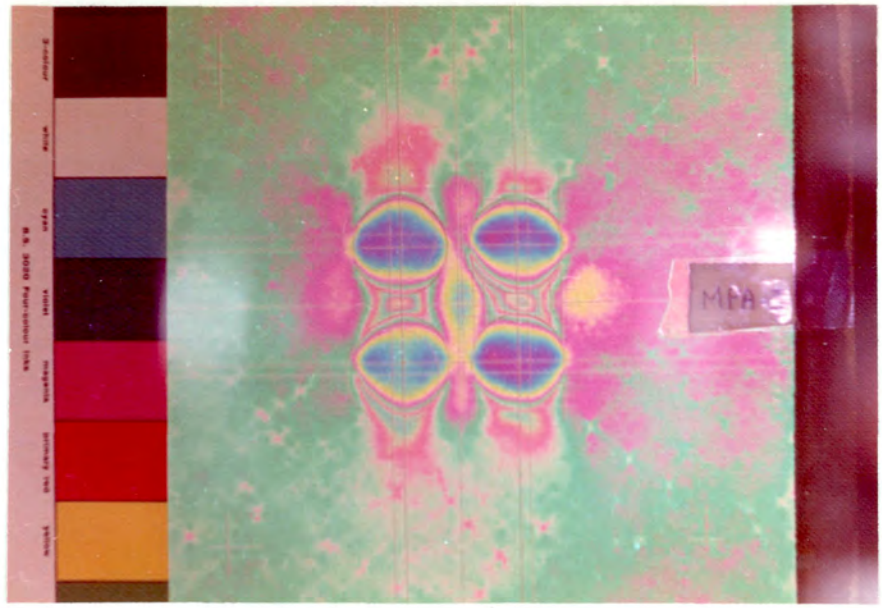


(b)
1800 p.s.i.

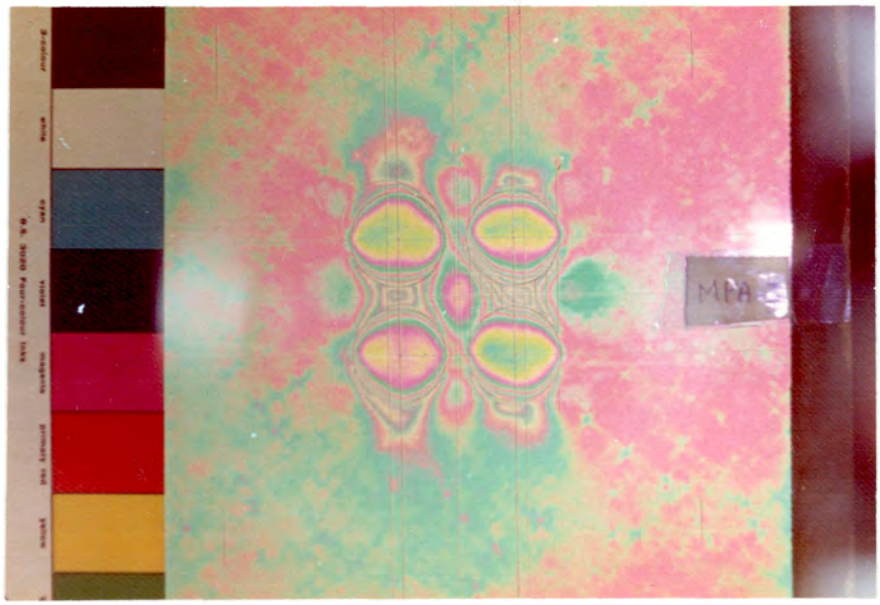


(c)
3240 p.s.i.

Figure 6-21



(d)
5100 p.s.i.



(e)
6600 p.s.i.

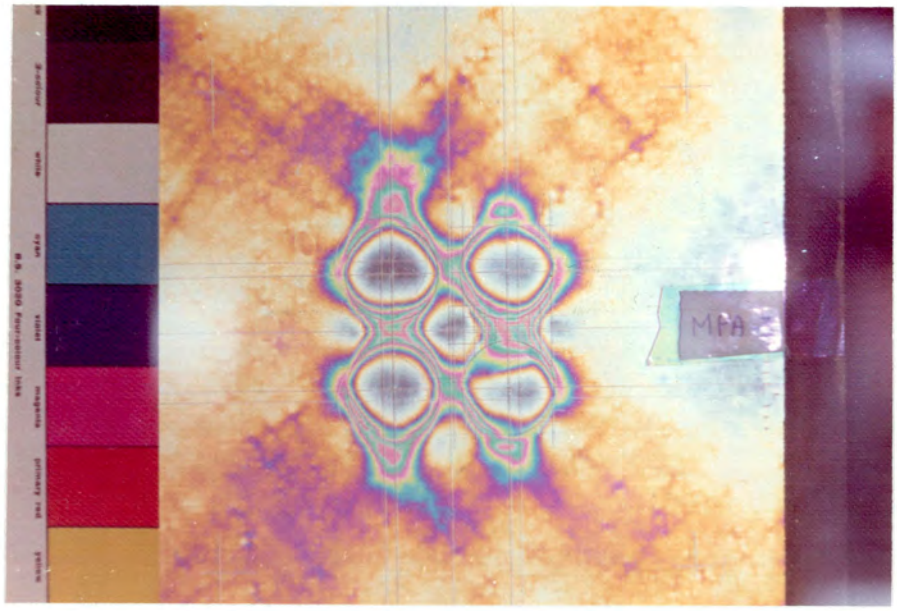


(f)
8070 p.s.i.

Figure 6-21 (Cont'd)



(g)
10050 p.s.i.



(h)
0 p.s.i.

Figure 6-21 (Cont'd)

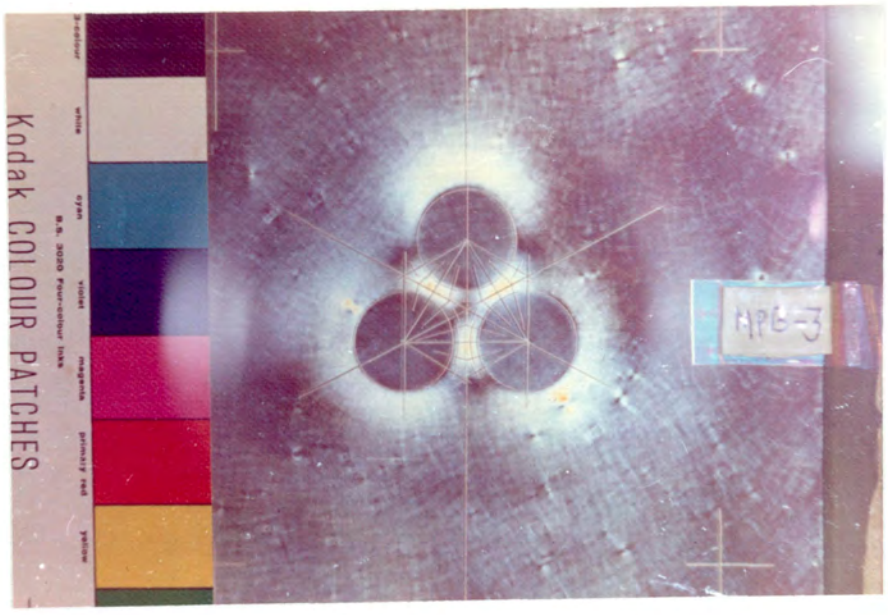
of symmetry of the particle array, a zone found to be "safe" from the strain analysis in chapter V, no residual strains were found.

Plate MPB-3 (Photographs on figure 6-22)

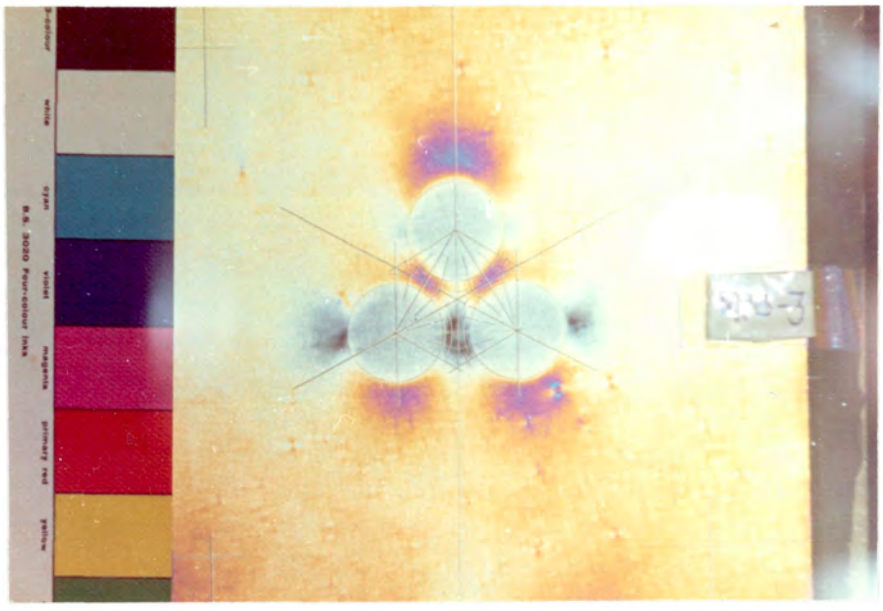
The most critical point on this particular plate had been found in the mortar zone directly between the two bottom particles of the array. It was found that the value of the shear strain at that point was generally low because the photographs indicated that load channelling through the bottom particles had occurred, causing a decrease of the compressive strain. But it was seen that, whereas at low loads (frames 'b' and 'c') the shear strain level in this particular zone was lower than in the adjacent aggregate particles, at a load of 4200 p.s.i. (frame 'd'), it was higher. In the following photographs the shear strain at that point relative to the shear strain value in the field continued to increase, although not at the rapid rates seen in the critical zones in plate MPA-3.

In other parts of the matrix, the strain response was found to be approximately linear up to the fifth photograph (a stress of 7050 p.s.i.) when high strain concentrations started to appear (a) between the aggregate particles aligned at 30 degrees with respect to the vertical axis, (b) around the aggregate inclusions and (c) on top of them. At 9390 p.s.i. and at 11,790 p.s.i., these high strain concentrations simply increased in value and the last photograph, taken upon removal of the load after failure indicated large residual strains in these zones which suggested that micro-cracking had occurred.

Examination of this series of photographs therefore confirmed that micro-cracking had initiated at the predicted point as also evidenced by the sudden deviation from linearity in the recorded tensile strain. It appeared that this micro-cracking had not subsequently progressed to a large extent. At later stages in the loading



(a)
0 p.s.i.



(b)
1260 p.s.i.



(c)
2640 p.s.i.

Figure 6-22



(d)
4200 p.s.i.



(e)
7050 p.s.i.



(f)
9390 p.s.i.

Figure 6-22 (Cont'd)



(g)
11790 p.s.i.



(h)
0 p.s.i.

Figure 6-22 (Cont'd)

micro-cracking appeared in other zones especially around the aggregate particles.

No cracks had been detected when the above plate was ground, washed with the "flaw detecting ink" and viewed under ultra-violet light. It was considered that the geometry of the system and the pattern of the strain disturbances had caused large zones to be subjected to micro-cracking and that sharp detectable flaws had not formed. Instead a high degree of "internal" disruption of the mortar matrix had occurred.

Plate MPC-2 (Photographs on figure 6-23)

Examination of the photographs in figure 6-23 indicated that the three particles aligned in the direction of loading had acted as a unit and had been largely unaffected by the presence of the other two particles (which behaved as individual units). The pattern of the strain distribution in the critical zones was seen to be closely similar to the one observed in the critical zones on plate MPA-3. Large shear-strain concentrations at the center of these critical zones were seen to occur fairly early in the loading sequence (frames 'c' and 'd') and at higher loads (frame 'e', 'f', 'g') these were seen to move around the aggregate particles. As in the MPA plates, evidence of load spalling in these critical zones had indicated that micro-cracking had progressed to a very high degree.

The residual strains after failure, seen on the last frame ('h') showed that more damage had occurred in these critical zones than at any other place.

Section 7. Discussion of Results and Conclusions

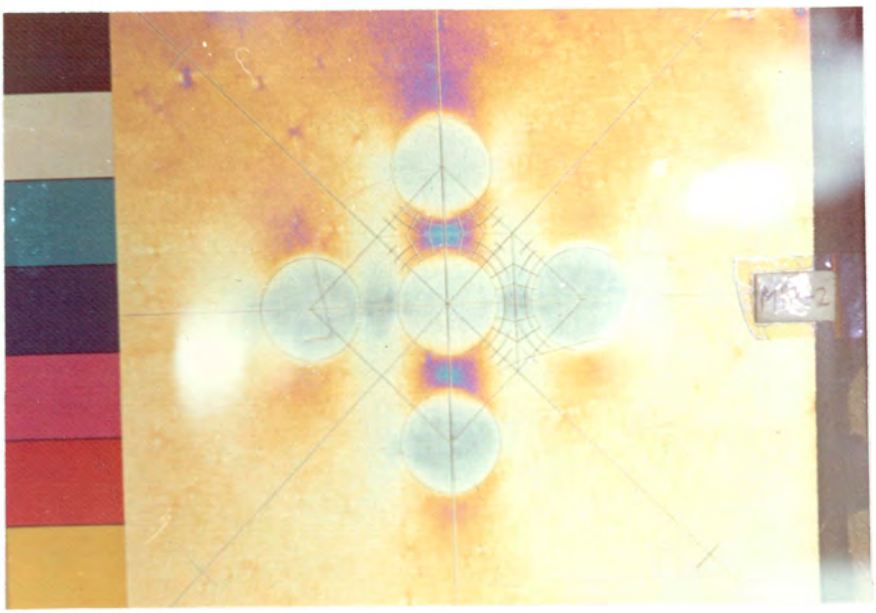
a) Applicability of Plate-Model Test Results to Concrete

Newman's[13] uniaxial compression tests have shown that the introduction of coarse aggregate in a mortar matrix reduces significantly



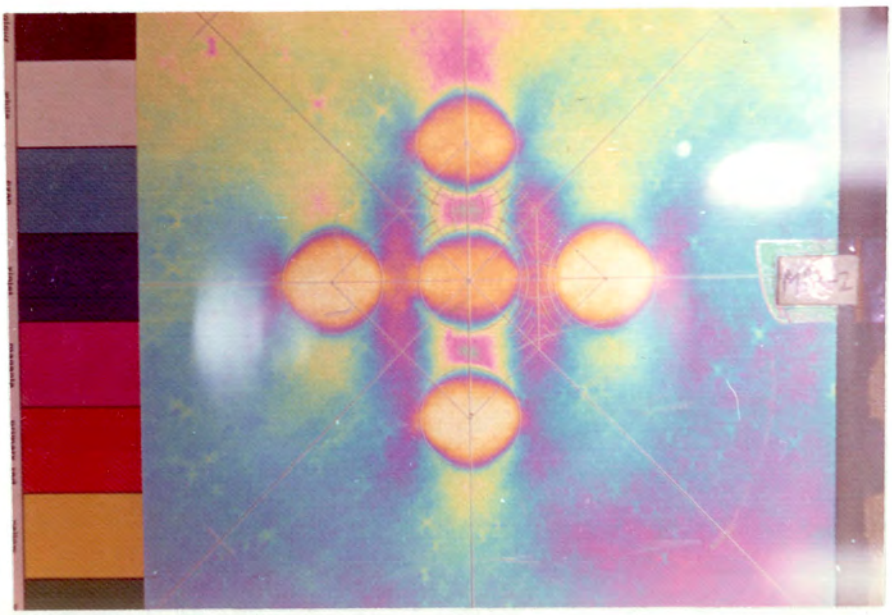
(a)

0 p.s.i.



(b)

1440 p.s.i.



(c)

2880 p.s.i.

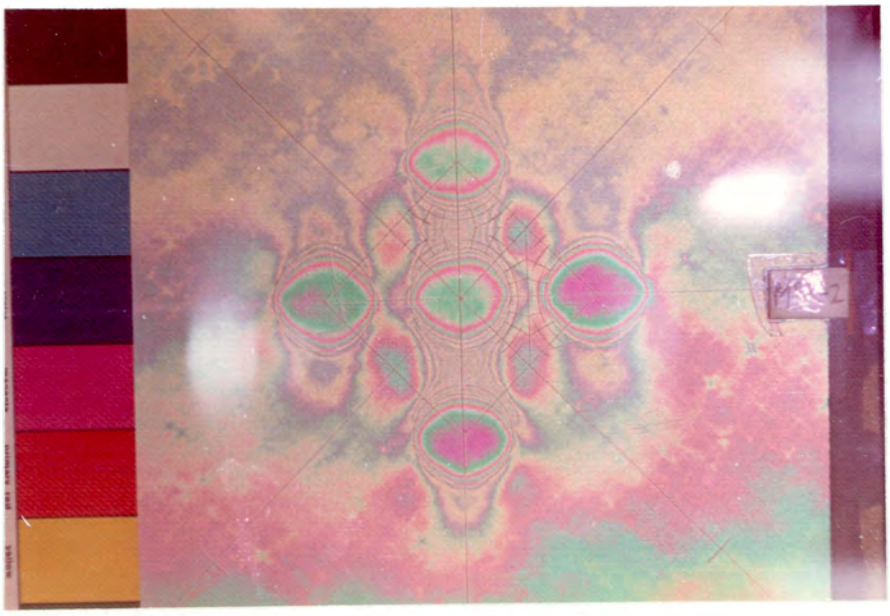
Figure 6-23



(d)
4710 p.s.i.



(e)
6600 p.s.i.



(f)
8820 p.s.i.

Figure 6-23 (Cont'd)



(g)
11130 p.s.i.



(h)
0 p.s.i.

Figure 6-23 (Cont'd)

the value of the minor principal composite strain (ε_3) required for fracture initiation (see figure 6-12). These tests were performed on cylinders containing various quantities of single-sized ground glass spheres in a mortar matrix, and a relation was established between the volume fraction of coarse aggregate and the level of minor principal composite strain required to initiate fracture.

The plate-model tests in the present series contained three different arrays of cylindrical aggregate particles with various spacings between particles representing volume fractions of coarse aggregate varying between 27% and 60%. The strain analysis in chapter V and the use of the fracture initiation envelope allowed the onset of micro-cracking to be predicted at certain points and at certain composite strain levels. Continuous strain readings on the plates during the tests to failure confirmed that fracture initiated at the level of composite strain predicted, and that the relationship between the composite strains required for fracture initiation and the percentage of aggregate was the same for all three particle arrays and similar to the relation obtained by Newman and three-dimensional test specimens within the same range of volume fractions of coarse aggregate (see figure 6-13).

Since the points where discontinuity strains were measured on the plate-models were in the mortar matrix and since the relation between the composite compressive strain required for fracture initiation and the volume fraction of coarse aggregate was the same for the plate-models and the three-dimensional specimens, it was concluded that fracture in these three-dimensional specimens had also initiated in the mortar matrix. The strain disturbances causing the low levels of composite strains at fracture initiation in the plate-models (the basic mechanisms of fracture initiation in such models) were

therefore considered most probably the same in "real" concrete.

The three models tested by the author and the one tested by McCreath (which gave similar results) can therefore be considered to comprise a valid two-dimensional representation of particles in concrete (containing single-sized glass-spheres) and the process of crack initiation and propagation in these plates is certainly a good indication of processes occurring "inside" the glass-marble concretes under load for the region of volume fractions of coarse aggregate investigated in the plate-models.

It must also be mentioned that the "elastic" strain analysis for the mortar matrix alone, used to study the discontinuity level of the plate-models, was therefore totally justified. The curves showing the strain disturbances (isochromatics, isotenics) in the various models (figures 5-12 to 5-55) can also be expected to give a valid indication of the strain disturbances in concrete before the onset of micro-cracking.

b) The Process of Crack Initiation and Propagation

It can now be said with almost absolute certainty that if the presence of round aggregate particles in a mortar matrix reduces so significantly the composite strains required for fracture initiation, it is because the presence of hard aggregate causes local high tensile strain concentrations in the mortar matrix (concentrations of the type seen in the models tested - see figures 5-12 to 5-55) enabling it to reach earlier at certain points the level of strain required for fracture initiation.

It should be noted that above a volume fraction of coarse aggregate of approximately 25%, there is relatively only a small change in the composite strains required to initiate cracking. A large change occurs between 0% (pure mortar) and 25%. It is not surprising

therefore that on the photographs taken during loading to failure and in the recorded strain data as well, only minor differences from one plate to another in the same series were seen since the volume fractions represented ranged from approximately 27% to 60%.

The mode of propagation of the micro-cracks was different in the present series of plates from those McCreath had observed. In the plate-models tested by the author, flaws, discernable using the fluorescent dyeing technique were not found in the zones where micro-cracking had initiated. Instead, gradual extension of these zones of internal micro-cracking until they reached the aggregate particle boundaries was detected. It was considered that the presence of the sharp flaws due to load that were visible in McCreath's[3] models (these flaws initiated at the center of symmetry of the aggregate particle array and moved to and around the aggregate inclusions) was due to the geometry of the particular particle array used which probably caused only relatively small zones to be subjected to micro-cracking. Flaws thus had an opportunity to develop at these points after sufficient micro-cracking had occurred. In certain models of the present series, zones of spalling of the mortar were noted when micro-cracking had had the possibility to develop to a high degree. In others micro-cracking had not reached the required level and there was no apparent disruption.

If the four models tested are now considered to represent fairly well single-sized glass-marble concretes, at least in the range of tests covering volume fractions of coarse aggregate from 27% to 60%, the basic process of crack initiation and propagation in such concretes can be described as follows. At a certain applied stress or composite strain level, micro-cracking initiates because of the high strain concentrations (mostly tensile) zones in the matrix, caused by the

hard aggregate particles. As the load increases further, the zones of micro-cracking in the matrix expand according to their position with respect to the surrounding aggregate particles and a sharp crack can occur at a certain point of sufficient strain intensity. Further load increases cause the material to become completely changed since some zones of mortar reaching the aggregate-mortar interface are completely disrupted. In other zones sharp cracks have possibly formed and moved towards the aggregate particles. Large cracks then form and they propagate along the easiest route in this "new" material which may or may not include the zones originally predicted to be critical. The propagation route definitely includes the aggregate-mortar interface which is the weakest link in the material[24]. The material then "breaks down" very shortly after the above stage when these large cracks have completely disrupted the specimen.

In the plate-models, "break down" occurs suddenly when large cracks form(as seen in model MPB-4, for instance). But in glass-marble concrete, because of the increased complexity of the material compared to a simple plate-model made mostly of mortar, more time is required for these large cracks to travel completely through the material.

It must be emphasized that in a concrete containing graded and more angular aggregate where the complexity of the material is even greater, large cracks might form well before the stage of complete disruption is reached.

CHAPTER VII

TESTS ON THREE-DIMENSIONAL CONCRETES

Section 1. Introduction

It was seen in the previous Chapter that the compressive strain of the composite material required for fracture initiation in single-sized glass-marble concretes (and in the plate-models) decreased with increasing volume fraction of coarse aggregate. This was found to be due to high strain concentrations (mostly tensile) in the mortar matrix caused by the presence of hard aggregate particles. It was felt that these strain concentrations would be higher, and thus the composite strains required for fracture initiation lower, if an angular aggregate was used instead of a round one.

It was therefore, decided to test in uniaxial compression (to determine the composite strains at fracture initiation) a series of cylinders (10" x 4" diameter) containing various volume fractions of single-sized coarse gravel aggregate in a mortar matrix. To allow a valid comparison with Newman's[13] glass-marble concrete test results, it was decided that, with the exception of the coarse aggregate particles, these cylinders would have the same characteristics as Newman's[13] test specimens.

Section 2. Testing Procedure

a) Materials

Six groups of three cylinders were cast. All the cylinders in one group contained the same volume fraction of coarse aggregate in a mortar matrix similar to that in the glass-marble concrete specimens and the plate-models (Cf. Chapter III, section 1.) Each group had a different volume fraction of coarse aggregate as follows: 0%, 10%, 20%, 30%, 40% and 50%.

The coarse aggregate was a Thames valley river gravel within the B.S.S. sieve size range $\frac{3}{4}$" - $\frac{3}{8}$".

b) Casting

All cylinders in each group were cast and compacted at the same time and in the same manner. Casting was carried out in three approximately equal layers, each layer being vibrated separately on a vibrating table. The time of vibration varied according to the characteristics of the various mixes in order to achieve the maximum possible compaction. At higher volume fractions generally, longer vibration times were needed. Vibration was concluded when an insignificant number of air bubbles were seen at the surface of the mix.

c) Air Content

At the same time as each group of specimens were cast, the air content of a similarly compacted portion of the mix was determined by means of the pressure pot method[8]. The percentages of air found are given in the following table:

% Coarse Aggregate	% Air in Mix	% Air in Matrix
0	4.05	4.05
10	4.25	4.70
20	3.45	4.30
30	3.00	4.30
40	2.90	4.85
50	2.15	4.30

Table 7-a

Examination of the above showed that the air content in the mortar matrix had not significantly varied from one mix to another.

It was therefore concluded that the mortar matrix phase could be regarded as similar in properties regardless of coarse aggregate content.

d) Curing

The cylinders were cured in the standard manner described in Chapter III. This procedure was also followed for the curing of Newman's[13] specimens.

e) Preparation of Specimens for Testing

When the cylinders were removed from the water after 27 days, the ends of each were ground using an Abwood grinding machine with a diamond impregnated polishing wheel. The resulting ground faces were found to be plane and parallel to within $^{1}/_{1000}$ of an inch and perpendicular to the axis of the cylinder.

A few days prior to testing, the surface of each specimen was carefully scraped to remove all latence before attaching the strain gauges. Four 60 mm electrical resistance strain gauges (PL-60) were placed at equal distances from each other around the mid-circumference of each cylinder. Two opposite gauges were aligned axially and two laterally. Care was taken to avoid the zones where there were cavities in the concrete surface due to air bubbles emprisoned during casting. The gauges were fixed on the concrete surface with P.S. adhesive and left to cure for at least 24 hours before testing.

f) Loading System and Strain Recording

Each cylinder was tested to failure in uniaxial compression in a 300 ton force Amsler loading frame. A spherical seating unit (6" diameter) was placed on top of each specimen to ensure axiality of applied load.

Pressure to the loading frame ram was controlled by an Amsler Hydro-Pacer. It was thus possible to apply to each cylinder a constant rate of applied compressive axial strain of approximately 300 micro-strains per minute.

The strains from the four gauges and from a pressure transducer (calibration shown on figure 6-2) connected to the Amsler pressure control cabinet were continuously recorded by a Peekel data-logger reading at a speed of one channel per second. They were recorded in the following order : the first axial gauge, the first lateral gauge, the pressure transducer, the second lateral gauge and the second axial gauge. In this way, a minimum time (and therefore strain) interval was kept between the two readings of the lateral gauges. These two values and the two values of the axial strain were averaged, every cycle of five readings being considered as a single load stage corresponding to the pressure transducer reading.

Section 3. Compressive Composite Material Strain at Fracture Initiation

A method allowing the strains at fracture initiation (or discontinuity) on three-dimensional concrete specimens to be determined with precision was discussed in chapter IV and an example of the use of this method was described. The method was based on calculations of volumetric strain differences between the points on the volumetric strain ($\Delta V/V0$) against minor compressive principal strain (ε_3) graph and a chosen best straight line representing the linear portion of the curve on the graph. Fracture was said to have initiated when these volumetric differences showed that a significant increase in the volumetric strain (more than 2 micro-strains) made the data points deviate from linearity. It was also mentioned

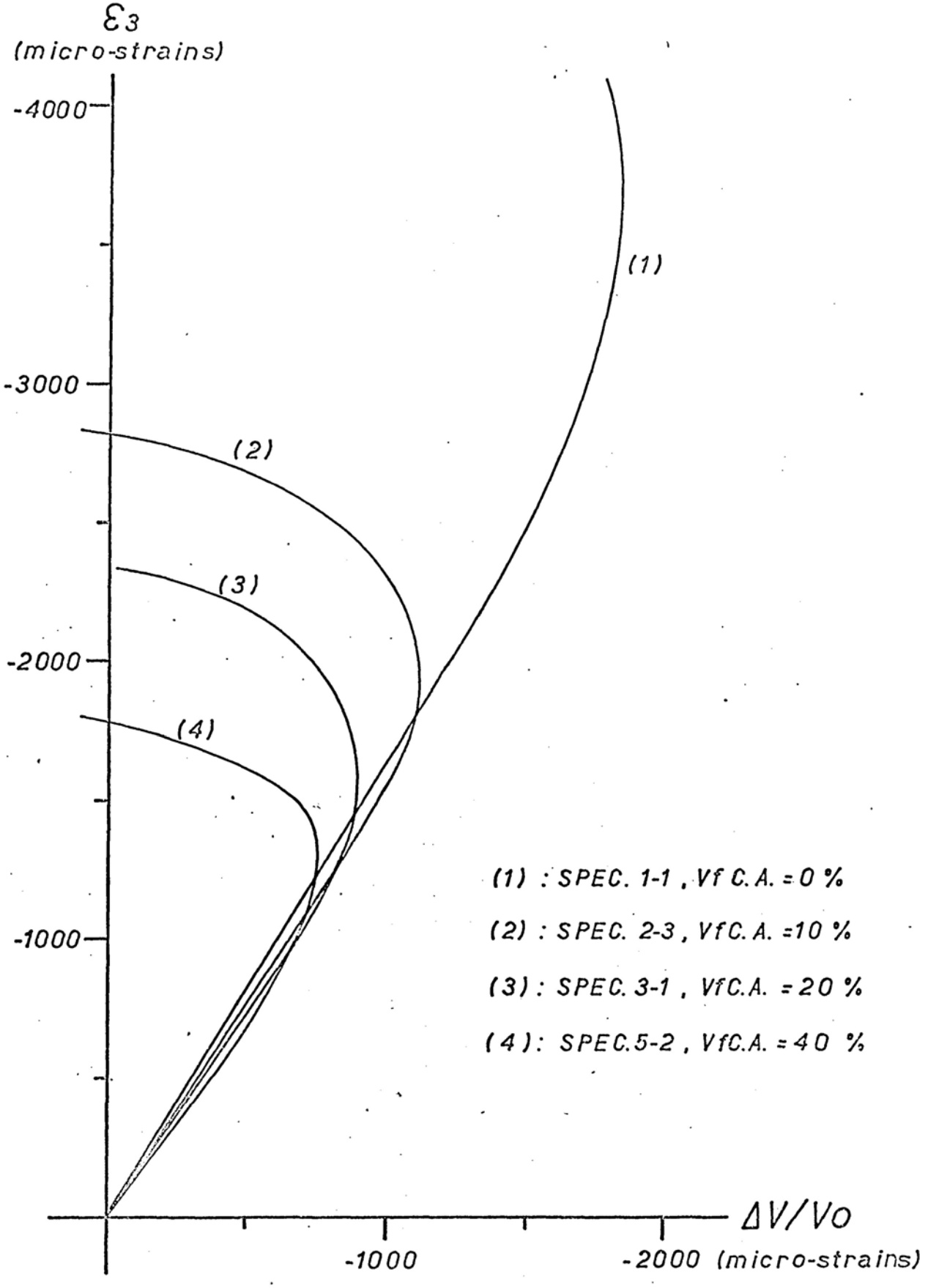
that, in the linear portion of the curve, the data points were usually found to lie at random in a $\pm$ 2 micro-strain band caused by possible errors in the strain recording techniques.

This method was also used on the present series of specimens to determine the stage at which fracture initiation occurred.

Unfortunately, on four specimens out of 18, it was impossible to determine a valid discontinuity point either because the strains in the linear portion of the curve showed an unusually large degree of variation or because in certain cases a sudden decrease, rather than increase, in the volumetric strain was noted. It was considered that the strain gauge readings on these cylinders did not accurately represent the behaviour of the concrete specimen as a whole.

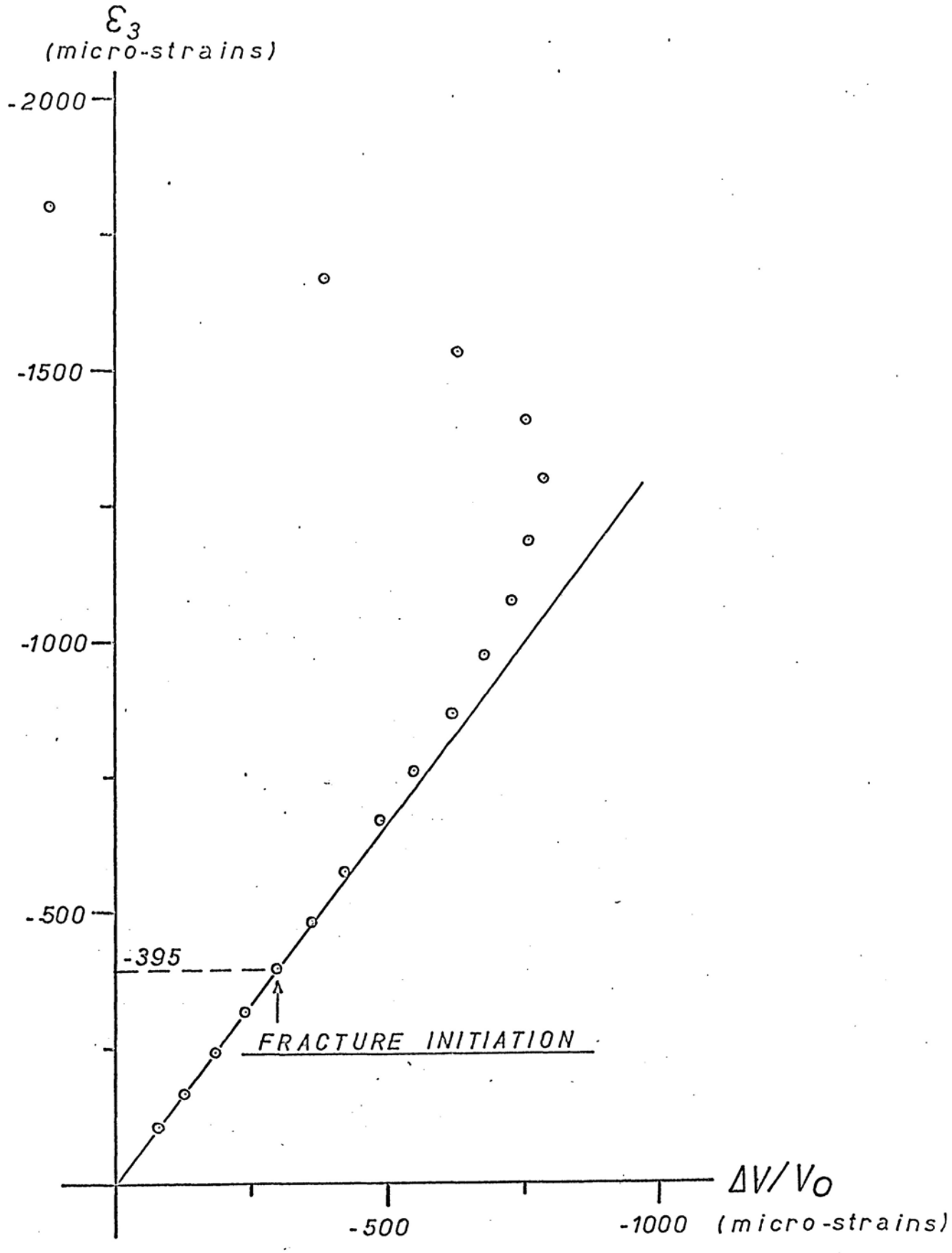
In two other cases, the discontinuity strains for one specimen in a group of three were found to be extremely low. It was considered that this was probably due to poor adhesion and consequent slipping of a gauge on the concrete surface. It was felt very unlikely that such a variation in the discontinuity properties of three specimens having similar failure stresses (within group variation of less than 4%) could occur. The other two values of the strains at discontinuity showed a very close agreement and their average was considered representative for that group.

Figure 7-1 shows typical relationships between volumetric strain ($\Delta V/VO$) and axial strain (ε_3) for four cylinders containing various volume fractions of coarse aggregate. In figures 7-2, 7-3, 7-4 and 7-5, the same relationships are plotted to a larger scale. (For clarity, only selected load stages are plotted). On these figures, the points of fracture initiation are shown together with the best straight line fitting the linear portion of the relationships. In table 7-B, the strains at discontinuity are given together



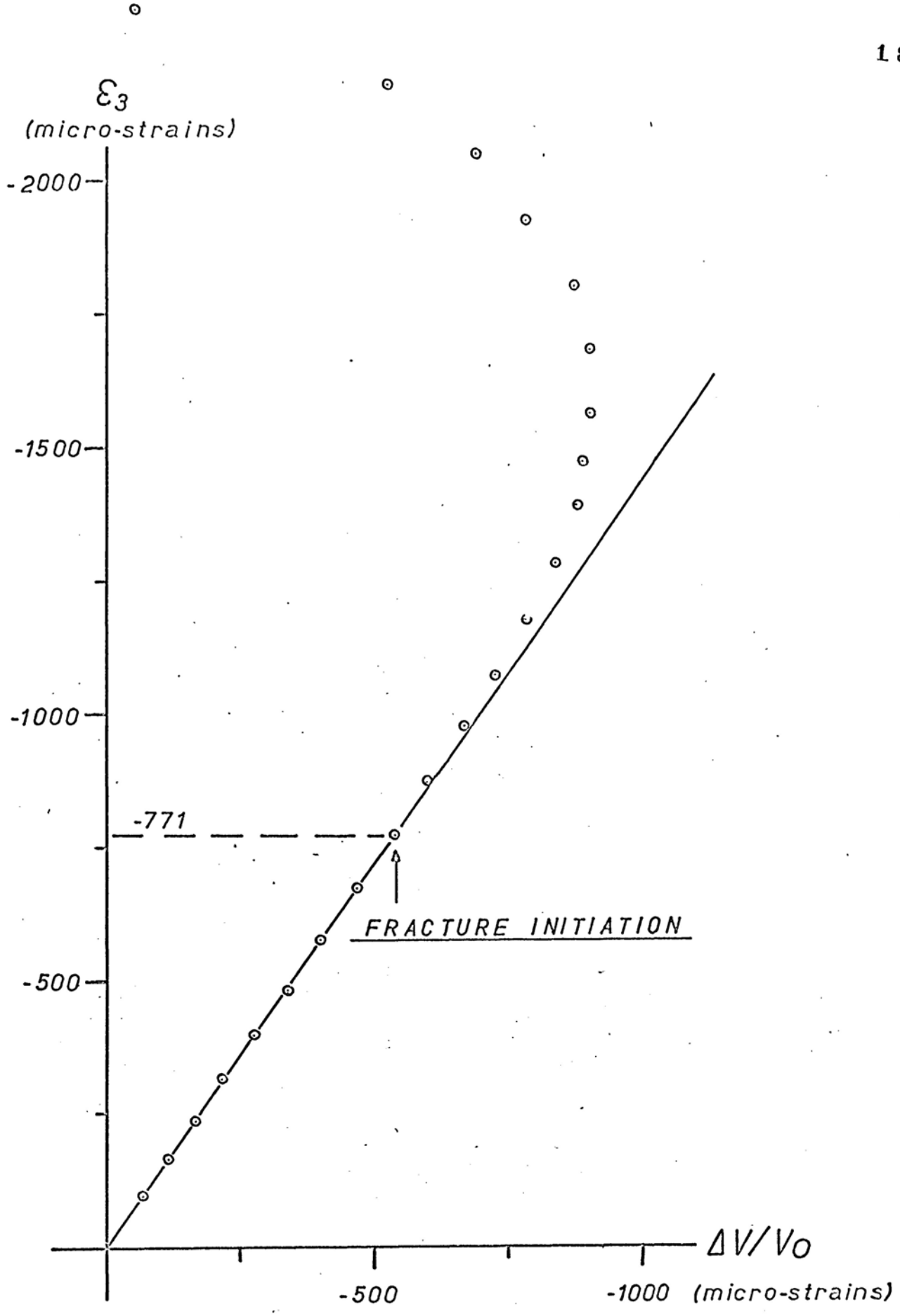
COMPARED CURVES
FOR VARIOUS SPECIMENS

fig. 7-1



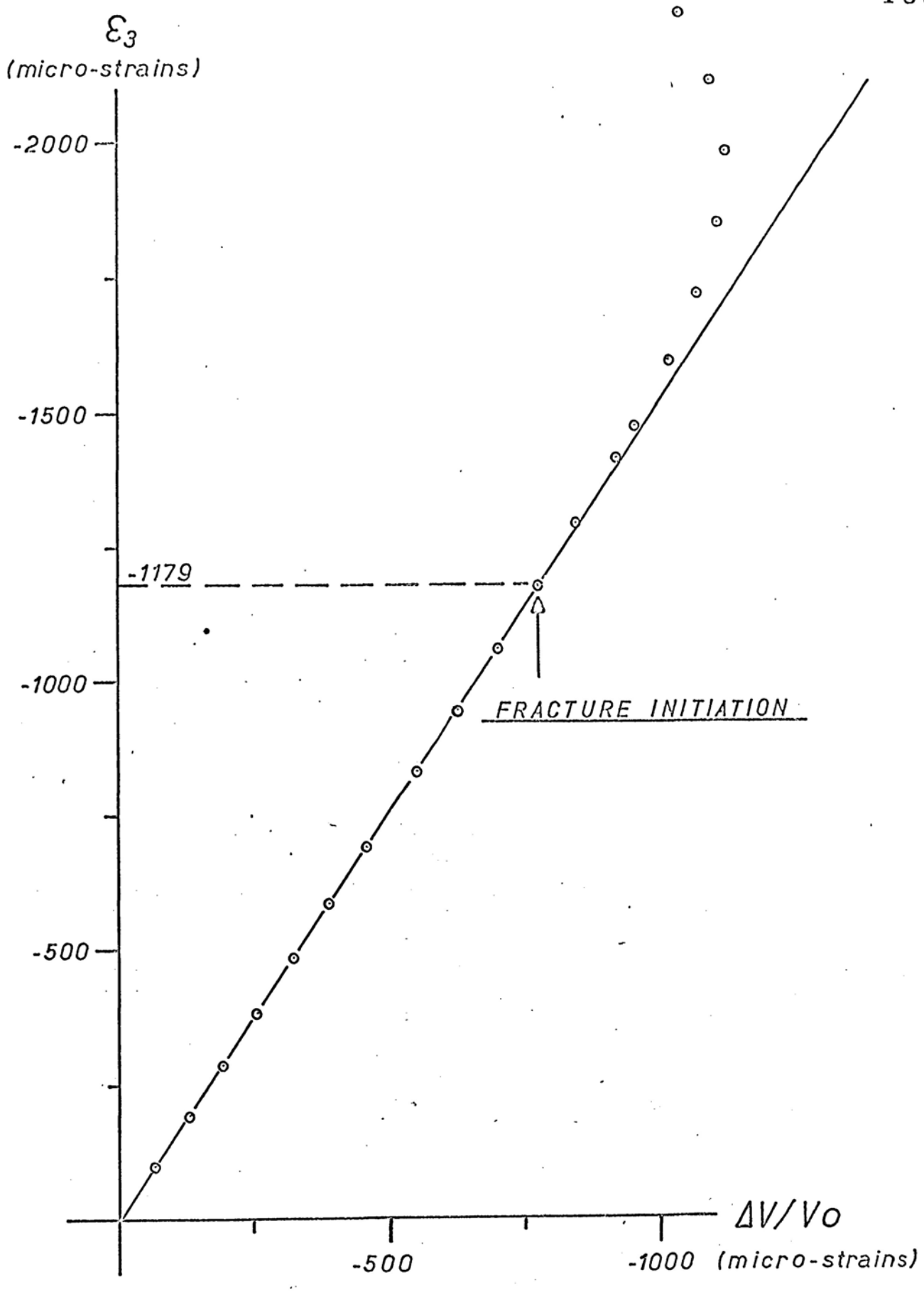
SPECIMEN 5-2 $V_f = 40\%$

fig. 7-2



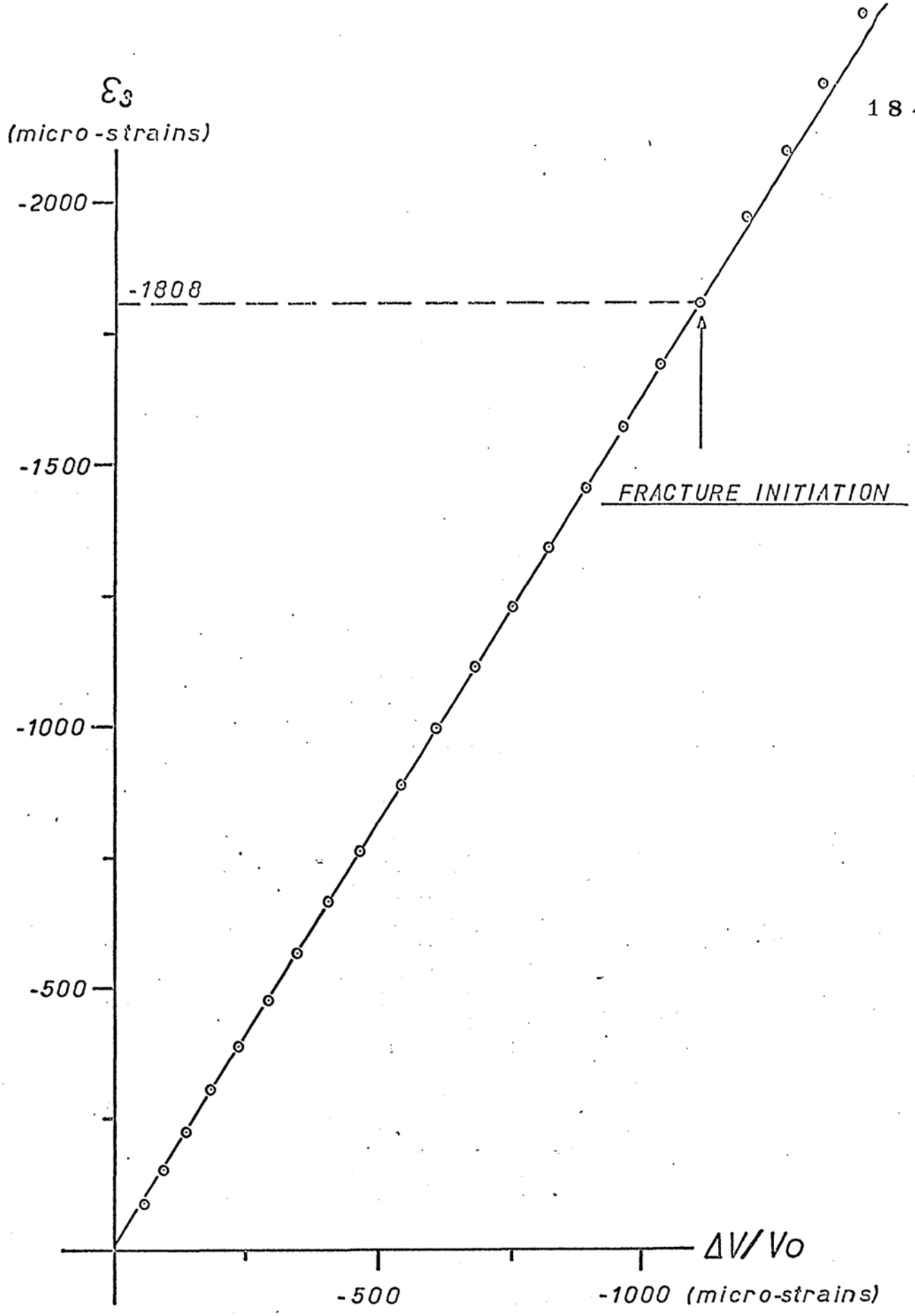
SPECIMEN 3-1 $V_f = 20\%$

fig. 7-3



SPECIMEN 2-3 V_f = 10 %

fig. 7-4



SPECIMEN 1-1 $V_f = 0\%$

fig. 7-5

TABLE 7-B

GRAVEL CONCRETE TEST RESULTS

SPEC.	% V_f C.A.	$(\varepsilon_1)_{f.i.}$ (micro-strains)	$(\varepsilon_3)_{f.i.}$ (micro-strains)	$(\sigma_3)_{f.i.}$ (p.s.i.)	$(\sigma_3)_{ult}$ (p.s.i.)
1-1	0	352	-1808	6900	10,920
1-2	0	338	-1745	6500	11,070
1-3	0	388	-1874	6910	10,880
Mean	0	359	-1809	6770	10,960
2-1	10	(65)*	(-439)*	(1770)*	8,830
2-2	10	223	-1152	4620	8,940
2-3	10	201	-1179	4520	8,630
Mean	10	212	-1165	4570	8,800
3-1	20	119	-771	3300	8,130
3-2	20	(51)*	(-270)*	(1240)*	7,920
3-3	20	126	-685	3230	8,190
Mean	20	122	-728	3265	8,080
4-1	30	-	-	-	8,760
4-2	30	-	-	-	8,780
4-3	30	111	-669	3690	8,380
Mean	30	-	-	-	8,640
5-1	40	59	-402	2020	7,790
5-2	40	47	-395	2260	7,520
5-3	40	66	-366	2160	7,750
Mean	40	57	-388	2150	7,690
6-1	50	49	-328	2160	8,100
6-2	50	-	-	-	8,320
6-3	50	-	-	-	7,930
Mean	50	-	-	-	8,120

* Results considered erroneous and not included in means

with the discontinuity and failure stresses for each specimen.

In figure 7-6, a graph showing the relation between the minor principal composite material strain at fracture initiation and the volume fraction of coarse aggregate is given. Specimen groups 4 and 6 are not shown on this graph since only one result per group was available and this was not considered sufficiently representative.

Section 4. Discussion of Results and Conclusions

On figure 7-7, Newman's[13] test results were plotted in a similar manner to figure 7-6, allowing a comparison to be made between the fracture initiation properties of glass-marble concretes and gravel concretes. As expected, it was found that in the gravel concretes, fracture had initiated at a significantly lower value of the minor principal composite material strain (ε_3) for all volume fractions of coarse aggregate considered.

It was therefore concluded that the angularity of the aggregate particles in such gap-graded mixes had a significant influence on the level of composite strain at fracture initiation and it was considered likely that the use of more angular aggregate (crushed rock for instance) would cause even greater decreases in the discontinuity strains of concrete.

It must be noted that the aggregate type and surface texture and not only the aggregate shape was dissimilar for the gravel and glass-marble concretes. However, Alexander, Wardlaw and Gilbert[24] have shown the bond quality to be related primarily to the type of aggregate and in particular to SiO_2 content, rather than the surface texture. The E-Glass used in the glass-marble concretes and the gravel aggregate both have similar and very high S_iO_2 contents. Thus it was considered valid to conclude that the shape of the

GRAVEL-CONCRETE TEST RESULTS

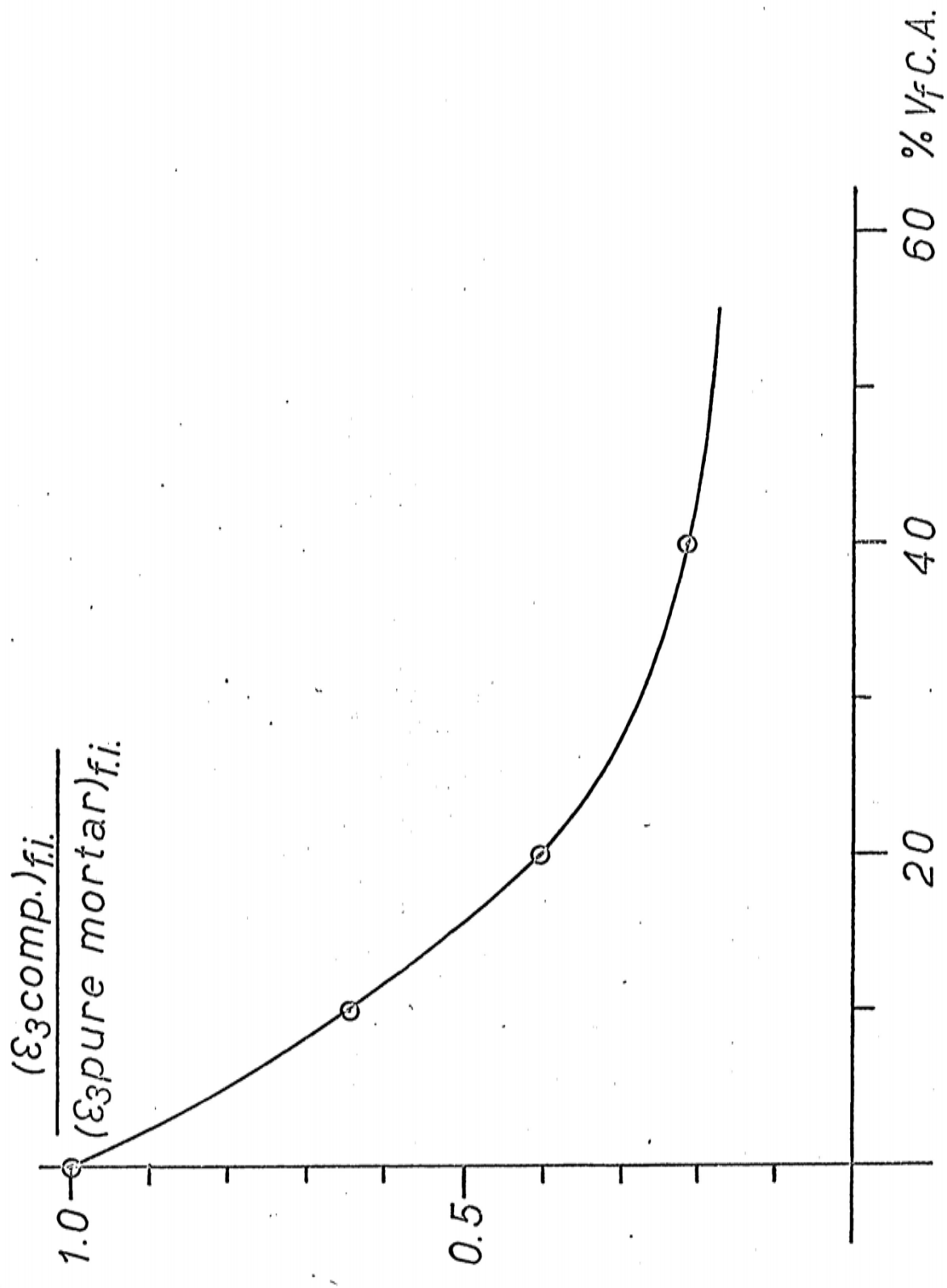


fig. 7-6

GLASS-MARBLE CONCRETE AND GRAVEL CONCRETE TEST RESULTS

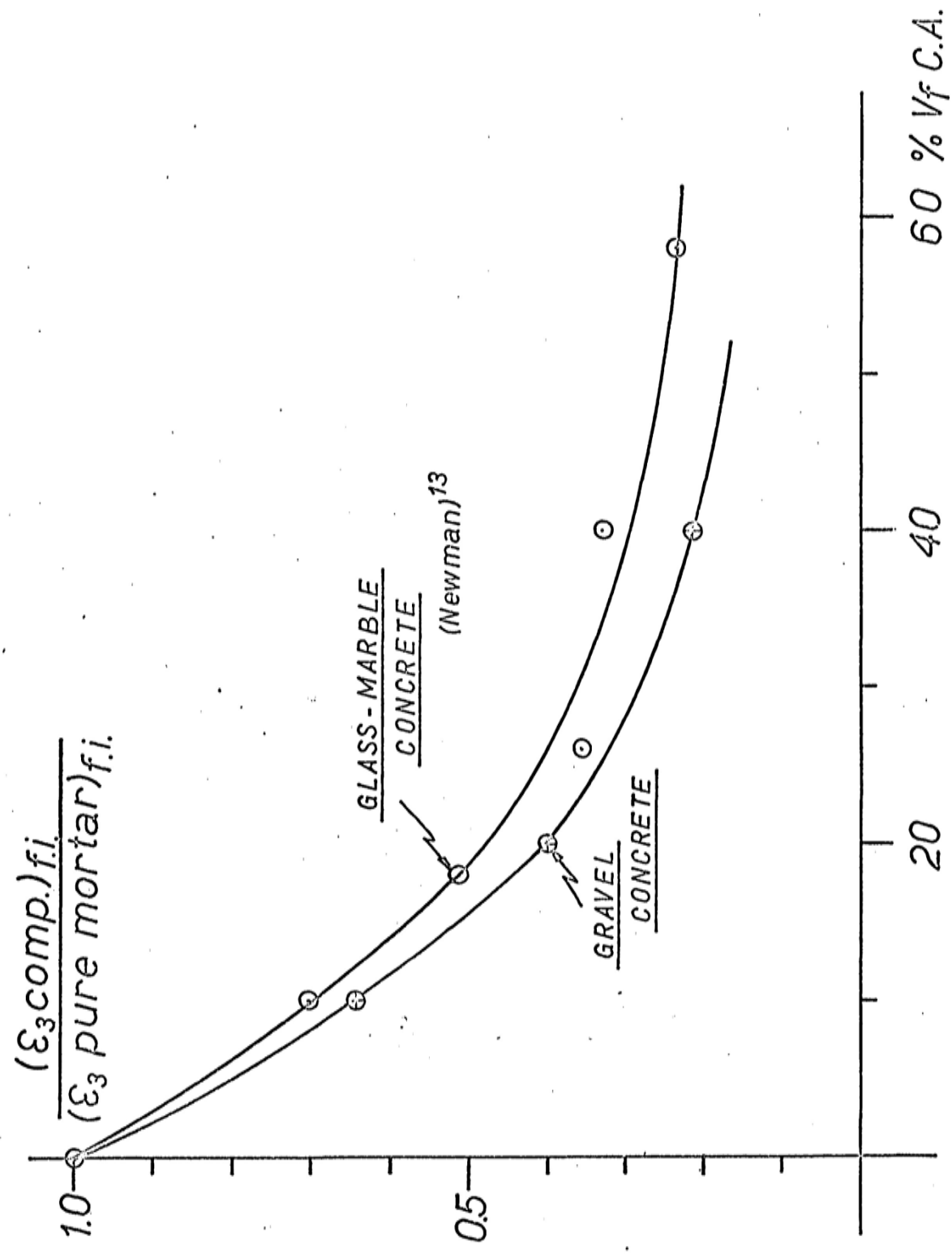


fig. 7-7

particles and not the bond quality was the main factor causing the values of the axial strain at fracture initiation to be different for the two types of concrete.

It was further concluded that the causes of internal cracking in gap-graded concrete containing an irregularly shaped gravel aggregate were therefore, most probably similar to those in glass-marble concrete (i.e. high tensile strain concentrations in the mortar matrix) since it was found that, as far as fracture initiation was concerned, these two types of concrete showed similar trends in the relation between strains at fracture initiation and volume fraction of coarse aggregate (see figure 7-7). However, the strain concentrations were higher and thus cracking occurred earlier in the gravel concretes because the aggregate particles were angular instead of round. This had been expected since the presence of discontinuities in a material usually causes higher stress concentrations as the shape of these discontinuities becomes more and more elliptical (or angular)[25-26].

CHAPTER VIII

CONCLUSIONS

In the present thesis, a particular type of concrete, consisting of single-sized glass spheres imbedded in a mortar matrix, was considered. Plate-models, representing thin two-dimensional slices of such a concrete were tested in uniaxial compression and the process of crack initiation and propagation was examined. These plate-models contained three different aggregate particle arrays, with various spacings between particles to represent various volume fractions of coarse aggregate.

From the plate-model tests, it was found that cracking always initiated in the mortar matrix, at a value of the minor (most compressive) principal strain of the composite material much lower than that required for fracture initiation in pure mortar. The presence of the hard aggregate particles was found to cause high tensile strain concentrations in the matrix and thus to enable it to reach at low values of the composite material strain the strains required for fracture initiation.

The tests to failure of the plate-models further showed that, after initiating in the mortar matrix, micro-cracking always propagated to, and around, the aggregate particles. Detailed conclusions of these tests are given in chapter VI section 7.

It must be mentioned, in addition, that another series of plates, with a different particle array, had been tested by McCreath[3] resulting in the same conclusions.

It was found that for all plates the relation between the volume fraction of coarse aggregate and the minor (most compressive) principal composite strain at fracture initiation was quantitatively similar (see figure 6-13) to the relation obtained by Newman[13] for uni-

axial tests on three-dimensional specimens of the concrete at least in the region of volume fractions covered by the plate-models. Thus it was concluded that these plate-models gave valid indications of the behaviour of the concrete with respect to the phenomenon of crack initiation and propagation.

It was felt that the above study represented a first step in the solution of the general problem of understanding the fundamental behaviour of concrete under load.

Tests carried out on gap-graded gravel concretes further showed that the behaviour of such concretes was similar to that of glass-marble concretes, although it was found that angular particles instead of round ones caused fracture to initiate at lower values of the composite material strain (see figure 7-7).

Therefore, in view of the above evidence, it can probably be concluded that the process of crack initiation and propagation in the plate-models basically represents that process in plain concrete under uniaxial compression.

Future Research

In the present study, the phenomenon of crack initiation and propagation was examined, but only in gap-graded concretes under uniaxial compression. Therefore, to fully understand the behaviour of normal plain concrete under load, many other parameters, concerned with both the material and loading characteristics, remain to be studied. These parameters can be grouped as follows:

- Matrix properties.
- Environmental Conditions.
- Aggregate grading and type.
- Loading rate, type and history.

As far as the cracking process is concerned, the matrix properties and environmental conditions are considered by the author to be of secondary importance.

Of prime importance is firstly the grading of the aggregate which is the basic difference between concrete in normal usage and the concretes considered in the present work. A gradation of aggregate sizes may cause higher strain concentrations, and thus earlier cracking, due to the superimposed effect of the large particles on the smaller ones. It may also influence the crack propagation process. In addition, the type of aggregate is considered of importance because it is the main factor affecting the aggregate-mortar bond strength[24]. Only high silica content aggregates were considered by the author in his investigation. It is felt that different types of aggregate and therefore different bond qualities may influence the process of crack propagation in concrete.

Secondly, it is considered that the effect of a predominantly tensile stress field should be investigated because in such a state of stress, the mechanism of fracture is probably different than in uniaxial compression. This is considered more important at this stage than complex states of stress (triaxial etc.).

Finally, as concrete is used in structural members and as such is submitted to long term and repeated loadings and to variable loading histories, it is felt that the response of concrete to such loads must also be investigated. It is important to determine how the cracking process will be affected and also how it will affect the behaviour of concrete in such cases. Up to now, little work has been done on this subject[27-28].

For the purposes of the future research suggested above, the author does not recommend the use of plate-models as described in

chapters V and VI because, if the parameters considered by the author to be important were to be included in plate-model tests, the specimens required would become too complex and difficult to test. The validity of the results obtained would therefore be doubtful. It is thus suggested that three dimensional tests only be carried out, at least if the parameters considered important by the author are to be investigated.

It should also be emphasized that investigators should always bear in mind the aim of this type of engineering research : better knowledge of the material to rationalize it's use and improve it's qualities as a building material.

REFERENCES

1. Richart, F.E., Brandtzaeg, A., and Brown, R.L. (1928). "A Study of the Failure of Concrete under Combined Stresses". University of Illinois, Eng. Expt. Stat., Bulletin No. 185, pp. 1-102.
2. Newman, K. and Newman, J.B., (1969). "Failure Theories and Design Criteria for Plain Concrete". Proceedings of the International Conference on Structure, Solid Mechanics and Engineering Design in Civil Engineering Materials, Southampton, (to be published). Paper 83, 33 pp.
3. McCreath, D.R., (1968). "The Fracture Mechanics of Concrete". Ph.D. thesis, University of London. 258 pp.
4. Griffith, A.A., (1920). "The Phenomena of Rupture and Flow in Solids". Philosophical Transactions of the Royal Society. 221-A pp. 163-198.
5. Griffith, A.A.,(1924). "Theory of Rupture" Proceedings of the First International Congress for Applied Mechanics, Delft. pp. 55-63.
6. Kaplan, M.F., (1968). "The Application of Fracture Mechanics to Concrete", in A.E. Brooks and K. Newman (Eds.), The Structure of Concrete. Cement and Concrete Association, London.
7. Orowan, E., "Fracture and Strength of Solids". Report on Progress in Physics. Vol. 12, 1948-49. pp. 185-232.
8. Neville, A.M., (1963). "Properties of Concrete". Publishers, Pitman and Sons, London.
9. Hoek, E., (1967). "Brittle Failure of Rock". Rock Mechanics Research Report No. 2, Imperial College, London.
10. Hsu, T.T.C., Slate, F.O., Sturman, G.M. and Winter, G., (1963) "Micro-cracking of Plain Concrete and the Shape of the Stress-Strain Curve". Proc. Amer. Conc. Inst. Vol. 60. pp. 209-224.

11. D...tu P.,(1958). "Study of the Stresses in Non-homogeneous Materials and it's Application to Concrete". Annales de l'Institut Technique du Batiment et des Travaux Publics. Vol. 11, pp. 55-57.

12. Swamy, N., (1969). "Aggregate-matrix Interaction in Concrete Systems" Proceedings of the International Conference on Structure, Solid Mechanics and Engineering Design in Civil Engineering Materials, Southampton (to be published). Paper 31, 15 pp.

13. Newman, J.B., "Behaviour of Concrete under Complex States of Stress". Ph.D. Thesis, University of London. To be submitted.

14. Dally, J.W. and Riley, W.F., (1965) "Experimental Stress Analysis" Publishers, McGraw-Hill. pp. 286-295

15. Navaratnarajah, V. (1965) "A Photo-elastic Method of Detecting Micro-cracks in Concrete". Journal of Scientific Instruments, Vol. 42, pp. 276-277.

16. Van Geen, R. Private Communication.

17. Duffy, J. and Mylonas, C., (1963) "An Experimental Study of the Effects of the Thickness of Birefringent Coatings" "Photoelasticity", Pergamon Press, New York.

18. Duffy, J. (1961) "Effects of the Thickness of Birefringent Coatings". Expt. Mech. Vol. 1, No. 3, pp. 74-82.

19. Durelli, A.J. and Riley, W.F., (1965), "Introduction to Photo-Mechanics". Prentice Hall (Publishers) pp. 246-253.

20. Muskhelishvili, N.I., (1953). "Some Basic Problems of the Mathematical Theory of Elasticity". 3rd. Ed. Publishers, P. Noordhoff N.V., Groningen, Holland. Trans. by J.R.M. Radak.

21. Newman, K., (1966). "Concrete Systems, Chapter VIII" in L. Holliday (Ed.), "Composite Materials" Elsivier Publishing Co. pp. 336-452.

22. Ward, M.A., (1969). "The Testing of Concrete Materials by Precisely Controlled Uniaxial Tension". Ph.D. Thesis, University of London. 312 pp.

23. Kaplan, M.F., (1963). "Strains and Stresses of Concrete at Initiation of Cracking and Near Failure". Proc. Amer. Conc. Inst., Vol. 60, pp. 853-879.

24. Alexander, K.M., Wardlaw, J. and Gilbert, D.J., "Aggregate-Cement Bond, Cement Paste Strength and the Strength of Concrete" in A.E. Brooks and K. Newman (Eds.), The Structure of Concrete (1968), Cement and Concrete Association, London pp. 59-81.

25. Timoshenko, S. and Goodier,J.N., (1951). "Theory of Elasticity" McGraw-Hill Book Co. New York. 506 pp.

26. Timoshenko, S., (1955). "Strength of Materials". 3rd. Edition. D. Van Nostrand Co. Publishers. 2 vols.

27. Rusch, H., (1960) Proceedings of the American Concrete Institute, Vol. 57.

28. Glucklich, J., "The Effect of Micro-cracking on Time-dependent Deformations and the Long-term Strength of Concrete" in A.E. Brooks and K. Newman (Eds.). The Structure of Concrete (1968) Cement and Concrete Association, London. pp. 176-189.